Identification and Investigation of Novel ALMS1 Interaction Partners in Cilia-Related Processes

Dissertation

der Mathematisch-Naturwissenschaftlichen Fakultät

der Eberhard Karls Universität Tübingen

zur Erlangung des Grades eines

Doktors der Naturwissenschaften

(Dr. rer. nat.)

vorgelegt von

Franziska Julia Wörz

aus Ludwigsburg

Tübingen

2023

Gedruckt mit Genehmigung der Mathematisch-Naturwissenschaftlichen Fakultät der Eberhard Karls Universität Tübingen.

Tag der mündlichen Qualifikation:	09.11.2023
Dekan:	Prof. Dr. Thilo Stehle
1. Berichterstatter/-in:	Prof. Dr. Doron Rapaport
2. Berichterstatter/-in:	Prof. Dr. Marius Ueffing

Erklärung zu thematischer/inhaltlicher Überschneidung von Dissertation und Masterarbeit

Aufgrund meiner vorangegangenen Masterarbeit können inhaltliche und thematische Überschneidungen zu dieser vorgelegten Dissertation bestehen.

Folgende Abschnitte die inhaltliche bzw. thematische Überschneidungen zur bisher unveröffentlichten Masterarbeit „ALMS1 interactome identification and its role in ciliogenesis using CRISPR/Cas9 gene editing and protein complex analysis“ von 2018 aufweisen können, wurden daher umformuliert, sowie Abbildungen modifiziert und neugestaltet:

- Summary
    - 1 Summary
- Zusammenfassung
    - 2 Zusammenfassung
- Introduction
    - 3.1 Cilia
    - 3.2 Ciliary dysfunction leads to diseases: Ciliopathies
- Material and Methods
    - 5 Materials
    - 6 Methods
- Aim
    - 4 Aim of the PhD study
- Results
    - 7.1 Generation of AMS1 deficient human retinal epithelium cell lines
    - 7.2 ALMS1 loss in hTERT-RPE1 single clones show variances in ciliary length
    - 7.7 Endogenous complex analysis revealed a new ALMS1 interactome
- Discussion
    - 8 Discussion and outlook
- References
    - 9 List of references

Die Masterarbeit wurde im August 2018 als gebundener Ausgabe im Prüfungsamt Molekulare Medizin in der Silcherstraße 5, 72076 Tübingen, Gebäude Nr. 370, Raum 109 abgegeben sowie auf ILIAS als PDF hochgeladen. Die Masterarbeit, im Rahmen des Masterstudiengangs Molecular Medicine an der Eberhard Karls Universität wurde mit einer 1,0 bewertet.

Tuebingen, 27th July 2023

Franziska Wörz

List of publications

Accepted Peer-Review Publication

Felix Hoffmann, Sylvia Bolz, Katrin Junger, Franziska Klose, Timm Schubert, **Franziska Woerz**, Karsten Boldt, Marius Ueffing, and Tina Beyer. 2022. TTC30A and TTC30B Redundancy Protects IFT Complex B Integrity and Its Pivotal Role in Ciliogenesis. Genes 2022, 13 (7), 1191; doi: https://doi.org/10.3390/genes13071191 [1]

Sebiha Cevik, Xiaoyu Peng, Tina Beyer, Mustafa S. Pir, Ferhan Yenisert, **Franziska Woerz**, Felix Hoffmann, Betul Altunkaynak, Betul Pir, Karsten Boldt, Asli Karaman, Miray Cakiroglu, S. Sadik Oner, Ying Cao, Marius Ueffing, Fowzan S. Alkuraya, Oktay I. Kaplan. WDR31 displays functional redundancy with GTPase-activating proteins (GAPs) ELMOD and RP2 in regulating IFT complex and recruiting the BBSome to cilium. Life Science Alliance May 2023, 6 (8) e202201844; doi: https://doi.org/10.1101/2021.06.10.445528 [2]

Submitted Manuscript

Franziska Woerz, Felix Hoffmann, Shibu Antony, Sylvia Bolz, Mohamed Ali Jarboui, Katrin Junger, Franziska Klose, Isabel F. Stehle, Karsten Boldt, Marius Ueffing, Tina Beyer. Interactome analysis reveals a link of the novel ALMS1-CEP70 complex to centrosomal clusters, Molecular & Cellular Proteomics, 2023, under review* [3]

Tobias Leonhard, Gaurav D. Diwan, Franziska Klose, Isabel F. Stehle, Katrin Junger, Marian Seda, Sylvia Bolz, **Franziska Woerz**, Robert B. Russell, Karsten Boldt, Dagan Jenkins, Marius Ueffing, Tina Beyer. Ciliopathy-associated missense mutations in IFT140 are hypomorphic and have edgetic effects on protein interaction networks. bioRxiv 2023.01.18.523235; doi: https://doi.org/10.1101/2023.01.18.523235 [4]

* This publication is part of this thesis.

Conference contribution

Conference Contribution

EMBO 5th European CILIA Conference (2022), Cologne, virtual conference
Poster presentation: Abstract #67: ALMS1 interactome identification and its role in ciliopathies (was presented by Felix Hoffmann)
Franziska Woerz, Felix Hoffmann, Katrin Junger, Sylvia Bolz, Franziska Klose, Karsten Boldt, Tina Beyer, Marius Ueffing

EMBO: Centrosome and Spindle Pole Bodies (2021), Denmark, virtual conference
Poster presentation: Abstract #8: ALMS1 ciliary protein complex mapping and phenotypic analysis reveal an ALMS1- γ Tubulin interaction that could promote basal body stability.
Franziska Wörz, Felix Hoffmann, Franziska Klose, Katrin Junger, Mohamed Ali Jarboui, Tina Beyer, Karsten Boldt, Doron Rapaport, Marius Ueffing

15th PRO RETINA Research-Colloquium (2021), Potsdam, virtual conference
Poster presentation: Abstract #904373: ALMS1 ciliary protein complex mapping and phenotypic analysis reveal an ALMS1- γ Tubulin interaction that could promote basal body stability.
Franziska Wörz, Felix Hoffmann, Franziska Klose, Katrin Junger, Mohamed Ali Jarboui, Tina Beyer, Karsten Boldt, Doron Rapaport, Marius Ueffing

Table of contents

List of Figures

List of Tables

Abbreviations

%	Percentage
°C	Degree Celsius
µg	Micrograms
µl	Microliter
A	Adenine
aa	Amino acid
ABC	Amonium bicarbonate Solution
ACN	Acetonitrile
Amp	Ampicillin
APS	Ammonium Persulfate
ATP	Adenosine triphosphate
BB	Basal body
BBSome	Bardet-Biedl-Syndrome protein complex
bp	Base pair
BPB	Bromophenol Blue
BSA	Bovine Serum Albumin
C	Cytosine
Cas9	CRISPR-associated Protein 9
CC	Connecting cilium
CEP250	Centrosomal protein 250 kDa
CEP70	Centrosomal protein 70 kDa
CRISPR	Clustered Regularly Interspaced Short Palindromic Repeats
CT	C-Terminal
CV	Ciliary vesicle
DAP	Distal appendages
DAPI	4’,6-Diamidin-2-phenylindol
ddH_2O	Ultra-pure water
ddNTP	Dideoxyribonucleoside- Triphosphate
dH_2O	Deionized water
dKO	Double knock-out
DMSO	Dimethylsulfoxid
DNA	Desoxyribonucleic acid
dNTP	Desoxynuceloside-Triphosphate
DTT	Dithiothreitol Solution

E.Coli	Escherichia coli
e.g.	Exempli gratia, for example
ECL	Enhanced chemiluminescence
et al.	and others
EtBr	Ethidium bromide
ex	Exon
FCS	Fetal calf sera
g	Gram
G	Guanine
GFP	Green fluorescent protein
GLUT4	Glucose transporter 4
h	Hour
HA	Hemagglutinin-Protein
HAc	Acetic acid
HCl	Hydrochloric Acid
HEK	Human Embryonic Kidney cells
hrs	Hours
hTERT-RPE	Human Telomerase Reverse Transcriptase-immortalized Retinal Pigmented Epithelial Cells
IAA	Iodacetamide Solution
IFS	Immunofluorescence Staining
IFT	Intraflagellar Transport
IP	Immunoprecipitation
IS	Inner segment
kb	Kilobases
KD	knockdown
KO	knock-out
l	Liter
LB	Lysis buffer
LB-Media	Luria-Bertoni Media
LC	Liquid chromatography
LFQ	Label-free quantification
m/z	Mass to charge ratio
mAb	monoclonal antibody
max.	Maximal
Mb	Mega base pairs

MetOH	Methanol
min	Minutes
mind.	At least
ml	milliliter
mM	Millimolar
MS	Mass spectrometry
MS/MS	Tandem mass spectrometry
MTOC	Microtubule organizing center
NaCl	Sodium Chloride
NGS	Next Generation Sequencing
NHEJ	Non Homologous End Joining
nM	Nanomol
NP-40	Nonident P40
NT	N-Terminus
OD	Optical density
OMIM	Online Mendelian Inheritance in Men
opt.	Optimal
OS	Outer segment
PAM	Protospacer adjacent motif
PBS	Dulbecco's Phosphate-Buffered Saline
PCR	Polymerase Chain Reaction
PEI	Polyethylenimine linear
PFA	Paraformaldehyde
PI 2,3	Phosphatase Inhibitor Cocktail 2,3
PIC	Protease Inhibitor Complex Complete
PP	Polypropylene
PPC	Photoreceptor precursor cells
Puro	Puromycin
PVDF	polyvinylidene difluoride
RFP	Red fluorescent protein
RFX	Regulatory factor X
RNA	Ribonucleic acid
rpm	Revolutions per minute
RT	Room temperature
SAP	Subdistal appendages
SDS	Sodiumdocecylsulfate
SDS-PAGE	SDS-polyacrylamide gel electrophoresis

sec	Seconds
Ser473	serine 473
sfGFP	super folder Green Fluorescent Protein
SF-TAP	Strep/Flag tandem affinity purification
siRNA	Small interfering RNA
SOC	super optimal broth with glucose
SpCas9	Streptococcus pyogenes
ssDNA	Single stranded DNA
STED	Stimulated Emission Depletion
T	Thymine
Taq	Thermus aquaticus
TBS	Tris-Buffered Saline
TBST	TBS-Tween
TFA	Trifluoracetic Acid
Thr308	threonine 308
TPR	tetratricopeptide repeat
tRNA	Transfer Ribonucleic acid
TTBK2	Tau tubulin kinase-2
TZ	Transition zone
u	Units
V	Volt
v/v	Volume per volume
w/v	Weight per volume
WB	Washing buffer
wt	wildtype
x g (rcf)	Relative Centrifugal Force

Acknowledgment

I would like to express my deepest gratitude to my two supervisors, Prof. Dr. Rapaport, and Prof. Dr. Marius Ueffing, for their invaluable guidance, exceptional ideas, and constant encouragement throughout my Ph.D. thesis. Their mentorship has been instrumental in shaping my academic journey, and I am profoundly grateful for the opportunity to work on this project under their supervision. Their unwavering support has not only fueled my personal growth but also contributed significantly to my academic development.

I would like to express my heartfelt gratitude to Dr. Tina Beyer and Dr. Karsten Boldt for their unwavering availability to address my "short" questions, engage in academic discussions, and address any concerns I had. Their exceptional support, kind words, and constructive criticism have been truly invaluable.

In addition, I would like to extend my sincere appreciation to the entire AG Ueffing team, with a special mention of Dr. Mohamed Ali Jarboui, Franziska Klose, Katrin Junger, Sylvia Bolz, Dr. Felix Hoffmann, Dr. Tobias Leonhard, Shibu Antony, and Isabel Stehle. I am immensely grateful for the stimulating discussions, motivational encouragement, and unwavering support they provided throughout my project. The memories of our "PhD movie nights" and the hilarious exchange of PhD-related memes will be cherished dearly. These moments have left an indelible mark on me, and I will fondly remember them.

Moreover, I want to thank Dr. Sally Williamson for her support and for proofreading this thesis.

I would like to extend a special and heartfelt gratitude to the following individuals who have been a tremendous source of support and unwavering advice throughout my journey: my boyfriend Felix, my parents Martina and Hartmut, my brother Philipp, my grandma Isolde, my aunt, my uncle, and my dear friends Vera, Ines, Monja, Carina, Anja and Jasmin. Your infinite support has meant the world to me, and I am truly grateful to have each of you by my side. Furthermore, I want to thank my beloved grandpa’s Harry and Karl-Heinz, that championed my academic achievements in heaven.

Thank you so much.

Franziska Wörz

1 Summary

Cilia, singularly projecting organelles found on most eukaryotic cells, play critical roles in human physiological processes [5]. They can be categorized mainly into two types: non-motile (primary) cilia and motile (secondary) cilia, both presenting high evolutionary conservation across species [6]. A cilium comprises a basal body, derived from the centrosome, which serves as foundation for the microtubule-based structure known as the axoneme. The axoneme facilitates the bidirectional transport of proteins (intraflagellar transport) between the proximal and distal regions of the cilium, which is crucial for cilia assembly and signaling. A critical regulatory region, known as the transition zone, acts as a gate regulating the diffusion of proteins from the cytoplasm into the cilium [7,8]. Any disruption in the proper functioning of cilia can lead to a diverse range of diseases, characterized by overlapping phenotypes, collectively referred to as ciliopathies. Currently, 35 ciliopathies have been identified, encompassing disorders such as the Alström syndrome (OMIM 203800) [9–11].

The Alström syndrome is a rare recessively inherited monogenetic condition with an incidence of 1 to 9 out of 1 million individuals [12,13]. Over 300 mutations within the *ALMS1* gene have been discovered, encompassing a vast array of phenotypic manifestations already occurring in infancy. These include cone-rode dystrophy leading to vision loss, Type 2 Diabetes, and childhood truncal obesity among others [14,15]. The *ALMS1* gene, located on chromosome 2, encodes a protein with a molecular weight of 461 kDa [16]. This protein is known to associate with both the centrosome and the basal body of cilia [16–18]. Despite published data, the specific molecular function of ALMS1 remains elusive, necessitating further investigation to unravel its functional significance.

The aim of this PhD study was to gain a better understanding of the molecular function of ALMS1 protein and its impact on the severity of this disorder. The working hypothesis centered on the involvement of ALMS1 in basal body protein interactions, essential for proper cilia morphology and transport to the cilium. To address this hypothesis and to decipher the ALMS1 function in cilia-related processes, phenotypical and protein complex analysis were performed.

Initially, ALMS1 deficient hTERT-RPE1 cells were generated using the CRISPR/Cas9 system, employing specific single guide RNAs (sgRNAs) targeting exon 8 and exon 10. *ALMS1* knock-out (KO) and control (Cas9 empty transfected cells) cells were used to identify the role of ALMS1 in cilia biology. *ALMS1* KO cells exhibit loss of ALMS1 accompanied by impaired cellular proliferation and shorter cilia compared to control cells. Furthermore, other centrosomal proteins, such as γ-tubulin were investigated, showing no differences in appearance to the control,

suggesting an upstream function, whereas CEP250 was mild but significantly reduced in ALMS1 deficient cells. These findings resembled the previously observed results from Knorz *et al.* [18]. Next, additional cilia and cilia-related markers were examined to further understand their expression and localization upon ALMS1 loss. While some markers, such as PCM1, remained unchanged, others such as RPGR displayed a compressed appearance. Further analysis and research are required to fully understand the functional relevance and implications of these observations and their significance in the context of cilia-related biology and disease-related mechanism.

To investigate a possible ALMS1-dependent mechanism, a protein complex analysis was conducted. Therefore, tags (sfGFP, RFP-HA) were introduced on endogenous level of *ALMS1* gene in HEK293T cells using the CRISPR/Cas9 method. These tagged cells were subsequently used for mass spectrometry analysis to identify novel ALMS1 interactors. Potential and novel interaction partners associated with cytoskeletal function, cell cycle regulation, metabolic function, transport, and post-translational protein modifications were revealed. One notable discovery was the identification of centrosomal protein 70 kDa (CEP70) as a highly abundant interactor of ALMS1. Further investigations, including affinity purification using full length CEP70 as well as CEP70 fragments (deletion analysis), were performed. Interestingly, protein complex analysis revealed, among others ALMS1 as an interactor of CEP70, hinting towards a strong interaction. Furthermore, ALMS1 as well as UBR4, ATG3, PLAA, UACA, TP53K, and BAX associate with the CEP70 region containing TPR domain and CT end. These results may indicate a potential role of CEP70-dependent cell loss. Due to enhanced cell loss, double KO of *CEP70* and *ALMS1* could not be achieved using CRISPR/Cas9. Silencing of CEP70 in wt cells showed not only a reduced ALMS1 localization at the BB, suggesting CEP70 upstream of ALMS1, but also an increase in cell loss. MRNA analysis of *BAX/BCL2* implicated an apoptotic process in CEP70 KD wt cells, while CEP70 KD in ALMS1 KO cells led to a shift towards cell survival compared to the control.

A final investigation of ALMS1 in a more retina-specific context was conducted. Retina gained from porcine and endogenous ALMS1-RFP-HA were used for a retina pull down. It revealed additional potential interaction partners implicated in signaling pathways, apoptosis and lipid metabolic processes, anatomical structure development, cell cycle regulation, and cilium organization. In the future, validation of these potential interaction partners is necessary to pin down the ALMS1 function.

In summary, this doctoral thesis shed light on the multifaceted functions of ALMS1 in various cellular processes. It indicated ALMS1 in the regulation of cellular proliferation, highlighting its role in the assembly and maintenance of cilia with implications for their functionality. Moreover, the involvement of *ALMS1* and *CEP70* in mRNA-mediated cell death processes was suggested, with CEP70 being upstream of ALMS1. However, further investigations are necessary to elucidate the intricate cellular and ciliary signaling pathways involved. The findings of this study provide valuable insights into the potential functions of ALMS1 and lay a solid foundation for future research endeavors, including investigations utilizing patient-derived cells to further comprehend the complexities of Alström syndrome.

2 Zusammenfassung

Zilien sind Organellen, die als einzeln hervorstehende Membranfortsätze auf den meisten eukaryontischen Zellen zu finden sind, deren Funktion essenziell für die menschliche Gesundheit sind [5]. Im Wesentlichen gibt es zwei Arten von Zilien, die beweglichen (sekundären) und die unbeweglichen (primären) Zilien, die zwischen verschiedenen Arten hochkonserviert sind [6]. Ein Zilium besteht aus einem Basalkörper, der sich vom Zentrosom ableitet und die Grundlage für das entstehende Mikrotubulirückgrat (Axonem) bildet. Das Axonem ermöglicht einen bidirektionalen Transport (intraflagellarer Transport) von Proteinen und anderen Stoffen, die für den Aufbau der Zilien und die ziliare Signaltransduktion wichtig sind. Eine *transition zone* fungiert als Tor zum Zilium, indem die freie Diffusion von Proteinen aus dem Zytoplasma in das Zilium eingeschränkt wird [7,8]. Jede Abweichung in der Funktion von Zilien kann zu einer Vielzahl von Krankheiten mit sich überschneidenden Phänotypen führen, die gemeinhin als Ziliopathien bezeichnet werden. Bislang wurden 35 Ziliopathien identifiziert, zu denen auch das Alström-Syndrom (OMIM 203800) gehört [9–11].

Das Alström-Syndrom ist eine seltene rezessiv vererbte genetische Erkrankung mit einer Inzidenz von 1 bis 9 in 1 Million Individuen [12,13]. Insgesamt wurden über 300 Mutationen im *ALMS1* Gen entdeckt, die ein breites Spektrum an phänotypischen Merkmalen umfassen, die bereits im Säuglingsalter auftreten. Dazu gehören unter anderem Zapfendystrophie, die zur Erblindung führt, Typ-2-Diabetes und Stammfettsucht bei Kindern [14,15]. Das *ALMS1* Gen, das sich auf Chromosom 2 befindet, kodiert ein Protein mit einem Molekulargewicht von 461 kDa [16]. Es ist bekannt, dass dieses Protein mit dem Zentrosom und mit dem Basalkörper der Zilien assoziiert ist [16–18]. Trotz der veröffentlichten Daten ist die genaue Funktion von ALMS1 jedoch nach wie vor unklar, sodass weitere Untersuchungen erforderlich sind, um seine funktionelle Bedeutung zu entschlüsseln.

Ziel dieser Doktorarbeit war es, ein besseres Verständnis der molekularen Funktion des ALMS1 Proteins und seiner Auswirkungen auf die Schwere dieser Erkrankung zu erlangen. Die Arbeitshypothese konzentrierte sich auf die Interaktionen von ALMS1 mit dem Basalkörper bzw. den zentrosomalen Proteinen, die für die korrekte Morphologie der Zilien und dem Transport von Proteinen zum Zilium unerlässlich sind. Um diese Hypothese zu untersuchen und die Funktion von ALMS1 zu entschlüsseln, wurden phänotypische Untersuchungen sowie Protein-Komplex-Analysen durchgeführt.

Zunächst wurden ALMS1-defiziente hTERT-RPE1-Zellen mit Hilfe des CRISPR/Cas9-Systems erzeugt, wobei spezifische *single guide* RNAs (sgRNAs) verwendet wurden, die auf Exon 8 und

Exon 10 abzielten. ALMS1-Knock-out (KO) - und Kontrollzellen (Cas9-transfizierte Zellen) wurden verwendet, um die Funktion von ALMS1 in der Zilienbiologie zu untersuchen. ALMS1-KO Zellen zeigen einen Verlust von ALMS1, der mit einer beeinträchtigen Zellproliferation und dem Vorhandensein kürzerer Zilien im Vergleich zu Kontrollzellen einhergeht. Darüber hinaus wurden andere zentrosomale Proteine wie γ-Tubulin und CEP250 untersucht. Der Phänotyp von γ-Tubulin unterscheidet sich nicht im Vergleich mit den Kontrollzellen, was auf eine vorgelagerte Funktion hindeutet. Hingegen war CEP250 in ALMS1-defizienten Zellen leicht, aber signifikant reduziert. Diese Ergebnisse ähnelten den zuvor von Knorz et al. beobachteten Ergebnissen [18]. Als Nächstes wurden zusätzliche Zilien und zilienverwandte Marker untersucht, um ihre Expression und Lokalisierung bei ALMS1 Verlust besser zu verstehen. Während einige Marker, wie z. B. PCM1, unverändert blieben, zeigten andere, wie z. B. RPGR, ein komprimiertes Erscheinungsbild. Weitere Analysen und Forschungsarbeiten sind erforderlich, um die funktionelle Bedeutung und die Implikationen dieser Beobachtungen sowie ihre Bedeutung im Zusammenhang mit der Biologie der Zilien und den krankheitsbezogenen Mechanismen vollständig zu verstehen.

Um einen möglichen ALMS1-abhängigen Mechanismus zu untersuchen, wurde eine Proteinkomplexanalyse durchgeführt. Dazu wurden Tags (sfGFP, RFP-HA) mit Hilfe der CRISPR/Cas9-Methode am C-Terminus des *ALMS1* Gens in HEK293T Zellen eingeführt. Diese endogen markierten ALMS1 Einzelklone wurden anschließend für die affinitäts-basierte Proteinaufreinigung verwendet, um neue ALMS1 Interaktionspartner zu identifizieren. Diese Proteine stehen mit der Funktion des Zytoskeletts, der Regulierung des Zellzyklus, der Stoffwechselfunktion, dem Transport und posttranslationalen Proteinmodifikationen in Verbindung. Eine bemerkenswerte Entdeckung war die Identifizierung des zentrosomalen Proteins 70 kDa (CEP70) als ein signifikanter Interaktor von ALMS1. Weitere Untersuchungen, einschließlich der Affinitätsaufreinigung unter Verwendung von nativem CEP70, sowie von CEP70 Fragmenten (Deletionsanalyse) wurden durchgeführt. Interessanterweise ergab die Analyse von Proteinkomplexen unter anderem, dass ALMS1 auch ein Interaktor von CEP70 ist, was auf eine starke Wechselwirkung hindeutet. Außerdem assoziiert ALMS1 ebenso wie UBR4, ATG3, PLAA, UACA, TP53K und BAX mit der CEP70-Region, die aus TPR-Domäne und dem CT-Ende besteht. Ein möglicher Doppel-KO aus CEP70 und ALMS1 konnte aufgrund eines erhöhten Zellverlusts nicht generiert werden. Die Hemmung der Genexpression von CEP70 (CEP70 KD), mittels RNA Interferenz, in Wildtypzellen (wt) zeigte nicht nur eine reduzierte ALMS1 Lokalisierung am BB, was auf eine vorgelagerte Funktion von CEP70 hindeutet, sondern auch einen erhöhten Zellverlust. Die mRNA Analyse von *BAX/BCL2* wies auf einen

apoptotischen Prozess in CEP70 KD behandelten wt Zellen hin, während die Hemmung von CEP70 in ALMS1 KO Zellen zu einer Verschiebung in Richtung Zellüberleben im Vergleich zur Kontrolle führte.

Eine abschließende Untersuchung von ALMS1 wurde in einem retinaspezifischen Kontext durchgeführt. Retinas von Schweinen und endogen markierten ALMS1-RFP-HA Zellen wurden für einen Retina-Pull-Down mit einem angepassten SDS-Protokoll verwendet. Dabei wurden zusätzliche potenzielle Interaktionspartner gefunden, die an Signalwegen, Apoptose und Lipidstoffwechselprozessen, der Entwicklung anatomischer Strukturen, der Regulierung des Zellzyklus und der Organisation des Ziliums beteiligt sind. In Zukunft ist eine Validierung dieser potenziellen Interaktionspartner erforderlich, um die Funktion von ALMS1 genau zu bestimmen.

Insgesamt wirft diese Thesis neues Licht auf die vielfältigen Funktionen von ALMS1 in verschiedenen zellulären Prozessen. Sie zeigt, dass ALMS1 an der Regulierung der zellulären Proliferation beteiligt ist, und hebt die Rolle beim Aufbau und der Erhaltung von Zilien hervor, sowie Auswirkungen auf deren Funktionalität. Außerdem wird die Beteiligung von *ALMS1* und *CEP70* an mRNA-vermittelten Zelltodprozessen vorgeschlagen, wobei CEP70 *upstream* von ALMS1 liegt. Es sind jedoch weitere Untersuchungen notwendig, um die zugrundeliegenden komplexen zellulären und ziliären Signalwege aufzuklären. Die Ergebnisse dieser Studie bieten wertvolle Einblicke in die potenziellen Funktionen von ALMS1 und bilden eine solide Grundlage für künftige Forschungsarbeiten, einschließlich Untersuchungen mit patienteneigenen Zellen, um die Komplexität des Alström-Syndroms besser zu verstehen.

3 Introduction

3.1 Cilia

Cilia are small, elongated antenna-like organelles presented on nearly every eukaryotic cell in the human body [5]. They were first described as “thin feet or little legs” on protozoa by Anthony van Leeuwenhoek in 1675 [19]. The eponym of “cilia” was introduced by Otto Muller in 1786 after the Latin word for eyelid or eyelashes [19]. But it was not until the 19th century that the difference between motile and non-motile cilia was first identified and described. However, early studies concentrated rather on motile cilia and their resemblances to eukaryotic flagella than on non-motile cilia, a structure that was discerned as a rudimentary cellular structure. In the last 20 years, immotile cilia have gained more and more interest, and importance due to their involvement in essential cellular signaling and developmental pathways [19]. Both types of cilia are crucial for human health, ensuring various processes, such as signaling, transportation and photo-, chemo-, mechanosensation [1,7,20] (Wörz unpublished Master thesis, 2018 [21]).

3.1.1 Primary and secondary cilia

Cilia are specialized, evolutionarily conserved structures, that include mainly two types of cilia, the primary (non-motile, immotile) and secondary (motile) cilia (Figure 1). Secondary cilia can be found exemplarily in spermatozoa flagella to drive sperm motility and in the respiratory tract, where their beating behavior exert mucus clearance. They are composed of a central pair of microtubules and a doublet of nine microtubules (9+2), accompanied by auxiliary inner as well as outer dynein arms and radial spokes (Figure 1). In contrast to secondary cilia, primary cilia are static and exhibit a microtubule doublet arrangement, lacking the central pair of singlets (9+0) (Figure 1). They are mainly involved in sensory functions or cellular signaling and can be found inter alia as a specialized, light sensitive structure in photoreceptors in the retina of mammalian eyes [9–11,22,23] (Wörz unpublished Master thesis, 2018 [21]).

3.1.2 Structure of primary cilia

A cilium is composed from distal to proximal of, a ciliary tip, microtubule-based axoneme ensheathed by a ciliary membrane, a ciliary pocket, a transition zone (TZ) and a basal body (BB) (Figure 1) [7,8] (Wörz unpublished Master thesis, 2018 [21]).

The ciliary tip, exposed to the extracellular environment, exhibits an important function in ciliary length control, as well as functioning as a scaffold for signaling [24–26]. Some proteins like Gli transcription factors, that are involved in the Sonic hedgehog signaling pathway accumulate at the ciliary tip [27,28]. Recent studies also showed the capability of the ciliary tip to perform

exocytosis with unknown fate of ectosomes (small vesicles) [29–31]. These findings could connect exocytosis and signaling pathways, because exocytosis of ectosomes, enriched with activated signaling-related membrane proteins, takes place mostly after signaling activation [29]. Furthermore, a similar process was observed by Young in 1967 in photoreceptor cells. Small vesicles from elder discs from the tip are released for recycling by phagocytosis (photoreceptor disc shedding) [32,33] (Wörz unpublished Master thesis, 2018 [21]).

The axoneme is the central microtubule backbone composed of alpha and beta tubulin, while only alpha tubulin is acetylated [34]. It has a length that ranges from 1 to 9 µm depending on the cell type [35]. The axoneme ensures ciliary stability, growth, length, and transportation of essential cargos along the cilium [36–39]. Since cilia lack the ability for biosynthesis, cilia assembly and maintenance are dependent and regulated inter alia by the intraflagellar transport (IFT). The IFT machinery carries essential cargos in a motor-protein driven bidirectional manner along the cilium. There are two multiprotein complexes of IFTs, the IFT-A and IFT-B. The IFT-A complex, comprises of six subunits, is crucial for the retrograde transport from the ciliary tip towards the base, which is mediated by the motor protein dynein. The IFT-B, a complex of 16 subunits, is responsible for the kinesin dependent anterograde transport of cargo from the base to the ciliary tip [1,36,37]. The ciliary membrane is an extension from the cellular plasma membrane exhibiting various signaling receptors, for example G-protein coupled receptors, and undergoes remodeling during ciliogenesis. It is crucial for detecting, selecting and transducing extracellular signals to ensure communication with the surroundings e.g. for cell migration, development and differentiation [40–43] (Wörz unpublished Master thesis, 2018 [21]).

The ciliary membrane is connected via Y-shaped linkers to the proximal region of the ciliary membrane, also called the transition zone (TZ). The TZ is known as the ciliary gate, controlling entry and exit of ciliary proteins by inhibiting free diffusion and therefore selects proteins for transport along the cilium [44] (Wörz unpublished Master thesis, 2018 [21]).

The BB, in mitotic cells called centrosome, is a modified centriole (mother centriole), that forms the basis of a protruding cilium [45]. The BB, approximately 500 x 200 nm in size, is made of triplet microtubule arrangements, which are extending and finally become the ciliary axoneme [45–47]. The basal body fuses with the plasma membrane and is stabilized by transition fibers (distal and/or subdistal appendages (DAP and SAP)) by anchoring it to the poorly defined ciliary pocket [11,48]. The ciliary pocket at the lower part of a cilium connects the ciliary membrane with the plasma membrane. It is a highly dynamic area where endocytosis of ciliary receptors

(recycling) and the fusion of membrane protein, containing ciliary vesicles, occurs [49,50] (Wörz unpublished Master thesis, 2018 [21]).

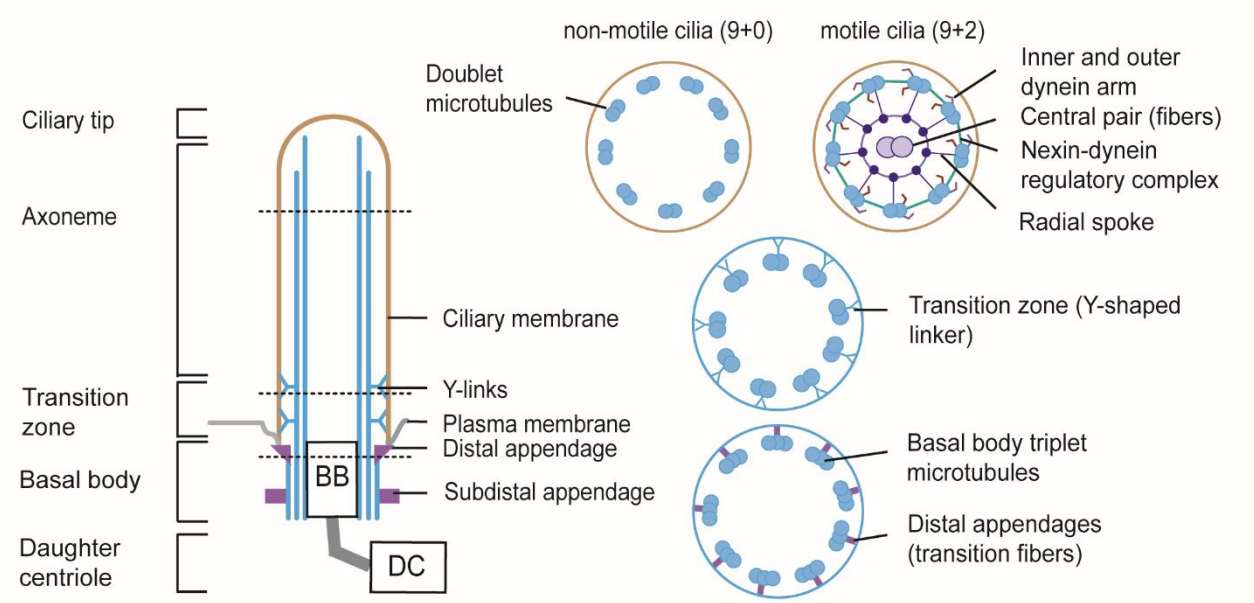

Figure 1 Structure of primary and secondary cilia
An overview of the motile (primary) and non-motile (secondary) ciliary structure. A simplified cilium is depicted on the left side, that is composed of a ciliary tip, an axoneme surrounded by a ciliary membrane, a transition zone (TZ), and a basal body (BB). Transversal planes (dashed lines) through the cilium show on the right site the different structures of non-motile, motile cilia, the transition zone, and the basal body. Non-motile cilia exhibit a 9+0 microtubule arrangement, while motile cilia show a 9+2 microtubule structure with inner and outer dynein arms, radial spokes, and nexin-dynein regulatory complexes. The double microtubule structure of the TZ is connected via Y-links with the ciliary membrane.
The BB, a modified centriole, exhibits a triple microtubule structure that is linked via transition fibers to the ciliary membrane. Reproduced and modified after [9,21,51], Wörz unpublished Master thesis, 2018 [21].

3.1.2.1 Specialized cilium: Connecting cilium in mammalian photoreceptors

The human retina, located in the fundus of the eye, consists of various layers including different cell types. The retinal nerve layer comprises of five classes of neurons, including photoreceptor cells, horizontal, bipolar, amacrine and ganglion cells [52]. Furthermore, the retina includes the retinal pigment epithelium (RPE) and three types of glial cells [52–55]. Photoreceptors are present in the retina's outer nuclear layer of the mammalian eye. They are responsible for vision, by recognizing, absorbing, and transforming signals (photons) into electrical stimuli and transmitting them through the inner retinal neuron and the optic nerve to the primary visual cortex in the brain [56,57], (Wörz unpublished Master thesis, 2018 [21]). There are two types of photoreceptors. The rods, that enable peripheral vision despite low light conditions and the cone cells (cones) for the facilitation of color vision [56,58,59]. They co-exist in the retina and share a very similar structure, except of their appearance. While rods present a rod-shaped structure with elongated outer segments, the cones have a truncated conical shape. However, both cell types exhibit a synaptic zone, a nucleus, an inner and an outer segment [60,61]. The inner and

the outer segment are connected through a modified and specialized connecting cilium. The function of the connecting cilium with its transition zone (TZ) is to connect the metabolic machinery from the inner segment with the light-sensitive outer segment. Therefore, the connecting cilium is crucial for the phototransduction cascade as well as the transport of essential proteins (e.g., rhodopsin) and lipids from the inner to the outer segments [48,62] (Wörz unpublished Master thesis, 2018 [21]).

Photoreceptors and their connecting cilium are highly complex, which makes them susceptible to mutations in ciliary and cilia-related genes leading to retinal degeneration [54] (Wörz unpublished Master thesis, 2018 [21]).

3.1.3 Centrosomal structure and function

Centrosomes, acknowledged as the microtubule organization center (MTOC) are essential for cell signaling/transportation, cell division and motility among species [63]. The centrosome is typically 200 nm in diameter and has a length of approximately 500 nm (0.4-1 µm) [46,47]. It consists of microtubule-based centrioles (mother and a daughter centriole), that have a barrel-shaped structure with a nine-fold symmetry [64]. The difference between the two centrioles lies in their maturation state, where the mother centriole is exclusively defined as mature and has appendages at its distal end to achieve centrosome-related functions, such as microtubule anchoring, plasma membrane docking and cilia formation (Figure 2) [23,65,66]. The daughter centriole lacks these appendages. The proximal end of the mother centriole is thought to be important for the formation of a cartwheel, that is needed for the assembly of the daughter centriole [67]. The centrosome is embedded in an electron-dense proteinaceous matrix (PCM), which is important for microtubule nucleation (Figure 2) [46]. Microtubules (MT) consists of α-β heterodimers, and undergo dynamic processes, that are highly geometrical defined. There are many centrosome-associated proteins and factors, which serve as linker proteins to facilitate the dynamic assembly and disassembly of microtubules. One PCM protein is γ-tubulin, which belongs to the tubulin super-family. It is the essential basis for the MT nucleating molecular machinery called the γ-Tubulin Ring Complex (γ-TURC). It consists of a multi-subunit protein complex, a γ-Tubulin Small Complex (γ-TUSC) and a variety of γ-Tubulin Complex Proteins (GCPs). The recruitment of γ-TURC to different MTOCs happens due to γ-TURC -tethering proteins [46].

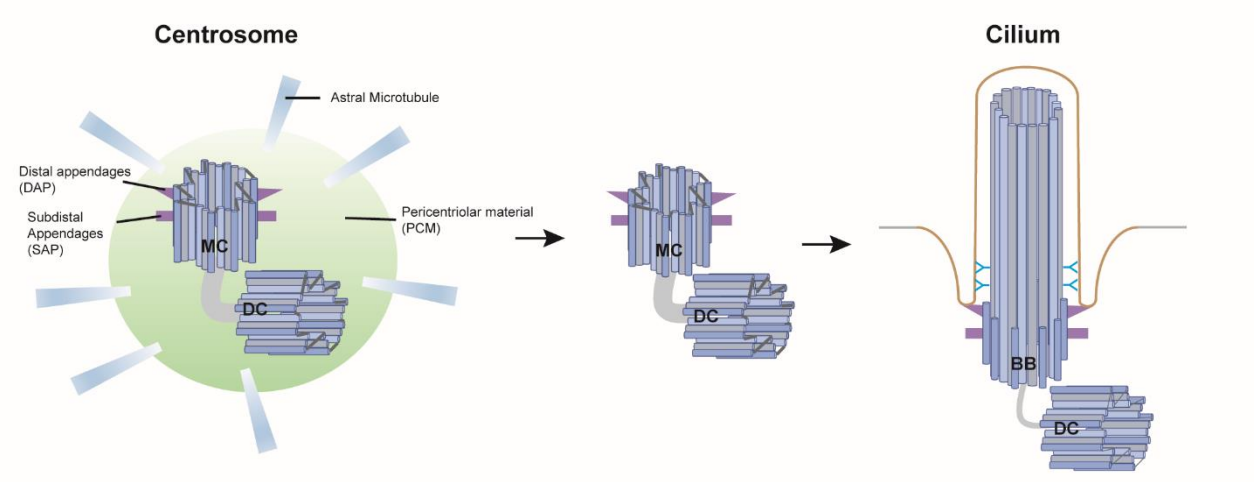

Figure 2 BB derives from the centrosome
The centrosome is a cellular structure composed of a mother and a daughter centriole surrounded by pericentriolar material (PCM). A centrosome is made of a nine-triplet microtubule structure, functioning as a microtubule organizing center (MTOC). During the resting phase (G0) of cells, the centrosome assumes the name basal body, which is important for cilia formation. Figure was reproduced and modified after [46] and Wörz unpublished Master thesis, 2018 [21].

3.1.3.1 Family of centrosomal proteins

Centrosomal proteins (CEP) associate with centrosomes and are important for centriole biogenesis and cell cycle progression control. To date, the centrosomal proteins belong to a family that consists of 31 proteins. They influence microtubules in terms of nucleation, posttranslational modifications, and de-/ polymerization. Furthermore, CEPs alter microtubule-associated proteins in their activity and localization [68,69].

3.1.3.2 Centrosomal protein 70 kDa (CEP70)

One member of the CEP family is the Centrosomal protein 70 kDa (CEP70), that was first described in 2003, where it was found in a proteomic study of human centrosome [70]. *CEP70* gene is localized on chromosome 3, exhibits 18 exons and encodes a protein of 597 amino acids (aa) that is associated with the centrosome and basal body of cilia [71–73]. The protein itself has two coiled coil domains in the C-terminal (CT) region, a TPR near the N-terminus (NT) and is conserved among species [72,74]. CEP70 is rarely studied in comparison to other CEPs [69], but it was shown to play an important role in microtubule stabilization and acetylation by interacting with Histone deacetylase 6 (HDAC6) [70]. CEP70 interacts through its coiled coil domains with γ-tubulin at the centrosome and regulates mitotic spindle assembly [74]. It was also shown that the γ-tubulin and CEP70 interaction is mediated through the deubiquitinase activity harboring tumor suppressor protein cylindromatosis (CYLD). Thereby, CYLD deubiquitinates CEP70, which promotes the protein-protein interaction and its localization at the centrosome [75]. Moreover, Wilkinson et al demonstrated that a depletion of CEP70 contributes

to shorter cilia with no obvious basal body defect in zebrafish embryos [72]. Despite the published data, the exact molecular function of the CEP70 protein needs to be elucidated in mammalian cells.

3.1.4 Primary ciliogenesis

The formation or assembly of cilia is termed ciliogenesis, which is tightly associated to the cell cycle, cell confluency and signaling activation [43,45,76]. Initially, it was thought, that cilia assembly occurs mainly in G1 or in quiescent cell (G0) phases and the cilium gets degraded (cilia disassembly) before cell cycle re-entry. However, recent research suggests ciliogenesis events throughout the cell cycle [77]. Despite the published data, the exact molecular mechanism of cilia formation is still elusive. Nevertheless, an extracellular and an intracellular pathway for ciliogenesis are postulated [78] (Figure 3). In the extracellular pathway, the mature centriole migrates straight towards the plasma membrane, where it attaches with its distal appendages. The intracellular pathway includes the formation of ciliary vesicles and a nascent cilium before docking at the plasma membrane [78] (Wörz unpublished Master thesis, 2018 [21]).

The length of primary cilia can vary between 1 µm to 10 µm dependent on cell type, microtubule dynamics (de-/polymerization), and other mechanism, that are described above [43,79,80] (Wörz unpublished Master thesis, 2018 [21]).

3.1.4.1 The basal body assembly drives cilia formation

The initiation of cilia assembly depends on the binding of DAPs to the plasma membrane. The ciliary vesicle formation is orchestrated by RAB GTPases (Rab11-8 cascade) and the IFT20 protein. At first, the C2 domain-containing protein 3 (C2CD3) protein associates with the distal end of the BB and induces the DAP formation. DAP proteins, such as CEP89 and CEP164, are recruited by CEP83. CEP164 plays a relevant function during early cilia assembly by ensuring ciliary vesicle formation and the binding of the BB to the cell surface. Moreover, it is responsible for the recruitment of several proteins, such as the tau tubulin kinase-2 (TTBK2), which leads to a dissociation of the Centriolar coiled-coil protein of 110 kDa (CP110) protein from the BB. The TBBK2 protein is a negative regulator of cilia assembly and by the loss of this protein, ciliogenesis takes place [81]. The anchoring of microtubules is mediated by SAPs. Two important SAPs are cenexin and centriolin, that play an important role in endosomal trafficking and ciliogenesis. Furthermore, SAP proteins interact with the Bardet-Biedl syndrome 4 protein (BBS4), a member of the Bardet-Biedl syndrome protein complex (BBSome). The BBSome mediates the anchoring of microtubules [81]. An inaccurate function of the BBSome is linked to a

rare disease called the Bardet Biedl syndrome, which shows the necessity of proper functioning SAPs in ciliogenesis.

Another necessity for cilia assembly, is the pericentriolar material (PCM), that are electron-dense granules surrounding pericentriolar satellites. These includes many proteins, such as CEP290 and the integral centriolar satellite protein PCM1, which recruit Rab8 to the basal body resulting in cilia development [81,82] (Wörz unpublished Master thesis, 2018 [21]).

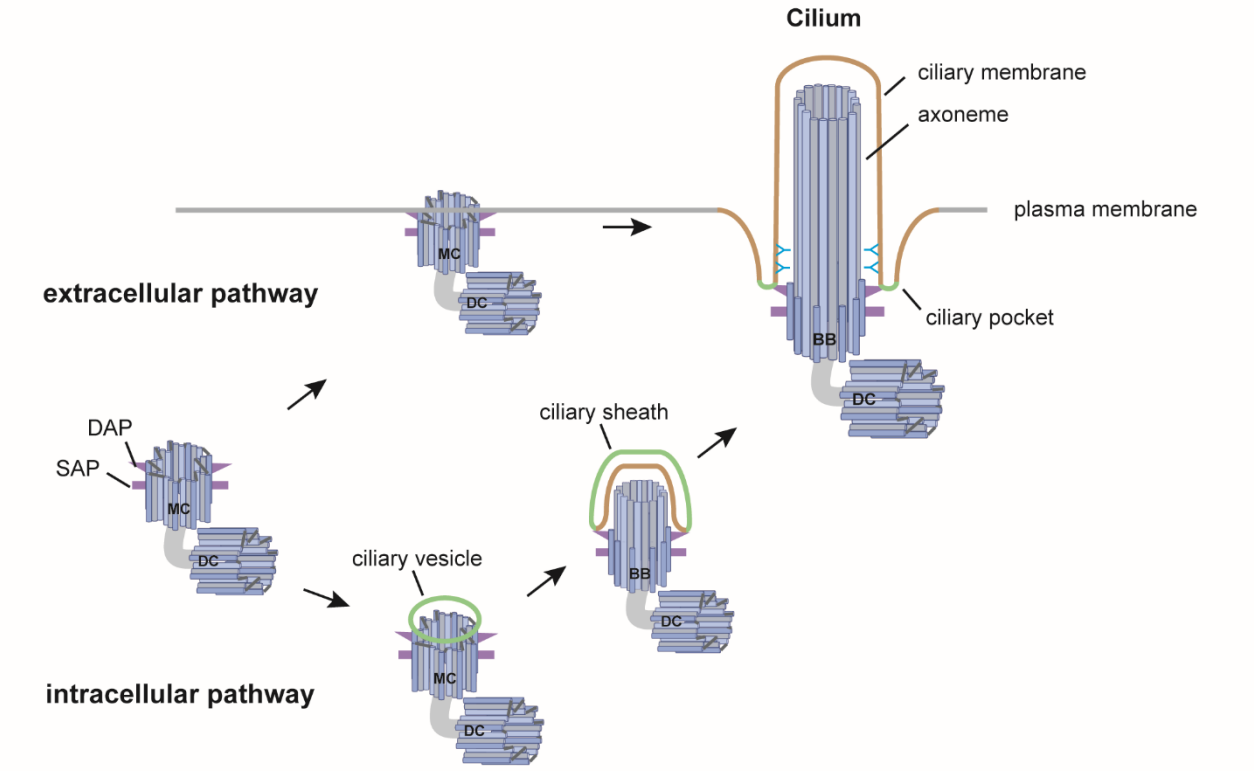

Figure 3 Initiation of ciliogenesis
A simplified representation of the extra- and intracellular pathway of initiating cilia formation based on basal body formation. In the extracellular pathway the mother centriole migrates and associates with its distal appendages (DAP) to the plasma membrane, which initiates the formation of a mature cilium. The intracellular pathway, ciliary vesicles assembly occurs at the distal appendages of the mother centriole, leading to axoneme growth and ciliary membrane formation (ciliary sheath). Finally, the premature cilium fuses with the plasma membrane, where cilia elongation takes place. Reproduced and modified after [83,84].

3.1.5 Signaling function of primary cilia

Primary cilia are also known to mediate different signaling pathways, such as Sonic Hedgehog (Shh, Hh) [85,86], transforming growth factor beta (TGF-β) [87–89], Hippo signaling [90,91], Wnt signaling [92], mammalian target of rapamycin (mTOR) [91,93], G protein coupled receptor (GPCR) and platelet-derived growth factor receptor alpha (PDGFR-α) among others [94,95]. These signaling pathways are important inter alia for development, homeostasis, energy metabolism, cell proliferation, autophagy, and protein synthesis [41,96–98].

Exemplarily, the PDGFR pathway is important for cell survival, growth regulation, cell proliferation, cell migration, embryonic development and maintaining tissue homeostasis [95,99]. PDGFR belongs to the receptor tyrosine kinases (RTKs), that regulates signaling events through primary cilia. RTKs comprise the most extensive group of enzyme-linked receptors with over 50 members, including inter alia insulin receptor (IR) and insulin like growth factor receptor (IGFIR) [95]. They also engage in cross-talk with other receptor systems and may utilize G proteins, GRKs, and β-arrestins to regulate diverse cellular responses [95], highlighting the dynamic processes mediated through signaling pathways.

There are two isoforms of PDGFR, PDGFR-α and PDGFR-β, that function in hetero- and homodimers facilitating cellular and tissue specific processes, with PDGFR-α primarily appearing in the cilium [22,100,101]. Activation of PDGFR-α occurs through phosphorylation induced by the ligand PDGFR-AA, followed by its localization to the ciliary membrane. Once activated PDGFR-α triggers downstream signaling pathways like MEK1/ERK1/2 and PI3-Akt-mTOR, leading to cell-cycle re-entry, cytoskeletal development, cell migration, differentiation and tissue homeostasis [99,102]. Defects in the PDGFR signaling pathway are linked to kidney and liver diseases, fibrosis and tumorigenesis [99,103].

3.2 Ciliary dysfunction leads to diseases: Ciliopathies

Ciliary defects, commonly known as ciliopathies, can result in photoreceptor development defects, in disturbed signal transduction, as well as retinal degeneration [104,105]. Many proteins linked to ciliopathies are involved in ciliary trafficking and cilia-related processes. Upon mutation, these proteins lead to a variety of syndromic diseases [9]. To date, there are up to 35 ciliopathies known, that share similar clinical features including obesity, type 2 diabetes and cone-rod dystrophy [9]. The prevalence of all ciliopathies is estimated to affect 1:1000 individuals worldwide [106,107]. One of these ciliopathies is the Alström Syndrome (Wörz unpublished Master thesis, 2018 [21]).

3.2.1 The Alström syndrome

The Alström Syndrome (AS, ALMS, OMIM #203800) is an ultra-rare disorder, that affect 1 to 9 out of 1 million individuals [12,13]. This disease is autosomal-recessively inherited, which means that two heterozygous carriers (one allele from the mother, one allele from the father) have a chance of 25% to conceive a child suffering from ALMS. People who are heterozygous carriers of this disease, exhibit no syndromic manifestations. This disease was first described in a Scandinavian medical journal in 1959 by Carl-Henry Alström [15,108]. He examined three children that exhibit a similar phenotype to the Bardet-Biedl Syndrome (BBS, OMIM #209900).

Both syndromes are also named “obesity ciliopathies”, and share similar clinical features such as obesity, retinal degeneration, and type 2 diabetes [107], but also show clinical differences (Table 1) [15,109]. Polydactyly was, to my knowledge, only observed in BBS patients. ALMS is a multisystemic disorder, that includes defects in numerous organs of the human body. Alström syndrome patients suffer from cone-rod dystrophy, insulin resistance (Type 2 Diabetes), childhood obesity (truncal obesity), sensorineural hearing impairment/loss and dilated cardiomyopathy among others. Furthermore, not every ALMS patient will develop the same symptoms, so it is a highly heterogeneous disease. The disease presents in infancy, and first symptoms to appear are nystagmus, light sensitivity, and truncal obesity, followed by complete blindness by school age. Until now, there are approximately 950 reported cases worldwide, and no applicable therapeutic approach is available [12,16] (Wörz unpublished Master thesis, 2018 [21]).

Table 1 Comparison between two obesity ciliopathies: Alström syndrome and Bardet-Biedl syndrome
Compressed overview of prevailing phenotypical features presented in patients suffering from Alström and Bardet-Biedl syndrome [15,110].

Disease features	**Alström syndrome**	**Bardet-Biedl syndrome**
Inheritance	Autosomal - recessive	Autosomal - recessive
Vision impairment	Yes, cone-rod dystrophy (infancy)	Yes, Retinal dystrophy (age ~7)
Hearing impairment/loss	90%	Usually not
Mental retardation	Normal mental development, sometimes delayed	Yes, cognitive impairment (50 - 90 %)
Extremities	Short, stubby fingers, wide flat feet	Poly-/syndactyly (79%)
Endocrine impairment	Obese, Type 2 Diabetes (89%)	Obese, Type 2 Diabetes (5-15%)
Heart involvement	Yes, dilated cardiomyopathy	Very rare

3.2.2 The Alström syndrome gene and protein function

The *ALMS1* gene is located on the short arm of chromosome 2 at position 13 (2p13). It exhibits 23 exons (12928 nucleotides) and codes for an approximately 0.5 MDa protein with 4169 amino acids (aa). The *ALMS1* gene has three mutational hotspots: exon 8, exon 10 and exon 16. Until now, over 300 mutations have been reported, with 49% percent occur in exon 8, but this high percentage could be due to this exon’s size (6.1 kDa). The vast majority are nonsense or frameshift mutations, that lead to a truncated protein [17]. It is not clear yet, how stable the truncated mRNA is and if it is translated into protein or degraded due to nonsense-mediated

decay. The ubiquitously expressed ALMS1 protein is not well conserved among species (except the short ALMS1 motif) and has a low expression level [16,111]. ALMS1 has several domains with unknown function: a large tandem repeat domain (TRP), three coiled-coil domains and a ~130 residue at the C-terminus (CT) called the ALMS1 motif [17]. The latter was shown to interact with alpha-actinin and NKCC2 [112]. Furthermore, Knorz et al showed that two regions of the ALMS1 protein are important for centrosomal localization. These regions include a small internal fragment (residue 2261-2602) and the CT (residue 3176-4169) containing the ALMS1 motif. The ALMS1 motif sequence shares similarities to the centrosomal protein CEP295/KIAA1731, which is able to associates with the centrosome and might be involved in microtubule organization and centriole biogenesis [18,113,114] (Figure 4) (Wörz unpublished Master thesis, 2018 [21]).

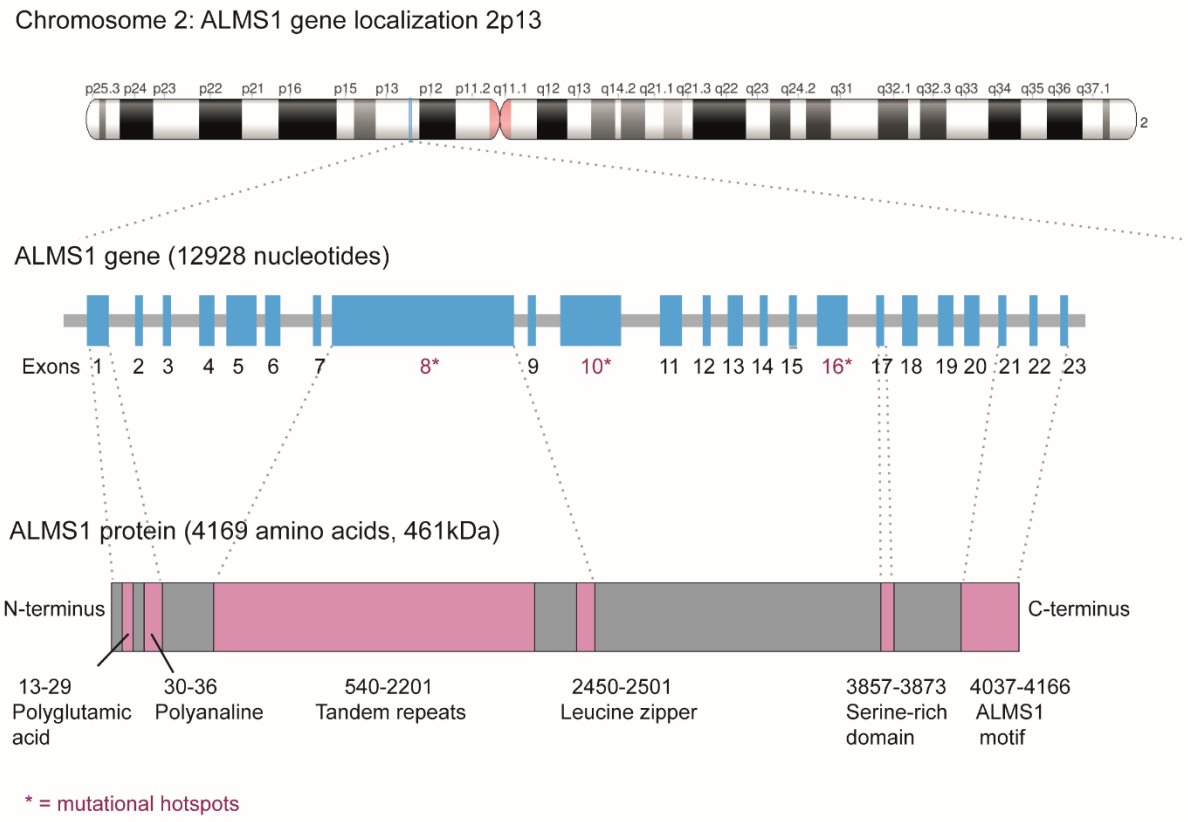

Figure 4 Overview of *ALMS1* gene localization and its protein
The *ALMS1* gene is located on chromosome 2 (top panel), consisting of 23 exons (light blue) with three mutational hotspots in exon 8, 10 and 16 (middle panel, marked in red). It codes for a 461 kDa protein, that shows various functional domains with unknown functions. A large tandem repeat domain (TPR), three short predicted coiled-coil domains, and an approximately 130 residues at the C-terminus called the ALMS1 motif, are depicted in magenta. This figure was reproduced and modified after [17,115], Wörz unpublished Master thesis, 2018 [21].

The ALMS1 protein localizes microtubule-independent at the proximal end of mother and daughter centriole, as well as the BB of a cilium and associates with γ-tubulin. ALMS1 deficient cells, e.g. fibroblasts, exhibit a normal appearing morphology of cilia and microtubule

cytoskeleton, which suggests a more functional role of ALMS1 [116]. The ALMS1 protein is suggested to be essential for cilia maintenance and function, cell cycle control, endosomal trafficking, homeostasis of metabolism and differentiation of cells [16,17]. The role of the ALMS1 protein in ciliogenesis still needs to be elucidated. To date, some studies propose an ALMS1 involvement in primary cilia formation and centrosomal cohesion [16,18,66,117], while others indicate an indirect role of ALMS1 in cilia assembly and disassembly [118,119]. ALMS1 was also postulated to be involved in ciliary and cilia-related signaling. María Álvarez-Satta *et al.* showed an ALMS1 involvement in the transforming growth factor beta/bone morphogenetic protein (TGF-beta/BMP) signaling pathway [87]. This pathway is essential for cell proliferation, differentiation and cell survival mechanism and is also associated with other signaling pathways, such as Sonic Hedgehog (Shh), Wnt, Hippo, Notch, mitogen-activated protein kinase (MAPK), or phosphoinositide 3-kinase (PI3K)-Akt. In this study, they used knock-down ALMS1 hTERT-RPE1 cells, that exhibit longer and bended cilia with an impaired TGF-beta/BMP signaling due to a reduced SMAD2/3 activation in TGFβ-1 stimulated cells [87]. Bea-Mascato *et al.* also showed that a loss of ALMS1 in HeLa and hTERT-BJ-5ta leads to an impaired TGFβ signaling pathway, that facilitates a decrease in cell migration and adhesion of cells [88]. The involvement of ALMS1 in Shh is debated due to the lack of polydactyly in ALMS patients. In spite of the published data, the molecular function of ALMS1 is still not fully understood (Wörz unpublished Master thesis, 2018 [21]).

Presently, there is no applicable therapeutic approach available for these patients. As a first potential treatment for nonsense-mediated ciliopathies, Eintracht *et al.* investigated BBS and AS patient derived fibroblasts with nonsense mutations while treating them with translational readthrough inducing drugs (TRIDS). They showed that two TRIDS can restore ciliary function by inducing IFT88 expression and correct localization of SSTR3 in patient-derived fibroblasts [107].

4 Aim of the PhD study

The Alström syndrome, an autosomal recessive monogenic disorder, exhibits a low prevalence ranging from 1 to 9 cases per one million individuals [12,13]. There are over 300 mutations identified so far, presenting a diverse spectrum of phenotypic features that already manifest during infancy. These manifestations include various clinical features such as blindness due to retinal degeneration resulting in visual impairment, Type 2 Diabetes, and childhood obesity, among others [14]. The *ALMS1* gene, located on chromosome two, encodes a large protein of 461 kilodaltons (kDa), which poses challenges for functional investigation [16]. Notably, it has three mutational hotspots in exon 8, 10 and 16 with most mutations being missense or frameshift mutations, suggested to result in truncated or absent protein [17].
The ALMS1 protein is known for its association with both the centrosome and the basal body of cilia. Its function is postulated within multiple cellular processes, including metabolism, cell proliferation and signaling pathways [16,17]. However, despite the published data, the exact molecular function of ALMS1 remains enigmatic, emphasizing the need for further investigations to unravel and understand the ALMS1 (patho-) mechanism in the future.

This PhD study aimed to gain a deeper understanding of the molecular function of the ALMS1 protein and its influence on the severity of the associated disorder. The main hypothesis focused on the protein interactions of ALMS1 enabling a functional basal body. This well-regulated sub complex is crucial for transport of proteins and other particles to the cilium, necessary for maintaining correct ciliary structure and ensuring proper ciliary function. This includes its sensory capacities as well as the transduction of signals and their impact on cell cycle. To investigate this hypothesis and to better understand the role of ALMS1 in cilia and cilia-related processes, phenotypical and protein complex analysis was combined to link ALMS1 interactions to functional data and exclude coincidences. This may help to identify the underlying (patho-) mechanism of ALMS1 in Alström disease. To achieve this overall objective, the following aims have been defined in detail.

The first aim of this study is to investigate the molecular function of ALMS1 in cilia biology and to gain initial insights into its underlying disease-causing mechanism. For functional analysis, CRISPR/Cas9 mediated ALMS1 knock-outs (KO) will be generated in human retinal epithelium cell lines (hTERT-RPE1). In literature, the ciliary length is highly discussed in ALMS1 mutant models and either suggest a direct or an indirect function of ALMS1 in cilia formation. Therefore, the ciliary length and ciliation will be assessed in ALMS1 KO cells. Additionally, structural protein

localization, such as cilia and cilia-related marker, will be analyzed, which will provide novel insight into ALMS1 function. Moreover, the influence of native and mutant ALMS1 on cellular behavior, such as viability and proliferation rate, will be observed. This may help to gain further knowledge on the molecular function of ALMS1 and how mutation may cause or influence the severity of the Alström syndrome.

The second aim is to identify interactors of ALMS1 to draw conclusions on potential functions of ALMS1. Since, proteins usually fulfill their biological role in complexes rather than isolated, investigating, and validating protein networks can elucidate their biological function as well as their disease-related implications. To achieve this, the CRISPR/Cas9 method will be employed to insert specific sequences (e.g. coding for peptide and fluorescence tags) into the *ALMS1* gene of HEK293T cells, which will be further utilized for protein complex analysis. Validation of the gained ALMS1 network will be translated into functional analysis to examine e.g. localization of potential interaction partners in native and mutant ALMS1 hTERT-RPE1 cells. Furthermore, epistasis experiments will be conducted to understand the functional interplay of novel interactors and ALMS1. This interactome study will reveal novel and potential interactors of ALMS1, which will shed light on its function in cilia and cilia-related processes.

The third aim will be to identify tissue specific interaction partners of ALMS1 by using previously generated endogenously tagged ALMS1 for a retina-specific pull down. Despite the fact, that human ALMS1 is not well conserved among species, it shows partial sequence similarities in porcine ALMS1. This approach will present novel retina-specific interactors of ALMS1, which will enable definition of tissue specific candidates relevant for understanding loss of vision in ALMS patients in the future.

These findings will give new insights and hint towards an underlying mechanism leading to Alström disease, which will be critical for developing therapeutic strategies with specific treatments. Furthermore, this study will show, that the discovery of CRISPR/Cas9 as well as the highly sensitive mass spectrometry method laid the cornerstone to study larger proteins like ALMS1.

5 Materials

5.1 Consumables

Material	Supplier
96 Well Lightcycler Plate	Sarstedt AG & Co. KG
Adhesive qPCR Seal	Sarstedt, Inc
BD 3 ml Syringe Luer -Lok™ Tip	Becton Dickinson
BD Microlance™ 3	Becton Dickinson
Cell Chip™	Tecan Group AG
Cell Scraper	Sarstedt AG & Co. KG
Colour coded insert, mixed	Sarstedt AG & Co. KG
Cover Glasses Ø12 mm	VWR
Cultube sterile culture tubes Tube with cap, polystyrene, 25/tray 17 mm x 95mm H.	Simport, Canada
Disposal Bag	Carl Roth GmbH & Co.KG
Eppendorf CombiTips	Eppendorf AG
Falcon 15ml Polypropylene Round-Bottom Tube	Corning
Filter tips 10, 20, 100, 200, 1000	Biozym Scientific GmbH, nerbe plus GmbH & Co. KG
Gel Loading Tips 0.5-200 µl, round	VWR
Gloves Nitrile XS, S	ABENA
Hybond-P PVDF Transfer membrane	GE Healthcare
Microscope slides 26 x76 mm	R. Langenbrinck GmbH
Microscope slides 26 x76mm	R. Langenbrinck GmbH
Multiply® -µStrip 8-strip	Sarstedt AG & KO. KG
Multiply®-Pro cup 0.2 ml	Sarstedt AG & Co. KG
Nitrile /Powder-Free Medical Examination Gloves XS	Abena
NuPAGE™ 4-12% Bis Tris Gel	Thermo Scientific, USA
NU-PAGE™ 4-12% Bis-Tris Gel	Invitrogen by Thermo Scientific
Parafilm M	Bemis Company, Inc.
Pasteur Capillary Pipettes 230 mm	Wilhelm Ulbrich GdbR

Peha-soft nitrile Guard XS	Paul Hartmann AG
Pipet tips with microcapillary for loading gels 1-200 µl	VWR
PP Cryo Tubes 1.8 ml	NUNC
PP insert with Bottom Spring 0.20mL	Supleco
PP tubes 15 ml, 50 ml	Sarstedt AG & Co. KG
Precision Wipes Kimtech Science	Kimberly Clark® Professional
Receiver Columns 20 µm	Macherey-Nagel GmbH & Co. KG
Safe-Lock Tubes 0.5 ml, 1.5 ml, 2 ml	Eppendorf AG
Serological pipettes 2 ml, 5 ml, 10 ml, 25 ml, 50 ml	Corning
StageTips 200µl pipette tip	Thermo Scientific
Tissue dishes 10 cm, 14 cm	Thermo Scientific
VWR® Tissue Culture Plates 96, 48, 24, 12, 6 well	VWR

5.2 Chemicals

Material	**Supplier**
0.05 % Trypsin-EDTA	Thermo Fisher Scientific
1,4-Dithiothreitol (DTT)	Merck KGaA
10x Dream Taq Buffer	Thermo Scientific
2-Iodacetamide (IAA)	Merck KGaA
5x Phusion GC buffer	Thermo Scientific
5x Phusion HF buffer	Thermo Scientific
6x DNA Loading Dye	Thermo Fisher Scientific
Accustain® Crystal Violet Solution (2.3% w/v	Sigma Aldrich
Acetonitrile (Chromasolve® LC-MS)	Sigma-Aldrich
Acrylamide/Bis Solution 37.5:1 (30% w/v, 2.6% C)	Serva
Adenosine 5’-triphosphate	New England BioLabs® Inc
Agar-Agar	Carl-Roth GmbH & Co. KG
Agarose	Lonza Group Ag
Albumin Fractio V	Carl-Roth GmbH & Co.KG
Ammonium bicarbonate (ABC)	Sigma-Aldrich

Ammonium Persulfate (APS, w/v = 10%, electr.grade, 98%)	Sigma Aldrich
Ampicillin sodium salt (100 mg/ml)	Carl-Roth GmbH & Co. KG
Anti-FLAG® M2 Agarose A2220-5ml	Sigma- Aldrich
ATP 10 mM	Fermentas GmbH
BIO-RAD PROTEIN ASSAY (5x Bradford Concentration)	Bio-Rad Laboratories GmbH
BIO-RAD PROTEIN ASSAY (5x)	BioRad
Bovine Serum Albumin (BSA, 10 mg/ml)	Carl-Roth GmbH & Co. KG
Bromphenol Blue (0.05%, BPB)	Sigma Aldrich
Chloramphenicol 100 mg/ml	Carl-Roth GmbH &Co. KG
Chloroform	Merck KGaA
DAPI	Sigma Aldrich, Thermo Fisher
Deoxynucleotide (dNTP) Solution 10mM	New England BioLabs® Inc
Dimethyl sulfoxide (DMSO)	ApplyChem
DMSO 100%	Thermo Sientific
dNTPS 10 mM (qPCR)	Promega
Dream Taq DNA Polymerase 500U, 5 U/µl	Thermo Scientific
Dream Taq Green Buffer (10x)	Fermentas/ Thermo Fisher Scientific
Ethanol p.a.	VWR
Ethidium bromide	AppliChem GmbH
F-5302 Phusion DNA Polymerase 20 U/µl	Thermo Fisher Scientific
Fast Digest BpiI	Thermo Scientific
FastDigest BbsI	Thermo Scientific
Flag Beads	Sigma-Aldrich
Flag Peptides	Sigma-Aldrich
Fluoromount-G®	SouthernBiotech
Gateway® BP Clonase™ II	Invitrogen by Thermo Scientific
Gateway® LR Clonase™ II	Invitrogen by Thermo Scientific
Gene Ruler 1 kb Plus	Thermo Fisher Scientific
Geneticindisulfat (G418) Lösung CELLPURE® 50mg/ml,steril	Carl-Roth GmbH &Co. KG
GFP-Trap®_A	Chromotek
Glacial Acetic Acid p.a	Merck KGaA

Glacial Acetic Acid p.a.	Merck KGaA
Glycerol	Carl-Roth GmbH & Co. KG
Glycine	Carl-Roth GmbH & Co. KG
Goat Serum (NGS)	Merck KGaA
Harnstoff ≥99.5%,p.a., Bio-Science-Grade	Carl-Roth GmbH &Co. KG
HPLC water	VWR
Hydrochloric Acid 32% p.a. (HCl)	Merck KGaA
Insulin (bovine)	Sigma- Aldrich
Isopropanol	Honeywell
jetPrimer® versatile DNA/siRNA transfection reagent	Polyplus
Kanamycin Sulfate 100 mg/ml	Carl-Roth GmbH &Co. KG
Lipofectamine™ P3000 Reagent	Thermo Fisher Scientific
Methanol	Honeywell
MG-132	Alfa Aesar
Milk powder, Blotting grade, dry, non-fat	Carl-Roth GmbH &Co. KG
Millipore water	Merck Millipore
M-MLV- RT 5x Buffer	Promega
M-MLV-polymerase (reverse Transcriptase)	Promega
Nonident P40 (NP40)	F-Hoffmann-La Roche
Nuclease free water	Promega GmbH
NuPAGE® MOPS 20x Running Buffer (20x)	Novex by life technologies
P3000™ Reagent	Thermo Fisher Scientific
PageRuler TM Prestained Protein Ladder (170 kDa)	Thermo Scientific
Penicillin/Streptomycin antibiotics (P/S) (10,000 Units/ml; 10 mg/ml)	Thermo Fisher Scientific
peqGold TriFast	PeQLab
Phosphatase Inhibitor Cocktail 2 (PI2)	Sigma-Aldrich
Phosphatase Inhibitor Cocktail 3 (PI3)	Sigma-Aldrich
Phusion High Fidelity DNA Polymerase	Thermo Scientific, USA
Pierce® Anti-HA Agarose 26181	Thermo Scientific

PierceTM ECL plus Western Blotting Substrate	Thermo Fisher Scientific
PlasmidSafe ATP-dependent DNase	Epicentre®
PlasmidSafe buffer 10x	Epicentre®
Poly-D-lysine hydrobromide 100x	Sigma- Aldrich
Polyethylenimine linear (PEI)	PolySciences, Inc
Polynucleotide kinase buffer (PNK) 10x	Epicentre®
Ponceau S (w/v = 1%)	Sigma Aldrich
ProSieve™ QuadColor™ Protein Marker 4.6-300kDa	Biozym Scientific GmbH
Protease Inhibitor Complex Complete (PIC)	F-Hoffmann-La Roche
Protein Marker 180kDa	Thermo Fisher Scientific
Puromycin	Life Technologies
QuickExtract™ DNA Extraction Soln. 1.0	Lucigen Coorporation
Random Primers	Promega
RapiGest™ SF Surfactant	Waters Corportation
S.O.C Medium	Invitrogen
Sodium Chloride	Merck KGaA
Sodiumdodecylsulfate SDS Solution 10% (w/v= 10%; SDS dust-free pellets >98%)	Sigma Aldrich
Sso Advanced Universal SYBR® Green Supermix	BioRad
T4 DNA Ligase	F-Hoffmann-La Roche AG
T4 polynucleotide kinase	New England BioLabs® Inc
TBS	In-house
TEMED	Merck
TriFast	VWR
Trifluoracetic Acid (eluent additive for LC-MS, v/v = 5 %) (TFA)	Fluka
Tris ultrapure	AppliChem GmbH
Tris(hydroxymethyl) Aminomethane (TRIS or TRIZMA)	Sigma Aldrich
Triton® X-100	Sigma Aldrich

Trypan Blue solution 0.4 % liquid, for microscopy	Sigma Aldrich
Trypsin NB Sequencing Grade, modified from porcine pancreas	Serva Electrophoresis GmbH
Tryptone/Peptone from Casein	Carl-Roth GmbH &Co. KG
Tween®20	Sigma Aldrich
Water for HPLC	VWR
Yeast Extract	Carl-Roth GmbH &Co. KG
β-Mercaptoethanol	Sigma Aldrich

5.3 Buffer and solutions

5.3.1 Proteomics

0/5 solution

TFA 100%	50 µl
HPLC water	950 µl

50/5 solution

TFA 100%	50 µl
Acetonitrile (50 %)	950 µl

80/5 solution

TFA 100%	50 µl
Acetonitrile (80 %)	950 µl

Acetic Acid (HAc) 1 M

HAc	100 µl
H_2O	1.65 ml

Acetic Acid (HAc) 50 mM

HAc 1 M	1 ml
H_2O	19 ml

Acetonitrile v/v = 50 %

Acetonitrile	50 ml
HPLC water	50 ml

Acetonitrile v/v = 80 %

Acetonitrile	80 ml
HPLC water	20 ml

Ammonium bicarbonate Solution (ABC)

ABC	19.8 mg
HPLC water	5 ml
	→ homogenize

Bradford Dilution 1 x

Bradford 5	2 ml
HPLC water	8 ml
	→ store at 4 °C, dark

BSA buffer 10x (10 mg/ml)

BSA	100 mg
HPLC water	10 ml
	→ homogenize and store 20µl aliquots at -20°C

Dithiothreitol Solution (DTT)

DTT	15.4 mg
HPLC water	1 ml
	→ homogenize

Flag Elution buffer (= Flag Peptide)

FLAG-Peptide	4 mg
TBS 1 x	800 µl
	→ 20 µl stock solution mixed with 480 µl 1 x TBS

Glycine buffer

Glycine	1.501 g
HPLC water	80 ml
	→ adjust pH to 2.5 with concentrated HCl
	→ fill up to 100 ml with HPLC water

	→ store at RT

Iodacetamide Solution (IAA)

IAA	55.5 mg
HPLC water	1 ml HPLC water
	→ homogenize

Lysis buffer

HPLC water	8.5 ml
10 x TBS	1 ml
NP40	55 µl
	→ homogenize, store at 4 °C
	→ add PI3, PI2 and PIC 50 x before usage

PIC 50 x

PIC 50 x	1 tablet
	1 ml HPLC water
	→ aliquot in 420 µl
	→ store at -20 °C

Polyethlyenimine Solution (PEI)

PEI	100 mg
Sodium Chloride (pH 5.5)	900 ml
	→ adjust pH to 7.8
	→ fill up to 1 l with Sodium Chloride (pH 5.5)
	→ stir over night
	→ check pH
	→ sterile filtrate
	→ aliquot 50 ml and store at 4 °C

RapiGest SF Surfactant

RapiGest SF Surfactant (1 mg)	1 vial
HPLC water	50 µl
	→ homogenize, store at 4 °C

SDS solution 5 %

SDS	2.5 g
1x TBS	50 ml
	→ homogenize, store at RT
	→dilute 1:500 (0.01 % SDS)

Sodium Chloride solution

NaCl	8.77 g
Millipore water	900 ml
	→adjust pH to 5.5
	→ fill up to 1 l

TBS 10 x

Tris ultrapure	180 g
NaCl	440 g
Millipore water	3.5 l
	→ adjust pH to 7.4
	→ full up to 5 l
	→ autoclave

TBS 1x

TBS 10 x	5 ml
Millipore water	45 ml

Tris base buffer 1 M

Tris ultrapure	12.114 g
HPLC water	60 ml
	→ homogenize and adjust pH to 10.4
	→ fill up to 100 ml with HPLC water
	→ store at RT

Tris Urea buffer stock

Urea	12 g
Tris ultrapure 50 mM	788 mg
HPLC water	80 ml
	→adjust pH to 7.5
	→ fill up to 100 ml with HPLC water

Tris Urea buffer 1

Tris Urea buffer stock	1 ml
Trypsin solution 0.5 µg/µl	10 µl

Tris Urea buffer 2

Tris Urea buffer stock	1 ml
DTT 100 mM	10 µl

Trypsin Solution (1µg/µl, 25µg)

Trypsin vial	→ Centrifuge
HAc (50 mM)	50 µl
	→ homogenize (vortex) and centrifuge
	→ store at -20 °C

Washing buffer

HPLC water	8.66 ml
TBS 10 x	1 ml
NP40	12 µl
	→homogenize, store at 4 °C
	→ add PI2 and PI3 before usage

5.3.2 Immunoblotting

APS solution

Ammonium Persulfate	1 g
HPLC water	10 ml
	→ homogenize
	→ aliquot and store at -20 °C

Blocking solution 5 %

Milk or BSA	5 g
TBST 1 x	90 ml
	→ fill up to 100 ml
	→ store at 4 °C

Comassie solution

Commassie Brilliant Blue-G250	4 g
Millipore water	1 l
	→ homogenize
	→ store at RT and in the dark

ECL plus Western Blotting substrate

Solution A	975 µl
Solution B	25 µl
(1:40)	→ incubate PVDF membrane for 2 min in the dark at room temperature before taking pictures

ECL Western Blotting substrate

Detection reagent 1	500 µl
Detection reagent 2	500 µl
(1:1)	→ incubate PVDF membrane for 2 min in the dark at room temperature before taking pictures

Laemmli buffer 5 x

Tris HCL buffer	8.33 ml
SDS solution (20%)	12.5 ml
Gylcerol	25 ml
β-Mercaptoethanol	1.75 ml
Bromphenol Blue	0.25 g
Millipore water	50 ml
	→ homogenize, aliquot and store are -20 °C

MOPS buffer 1x

MOPS buffer 20 x	50 ml
VE water	950 mll

Ponceau S solution 10 x(Stock)

Ponceau S	1 g
VE water	45 ml
Acetic acid	50 ml

	→ fill up to 100 ml with VE water → store at RT, in the dark

Ponceau S solution 1 x

Ponceau S solution 10 x (Stock)	Dilute 1:10 with VE water → store at RT and in the dark

Running buffer 10 x

Glycin	750 g
Tris base	150 g
SDS	50 g
VE water	4.5 l → homogenize and fill up to 5 l

Running buffer 1x

Running buffer 10 x	Dilute 1:10 with VE water

SDS solution 10 %

Sodiumdodecylsulfate (SDS)	50 g
Millipore water	400 ml → homogenize and fill up to 500 ml

TBST 1x

TBS 10 x	100 ml
Tween® 20	1 ml
VE water	900 ml

Tris HCl buffer (1.5 M)

Tris base	90.8 g
VE water	450 ml → adjust to pH 6.8 (stacking gel) and pH 8.8 (separation gel). → fill up to 500 ml with VE water

Western buffer 10 x

Glycin	144.13 g
Tris base	30.29 g

VE water	900 ml →homogenize and fill up to 1 l

Wester buffer 1 x

Western buffer 10 x	100 ml
Methanol	200 ml
VE water	700 ml

5.3.3 Nucleic acid method

Agarose gel 1%

Agarose	1 g
TBE 1 x	100 ml
Ethidium bromide	4 µl

5.3.4 Cloning

Ampicillin solution (100 mg/ml)

Ampicillin	1 g
HPLC water	10 ml → aliquot and store at -20 °C

LB Agar

LB medium	400 ml
Agar agar	6 g → autoclave Pour LB agar plates: → boil up LB Agar and cool down (~ 55 - 60 °C) before adding antibiotics (1:1000)

LB Medium

Trypton	50 g
Yeast Extract	25 g
NaCl	50 g
VE water	4.5 l

	→homogenize →adjust pH to 7.0 with 5 N NaOH →fill up till 5l with VE water

Kanamycin solution (50 mg/ml)

Kanamycin	500 mg
HPLC water	10 ml
	→ aliquot and store at -20 °C

Chloramphenicol Solution (100mg/ml)

Chloramphenicol	1 g
Ethanol p.a.	10 ml
	→ aliquot and store at -20 °C

5.3.5 Cell culture

Dulbecco's Modified Eagle Medium – high glucose (DMEM)	Sigma-Aldrich, Gibco
Dulbecco's Phosphate Buffered Saline (1x, DPBS), [-] $CaCl_2$, [-] $MgCl_2$	Thermo Fisher Scientific, Gibco
Fetal Bovine Serum (FBS)	Sigma-Aldrich

Cryo medium

nFBS	3.6 ml
DMSO (100%)	400 µl
	→ homogenize

Culturing medium

DMEM-high glucose	500 ml
10 % fetal Bovine Serum	50 ml
100x Antibiotic-Antimycotic (P/S)	2.5 ml

Starvation medium

DMEM-high glucose	500 ml

5.3.6 Localization studies

DAPI

DAPI 1 mg/ml	1 µl

PBS	10 ml → store at 4 °C, in the dark
Normal goat serum (NGS)	
NGS BSA PBST	10 % 1 % In 0.1 % PBST

Paraformaldehyde (PFA) 4 %

Paraformaldehyde PBS	4 g 50 ml → dissolve and heat up till 55-60 °C → Fill up with 50 ml PBS. → Stir for 45 min, → adjust pH to 7.4 → store at -20 °C

PBST (0.3 %)

PBS Triton	25 ml 75 µl → homogenize and aliquot → store at -20 °C

Poly-D-Lysine 1 x

Poly-D-Lysine 100 x PBS	500 µl 49.5 ml →store at 4 °C

5.3.7 Crystalviolet

Acetic Acid 20 %

Acetic acid 100 % VE water	100 ml 900 µl

Crystalviolet 0.2 %

Crystalviolet 100 % Ethanol 20 %	4.35 ml 45.65 ml

5.4 Bacteria

Bacteria	Supplier
E. coli - Library Efficiency® DH5α Competent Cells	Invitrogen, in house
E. coli - One Shot® CcdB Survival™ 2T1^{R} compentent cells	Invitrogen, in house

5.5 Human cell lines

HEK293T – human embryonic kidney cells expressing large T antigen of SV40 (CRL-3216)	American Type Culture Collection
hTERT-RPE1- Human Telomerase Reverse Transcriptase-immortalized Retinal Pigmented Epithelial Cells	American Type Culture Collection

5.6 Plasmid

Plasmid	Antibiotic resistance	Company
pSpCas9(BB)-2A-Puro (PX459) V2.0 8 (gift from Feng Zhang)	Amp^{R}, Puro^{R}	Addgene
pJET1.2/blunt Cloning Vector	Amp^{R}	Thermo Scientific Fisher
pGEM-T-Easy Vector	Amp^{R}	Promega
pEBTerBI-CLIP-CEP70 was a gift from Kai Johnsson (#136870)	Amp^{R}	Addgene
pEBTetBI-CLIP-ALMS1 was a gift from Kai Johnsson (#136877)	Amp^{R}	Addgene
pDONR201	Kan^{R}	A gift from R. Roepman, Nijmegen, Invitrogen
pDEST (pcDNA 3.0 backbone) modified with C- or N-terminal StrepFLAG tag	Amp^{R}	Invitrogen modified by CJ Gloeckner [120]

5.7 Oligonucleotides (sgRNA)

Name	Oligonucleotide sequence	Company
ALMS1 ex 10 bottom	AAACTGCTAATAAGGGTATGGTTAC	IDT
ALMS1 ex 10 top	CACCGTAACCATACCCTTATTAGCA	IDT
ALMS1 ex 8 bottom	AAACCTTCCTCCCTGCTATCTGTTATAC	IDT
ALMS1 ex 8 top	CACCGTATAACAGATAGCAGGGAGGAAG	IDT
CEP70 ex 5 bottom	AAACGTATCATGTTCTGTTGACATC	IDT
CEP70 ex 5 top	CACCGATGTCAACAGAACATGATAC	IDT
CEP70 ex 6 bottom	AAACACTTAGTGATTCATCCTCCAC	IDT
CEP70 ex 6 top	CACCGTGGAGGATGAATCACTAAGT	IDT

5.8 Primer genomic

Name	Oligonucleotide sequence	Company
ALMS1 ex 23 forward	CCCTCATTGGTGAGTCAGATAC	IDT
ALMS1 ex 23 reverse	TCATTGTAACACACAGGCCATTGG	IDT
ALMS1 ex 8 forward	GCAGAGAGCAAAGTCAGTATG	IDT
ALMS1 ex 8 reverse	TTTCATTGGCTAAGCTTCCTC	IDT
sfGFP reverse	AGCTCATCCATGCCATGTGTAATC	IDT
ALMS1 ex 10 forward	ACCCTTGGCTGTCAGAATTAG	IDT
ALMS1 ex 10 reverse	GATGTTGAGGAGAGGGAGAATG	IDT
ALMS1 ex 23 forward	CAGATCCTCTTTCCTGAACCTTTCG	IDT
CEP70 ex 6 forward	GAAATGAACTTCAGCTAGAGCA	IDT
CEP70 ex 6 reverse	GAATTCATAACTCAGTACCTGT	IDT

5.9 Primer Sequencing

Name	Oligonucleotide sequence	Company
pJET1.2 Forward	CGACTCACTATAGGGAGAGCGGC	Thermo Scientific Fisher/IDT
pJET1.2 Reverse	AAGAACATCGATTTTCCATGGCAG-	Thermo Scientific Fisher/IDT
SP6 promotor forward	TATTTAGGTGACACTATAG	IDT
T7 promoter reverse	TAATACGACTCACTATAGG	IDT
U6 forward	GAGGCCCTATTTCCCATGATTCC	IDT

U6 reverse	GGAGTAGCCTTATTTTAACTTGCTATT	IDT
EGFP-C forward	CATGGTCCTGCTGGAGTTCGTG	IDT
SV40pA-R reverse	GAAATTTGTGATGCTATTGC	IDT
CMV forward	CGCAAATGGGCGGTAGGCGTG	IDT

5.10 Primer qPCR

Name	Oligonucleotide sequence	Company
ABCA4 forward	CATCCTGTTCCACCACCTCA	IDT
ABCA4 reverse	CTGTGTCCTCCAACATGGCT	IDT
ALMS1 ex 10 forward	CTGATGCAGTCACTCAGATAACA	IDT
ALMS1 ex 11 reverse	ACTGAAGATGATGAGGCAAACT	IDT
ALMS1 ex 4 forward	GCTTCTCCTGATTTGCCTTTG	IDT
ALMS1 ex 5reverse	CTATAAGCGGGTGCTGAGATAC	IDT
BAX forward	TTTGCTTCAGGGTTTCATCCA	IDT
BAX reverse	CTCCATGTTACTGTCCAGTTCGT	IDT
BCL2 forward	TCGCCCTGTGGATGACTGA	IDT
BCL2 reverse	CAGAGACAGCCAGGAGAAATCA	IDT
CEP70 ex 11 reverse	GCTTCTTCACCTGCTGTTTA	IDT
CEP70 ex 3 forward	GGATTCCAGTCAACCATCAG	IDT
CEP70 ex 5 reverse	CAAATTCTGTCTCATCCTTTGTG	IDT
CEP70 ex 9 forward	CAGAAATCTGGATGCCTCAC	IDT
GAPDH forward	GCAAATTCCATGGCACCGT	IDT
GAPDH reverse	GCCCCACTTGATTTTGGAGG	IDT
GUSB forward	AGAGTGGTGCTGAGGATTGG	IDT
GUSB reverse	CCCTCATGCTCTAGCGTGTC	IDT
OCT3/4 forward	GTTCTTCATTCACTAAGGAAGG	IDT
OCT3/4 reverse	CAAGAGCATCATTGAACTTCAC	IDT
OPN1SW forward	ACCATTGGTATTGGCGTCTC	IDT
OPN1SW reverse	GGAGAGAGGCACAATGAAGC	IDT
PAX6 forward	CCGGCAGAAGATTGTAGAGC	IDT
PAX6 reverse	GCCCGTTCAACATCCTTAGT	IDT
RCV1 forward	ACACCAAGTTCTCGGAGGAG	IDT
RCV1 reverse	ACTTGGCGTAGATGCTCTGG	IDT
RPE65 forward	GCCCTCCTGCACAAGTTTGACTTT	IDT
RPE65 reverse	AGTTGGTCTCTGTGCAAGCGTAGT	IDT

5.11 Tag Sequences

5.11.1 sfGFP (gBlock® Gene Fragments, IDT)

AGAGTGACCAATCAACTTCTGGGGAGAAAAGTCCCATGGGACAGCAAAGGAGAAGAACTTT
TCACTGGAGTTGTCCCAATTCTTGTTGAATTAGATGGTGATGTTAATGGGCACAAATTTTCT
GTCCGTGGAGAGGGTGAAGGTGATGCTACAAACGGAAAACTCACCCTTAAATTTATTTGCA
CTACTGGAAAACTACCTGTTCCATGGCCAACACTTGTCACTACTCTGACCTATGGTGTTCAA
TGCTTTTCCCGTTATCCGGATCACATGAAACGGCATGACTTTTTCAAGAGTGCCATGCCCGA
AGGTTATGTACAGGAACGCACTATATCTTTCAAAGATGACGGGACCTACAAGACGCGTGCT
GAAGTCAAGTTTGAAGGTGATACCCTTGTTAATCGTATCGAGTTAAAAGGTATTGATTTTAAA
GAAGATGGAAACATTCTCGGACACAAACTCGAGTACAACTTTAACTCACACAATGTATACAT
CACGGCAGACAAACAAAAGAATGGAATCAAAGCTAACTTCAAAATTCGCCACAACGTTGAA
GATGGTTCCGTTCAACTAGCAGACCATTATCAACAAAATACTCCAATTGGCGATGGCCCTGT
CCTTTTACCAGACAACCATTACCTGTCGACACAATCTGTCCTTTCGAAAGATCCCAACGAAA
AGCGTGACCACATGGTCCTTCTTGAGTTTGTAACTGCTGCTGGGATTACACATGGCATGGA
TGAGCTCTACAAATGACACAAGTTTATTTTCCTCAGAGCCTTGGAATTCTATTTTATGAACCT
AGAGAAGCAGAATCCTTACTTTTGTGAGTCTGGTTGAATAAAGCTTATTCTTTGTCCATGTGT
ATTTTAGAAATAGTAACTTCTAAAGAGTCTGGAACAAAGTGGTGATTAAAATTCCTAATGGTT
TGGGAGCAATACTTTCTGCATAGTGGCCTTGTCCAATGGCCTGTGTGTTACAATGATATGAT
CATTTCTCAAGAATAAGTCCCTTTTTGTATGTGTTTTTATACTTTTAGAAAATAAAAACTTTAG
ATTAACTCTCTGGGGAGAAAAGTTCCCTGGG

5.11.2 ALMS1 CT RFP-HA (gBlock® Gene Fragments, IDT)

GGCCATATGCATACGCAGGCTCTGGGGAGAAAAGTTCCCTGGGAGGCCTCTCCTTATGCT
ACTGTATGTGGGAACTGATGGATTATCTGTGTCTCTATAGAAATAATAGATATTGATTACAGA
TCCTCTTTCCTGAACCTTTCGTGAAGTATTTTTTATATGACGACCATAGTTTCTGAAGCAGAG
TAAAATGAACAAGATTTGAATAGGACCACACTGATTCTCCTTGGTGACATGGATGCAGGGA
GGAGAGGCATCTGCCTCTGATGGCAGTAATATCTAACTTCTTTCCTGCCTTTCTTTTCTTCTA
CAGAGAGTGACCAATCAACTTCTGGGGAGAAAAGTCCCATGGGACGGTGGGGGTTCTGGC
GGGGGAAGCGGAGGTGGTTCAGCGTCCAGTGAAGACGTTATAAAGGAATTTATGAGATTTA
AAGTCCGGATGGAAGGAAGTGTAAACGGCCACGAATTCGAGATCGAGGGGGAGGGGGAG
GGTAGACCCTATGAGGGTACACAAACCGCCAAGCTTAAAGTGACCAAGGGCGGACCACTC
CCGTTTGCATGGGACATCCTTAGCCCGCAGTTCCAATACGGTTCAAAAGCCTATGTGAAAC
ACCCCGCAGACATACCAGATTATCTGAAACTTTCCTTCCCCGAGGGTTTCAAGTGGGAGCG
AGTGATGAACTTTGAAGACGGTGGAGTTGTGACAGTCACCCAGGATTCCTCACTCCAAGAC
GGTGAATTCATCTACAAGGTGAAGCTTAGGGGCACAAATTTTCCCAGTGATGGCCCTGTCA

TGCAAAAAAAAACTATGGGATGGGAAGCATCAACTGAGAGAATGTACCCCGAAGATGGAGC
CTTGAAGGGAGAAATAAAAATGAGGCTTAAACTCAAAGATGGAGGACACTACGATGCCGAA
GTGAAAACCACATACATGGCAAAAAAACCGGTACAGCTGCCCGGAGCCTACAAAACTGACA
TCAAATTGGACATTACTAGTCATAATGAAGATTACACTATTGTAGAACAGTATGAAAGAGCC
GAGGGAAGACATAGCACGGGAGCGGGCGGCGGGAGTTACCCGTACGACGTGCCCGATTA
TGCGTGACACAAGTTTATTTTCCTCAGAGCCTTGGAATTCTATTTTATGAACCTAGAGAAGC
AGAATCCTTACTTTTGTGAGTCTGGTTGAATAAAGCTTATTCTTTGTCCATGTGTATTTTAGA
AATAGTAACTTCTAAAGAGTCTGGAACAAAGTGGTGATTAAAATTCCTAATGGTTTGGGAGC
AATACTTTCTGCATAGTGGCCTTGTCCAATGGCCTGTGTGTTACAATGATATGATCATTTCTC
AAGAATAAGTCCCTTTTTGTATGTGTTTTTATACTTTTAGAAAATAAAAACTTTAGATTAACTC
TCTGGGGAGAAAAGTTCCCTGGGGACTTCGAACTGGAATTCGTA

5.12 Primary and secondary antibodies

5.12.1 Primary Antibody

Antibody name	Product number	Biological source	Dilution (IFS/WB)	Company
Acetylated tubulin	ab24610	Mouse	1:250/1:2500	Abcam
AKT	10176-2-AP	rabbit	-/1:1000	Proteintech
ALMS1 IgG	27231-1-AP	rabbit	1:750	Proteintech
ALMS1 IgG	Ab84892	Rabbit	1:1000	Abcam
ALMS1 IgG	NB100-97823	Rabbit	1:1000/ 1:500	Novusbio
ARL13B IgG	73-287	mouse	1:200	Neuromab
ARL13B IgG	17711-1-AP	rabbit	1:150	Proteintech
CEP250/CNAP1	14498-1-AP	rabbit	1:100	Proteintech
CEP70	ab227456	rabbit	1:500/1:1000	Abcam
GAPDH	D16H11	Rabbit	-/1:10.000	Cell Signaling Technology
Glutamylated tubulin (GT335)	A27791601	mouse	1:1500/-	Adipogen
GSK-3α/β	D75D3	rabbit	-/1:1000	Cell Signaling
PCM1	19856-1-AP	rabbit	1:200/-	Proteintech
p-GSK3 beta (F-2)	sc-373800	mouse	-/1:500	Santa Cruz
Phospho-AKT	139H12	rabbit	-/1:2000	Cell Signaling

(Ser473)				
Rootletin	Sc-374056	mouse	1:250	SantaCruz
RPGR IgG	HPA001593	rabbit	1:500	Sigma-Aldrich
TUBGCP2	25856-1-AP	rabbit	1:100	Proteintech
γ-Tubulin (TUBGC1)	NB-120-11318	rabbit	1:1000	Novusbio

5.12.2 Secondary Antibody

Host	**Fluorescence spectrum**	**Dilution**	**Product**	**Company**
Goat anti-mouse	568 nm, red	1:350	Alexa Fluor	Thermo Fisher Scientific
Goat anti-mouse	488 nm, green	1:350	Alexa Fluor	Thermo Fisher Scientific
Goat anti-mouse	647 nm, far-red	1:350	Alexa Fluor	Thermo Fisher Scientific
Goat anti-mouse	HRP	1:7500	-	Jackson ImmunoResearch
Goat anti-rabbit	568 nm, red	1:350	Alexa Fluor	Thermo Fisher Scientific
Goat anti-rabbit	488 nm, green	1:350	Alexa Fluor	Thermo Fisher Scientific
Goat anti-rabbit	HRP	1:7500	-	Jackson ImmunoResearch
Goat-anti rabbit	647 nm, far-red	1:350	Alexa Fluor	Thermo Fisher Scientific

5.13 Kits

Name	**Company**
Gateway® BP ClonaseTM II Enzyme Mix	Invitrogen Thermo Scientific, USA
Gateway® LR ClonaseTM II Enzyme Mix	Invitrogen Thermo Scientific, USA
JetPRIME®	Polyplus
Lipofectamine™ 3000 Transfection Kit	Thermo Fisher Scientific
Monarch® Plasmid Miniprep Kit	New England BioLabs Inc.
PeqGold Cycle -Pure Kit	VWR

PeqGold Tissue DNA Mini Kit	VWR
PureYield™ Plasmid Midiprep System	Promega GmbH
QIAquick® PCR Purification Kit	Carl Roth GmbH & Co.KG
TriFECTa® Kit DsiRNA Duplex CEP70	IDT
EZ-PCR Mycoplasma Detection Kit	Sartorius Biological Industries

5.14 Equipment

Equipment	Company
2 Channel Jumbo Display Clock Timer	Carl Roth GmbH & Co.KG
Agarose gel chamber	Bio-Rad Laboratories, Inc.
Agarose gel comb	Bio-Rad Laboratories, Inc.
ApoTome2, Imager.Zi Ax10	Carl Zeiss AG
Axio Vert. A1 Microscopy	Carl Zeiss AG
BioRad T100™ Thermal Cycler	BioRad
Blotting Chamber	BioRad
Brand® Accu-jet® Pipetboy	Sigma-Aldrich
Centrifuge 5415 R	Eppendorf AG
Chemi Imgager Fusion FX	Vilber
Duran® baffled flask	DWK Life Sciences
Ecotron Incubation Shaker	Infors HT
FIBERLite® F15-8x50C	Thermo Scientific
Filter system	Millipore Filterunit Express Plus
HERACell 150i CO2 Incubator	Thermo Scientific
Heraeus Fresco 17 Centrifuge	Thermo Scientific
Heraeus Multifuge X3R Centrifuge	Thermo Scientific
Incubator	Memmert GmbH & CO.KG
Laboport® Mini Vacuum Pump	KNF Neuberger, Inc.
Leica TCS SP8 Scanning Microscope	Leica Microsystems IR GmbH
MiniStar Centrifuge	VWR
MSC-Advantage	Thermo Fisher Scientific
MWG Biotech Inc Primus 25 Thermal Cycler	Cole-Parmer GmbH
NanoDrop 1000 Spectrophotometer	PeqLab
NeoLab Intelli-Mixer	NeoLab
Pipettes 10 µl, 100 µl, 1000 µl Diamond	Gilson

Power Pack™ Basic	Bio-Rad Laboratories, Inc.
PrimoVert Microscopy	Carl Zeiss AG
qPCR Cycler	BioRad
Rotilabo®-precision glass cuvette, micro, quartz glass, seamed lid, 0,7 ml	Carl Roth GmbH & Co.KG
Savant RVT400 Refrigerated Vapor Trap	Thermo Scientific
Savant SPD111V SpeedVac Concentrator	Thermo Scientific
STED	Leica
Systec DX-150, DX-23 Autoclave	Systec GmbH
T70 UV/VIS Spectrometer	PG Instruments Ltd.
Tecan Spark 10M Luminescence Reader	Tecan Group AG
Thermo-Shaker	Universal Labortechnik GmbH & KO.KG
Vortex-Genie2	Scientific Industries, Inc
Water bath VWB 18	VWR
WB Chamber	BioRad
Zeiss Axio Imager Z1 ApoTome Microscope	Carl Zeiss Microscopy GmbH

5.15 Liquid chromatography and mass spectrometry (LC-MS/MS)

	Company/Supplier
Acclaim PepMap100 C18	Thermo Scientific
Orbitrap Fusion™ Tribrid	Thermo Scientific
Ultimate3000 RSLCnano systems	Thermo Scientific
Acclaim PepMap RSLC C18	MPI of Biochemistry
QExective Plus	Thermo Scientific
µPAC nano column (50 cm, C18)	Thermo Scientific
µPAC trapping column	Thermo Scientific

5.16 Software

Software	**Company/Supplier**
Adobe Illustrator CS5.1	Adobe System Inc.
Adobe Photoshop CS5.1	Adobe System Inc.
Adobe Photoshop CS5.1	Adobe System Inc.
BioEdit v7.0.5.3	Tom Hall, Ibis Therapeutics

EASYWin32 5.17.295	Herolab GmbH
FIJI (ImageJ) 1.53q	Wayne Rasband
Leica Application Suite X (LasX; 3.5.7)	Leica Microsystems
Mascot 1.6.1.0	Matrix Science
MaxQuant 1.6.1.0	MPI of Biochemistry
Mendeley	Mendeley Ltd.
Microsoft Office 2016	Microsoft Corporation
NeuronJ (Plugin; FIJI) 1.4.3.	Erik Meijering
Perseus 1.6.5.0	MPI of Biochemistry
Scaffold 3.0, 4.0, 5.0	Proteome Software Inc
SparkControl 2.2	Tecan Group AG
ZEN 3.0 (blue edition)	Carl Zeiss Microscopy GmbH

5.17 Databases, online tools, and web links

Databases	**Web links**
Benchling	https://benchling.com
BioGRID	https://thebiogrid.org/
CCTop- CRISPR/Cas9 target online predictor	http://crispr.cos.uni-heidelberg.de
Ensembl	http://www.ensembl.org/index.html
Expasy	https://web.expasy.org/translate/
GetGo	http://getgo.russelllab.org
Multalin	http://multalin.toulouse.inra.fr/multalin/multalin.html
NCBI	www.ncbi.nlm.nih.gov/
NCBI BLAST	https://blast.ncbi.nlm.nih.gov/Blast.cgi
NCBI Primer-BLAST	https://www.ncbi.nlm.nih.gov/tools/primer-blast/
NCBI Protein	www.ncbi.nlm.nih.gov/sites/entrez?db=protein
NCBI PubMed	https://pubmed.ncbi.nlm.nih.gov/
PrimerQuest™ Tool	https://eu.idtdna.com/pages/tools/primerquest
Reactome	https://reactome.org/
Reverse Complement	https://www.bioinformatics.org/sms/rev_comp.html
Sequence Variant Nomenclature	http://varnomen.hgvs.org/ Version 20.05
Sequencing	www.gatc-biotech.com https://www.eurofinsgenomics.eu/de/home/

	https://web.expasy.org/translate/
Signaling pathways	https://www.genome.jp/kegg/pathway.html
Statistics	https://www.estimationstats.com/#/
String	https://string-db.org/
Swissprot	www.expasy.ch/sprot/
SysCilia Gold Standard	http://www.syscilia.org/goldstandard.shtml
TIDE: Tracking of Indels by Decomposition	https://tide.nki.nl/
Uniprot	http://www.uniprot.org/
The Human Protein Atlas Version 23.0	https://www.proteinatlas.org/

6 Methods

6.1 Proteomics

6.1.1 Immunoprecipitation

Endogenously CT tagged ALMS1 cells (see 0) were used for immunoprecipitations (IP). Beside the endogenous tagged cells, overexpression plasmids containing the sequence of the protein of interest (e.g. CEP70, Raf1) with a Strep-Flag tag were used. All steps for an IP were done on ice or 4 °C to preserve proteins.

Around 4 million HEK293T cells were plated on 14 cm petri dishes. For an IP with overexpression constructs, cells were transfected with 1 ml PEI and 8000 ng DNA per 14 cm petri dishes for at least 48 hrs. For the sfGFP-IP cells were starved overnight (ON) to stop proliferation and to induce cilia formation. When cells reached 100% confluency, the medium was discarded, cells were washed with PBS and scraped of the plate with 1 ml lysis buffer (1x TBS, 0.5 Nonidet P40 (Roche), 1 % phosphatase inhibitor cocktail 2 and 3 (Sigma), Protease Inhibitor Complexe Complete (Roche)) on ice. The lysate was incubated on an end-over end shaker (NeoLab) for 30 min, followed by a 10 min incubation at 10000 xg. The supernatant was used to determine its protein concentration using the Bradford Assay. (Wörz unpublished Master thesis, 2018 [21], Woerz *et al.*, under review [3])

Per sample, 50 µl mixed GFP beads, 25 µl mixed Flag and 25µl HA beads were prepared. All the following steps were performed on ice. The beads were centrifuged after each washing step for 1 min at 5000 x g and the supernatant was removed. First, the beads were washed once with 600 µl 1x TBS. Then, 500 µl lysis buffer was pipetted onto the beads and centrifuged. Afterwards, the beads were washed twice with 500 µl washing buffer (1x TBS, 0.5 Nonidet P40 (Roche), 1% phosphatase inhibitor cocktail 2 and 3 (Sigma)) followed by centrifugation. In a last step, 1x mixed bead volume of washing buffer was added onto the beads and thoroughly mixed and divided into new Eppendorf tubes. (Wörz unpublished Master thesis, 2018 [21], Woerz *et al.*, under review [3])

5-10 mg protein was mixed with the appropriate and previously washed HA, Flag or sfGFP Beads. The lysate-bead mixture was incubated for 1 h at 4 °C on an end over end shaker. Lysate with HA beads were used for an on-bead digest described in 6.1.5, whereas the lysate - sfGFP beads mixture was used for an in-solution digest. Lysate with Flag Beads were either used for on-bead digest or in-solution digest. Before elution of proteins from beads for the in-solution digest was conducted, the samples were added onto a column and washed three times

with 500 µl washing buffer. (Wörz unpublished Master thesis, 2018 [21], Woerz *et al.*, under review [3])

For elution of the protein of interest, the GFP beads lysate mixture was first incubated with a 100 µl acid glycine buffer (0.2 M, pH 2.5) and then neutralized with 10 µl 1 M Tris base buffer (pH 10.4). Flag peptide was used to elute proteins from Flag beads. Therefore, 100 µl Flap peptide was added for 10 min at 23 °C and 500 rpm to the beads. HPLC water was added to the eluate get a total volume of 200µl for protein precipitation (see 6.1.3). (Wörz unpublished Master thesis, 2018 [21], Woerz *et al.*, under review [3])

6.1.2 Bradford assay

For the Bradford assay, 180 µl HPLC water was added to 20 µl 10x bovine-serum-albumin (BSA) solution (10 mg/ml) and shortly mixed before usage. Table 2 displays the pipette scheme for the calibration dilution series with a total volume of 55.5 µl each. 5 µl per calibration dilution and 1 µl of undiluted or 1:5 diluted lysates were pipetted in triplicates into a 96 well plate. Each calibration sample and the experimental lysates were mixed with 250µl 1x Bradford reagent and measured. The OD was determined at 595 nm via Spark® Multimode Microplate Reader (Tecan). (Wörz unpublished Master thesis, 2018 [21])

Table 2 Pipette scheme for Bradford assay

BSA concentration [mg/ml]	Used volume 1x BSA [µl]	Used volume HPLC water [µl]	Lysis buffer [µl]	Total volume [µl]
0	0	50	5.5	55.5
0.2	10	40	5.5	55.5
0.4	20	30	5.5	55.5
0.6	30	20	5.5	55.5
0.8	40	10	5.5	55.5
1.0	50	0	5.5	55.5

6.1.3 Protein precipitation

For precipitation, chemicals were added one by one to the eluate (from 6.1.1), vortexed and centrifuged. First 800 µl LC-methanol was pipetted to the eluate and centrifuged for 2 min at 9000 x g. 200 µl Chloroform was added and again centrifuged for 2 min at 9000 x g. For precipitation, 600 µl HPLC water was used and centrifuged for 2 min at 16000 x g. The interphase of the two appearing phases, was further used by adding 600 µl LC-methanol. A final centrifugation step for 4 min at 16000 x g was conducted to obtain a pellet, which is further used for protein digestion (see 6.1.4). (Wörz unpublished Master thesis, 2018 [21])

6.1.4 Protein digest (in solution)

The pellet was resuspended with 30 µl 50 mM ammonium bicarbonate (ABC), 4 µl RapiGest and 1 µl 100 mM dithiothreitol (DTT) by vortexing, followed by a 10 min incubation at 60 °C, 500 rpm. A 30 min incubation with 1 µl iodacetamide (IAA) in the dark at room temperature (RT) was conducted. 1 µl of 50 µg Trypsin (0.5 µg/µl) was pipetted to the probes and incubated ON at 37 °C. After adding 1.7 -1.9 µl 100% TFA (final concentration: 5 % TFA) to the mixture and an incubation of 10 min at RT, it was centrifuged at 22 °C at 16.000 x g for 15 min. (Wörz unpublished Master thesis, 2018 [21])

StageTips are used to purify the samples with 80/5, 50/5 and 0/5 solutions of 5 % TFA and 80 %, 50 % ACN or HPLC water. The following order was used per sample: 20 µl 80/5 solution was added to the Stage Tip matrix, followed by a 20 µl 0/5 solution washing step. The sample was added, followed by 20 µl 0/5 solution. Elution was implanted with 20 µl 50/5 solution and 20 µl 80/5. A SpeedVac for volume reduction was used to a maximum of 5 µl. Approximately 10 µl 0.5 % TFA was added to the sample to gain a total volume of 15 µl. 5 µl of this solution was measured using mass spectrometry. (Wörz unpublished Master thesis, 2018 [21])

6.1.5 On-bead digest

After Immunoprecipitation of Flag and RFP-HA samples, descripted in 6.1.1, an On Bead Digest was performed. After the lysate-bead incubation the beads were washed 3x times with 1xTBS (with PI2, PI3 for HA Beads) with centrifugation steps in between at 5000 x g for 1 min at 4°C. The supernatant was removed and 60µl of a Urea-Tris buffer (pH7.5) with 0.5µg/µl Trypsin Solution was added to the beads and incubated on a ThermoShaker with 800 rpm at 27 °C for 30 min, followed by centrifugation for 0.5min at 5000 x g. From here, the supernatant was collected after each centrifugation step while washing the beads. The beads were washed twice with 50µl Urea-Tris buffer with 10µl DTT. 2µl IAA was added to the supernatant and incubated overnight in the dark at RT. On the next day, the enzymatic digestion was stopped by adding 1-5.5µl 100% TFA. The probes were centrifuged for 15min at 16000 x g at RT before they were stage tipped (described in 6.1.4). (Woerz *et al.*, under review [3])

6.1.6 Tissue lysis

Porcine eyes were obtained from the slaughterhouse (Tuebingen). The eyes and the following steps were performed on ice/4 °C. Clean porcine eyes were cut open below the ciliary muscle to remove the lens and the vitreous body. Ice-cold PBS was added to the open eye. In the next step, the clear retina layer was detached and immediately transferred into lysis buffer (1 x TBS, 0.5 Nonidet P40 (Roche), 1 % phosphatase inhibitor cocktail 2 and 3 (Sigma), 50x Protease

Inhibitor Complex Complete (Roche)) on ice. Two to four retinas were pooled and stored at -80 °C until tissue specific protein complex analysis via SDS-based bait purification was conducted.

6.1.7 Tissue specific protein complex analysis via SDS-based bait purification

Cell lysate, HA beads (Pierce ® Anti-HA Agarose, Thermo Scientific) were prepared on ice like described in 6.1.1. 6 to 10 mg total protein of endogenously HA-tagged ALMS1 (bait) and HEK293T wild type (control) cell lysate were added to the beads and incubated for 1 h at 4 °C, 35 rpm on an end-over-end shaker. After centrifugation at 10.000 x g for 10 min at 4 °C, the supernatant was discarded, and the beads were washed twice with wash buffer (with 1 % PI2 and 1 % PI3). The beads were incubated once with 0.01 % SDS for three minutes at room temperature, followed by 1 min at 5000 x g centrifugation at 4 °C. The supernatant was discarded, and the beads were washed three times with wash buffer. A minimum of 2 mg tissue lysate (porcine retina, 2 - 4 mg) were added to the washed beads and incubated for 90 min at 4 °C on an end-over-end shaker. After centrifugation, the beads were washed once with wash buffer and three times with 1x TBS (with 1 % PI2 and 1 % PI3). The further procedure to digest proteins on beads till stage tipping can be read in 6.1.5.

6.1.8 Mass spectrometry (LC-MS/MS) analysis

An Ultimate3000 RSLCnano (Thermo Scientific) was coupled with a nano spray ion source to the Orbitrap Fusion Tribrid mass spectrometer (Thermo Scientific) or Q Exactive Plus (Thermo Scientific). The tryptic peptide mixtures were loaded onto a nano trap column (Q Exactive Plus: 300 µm i.d. x 5 mm precolumn, packed with Acclaim PepMap100 C18, 5 µm, 100 Å. Thermo Scientific; Orbitrap Fusion: 2 mm × 10 mm, µPAC™ Trapping column, 300 nm, 100–200 Å, PharmaFluidics). For injection the flow rate of 30 µL/min in 0.1 % trifluoroacetic in HPLC grade water. The peptides were eluted after 3 min and separated on an analytical column (Q Exactive Plus: 75 µm i.d. x 25 cm, Acclaim PepMap RSLC C18, 2 µm, 100 Å. Thermo Scientific; Orbitrap Fusion: 315 µm × 50 cm, µPAC™ nano-LC columns – 50 cm µPAC™ C18, 300 nm, 100–200 Å, PharmaFluidics). The flow rate was at 300 nL/min over 82 min with a linear gradient from 2 % to 30 % of buffer B (80 % acetonitrile and 0.08 % formic acid in HPLC water) in buffer A (2 % acetonitrile and 0.01 % formic acid in HPLC water). A short gradient from 30 % to 95 % buffer B in 5 min enables the elution of remaining peptides. The subsequent analysis of the eluted peptides was performed on the Orbitrap Fusion Tribrid mass spectrometer (Thermo Scientific) or Q Exactive Plus (Thermo Scientific). With the Q Exactive Plus, ten of the most intense peptide ions, from the high-resolution MS prescan with a mass range between 335 and 1500, were selected for fragment analysis due to their intensity (at least 200 counts) and their charge (at

least double charged). The Orbitrap Fusion was run in top speed mode with 3s- cycle time. The HCD value of 26 (Q Exective) and 30 (Orbitrap Fusion) for a normalized collision energy was used. The fragments were detected with a resolution of 17,500 (Q Exactive) or in the ion trap (Orbitrap Fusion). The lock mass option was activated and set to a background signal with a mass of 445.12003. 20 or 60 s dynamic exclusion was set to exclude every ion, that was selected for fragmentation. (Wörz unpublished Master thesis, 2018 [21], Woerz *et al.*, under review [3])

6.1.9 Experimental design and statistical rationale

MS/MS data were analyzed using MaxQuant software (version 1.6.1.0). Trypsin/P was selected as the enzyme for digestion, allowing for a maximum of two missed cleavages. For variable modifications, methionine oxidation and N-terminal acetylation, while for fixed modifications, cysteine carbamidomethylation were chosen. Label-free quantification with a with the minimum ratio count of two and no fast LFQ were used for data analysis. The re-quantify was set. The human SwissProt database (release 2014-11, 2021-05) and the sus scrofa proteome database (released in 202110) was selected for peptide and protein identification. MaxQuant contaminant search was applied to excluded contaminants. A minimum peptide number of 1 and a minimum peptide length of 7 was tolerated and accepted. Unique and razor peptides were chosen for quantification. MaxQuant settings of each experiment can be found in 10.7.1, 10.7.3, 10.10.1, 10.10.3, respectively. (Woerz *et al.*, under review [3])

The Perseus software (version 1.6.5.0) was applied for statistical analysis. A minimum of four to six or five to eight biological replicates and controls were available for statistics. For sfGFP-tagged ALMS1 eight biological replicates, for HA-tagged ALMS1, as well as for CEP70::NSF six biological replicates. Potential contaminants, peptides only identified by site or reverse sequence were excluded for all data. Within the groups, minimum half of the samples should have valid values (sfGFP: 5, and Flag: 4). Furthermore, mean, standard deviation and coefficient of variation values of the groups was intended. Identified proteins were analyzed and classified in two Tier system. Tier 1 interactors were stringently analyzed with significance A (Benjamini-Hochberg FDR < 0.05) and Student's t-test (Permutation based FDR <0.05). Tier 2 contains additional proteins with a less stringent analysis (Significance A Benjamini Hochberg FDR < 0.05 and Student's t-test *p*-value $p < 0.05$). The two-sample-test was applied to identify stable proteins, that are enriched within groups. Network was created using experimental and functional interactions extracted from curated database using STRING [121] and visualized in Cytoscape 3.9.1 (https://cytoscape.org/) [122]. (Woerz *et al.*, under review [3])

6.2 Immunoblotting

HEK293T and hTERT-RPE1 WT, KO and/or tagged single clone cells were seeded in 10 or 14 cm petri dishes. Confluent cells were starved overnight (HEK293T), while retinal epithelial cells were starved for three days with Dulbecco's Modified Eagle's Medium (DMEM-high glucose) without supplements. Cells were lysed with lysis buffer (0.5 % Nonidet-P40, 2 % protease inhibitor mixture (Roche) and 1 % phosphatase inhibitor cocktail I and II (Sigma Aldrich). The lysate was incubated for 30 min. on an end over end rotator (NeoLab) at 4 °C, followed by a centrifugal step for 10 min at 10,000 x g at 4°C. The supernatant was used for protein concentration measurement with a Bradford Assay (see 6.1.2) to get an equal amount of protein per experiment. Lysates were stored at -20°C (short time), -80 °C (long term) or directly used for Immunoblotting. A SDS-PAGE (8-12 %) was done and the separated proteins were transferred onto a PVDF membrane (GE Healthcare) for 90 min, 90 V at 4 °C. The PVDF membranes were blocked with 5 % fat-free dry milk or 1-5 % BSA dissolved in 1x TBST depending on the used antibody. Followed by an incubation with primary antibodies over night at 4 °C and secondary antibodies for 1 h at room temperature. The PVDF membrane was incubated with Pierce™ ECL Plus Western Blotting solution 40:1 (Thermo Scientific) for 2 min in the dark and the specific proteins were visualized using the Western Blot and Chemi Imager Fusion FX (Vilber). Images were edited by using Adobe Photoshop CS5 and Adobe Illustrator CS5.

Quantification of protein level was performed using ImageJ. Lanes were elected and a profile plot generated, which shows the densities of bands. The area of these bands was measured, and the values were normalized against the loading control. These relative densities of one blot can be further used to compare the intensities of bands in different samples.

6.3 Methods of nucleic acid analysis

6.3.1 Spectrophotometric measurement of DNA and RNA concentration

The (plasmid-) DNA and RNA concentration was measured with a NanoDrop (PeqLab). 2 µl Plasmid-DNA or RNA was transferred onto the NanoDrop and the concentration was determined via the optical density at wavelength 260 nm for DNA and 230 nm for RNA. The DNA/ RNA concentration was indicated in ng/µl. To determine the purity of plasmid DNA, the plasmid-DNA $OD_{260/280}$ was evaluated. (Wörz unpublished Master thesis, 2018 [21])

6.3.2 Polymerase chain reaction (PCR)

To amplify specific DNA fragments *in - vitro, the* Polymerase Chain reaction (PCR) was conducted. A Thermocycler (Cole-Parmer GmbH, BioRad T100™ Thermal Cycler) for

amplification of target DNA was used. The pipette scheme is described in Table 3 and the Thermocycler condition in Table 4. (Wörz unpublished Master thesis, 2018 [21])

Table 3 PCR reaction pipette scheme

Components	Volume per approach (µl)
Green Buffer (10x)	2
dNTP (10 mM)	0.2
Dream Taq	0.3
Primer reverse (1:10)	1
Primer forward (1:10)	1
DMSO (1 %)	0.2
ddH_2O	Add to total volume of 18-19 µl
Template DNA	1-2
Total	20

Table 4 PCR thermocycler condition (DreamTag polymerase)

Time	Temperature (°C)	Cycles
5 min	95	
30 sec	95	x 40
40 sec	55-62	
2 min	72	
5 min	72	
Hold	4	

Primer pair	Temperature (°C)	Further information
ALMS1 ex 23 for + sfGFP rev;	Annealing: 62.8 for 10 s	Elongation time: 2 min
ALMS1 ex 23 for + ALMS1 ex 23 rev	Annealing: 60.7	Elongation time: 3 min
ALMS1 ex 8 for und rev	Annealing: 62°C	Add 1 % DMSO and 4 µl of Green Buffer (10x) and 0.4 µl dNTP, Elongation time: 1 min
ALMS1 ex 10 for + rev	Annealing: 62°C	Elongation time: 1 min
CEP70 ex 6 for + rev	Annealing: 60.7	Elongation time: 40 sec

6.3.3 Gel electrophoresis

PCR products were separated for up to 40 min at 100 V using agarose gel electrophoresis. A gel of 1 to 2 % was used to separate DNA fragments by their size of 200 bp - ca. 2000 bp. Agarose powder was solved in 1x TBE and mixed with 4 µl Ethidium bromide to detect DNA. (Wörz unpublished Master thesis, 2018 [21])

6.3.4 RNA Isolation

RNA was isolated from hTERT-RPE1 single clone cells after no starvation and three days of starvation by using TriFast (VWR) under the hood. All steps were performed with filter tips, on ice/4 °C and under the hood. Cells were first washed with 5 ml PBS. 1 ml TriFast (VWR) was pipetted onto a 10 cm petri dish, equally dispersed and incubated for 5 min at room temperature and in the dark. Cells were scratched off the plate and transferred into a 1.5 ml Eppendorf tube. 200 µl chloroform was added to separate proteins from the nucleic acid. The mixture was vortexed strongly, followed by a 5 min incubation at room temperature. Samples were centrifuged for 5 min at 12.000 x g at 4 °C. The upper phase, that includes the RNA, was transferred in a new 1.5 ml Eppendorf tube with 500 µl isopropanol to precipitate the RNA. The solution was vortexed strongly, incubated for 10 min on ice and centrifuged for 10 min at 12.000 x g at 4°C. The supernatant was discarded, and the white pellet was washed twice with 1 ml 75 % ethanol with centrifugal steps in between at 12.000 x g at 4 °C for 10 min. The pellet was air dried under the hoof at room temperature until the pellet could be resuspended with 30 µl nuclease-free water and incubated at 56 °C for 10 min at 300 rpm. The RNA concentration of the samples was measured with NanoDrop® ND-1000 Spectrophotometer (PeQLab) and the final concentration of 0.1 µg/µl was calculated for cDNA synthesis. (Woerz *et al.*, under review [3])

6.3.5 cDNA synthesis

All steps for cDNA synthesis were performed with filter tips and at room temperature. The described volume is for one sample. 7 µl nuclease free water, 1 µl hexamer (500µg/ml) and 20µl RNA (0.1 µg/µl) were mixed carefully, incubated at 70 °C for 5 min and quickly transferred onto ice for 5 min. The solution was shortly centrifuged. 10 µl M-MLV RT 5x buffer, 2.5 µl dNTPs (mM), 8.5 µl nuclease-free water and 1 µl M-MLV polymerase (reverse transcriptase) was carefully mixed on ice. Both solutions were now combined by carefully pipetting up and down, followed by a short centrifugal step. CDNA synthesis was performed according to the following incubation steps: 10 min at 23 °C, 50 min at 50 °C and 15 min at 70 °C to deactivate the reverse

transcriptase. CDNA was stored at -20 °C or at -80 °C for long term storage. (Woerz *et al.*, under review [3])

6.3.6 Real-time PCR (qPCR)

The expression level of a gene of interest can be quantified using real time PCR (qPCR). Mastermix with SYBR Green and qPCR conditions are listed in Table 5 and Table 6. The PCR was performed on a BioRad qPCR Cycler (BioRad) with one or three biological replicates. Analysis and quantification were conducted with the corresponding program from BioRad. For a relative quantification of the results, two housekeeping genes, GAPDH (Glycerinaldehyd-3-Phosphat Dehydrogenase) were used as a reference gene due to its constant expression level in cells. ΔCp or ΔΔCt was calculated. Finally, normalization was conducted to the used control cells. (Woerz *et al.*, under review [3])

Table 5 Pipette schema for real-time PCR (qPCR)

Components	Volume per approach (µl)
2x Sso SYBRGreen MM	5.5
Primer reverse (1:10)	0.5
Primer forward (1:10)	0.5
Nuclease-free water	3.5
Total	10
cDNA	1

Table 6 BioRad cycler condition for qPCR

Time	Temperature (°C)	Cycles
1 min	95	
10 sec	95	x 40
30 sec	60	
5 sec, 0.5 °C/cycle	65	Melting curve
5 sec, 0.5 °C/cycle	95	
Hold	4	

6.4 Cloning of plasmids

6.4.1 Oligonucleotide phosphorylation and annealing

The design of the oligonucleotides (gRNA) was done with the program CCTop and ordered from IDT (integrated DNA Technology). The following pipette schema can be found in Table 7. The annealing of the gRNAs was done using a thermocycler. The conditions used for

phosphorylation and annealing of gRNAs in a thermocycler can be found in Table 8. (Wörz unpublished Master thesis, 2018 [21], Woerz *et al.*, under review [3])

Table 7 Pipette schema of phosphorylation and annealing of oligonucleotides

Components	Volume per approach (µl)
sgRNA top (100 mM)	1
sgRNA bottom (100 mM)	1
PNK buffer	1
T4 PNK	1
ddH_20	6
Total	10

Table 8 Thermocycler conditions for annealing of the oligonucleotides

37 °C	30min
95 °C	5min
Ramp down to 25°C with 5°C per minute	

6.4.2 Restriction enzyme digest and ligation

Restriction enzymes were used to cleave the desired plasmid on their specific recognition site. Afterwards, DNA ligase circulates the plasmid via inserting the desired gRNA. The ligation approach was performed according to the following protocol in Table 9, incubated for 1 h (Table 10) and treated with PlasmidSafe exonuclease (Table 11). (Wörz unpublished Master thesis, 2018 [21], Woerz *et al.*, under review [3])

Table 9 Pipette scheme of cloning sgRNA into PX459

Components	Volume per approach (µl)
pSpCas9-vector (100 ng)	1
Diluted Oligonucleotides (1:100)	2
FastDigest Buffer	2
DTT 10 mM	1
ATP 10 mM	1
FastDigest BbsI	1
T4 Ligase	0.5
ddH_20	11.5
Total	20

Table 10 Ligation incubation reaction

Cycle number	Condition

1-6	37°C for 5 min, 21°C for 5 min

Table 11 Exonuclease reaction pipette scheme

Component	Volume per approach (µl)
Ligation reaction	11
PlasmidSafe buffer 10x	1.5
ATP 10 mM	1.5
PlasmidSafe exonuclease	1
Total	15

6.4.3 Cloning pJET1.2 vector

The CloneJET PCR Cloning Kit was used to introduce the sfGFP and RFP-HA tag sequence into the pJET 1.2/blunt Cloning Vector to generate CT- ALMS1-tagged human cell lines for affinity purification and proximity labeling.

The “Blunt-End Cloning protocol” was used to insert the tag sequences into the pJET1.2/blunt Cloning Vector (50 ng/µl). Table 12 shows the reaction mixture that was prepared on ice. The ligation mixture was shortly vortexed and briefly centrifuged, followed by a 30 min incubation at RT. Afterwards, a transformation can be set up (see 6.4.5). (Woerz *et al.*, under review [3])

Table 12 Pipette scheme for cloning reaction (pJET)

Component	Volume per approach (µl)
2X Reaction buffer	10
Tag sequence	1
pJET1.2/blunt Cloning Vector (50 ng/µl)	1
T4 DNA ligase	1
Nuclease-free water	7
Total	20

6.4.4 Gateway Cloning

Gene-specific primer, containing full-length attb1 and attb2 sequences, were created and purchased from IDT. PCRs and BP clonase (Invitrogen) recombination reactions were performed following the provided protocols (Table 13, Table 14, Table 16). The obtained recombinant product in the entry vector was transformed into *E.Coli* DH5α through heat shock. LR Reaction (Invitrogen) was conducted to clone the DNA fragments into the desired destination vectors (Table 15, Table 16), followed by another transformation into *E.Coli* DH5α. DNA isolation was performed using the Monarch®Plasmid Miniprep Kit (BioLabs) and the PureYield® Plasmid

Midiprep Protocol System (Promega). To confirm successful cloning, purified plasmid DNA was sent in for sequencing (see 6.4.11). (Woerz *et al.*, under review [3])

Table 13 PCR reaction pipette schema for adding attb sites

Components	Volume per approach (µl)
5x HF Buffer	5
dNTP Mix (10 mM)	0.5
Attb1 1:10	1.3
Attb2	1.3
Template (10ng/µl)	1
Phusion Tag Polymerase	0.5
HPLC water	15.4
Total	25

Time	Temperature (°C)	Cycles
2 min	98	
30 sec	96	x 25
40 sec	66	
2 min- 2 min 30 sec	72	
5 min	72	
Forever	16	

Table 14 BP reaction pipette schema and incubation time

Components	Volume per approach (µl)
Vector (pDONR201,100 ng/µl)	1
PCR Product 1st PCR	3
BP Clonase II	1
Total	5

Table 15 LR reaction pipette schema

Components	Volume per approach (µl)
Vector (pEST,100 ng/µl)	1
Midipreped pDONR + Insert (100 ng/µl)	1
LR Clonase I	1
ddH_2O	3
Total	5

Table 16 Incubation procedure for BP and LR reaction

Temperature (°C)	Time per cycler
25	1-4 hrs or ON (depending on the size of the protein of interest)

6.4.5 Bacterial transformation

Chemically competent *E.coli* DH5α or *ccdB survival* were used for plasmid amplification. 1 to 5 µl plasmid DNA was mixed with 50 µl competent *E.coli or* 25 µl *ccdB survival* bacteria. After 45 min on ice, a heat shock for 45 sec at 42 °C was conducted. The transformed bacteria were placed on ice for 2 min, before adding 250 µl S.O.C medium. Incubation for 60 min at 37 °C with 160 rpm in a shaker incubator was performed. The bacteria cell suspension was plated onto LB agar plates and incubated for 12 to 24 h at 37 °C. Single colonies were transferred into baffled flasks with LB medium and antibiotics (100 µg/ml). It was incubated at 160 rpm, 37 °C in a shaking incubator overnight. (Wörz unpublished Master thesis, 2018 [21])

6.4.6 Bacterial glycerol stock

500 µl 80 % Glycerol and 500 µl competent *E.coli* cell suspension were thoroughly mixed in a cryo tube. The glycerol stock was stored long-term at -80°C. (Wörz unpublished Master thesis, 2018 [21])

6.4.7 Genomic DNA Isolation

To isolate und purify genomic DNA, the short protocol “Tissue DNA Mini Kit” from “PeqGold Tissue DNA Mini Kit” by VWR was used.

First, the pellet of human cell lines was resuspended with 400 µl alkaline lysis buffer, 20 µl proteinase K and 15 µl RNase (20 mg/ml) followed by an incubation for 15 min at 50 °C in a Thermo-Shaker (Universal Labortechnik). Second, the solution was mixed with 200 µl DNA binding buffer and transferred on a DNA binding column. After centrifugation, 650 µl ethanol-containing DNA wash buffer was used twice, before the purified DNA was eluted with 50 µl nuclease-free water. DNA was stored at -20 °C. (Wörz unpublished Master thesis, 2018 [21])

6.4.8 Plasmid DNA purification (Miniprep)

Isolation of plasmid DNA from *E.coli* DH5α was performed with the Monarch® Plasmid Miniprep Kit according to the protocol provided by New England BioLabs® Inc..

All centrifugal steps were performed at 16.000 x g. 1 to 1.5 ml bacterial culture was centrifuged for 30 seconds. The pellet was resuspended carefully using 200 µl resuspension buffer. 200 µl plasmid lysis buffer was added and inverted gently until the solution becomes clear and viscous.

After 1 min incubation, 400 µl plasmid neutralization buffer was added and gently inverted until the color is uniformly yellow and has a precipitated form. This solution was incubated for 2 min and subsequently centrifuged for 5 min to clarify the lysate. Afterwards, the supernatant was transferred onto a spin column and centrifuged for 1 min. The silicate membrane was washed once with 200 µl plasmid wash buffer 1 to remove RNA, proteins and endotoxins and centrifuged for 1 min. 400 µl plasmid wash buffer 2 (with ethanol) was added with a subsequent 1 min centrifugation step. The spin column was transferred into a new 1.5 ml Eppendorf tube. 40 µl elution buffer (50 °C) was added onto the silicate membrane and incubated for 1 min. A final centrifugation step for 1 min was conducted. (Wörz unpublished Master thesis, 2018 [21])

6.4.9 Plasmid DNA Purification (high quality)

Isolation of high-quality plasmid DNA from bacteria was conducted according to the manufacturer protocol from ProMega Service GmbH. Thereby, the PureYield™ Plasmid Midiprep system was applied.

First, the overnight culture was centrifuged at 4000 x g for 10 min. The pellet was resuspended with 3 ml resuspension buffer and mixed with 3 ml lysis buffer. After 3 min at RT, 5 ml neutralization buffer was added. The suspension was centrifuged at 12000 x g for 15 min at RT. The supernatant was transferred onto a silicate membrane. Washed with 5 ml endotoxin removal buffer (Isopropanol) and 20 ml ethanol containing washing buffer. 400 - 500 µ nuclease-free water was used for elution of the plasmid DNA. (Wörz unpublished Master thesis, 2018 [21])

6.4.10 Purification of DNA from PCR

PegGold Cycle-Pure Kit by PEQLAB Biotechnologie GmbH, VWR was used to purify PCR products. Thereby, the short protocol “Cycle Pure Kit” protocol was followed. 20 µl PCR product was mixed with 80 µl CP buffer (4 times) and pipetted on a PerfectBind DNA Column. After washing twice with an ethanol-containing washing buffer, the purified PCR product was eluted with up to 40 µl deionized water or elution buffer. (Wörz unpublished Master thesis, 2018 [21])

6.4.11 Sanger sequencing

The constructs were sequenced by the company Eurofins Genomics (https://eurofinsgenomics.eu/de) and Microsynth Seqlab (https://srvweb.microsynth.ch/). Eurofins requirement included a mix of 5 µl purified PCR product or plasmid DNA and 5 µl of the appropriate primer. For sequencing with Microsynth, 3 µl Primer and 9 µl 100 ng/µl DNA (plasmid, PCR product) were required. (Wörz unpublished Master thesis, 2018 [21])

6.4.12 Purification of genomic DNA extraction (QuickExtract™)

Approximately 200 µl cell suspension was centrifuged for 3 min at 500x g. After supernatant was removed, the pellet was resuspended with approx. 200 µl QuickExtract™ DNA Extraction Solution (Lucigen) by vortexing for 15 seconds. The mixture was incubated for 6 min at 65 °C in a Thermo Shaker. Vortexed again for 15 seconds and incubated at 98 °C for 2 min. After cooling down, the extracted genomic DNA was stored at -20 °C until usage. 1 to 2 µl of this DNA was used for a PCR mastermix. (Wörz unpublished Master thesis, 2018 [21])

6.5 Cell culture

6.5.1 Thawing frozen human cell lines

Vials of HEK293T and hTERT-RPE1 cells were thawed at 37 °C and added under a sterile bench into 10 cm petri dishes with 500 ml DMEM – high glucose, FBS (v/v = 10 %) and 100x P/S (10.000 U/ml, v/v = 0,05 %). After cells attached on the surface, the medium was changed with 10 ml standard medium. The cells were grown under constant conditions (37 °C, 90 % humidity, 5 % CO_2) in an incubator. (Wörz unpublished Master thesis, 2018 [21])

6.5.2 Cell lines maintenance: splitting and seeding cells

The cells were splitted two to three times a week under sterile conditions at a confluency of 80 to 95 %. Therefore, cells were washed with 5 ml PBS (Dulbecco's Phosphate-Buffered, Saline, without $CaCl_2$ and without $MgCl_2$) and detached with 0.05 % Trypsin-EDTA (1 ml for HEK293T, 2 ml for hTERT-RPE1) for three to five minutes at 37 °C. 8 to 9 ml warm standard medium was added (total volume 10 ml per 10cm dish). HEK293T were splitted 1:20 or 1:10 and hTERT-RPE1 cells 1:10 or 1:5 for maintenance. Seeding cells were performed by counting cells using 10 µl diluted cell-medium suspension on a TecanReader chip. A TecanReader (Tecan Group AG) calculated cells/ml, which was used for calculating the desired number of cells per 10 cm dish or 24, 12 or 6 well plate. In general, cultured human cell lines were used at or post passage 3 for experiments. (Wörz unpublished Master thesis, 2018 [21])

6.5.3 Freezing of cultured cells

Frozen cells were stored in cryomedium (10 % DMSO in FBS) in liquid nitrogen (-192 °C). Therefore, cells from a 10 cm petri dish were detached before (see 6.4.2) and mixed with standard medium. Cells were transferred into a Falcon and, centrifugation for 3 min at 500 x g. The pellet was resuspended in 4 ml cryomedium and transferred in four PP cryo tubes (1 ml total volume per tube). The freezing procedure was followed in the exact order: 4 °C for 10 min, -20 °C for 60 min, -80 °C overnight and finally stored in liquid nitrogen. (Wörz unpublished Master thesis, 2018 [21])

6.5.4 Insulin treatment of cells

hTERT-RPE1 cells were seeded in a 6 well plate. 100% confluent cells were starved for 48 – 72 hrs with DMEM without supplements. A subsequent insulin treatment (1 µg/ml) for 15 min at 37 °C, 5 % CO_2. Cells were washed with PBS before lysis (see 6.1.1). Lysate was used for western blot (see 6.2).

6.5.5 CRISPR/Cas9 Knock-In of tags in the *ALMS1* gene

To endogenously tag *ALMS1* at the CT different tags with or without linker sequences were designed. CRISPR/Cas9 method was used to insert a 711 bp sfGFP and a 746 bp RFP-HA tag into the *ALMS1* gene in HEK293T cells. Single clones were selected, expanded, and verified first with PCR, gel electrophoresis, followed by Sanger sequencing. Proper tag insertion was verified via immunoprecipitation (IP). (Woerz *et al.*, under review [3])

6.5.6 Transfection of human cell lines

Transfection of hTERT-RPE1 cells to introduce indels was conducted according to the manufacturer protocols (Lipofectamine™ 3000 Reagent Protocol, jetPRIME® transfection reagent Short protocol-DNA transfection). For HEK293T cells, the transfection reagent PEI was used. (Wörz unpublished Master thesis, 2018 [21])

350.000 hTERT-RPE1 or 300.000 HEK293T cells per 2 ml were seeded into wells of a 6 well plate, 80.000 cells/ml in a 24 or 90.000 - 100.000 cells/ml in a 12 well plate before transfection. The cells were transfected after 6 h at a confluency of 60 - 70 %. (Wörz unpublished Master thesis, 2018 [21])

6.5.6.1 Lipofectamine 3000

Lipofectamine™ 3000 reagent and DMEM were mixed. Plasmid-DNA and P3000 Reagent were transferred to new DMEM. Subsequently, the diluted Lipofectamine™ 3000 reagent was transferred to the diluted plasmid DNA and incubated for 10 min at RT. The whole DNA-lipid complex solution was transferred dropwise onto the cells and incubated for 48 - 72 h at 37 °C, 5 % CO_2. Table 17 shows the used plasmid-DNA concentration and volumes. (Wörz unpublished Master thesis, 2018 [21], Woerz *et al.*, under review [3])

Table 17 Transfection pipette scheme with Lipofectamine3000

Culture plates	Cell number	DMEM (high glucose) without nFBS and P/S) (µl)	Lipofectamine® 3000 Regent per well (2µl/µg)	P3000™ Regent per well (2 µl/µg)	DNA concentration in total [ng]
6 well	300.000-	2x 125	5	2	1000

	350.000				

6.5.6.2 JetPRIME®

The transfection reaction was conducted according to the manufacturer protocol “jetPRIME® transfection reagent Short protocol - DNA transfection” from Polyplus. jetPRIME® buffer was mixed with 1000 ng DNA for 10 sec and centrifuged. 2 µl/µg jetPRIME® reagent was added, vortexed and centrifuged again. After 10 min incubation, the diluted DNA was transferred dropwise on the cells and incubated for 24 - 48h at 37 °C, 5 % CO_2. An overview of the transfection approach can be found in Table 18.

Table 18 Transfection with jetPRIME- overview

Culture plates	Cell number	Volume of JetPrime® buffer (µl) per well	Volume of JetPrime® reagent (µl) per well	DNA concentration in total [ng]
6 well	350.000	200	2	1000

6.5.6.3 PEI transfection

HEK293T cells were transfected with PEI (in-house made). PEI was mixed with the appropriate amount of DNA and incubated for 10 min before pipetting the whole solution dropwise onto the cells. The amount of used PEI and DNA can be seen in Table 19. The cells were incubated for 48 - 72 h at 37 °C, 5 % CO_2. (Woerz *et al.*, under review [3])

Table 19 Transfection with PEI-overview

Culture plates	Cell number (Cells/ml)	Volume of PEI (µl)	DNA concentration in total [ng]
14 well	Approx. 4 Mio	1000	8000

6.5.6.4 Knockdown of CEP70 using JetPRIME

HTERT-RPE1 control and KO cells were used at a 50 % cell density for CEP70 knock-down. Customized siRNAs were purchased from IDT. The manufacturer protocol “jetPRIME® transfection reagent Short protocol – siRNA transfection” from Polyplus was followed. An overview of used volumes can be seen in Table 20. The approach is described in 6.5.6.2 and the cells were incubated for 24 h - 72 h. (Woerz *et al.*, under review [3])

Table 20 CEP70 knockdown procedure using siRNA and JetPrime

Culture plates	Cell number	Volume of JetPrime® buffer (µl) per well	Volume of JetPrime® reagent (µl) per well	siRNA concentration in total [ng]

12-well	150.000	100	3	152-762
6-well	300.000	200	4	306-1524

6.5.7 Antibiotic selection of transfected human cell lines

Transfected cells were gained by antibiotic selection with puromycin. The desired concentration per human cell line and incubation time can be found in Table 21. Puromycin treated cells were stored in the incubator at 37 °C, 5 % CO_2. Due to an intrinsic puromycin resistance of hTERT-RPE1 cells, a higher puromycin concentration was used. (Wörz unpublished Master thesis, 2018 [21], Woerz *et al.*, under review [3])

Table 21 Conditions for Puromycin treatment of transfected cells

Human cell lines	Puromycin concentration (µg/µl)	Incubation time (d)
HEK293T	2-3	3
hTERT-RPE1	35-40	5

6.5.8 Generation of single clones

All steps for single clone selection were performed under a sterile bench. 1.000-4.000 cells per 100 µl were seeded in a 14 cm dish with 20 ml standard medium. Cells were then incubated for three to five days. Single colonies were washed with PBS and slightly detached with diluted 0.05 % trypsin (1:20 for HEK293T or 1:10 for hTERT-RPE1 cells) in PBS. Single clones were picked using a microscope (Zeiss) and added in a 24 well plate with 0.5 ml DMEM. The cells were expanded until freezing. DNA was extracted (6.4.12) and used for indel verification (6.4.12). (Wörz unpublished Master thesis, 2018 [21], Woerz *et al.*, under review [3])

6.5.9 Proliferation assay- Crystal violet

The Crystal Violet Assay was used to investigate the proliferation characteristics of human cell lines with their viability.

7.000 cells/per well of 24 well plates were seeded in triplicates on day zero. The following steps were performed under unsterile conditions. 0.5 ml of 0.2 % crystal violet (CV, Sigma Aldrich) in 20 % ethanol per well were carefully added to fixate and stain the cells at 6 hrs, 24 hrs, 48 hrs and 72 hrs after plating. Wells were washed 3 times with PBS to excess unbound dye. The 24 well plates were air dried at least ON. 1 ml 10 % acetic acid/ well was added to the air-dried wells to solubilize the stain by shaking with 200 rpm for 20 min at RT. The crystal violet absorption is determined using TecanReader at a wavelength of 585 nm. Excel (Microsoft, 2016) was utilized to compute the proliferation rate. (Woerz *et al.*, under review [3])

6.6 Localization studies

6.6.1 Immunofluorescence staining

Cells were plated onto autoclaved coverslips in a 12 well plate for localization studies and incubated for 48 - 72 h at 37 °C, 5 % CO_2. Single clones of transfected hTERT-RPE1 and HEK293T cells were carefully washed with PBS and starved with starvation medium for 48 hrs to 72 hrs (hTERT-RPE1) or less than 1 day (HEK293T) to induce cilia assembly. The following steps were conducted at RT and under non-sterile conditions. Furthermore, it was crucial to keep the coverslips moist. (Wörz unpublished Master thesis, 2018 [21])

Cells were fixated with 4 % PFA for 15 min or/and with -20 °C 100 % methanol for 5 min. The coverslips/cells were washed twice for 5 min with PBS and transferred with the cell side down onto a PBS drop on a parafilm in a humidity chamber for another 5 min. Cells were permeabilized for 5 min with 50 µl 0.3 % PBST (Triton) and blocked with 50 µl Normal Goat Serum (10 % NGS, 1 % BSA in 0.1 % PBST) or 1 - 5 % BSA (in PBS). 50 µl primary antibody (in NGS or BSA; see 5.12.1) was incubated for 1 h at RT or overnight at 4 °C. Cells were washed 5x times for 5 min with PBS before and after the 1 h incubation step with 50 µl secondary antibody (1:350 Alexa anti-mouse and rabbit in PBS; see 5.12.2). DNA was stained with 30 µl DAPI (1:10.000) for 5 min. Cells were washed twice for 5 min with PBS. The coverslips were once washed with A. bidest and were fixed (cell side downwards) onto a microscope slide with Fluoromount-G® (SouthernBiotech). The microscope slides were kept at 4 °C in the dark. The Zeiss Axio Imager Z1 ApoTome microscope (Zeiss) with AxioCam MRm camera and 40× (NA 1.3) and 63× (NA 1.4) oil immersion objective lenses was used to get images. Images were gained as Z-stacks and further processed and analyzed with Zeiss ZEN 3.0 Blue Edition. (Wörz unpublished Master thesis, 2018 [21], Woerz *et al.*, under review [3])

6.6.2 Ciliary length and ciliation measurement

To determine the ciliary length and ciliation, three biological replicates with four technical replicates were included. Ciliary staining was performed using ARL13B, while nuclei were stained with DAPI. Ciliary length and ciliation measurement was conducted either by hand or by using automated image analysis with the plugin ALPACA 1.0.1 [123] for Fiji [124]. The statistical analyses were conducted using unpaired Welch t-test (GraphPad Prism 5 software), considering unequal variances. Three asterisks indicate p-value < 0.001. The error bars represent mean with SD. (Woerz *et al.*, under review [3])

6.6.3 Intensity measurement

Intensity measurement was either performed by hand using Zen software (Zen blue) or automated using Fiji program. First the integrated density, derived from the mean intensity of the desired staining and the area was calculated. Furthermore, the mean intensity of the background and area were multiplate and subtracted from the integrated intensity to calculate the CTCF value. Analysis was conducted using Anova (Tukey) (GraphPad Prism 5 software). Error bars presents the mean with SD. Three asterisks indicate *p*-value < 0.001.(Woerz *et al.*, under review [3])

7 Results

The Alström Syndrome (ALMS, AS, OMIM #203800) is a rare multi-systemic autosomal-recessive disease, that affects individuals in early childhood. More than 300 mutations in the *ALMS1* gene are identified, that causes a variety of symptoms, such as the loss of vision during school age. Since 1959, where the disease was first described in three children by Carl-Henry Alström, the underlying molecular mechanism of this disease is still elusive.

New advances in research, such as the CRISPR/Cas9 method, made it possible to investigate the *ALMS1* gene by introducing indels (insertion, deletion) and study the native and mutated ALMS1 protein on a physiological level. The experimental workflow of this study is depicted in Figure 5. It shows the protein complex and phenotypic analysis to identify and investigate the interactome of ALMS1 and its role in cilia biology. By combining these two methods it is possible to connect probable protein interaction with an occurring phenotype and exclude coincidences. For protein complex analysis, tags were inserted into the C-terminal (CT) end of the *ALMS1* gene in HEK293T cells using CRISPR/Cas9 mediated homology-directed repair (HDR). Endogenously tagged *ALMS1* single clones were further used for protein complex analysis using liquid chromatography coupled to mass spectrometry (LC-MS/MS) to identify the ALMS1 interactome. Potential ALMS1 interactors were validated either with protein complex analysis and/or phenotypic analysis, such as the centrosomal protein 70 kDa (CEP70). Thereby, CEP70 was fused to a N-terminal Strep/Flag tag (NSF-CEP70) and used for protein complex analysis.
For phenotypic analysis, CRISPR/Cas9 mediated ALMS1 knock-outs (KO) in hTERT-RPE1 cells were generated. These cells and a control were then used for validation of potential ALMS1 interactors identified by proteomic analysis as well as to investigate BB, cilia and cilia-related functions and morphology. Therefore, localization studies, mRNA level and/or protein level analysis were applied to decipher the role of ALMS1 in cilia biology.

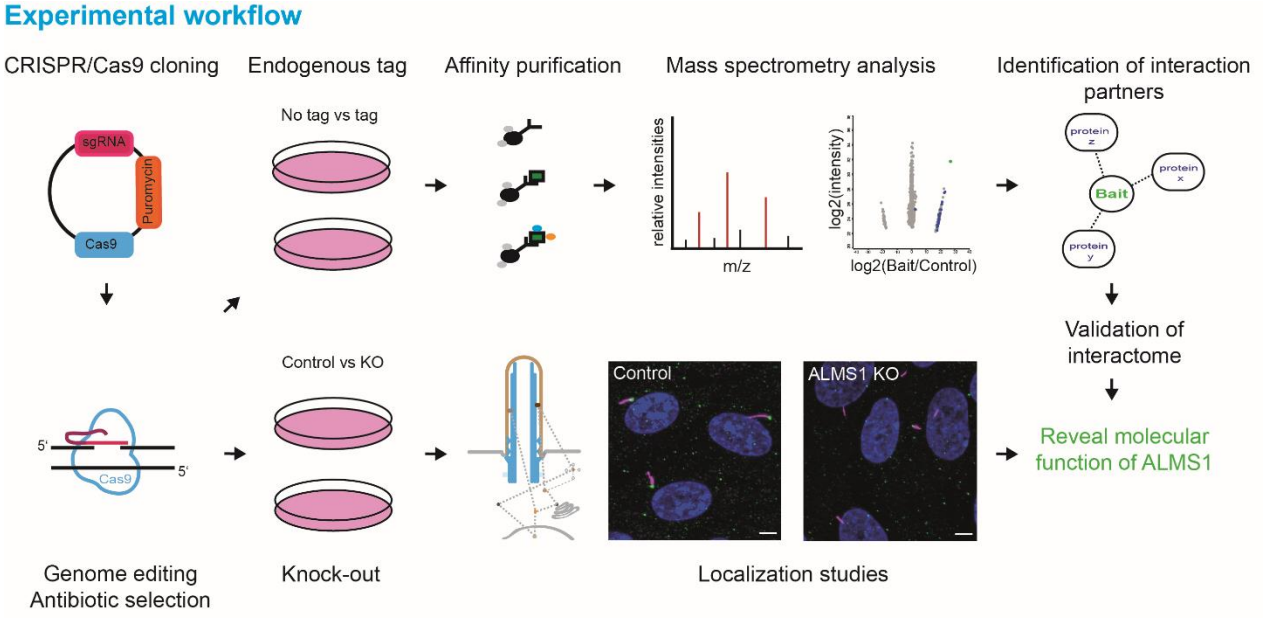

Figure 5 Schematic experimental workflow
This overview presents the experimental workflow including protein complex and phenotypic analysis. CRISPR/Cas9 plasmids containing sgRNA targeting specific regions of the *ALMS1* gene were used for genome editing to create knock-outs (KO). Additionally, an insertion of a desired sequence, such as sfGFP tag, on endogenous level can be performed by combining sgRNA and a repair construct. After antibiotic selection, cells were verified by Sanger sequencing. Cells harboring a protein tag were further used for immunoprecipitation (IP), followed by mass spectrometry and database dependent analysis to identify potential interaction partners of ALMS1. Localization studies of ALMS1 KO and control cells were performed to identify the role of ALMS1 in cilia biology. The combination of potential interaction partners and an observed phenotype enables the generation of hypotheses regarding an unknown protein function, facilitating further investigation. Figure was reproduced and modified after Wörz unpublished Master thesis from 2018 [21].

7.1 Generation of ALMS1 deficient human retinal epithelial cell lines

Cas9 mediated *ALMS1* KO in retinal pigmented epithelial cells (hTERT-RPE1) were generated to investigate the role of ALMS1 in cilia biology. The plasmid PX459 with specific sgRNAs targeting exons (ex) 8 and 10 were used single and simultaneously for transfection, followed by puromycin selection and single clone selection, as described before [125]. Extracted DNA was used for amplification of the region of interest via PCR and verified by Sanger sequencing. Indels, that contain base pair (bp) insertion and/or deletion were identified (Table 22, Figure 6).

In one single clone, a GG deletion occurred in ex 8 (c.7383_7384delGG, p.Glu3462Argfs*7), while in another single clone a T insertion in *ALMS1* ex 10 (c.8533_8534insT, p.Ser2846fs*) was introduced. By combining two sgRNAs, mutant cells harboring two mutations were generated. One single clone showed a homozygous 14 bp deletion in ex 8 and an A insertion in ex 10 (c.7370_7384del14, p.Asp2458Argfs*7,c.8535_8536insA, p.Ser2846Lysfs*38). The second single clone harbors a G insertion in ex 8 and heterozygous 199 bp insertion in ex 10 (p.Glu2462Glyfs*8, p.Ser2846Argfs*10) (Table 22, Figure 6).

All presented ALMS1 KOs led to frameshift mutations resulting in a predicted early stop codon. Therefore, these generated ALMS1 KOs, especially the ALMS1 ex 8-10 KO 2, were further used to investigate the role of ALMS1 in cilia biology.

Table 22 CRISPR/Cas9 mediated KO in *ALMS1* gene in human cells
HTERT-RPE1 cells transfected with CRISPR/Cas9 plasmid without sgRNA showed no alteration in the *ALMS1* gene and is therefore used as a control. Several KOs in the *ALMS1* ex 8 and/or ex 10 are created, leading to frameshift mutations and a predicted early stop codon. HGSC nomenclature version 2005 was used [126]. Ex = exon.

ALMS1 targeted region	**Induced indel**	**Mutation nomenclature**	**Name for simplicity**
Cas9 empty	No alterations	-	Control
ALMS1 exon 8	GG deletion leading to a frameshift mutation with an early stop codon	c.7383_7384delGG p.Glu3462Argfs*7	ALMS1 ex 8 KO
ALMS1 exon 10	T insertion leading to a frameshift mutation with an early stop codon	c.8533_8534insT p.Ser2846fs*	ALMS1 ex 10 KO
ALMS1 exon 8 and *ALMS1* exon 10	14 bp deletion in exon 8 and A insertion in exon 10 leading to frameshift mutations with early stop codons	c.7370_7384del14, p.Asp2458Argfs*7 c.8535_8536insA, p.Ser2846Lysfs*38	ALMS1 ex 8-10 KO 1
ALMS1 exon 8 and *ALMS1* exon 10	G insertion in exon 8 and 199 bp insertion in exon 10 leading to frameshift mutations with early stop codons	c.7382_7383insG p.Glu2462Glyfs*8; c.8536_8537ins199 p.Ser2846Argfs*10	ALMS1 ex 8-10 KO 2

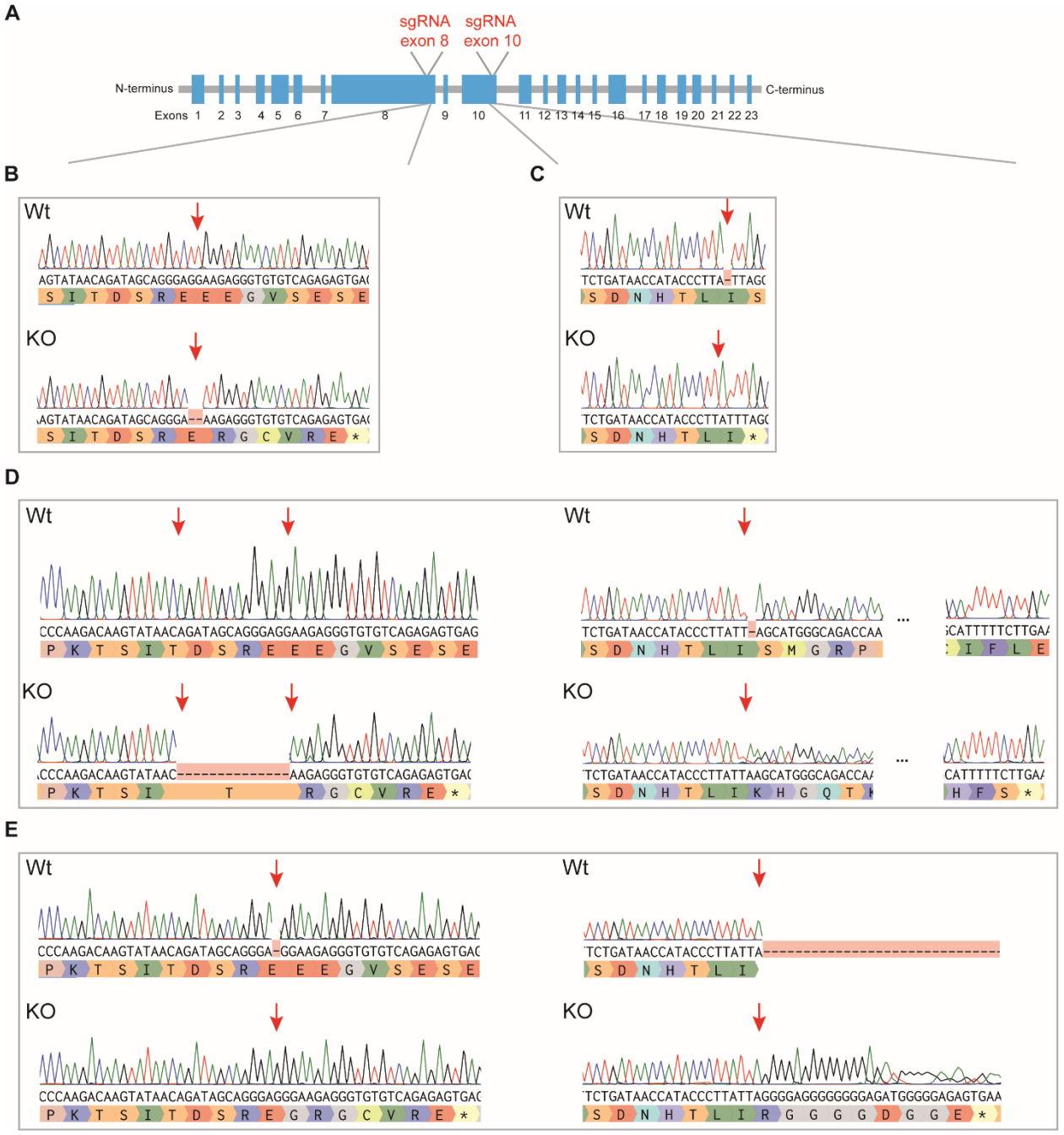

Figure 6 Verified CRISPR/Cas9 induced indels in the *ALMS1* gene in human retinal epithelial cells

A, A simplified schema of the *ALMS1* gene harboring 23 exons is presented. CRISPR/Cas9 mediated *ALMS1* KOs were generated in *ALMS1* ex 8 and/or *ALMS1* ex 10, indicated by two exon-specific sgRNAs.

B, An electropherogram of hTERT-RPE1 *ALMS1* native sequence (top panel) and an CRISPR/Cas9 mediated *ALMS1* ex 8 KO with their respective nucleotide and amino acid sequences are depicted. A homozygous GG deletion was introduced, leading to a frameshift mutation and an early stop codon (*) (c.7383_7384delGG, p.Glu3462Argfs*7).

C, A CIRPSR/Cas9 mediated *ALMS1* ex 10 KO single clone harboring a homozygous T insertion, leading to a frameshift mutation with an early stop codon (*) (c.8533_8534insT, p.Ser2846fs*). *ALMS1* wt sequence is depicted on the top panel, while *ALMS1* KO sequence on the lower panel.

D, By combining two sgRNAs a *ALMS1* KO in ex 8 and ex 10 in the same cells were verified. In *ALMS1* ex 8 a 14 bp deletion occurred (c.7370_7384del14, p.Asp2458Argfs*7), while an A insertion was introduced in *ALMS1* ex 10 (c.8535_8536insA, p.Ser2846Lysfs*38).

E, Another single clone with indels in *ALMS1* ex 8 (c.7382_7383insG, p.Glu2462Glyfs*8) and ex 10 (c.8536_8537ins199, p.Ser2846Argfs*10) was verified by Sanger sequencing.

On the top panels, the *ALMS1* native sequence of ex 8 or ex 10 are presented throughout A-C. Red arrows indicate the region, where indels occurred. Overview was created with Benchling [Biology Software], 2023, retrieved from https://benchling.com. Figure was modified and adapted after Woerz *et al.*, under review [3].

7.2 ALMS1 loss in hTERT-RPE1 single clones show variances in ciliary length

To further verify CRISPR/Cas9 mediated ALMS1 KOs, immunofluorescence staining was conducted. The ciliary marker, ARL13B, and the basal body/centrosomal protein ALMS1 were used for co-immunostaining. ARL13B is a small GTPase, that can be found on the ciliary membrane and plays an essential role in ciliogenesis and in Sonic Hedgehog signaling [35]. Here, ARL13B was used to visualize cilia, to show ALMS1 localization at cilia and to further identify changes in ciliary length upon ALMS1 loss.

In three out of four ALMS1 KO cells, including ALMS1 ex 10 KO and ALMS1 ex 8-10 KO 1 and 2, no localization of ALMS1 at the basal body of cilia was detected (Figure 7). In contrast, the ALMS1 ex 8 KO showed a reduced localization of ALMS1 at the BB, hinting towards a truncated ALMS1 protein with normal looking cilia compared to the control (Figure 7, right panel). To identify a potential defective ARL13B transport to the ciliary membrane resulting in shorter cilia, another ciliary marker, the acetylated tubulin was co-stained with ARL13B. Acetylation of tubulin is a post-translational modification of tubulins, regulating primary cilia and marking microtubule structures, such as the axoneme of cilia and the cytoskeleton of cells [127,128]. Acetylated tubulin showed also shorter cilia, with no difference in acetylated tubulin signal in control and ALMS1 ex 10 and ex 8-10 KO 1 and 2 cells (Figure 7).

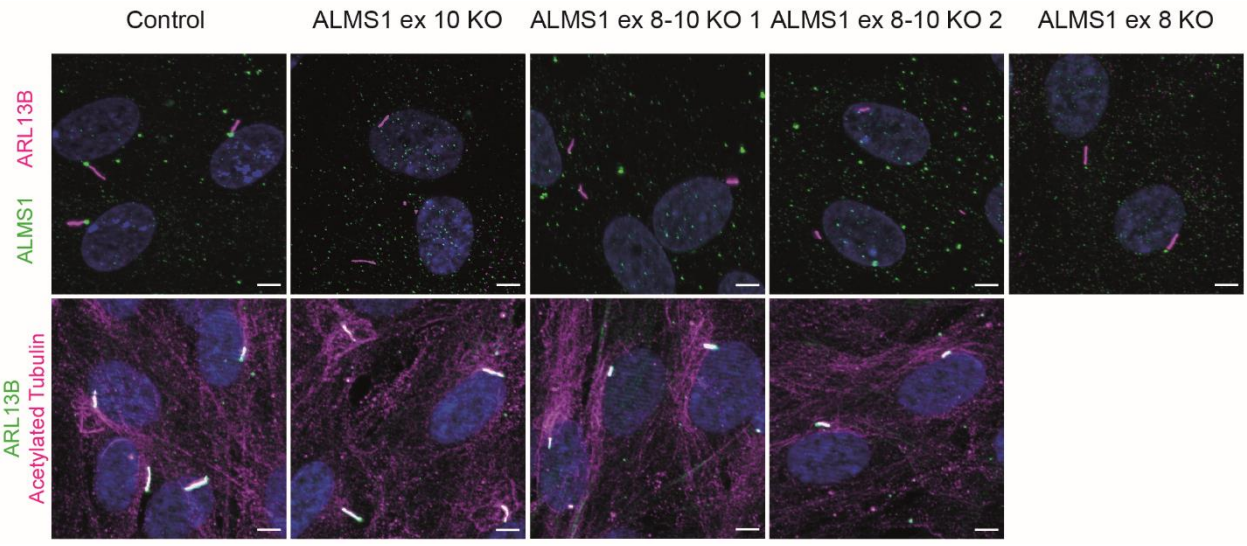

Figure 7 CRISPR/Cas9 mediated ALMS1 loss in hTERT-RPE1 cells
The picture shows from left to right, the CRISPR/Cas9 control (Control),the ALMS1 ex 10 KO, the ALMS1 ex 8 KO and 10 KO 1, and KO 2. ARL13B (magenta, green) and acetylated tubulin (magenta) were used as ciliary marker. ALMS1 and the centrosomal protein CEP250 are depicted respectively in green. Scale bar measures 5 µm. Figure was taken and modified after Woerz *et al.*, under review [3].

Next, ciliary length and ciliation were investigated with three biological replicates to identify a role of ALMS1 in cilia formation. Therefore, the ciliary marker ARL13B was used for measurements. In previous studies, significant variations in ciliary length between ALMS1 knockdown or KO models and ALMS-patient derived fibroblasts compared to controls were revealed [16,18,66,117].

In a first experiment, cells were starved for three days, and ciliary length was determined by hand due to high fluorescent background. 645 cilia were counted and measured for control, 681 cilia for ALMS1 ex 8 KO, and 476 cilia for ALMS1 ex 10 KO. Analysis was conducted using GraphPad Prism5 and an unpaired t-test with Welch's correction. While ALMS1 ex 8 showed no difference in ciliary length (ALMS1 ex 8 KO: $t(1309) = 0.1096$, $p = 0.9127$), ALMS1 ex 10 KO exhibit mild but significantly longer cilia (ALMS1 ex 10 KO: $t(969) = 5.877$, $p < 0.0001$) compared to the control cells. Furthermore, ALMS1 ex 10 KO harbors longer cilia (ALMS1 ex 10 KO: $t(969) = 6.142$, $p < 0.0001$) as ALMS1 ex 8 KO cells (Figure 8 A left panel). The mean of ciliary length of ALMS1 ex 8 KO was 4.035 µm ± 0.04388, of ALMS1 ex 10 KO 4.494 µm ± 0.06052 and of control 4.042 µm ± 0.04749. The ciliation was conducted by counting nuclei per cilia. There was a mild, but significant difference between the control (82.50 % ± 1.848) and ALMS1 ex 8 KO (71.75 ± 3.544), while ALMS1 ex 10 KO (59.25 % ± 2.839) showed a significant decrease in ciliation ($p < 0.001$) compared to the control and a mild decrease to the ALMS1 ex 8 KO cells (Figure 8 A right panel). With these results, ALMS1 ex 8 KO was excluded from this study and only KOs harboring a complete loss of ALMS1 were further investigated.

In a later experiment, cells were starved for two days and ciliary length measurement was performed using ALPACA (Accumulation and Length Phenotype Automated Cilia Analysis) [123]. 905 cilia were counted in control cells, 535 cilia for ALMS1 ex 8-10 KO 1 and 549 cilia in ALMS1 ex 8-10 KO 2 cells and analyzed using unpaired t-test with Welch's correction. ALMS1 KOs showed mild but significantly shorter cilia (ALMS1 ex 8-10 KO 1: $t(1384) = 10.68$, $p < 0.0001$; ALMS1 ex 8-10 KO 2: $t(1445) = 17.11$, $p < 0.0001$) compared to the control cells (Figure 8 B right panel). The mean of ciliary length of ALMS1 ex 8-10 KO 1 was 2.805 µm ± 0.02982 and 2.562 µm ± 0.02653 for ALMS1 ex 8-10 KO 2 cells, while the mean of control cells was 3.272 µm ± 0.03188 µm. Furthermore, the number of cilia in relation to the number of nuclei was counted (ALMS1 ex 8-10 KO 1: $t(18) = 3.489$, $p < 0.0026$); ALMS1 ex 8-10 KO 2: $t(20) = 3.927$, $p < 0.0008$), resulting in a significant decrease of ciliation between ALMS1 ex 8-10 KO 1 (68.84 % ± 1.581), ALMS1 ex 8-10 KO 2 (54.91 % ± 3.178) and control cells (68.84 % ± 1.581) (Figure 8 B left panel) (Woerz *et al.*, under review [3]). No significant difference in ciliation was observed between ALMS1 ex 8-10 KO 1 (55.88 ± 3.362) and KO 2 (54.91 ± 3.178).

In addition, the viability and proliferation rate using crystal violet were examined in ALMS1 KO and control cells for 0 hrs, 24 hrs, 48 hrs and 72 hrs. Within the first 48 hrs, no difference in proliferation rate was observed (Figure 8 C). The ALMS1 KO cells showed a mild, yet significant slower proliferation rate (p-value < 0.01, 0.1788 ± 0.05159) at 72 hrs compared to the control (0.2122 ± 0.08163).

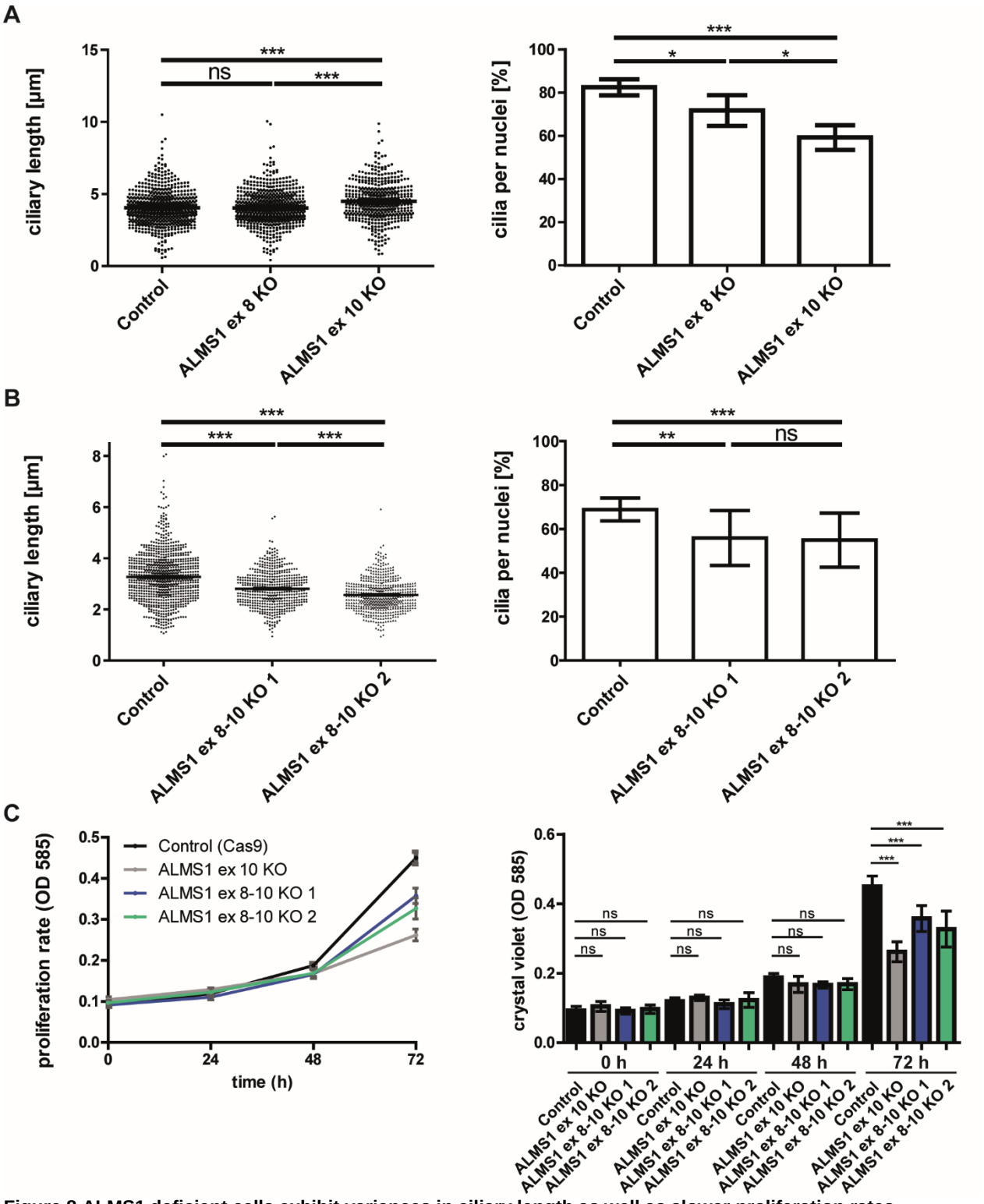

Figure 8 ALMS1 deficient cells exhibit variances in ciliary length as well as slower proliferation rates
A, HTERT-RPE1 control and ALMS1 KO single clones were starved for three days and used to assess the ciliary length. 645 of control, 681 of ALMS1 ex 8 KO and 476 of ALMS1 ex 10 KO are measured with their respectively ciliary length (left in µm) and ciliation (right in %). **B**, Ciliary length was determined after 48 hrs of starvation from 905 cilia for control, 535 for ALMS1 ex 8-10 KO 1 and 549 cilia for ALMS1 ex 8-10 KO 2. On the x-axis the control and the ALMS1 KO single clones are depicted. On the y-axis the ciliary length (µm) in the left graph and the ciliation (%) in the right graph is shown.

Analysis of three biological replicates (n=3) with respectively four ApoTOME pictures (magnification 40x) was conducted. An unpaired t-test with Welch's correction test was used. Error bars imply SEM. Ex = exon.
C, Control as well as ALMS1 deficient cells are presented with their proliferation rate at four different time points (0 hrs, 24 hrs, 48 hrs, 72 hrs). n=4.
P- values < 0.001 are indicated by ***, *p*- value < 0.01 by **, and *p*- value < 0.05 by *, and *p*-value > 0.05 are defined not significant (ns). Error bars represent SD. Figure was modified after Woerz *et al.*, under review [3].

As ALMS1 is a BB protein, centrosomal instability upon ALMS1 loss might lead to ciliary stability, transport and signaling defects, which was further investigated.

7.3 ALMS1 loss shows unaffected γ-tubulin

To decipher any centrosomal/BB defects upon ALMS1 loss, I first investigated the localization of two major components of centrosomes, the γ-tubulin (TUBGCP1 (TUBG1) and TUBGCP2 (GCP2)). Both γ-tubulin proteins are important for microtubule nucleation as well as cell proliferation and linked to brain malformations (TUBG1 (TUBGCP1) OMIM #615412, TUBGCP2 OMIM #617817) [46,129,130]. Again, ARL13B (magenta) was used as a ciliary marker and the basal body was stained with TUBGCP1 (Figure 9 A, upper panel, green) and TUBGCP2 (Figure 9 A, lower panel, green) in control and ALMS1 deficient cells (one biological replicate). Initially, immunostaining revealed no difference due to the differences of the background in all cells. However, quantification of γ-tubulin intensity displayed a high variability of the intensity of both γ-tubulin proteins, despite the background deduction (Figure 9 B, C). Furthermore, TUBGCP1 on protein level showed marginal differences in the intensity (Figure 9 D, E). GAPDH was used as a loading control. These results suggested γ-tubulin upstream of ALMS1 and an ALMS1 independent localization of γ-tubulin to the BB, that was also seen by Knorz *et al.* [18].

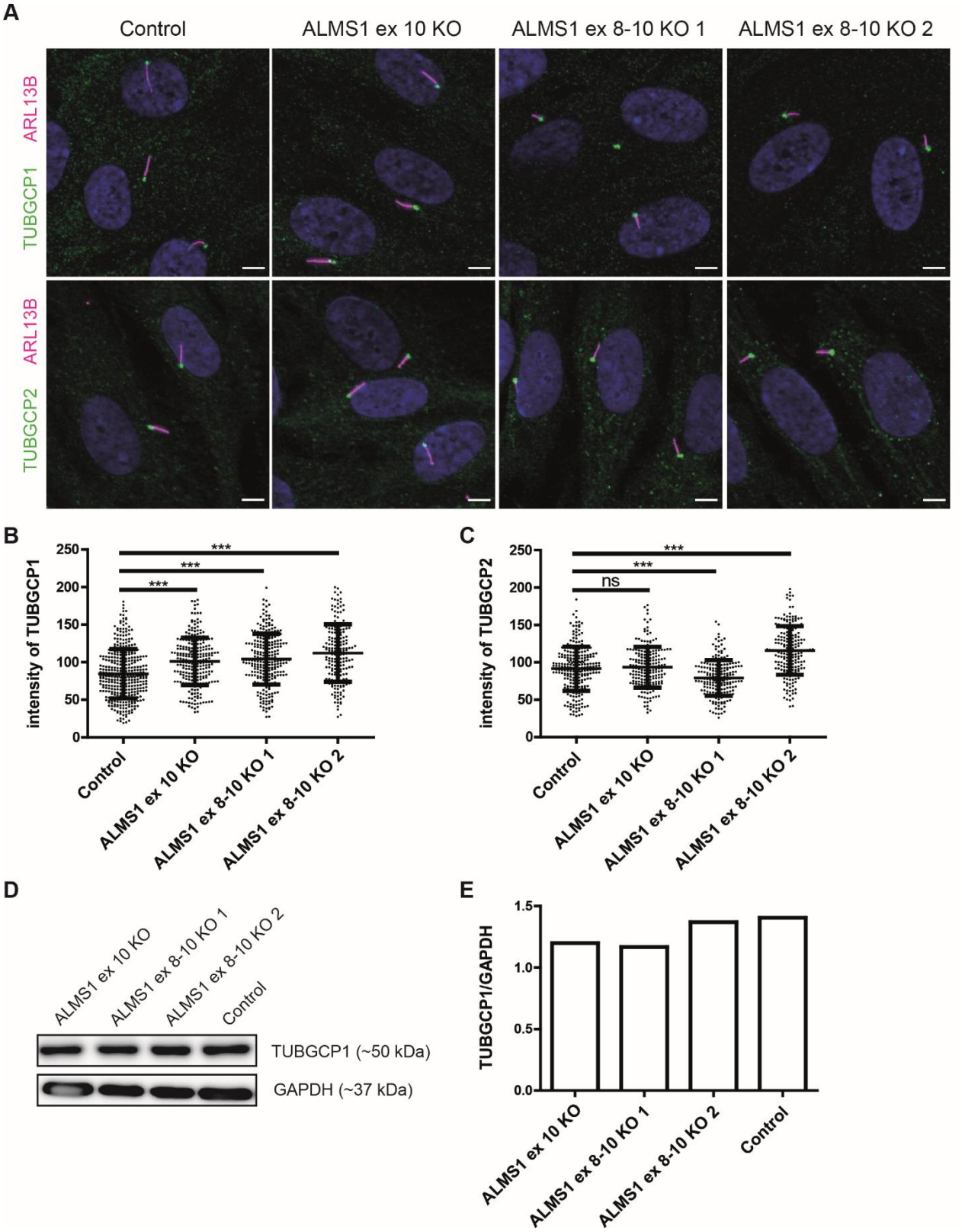

Figure 9 ALMS1 KO cells showed unaffected γ-tubulin

A, Immunostaining pictures of hTERT-RPE1 control cells, ALMS1 ex 10 KO, ALMS1 ex 8-10 KO 1 and KO 2 are presented. TUBGCP1 (upper panel) and TUBGCP2 (lower panel) were depicted in green, while the ciliary marker ARL13B was marked in magenta. Intensity measurement of TUBGCP1 (**B**) and TUBGCP2 (**C**) in control and ALMS1

deficient cells were shown, respectively. Results were visually displayed using a scatter dot blot, where each dot representing one cilium. For statistical analysis, the mean was applied. *P*-values < 0.001 are represented by ***, *p*-value < 0.01 by **, and *p*-value > 0.05 by *, and *p*-value above 0.05 are considered not significant (ns). Error bars represent the SD. Exon = ex. Fiji was used. **D**, Protein level of TUBGCP1 and the house keeping gene GAPDH were reviewed with western blot. **E**, Quantification of TUBGCP1 protein level was performed by measuring its intensity in hTERT-RPE1 control cells, ALMS1 ex 10 KO, ALMS1 ex 8-10 KO 1 and KO 2 (n = 1). The values were normalized against GAPDH (loading control). The mean was used for statistical analysis. Figure was modified after Woerz *et al.*, under review [3].

For further investigation of ALMS1 in cilia biology, one ALMS1 KO (ALMS1 ex 8-10 KO 2) will be shown in microscopy pictures, due to complete loss of ALMS1 in all ALMS1 KO cells.

7.4 ALMS1 deficient cells shows CEP250 decrease

To investigate other centrosomal-related proteins in ALMS1 deficient cells, immunofluorescence staining was performed with one biological replicate, respectively. Cilia were stained with ARL13B. The centrosomal protein CEP250 can be found at the BB in photoreceptors and is responsible for centrosome cohesion during interphase [69]. CEP250 was already linked to ALMS1, whereby CEP250 was reduced in ALMS1-depleted cells [18]. CEP250 staining revealed a high variability in signal while comparing control and ALMS1 deficient cells, whereby it seemed more reduced in ALMS1 deficient cells (Figure 10, left panel, Figure 11).

Further, the investigation also focused on rootletin (CROCC), the primary constituent of the ciliary rootlet. Rootletin plays a crucial role in connecting centrioles and ensuring accurate positioning of the basal body (BB) to facilitate ciliogenesis [131,132]. A similar rootletin localization was observed in ALMS1 KO and control cells, hinting towards an unchanged centriolar linker, that connects the mother and the daughter centriole resulting in proper centrosome cohesion and cilia stability (Figure 10, middle panel). Next, the centriolar satellite member PCM1, which is important for centrosome assembly and function by facilitating localization of centrosomal proteins, such as CEP250 to the BB, was investigated [133,134]. Immunostaining revealed an unaffected centriolar satellite member PCM1, suggesting no functional relation of ALMS1 and PCM1 (Figure 10, left panel).

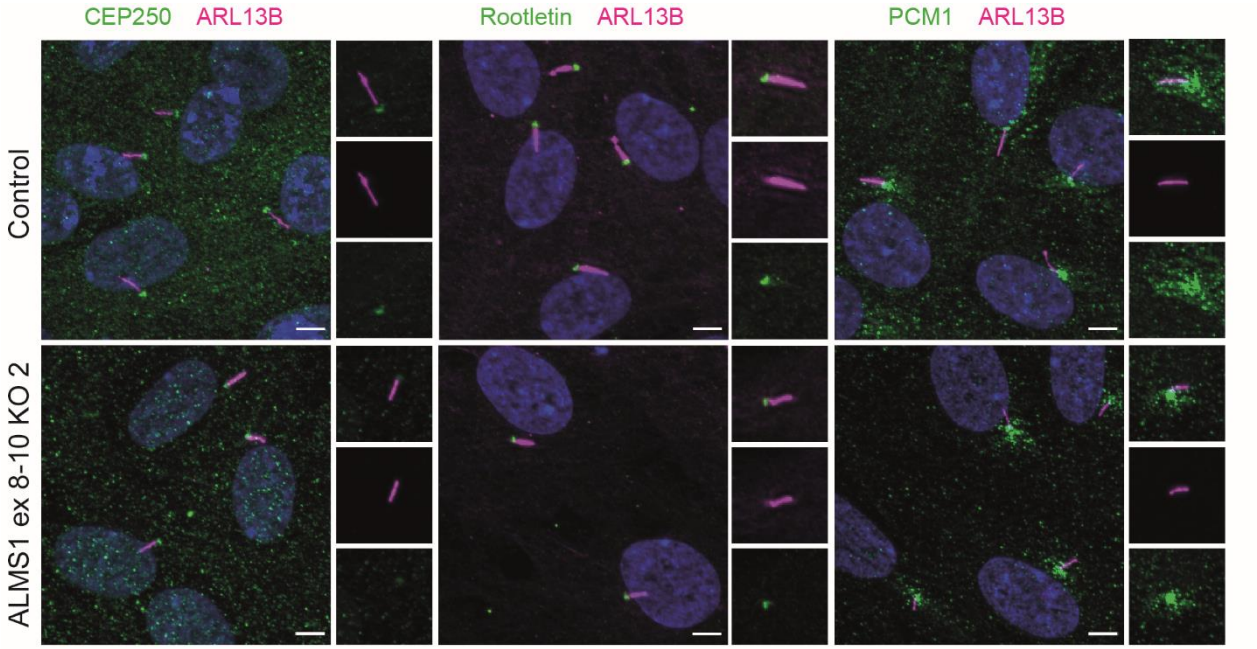

Figure 10 Centrosomal protein investigation in ALMS1 KO cells
Immunofluorescence staining in hTERT-RPE1 control (upper panel) and ALMS1 deficient cells (lower panel) was performed. Co-staining was conducted with ARL13B (magenta) and CEP250 (green, left panel), rootletin (green, middle panel) or PCM1 (green, right panel). DNA was stained in blue. Scale bar marks 5 µm. 40x magnification, ApoTome., n = 1. Figure was modified after Woerz *et al.*, under review [3].

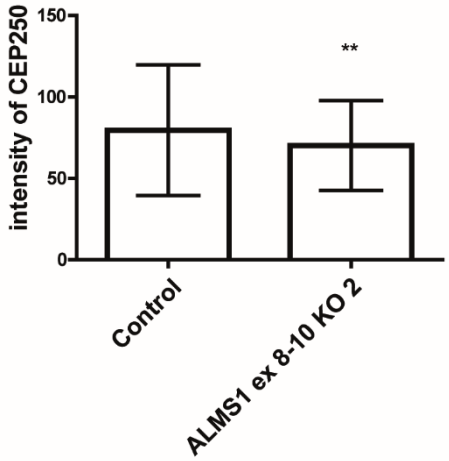

Figure 11 CEP250 is modestly reduced in ALMS1 ex 8-10 KO 2
CEP250 intensity measurement was conducted by hand, using Zen software. Unpaired Welch t-test was applied for analysis (GraphPad Prism 5 software). One biological replicate of control and ALMS1 ex 8-10 KO 2 were used. Two asterisks indicate a *p*-value < 0.01. Error bars imply SD.

7.5 Shorter cilia in ALMS1 deficient cells exhibit compressed transition zone

To investigate a potential role of ALMS1 in ciliary structure, stability and trafficking immunofluorescence staining was conducted. Control, with unaffected ciliary length, and ALMS1 deficient cells harboring shorter cilia were used. ARL13B was again used as a ciliary maker. Polyglutamylated tubulin, which is present at the proximal compartment of cilia, and is important for microtubule stability, was stained with GT335 [135]. Similar signals in control and ALMS1 KO

cells, suggesting comparable ciliary stability despite an ALMS1 loss (Figure 12, left panel). To assess intact ciliary trafficking, the intraflagellar transport protein IFT88, a reliable indicator was examined. ALMS1 deficiency showed no effect on IFT88 signal compared to the control, suggesting an unaffected transport system and related ciliary function (Figure 12, middle panel). Furthermore, Retinitis Pigmentosa GTPase Regulator (RPGR) protein, which localizes primarily to the transition zone, was checked due to its disease relevance in Retinitis pigmentosa (RP), including vision loss. A compressed RPGR was observed in ALMS1 KO cells compared to the control (Figure 12 right panel). The length of RPGR was measured using the plugin NeuronJ for Fiji [124].

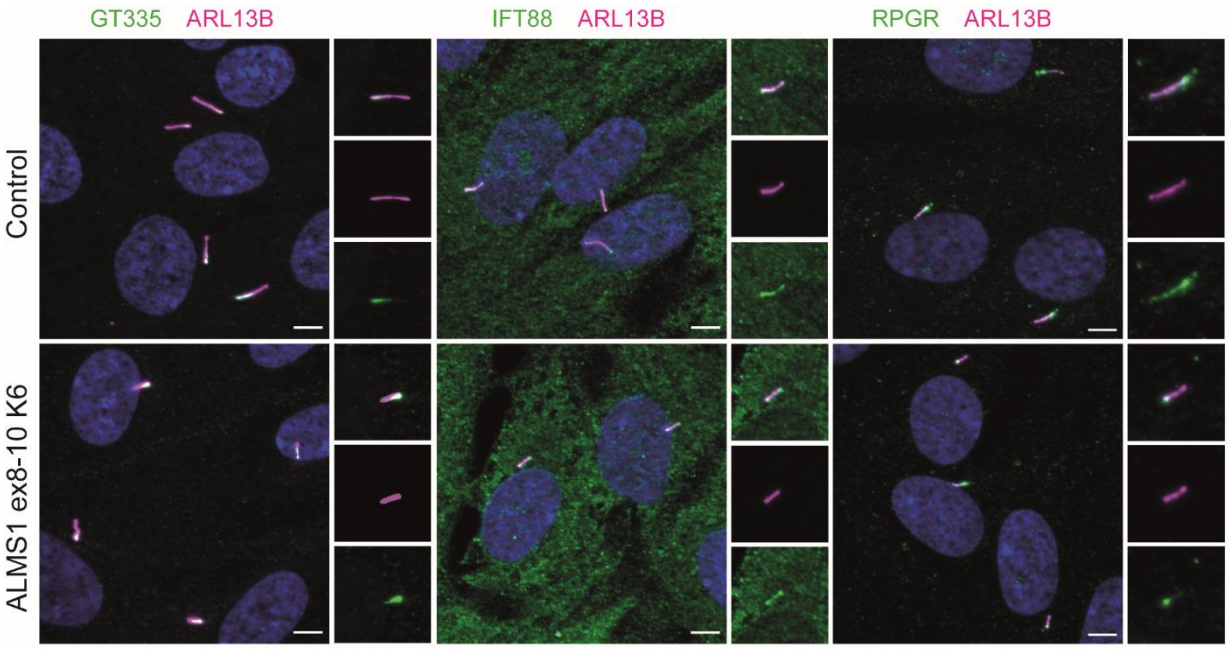

Figure 12 ALMS1 shows compressed transition zone with unaffected polyglutamylated tubulin and ciliary trafficking
Immunofluorescence microscopy pictures visualize cilia with ARL13B (magenta), polyglutamylated tubulin GT335 (green, left panel), intraflagellar transport protein IFT88 (green, middle panel) and transition zone protein retinitis pigmentosa GTPase regulator RPGR (green, right panel) in hTERT-RPE1 control and ALMS1 KO cells. DNA is shown in blue. Scale bar represents 5 µm. One biological replicate is presented. Figure was modified after Woerz *et al.*, under review [3].

ALMS1 KO cells, that harbor shorter cilia (Figure 8) showed a compressed transition zone (2.047 µm ± 0.08260, n=127) compared to the control (3.580 µm ± 0.1056, n=105) (Figure 13). Significance was evaluated using Welch unpaired t-test.

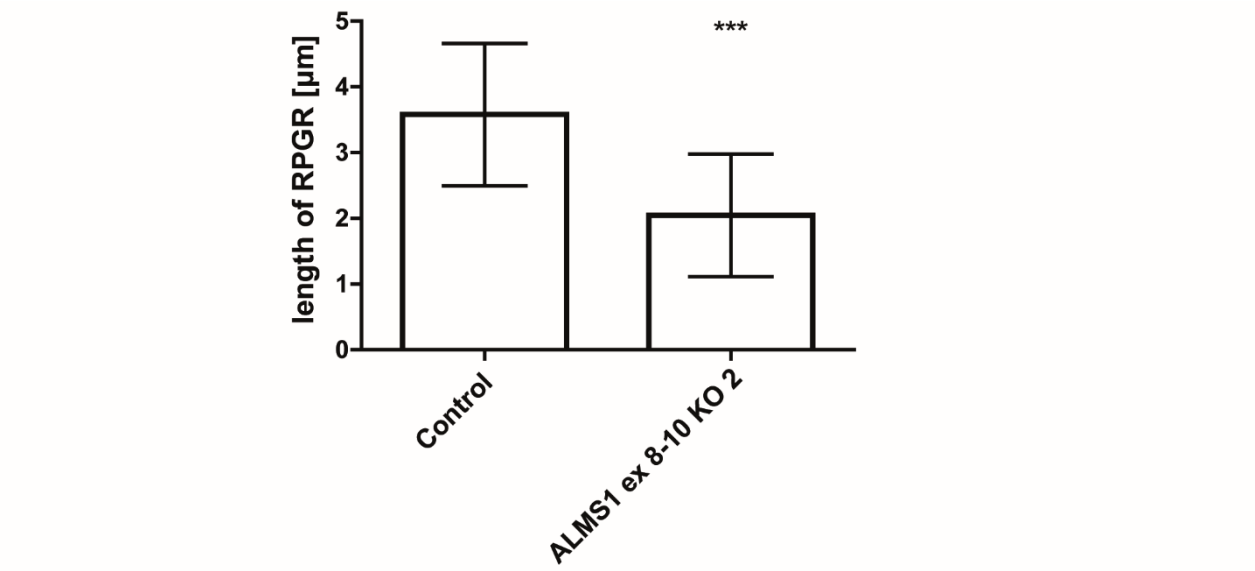

Figure 13 ALMS1 KO cells with shorter cilia show a compressed RPGR
Length measurement of RPGR was performed by hand, using plugin NeuronJ for Fiji [124]. Unpaired Welch t-test was applied for analysis (GraphPad Prism 5 software). One biological replicate of control and ALMS1 KO cells stained with RPGR were compared. Three asterisks indicate a *p*-value < 0.001. Error bars imply SD.

Phenotypical characterization of the generated ALMS1 KO cells revealed, that a loss of ALMS1 does not affect the localization of typical ciliary markers for stability (GT335) and intraflagellar transport (IFT88). However, the transition zone (RPGR) is significantly compressed, in ALMS1 KO cells compared to the wildtype, in addition to the previously described reduced ciliary length(Fig). Both findings definitively suggest a function of ALMS1 in ciliary context and needs to be further investigated.

7.6 Centrosomal and BB localization of endogenously tagged ALMS1

Following the phenotypical characterization of ALMS1 KO cells compared to control cells, the aim was to understand the mechanism leading to the observed phenotype. Therefore, protein complex analysis was conducted to gain novel and comprehensive insights into the involvement of ALMS1 in cilia and cilia-related processes. This approach enabled the identification of interaction partners for ALMS1, which can be further investigated for functional validation in a cilia specific context. Since, proteins usually fulfil their biological role as complex rather than isolated. The identification of protein-protein interactions is crucial to understand their physiological function. Even minor deviation can result in perturbations of the system and potentially cause various diseases. Consequently, a protein complex analysis using liquid chromatography coupled to mass spectrometry (LC-MS/MS) was performed to get further and novel hints towards the molecular function of ALMS1. Previous investigations of ALMS1 (ENSG00000116127) have faced challenges due to its large size with 461 kDa, hindering the study of full-length protein [118,136]. The advent of CRISPR/Cas9 technology has significantly

contributed to our understanding of protein function by enabling the precise tagging of endogenous proteins. Therefore, endogenously tagged *ALMS1* at the C-terminus (CT) were generated using the CRISPR/Cas9 method in human embryonic kidney (HEK293T) cells (Figure 14).

In a first step, specific sgRNA targeting the nucleotide sequence, followed by the PAM sequence before the stop codon of *ALMS1* at the CT end, was designed (Figure 14 A). Therefore, the online tool CCTop [137] was used and the sgRNA chosen, that had the lowest off target effects prediction in other exonic regions (see 10.2, Appendix Table 23). The sgRNA was cloned into the pSpCas9(BB)-2A-Puro vector (PX459, was a gift from Feng Zhang) [125,138] (Woerz *et al.*, under review [3]). For proper superfolder Green Fluorescent Protein (sfGFP, 711 bp long) tag insertion at the CT, a repair construct was created, and subcloned into the pJET plasmid. A benefit of this tag was to visualize tagged ALMS1 at the centrosome and at the BB of cilia and use it for affinity purification. The sfGFP construct harbors homology arms of approximately 355 basepairs (bp), flanked by the sgRNA-targeting sequence for *in vivo* linearization leading to higher repair efficiency [139]. Furthermore, two wobbled base pairs in the sgRNA targeting region were introduced to prevent renewed cutting of Cas9 (Figure 14 B, bold letters). Both plasmids (sgRNA containing PX459 and tag containing pJET) were used simultaneously for transfection of the cells. After antibiotic and single clone selection, an initial screening for a positive tag insertion in the *ALMS1* gene was conducted using purified genomic DNA for PCR and gel electrophoreses (see 10.4). Control cells showed one band at approximately 930 bp, while homogenously tagged cells presented one prominent band at the expected size of approximately 1614 bp (Appendix Figure 37 A). Lastly, Sanger sequencing revealed a successful insertion of the sfGFP tag into the CT end of the *ALMS1* gene (Figure 14 B; see 10.4 Appendix Figure 37 B). Seven homozygously sfGFP tagged ALMS1 single clones and eleven heterozygously sfGFP tagged ALMS1 cells out of 49 single clones were identified (see 10.4 Appendix Figure 37 C).

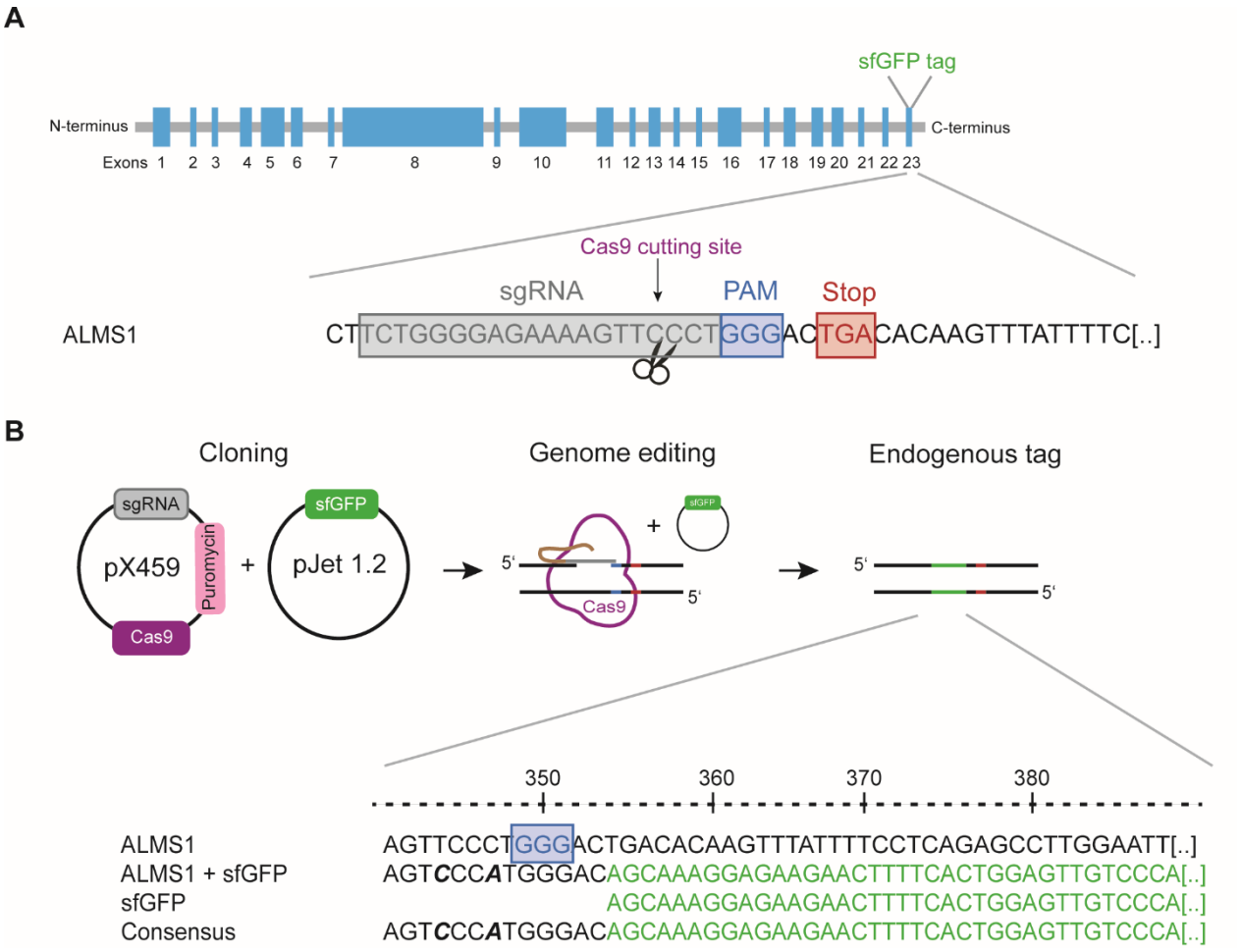

Figure 14 Workflow of CRISPR/Cas9-mediated endogenous tagging of *ALMS1*
A, The upper panel illustrates the *ALMS1* gene with 23 exons (blue) and introns (grey). The desired location for inserting the tag at the C-terminal (CT) end of ALMS1 is indicated. A native ALMS1 fragment is shown with the sgRNA binding site (grey) and PAM sequence (blue) downstream of the stop codon (red). Cas9 cuts (lilac) three nucleotides upstream of the PAM sequence.
B, Tag insertion was facilitated by a simultaneous transfection of CRISPR/Cas9 vector containing the clones sgRNA and a repair construct. The repair construct includes the super folder green fluorescent protein (sfGFP) along with homology arms. Single clones of endogenously sfGFP-tagged ALMS1 were confirmed by Sanger sequencing. Both plasmids are used for genome editing leading to endogenous tagging of ALMS1 (lower panel). The lower panel shows the results of the sequencing, displaying fragments of the ALMS1 native sequence, ALMS1 with the inserted sfGFP sequence, the sfGFP sequence itself, and the consensus sequence.
ROI = region of interest, [..] = continuous sequence. The CT nucleotide sequence of ALMS1 is depicted with the specific sgRNA (grey), PAM sequence (blue) and stop codon (red), Cas9 (lilac), sfGFP (green), puromycin (pink), protospacer (brown). Figure was taken and modified after Woerz *et al.*, under review [3].

Next, I investigated the localization of the sfGFP tagged ALMS1 (ALMS1-sfGFP) at the basal body and the centrosome (Figure 15 A). Therefore, homozygous single clones of untagged ALMS1 and ALMS1-sfGFP were co-stained with the ciliary marker ARL13B and an ALMS1 antibody (Figure 15 B, C). Untagged ALMS1 showed ALMS1 at the BB of ciliated cells (Figure 15 B) and ALMS1-sfGFP localize at the basal body of primary cilia, suggesting that tag insertion does not disturb ALMS1 localization (Figure 15 C) (Woerz *et al.*, under review [3]). Furthermore, ALMS1-sfGFP can be found in mitotic cells, exemplary at the spindle poles in metaphase,

anaphase, and telophase (Figure 15 D-F) (Woerz *et al.*, under review [3]). Taken together, data indicate a successful tag insertion into the *ALMS1* gene in HEK293T cells, while maintaining proper ALMS1 localization at the centrosome and BB, hence provide the ideal system to study ALMS1 interacting proteins.

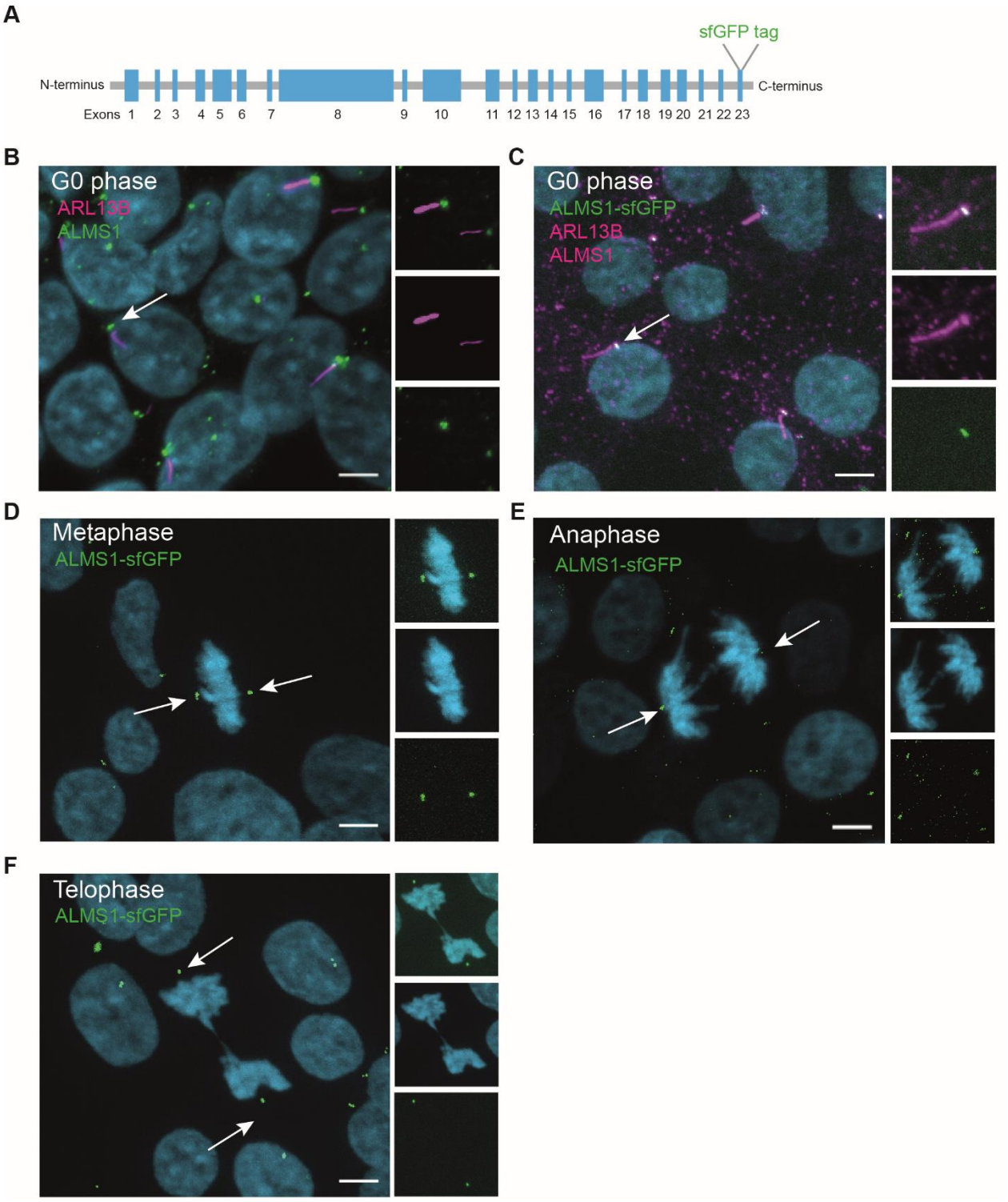

Figure 15 Fluorescent-tagged ALMS1 localizes to the basal body of cilia and to the centrosome during mitosis

A, Schematic overview of the *ALMS1* gene and the inserted sfGFP tag at the C-terminus (CT) of ALMS1 are presented.
B, HEK293T native cells (no tag) were co-stained with the ciliary marker ARL13B (magenta) and the basal body marker ALMS1 (green) antibody. Native ALMS1 localizes at the basal body of cilia (G0 phase). DAPI is depicted in light blue. The scale bar measures 5µm.
C, Endogenous tagged ALMS1-sfGFP (green) localizes at the basal body (magenta) of cilia (magenta) in resting cells (G0 phase). DAPI is depicted in light blue. The scale bar measures 5µm.
D-**F**, ALMS1-sfGFP (green) during different mitosis phases (Metaphase (D), Anaphase (E) and Telophase (F)) are shown. DAPI is represented in light blue. The scale bar measures 5µm.
Figure was taken and modified after Woerz *et al.*, under review [3].

7.7 Endogenous complex analysis revealed a new ALMS1 interactome

Receiving and investigating potential interaction partners of ALMS1 helps to narrow down the (patho-) mechanism of the ALMS1 protein. Therefore, eight biological replicates of ALMS1-sfGFP and control cells were used for protein complex analysis. HEK293T wildtype cells expressing untagged ALMS1 were used as a control, to identify false positive proteins binding to the beads unspecifically. Label free quantification of mass spectrometry (MS) data was conducted by using MaxQuant [140], followed by a statistical evaluation using Perseus [141]. First, proteins only identified by site, potential contaminants and reversed peptide sequences were filtered out of the proteomic dataset. Control and ALMS1-sfGFP replicates were grouped for comparison. The groups were filtered in at least five out of eight samples and should display valid number. Subsequently, missing values were replaced with the value zero for all LFQ intensities. The median values for each group were set and the ratios between specific ALMS1-sfGFP sample and control were determined. Further, the LFQ intensities and calculated ratios were transformed with the log2(x) (Figure 16 A) (Wörz unpublished Master thesis, 2018 [21]). ALMS1 interactors were identified due to enriched proteins with an outlier test significance A < 0.05 (Benjamini-Hochberg FDR < 0.05) and significantly enriched proteins Student's t-test p < 0.05 (Permutation-based FDR < 0.05 or p-value < 0.05) in all samples. Proteins, that are analyzed more stringently with the Permutation-based FDR are grouped into Tier 1, while proteins with a less stringent statistical test (p < 0.05) are included into Tier 2, as done before (Appendix Figure 37 D) [142,143]. Proteins, that are found with both tests were deemed to be specifically enriched in ALMS1-sfGFP samples compared to the control (Woerz *et al.*, under review [3]). The ALMS1 protein was found with a high sequence coverage of 50.6 % in ALMS1 sf-GFP cells (Woerz *et al.*, under review [3]). 32 proteins were grouped into Tier 1 (see 10.7.2 Appendix Table 26). Tier 2 contains in total 79 proteins (Figure 16 B, see 10.7.2 Appendix Table 27). To understand the biological relevance and gain insight into the underlying biological processes of these proteins, the Gene Ontology (GO) enrichment analysis by the Gene Ontology Consortium was applied [144,145] (Woerz *et al.*, under review [3]). By examining the enrichment of ALMS1-associated proteins within cellular components, valuable insights can be

gained into the potential involvement of ALMS1 in centrosomal and basal body function (Figure 16 C). A total of 15 proteins participate in microtubule cytoskeleton function, with nine of them being categorized as centrosomal components and grouped together with ALMS1 (TUBGCP2, CEP170, FLII, DYNC1LI2, TACC3, GNAI3, CEP70, BOD1L1, GSK3B) (Woerz *et al.*, under review [3]). This result suggests that these proteins, including ALMS1 have a shared involvement in the organization and regulation of centrosome, that plays a crucial role in microtubule dynamics and cellular processes such as cell division and intracellular transport (Woerz *et al.*, under review [3]).

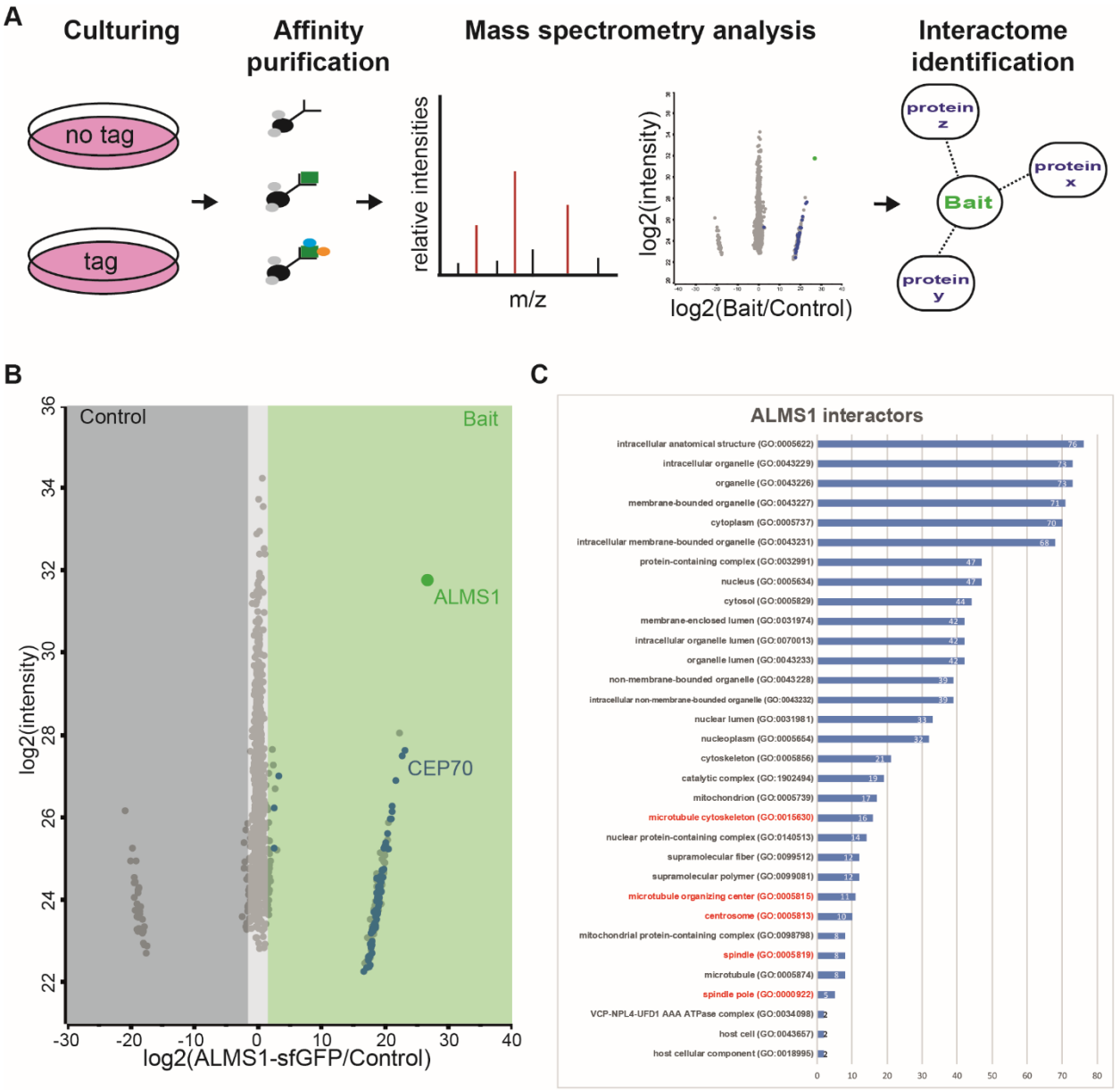

Figure 16 Protein complex analysis identified novel ALMS1 interactors
A, Native HEK239T and ALMS1-sfGFP cells were prepared for affinity purification, with a subsequent mass spectrometry and data dependent analysis with MaxQuant and Perseus. Finally, the ALMS1 network was identified.

B, The scatter plot visualizes on the x axis the ratio of mean ALMS1-sfGFP/mean and the y axis the log_2 intensity. Eight biological replicates of ALMS1-sfGFP and control samples were used for MS and data dependent data analysis, respectively. Proteins, that did not pass the Student's t-test and/or significance A are denoted by grey filled circles. The bait protein ALMS1 is depicted in green, while potential ALMS1 interaction partners are marked in blue (Tier 2).
C, The graph represents cellular processes identified with GO enrichment analysis of ALMS1 interactors using the knowledgebase provided by the Gene Ontology Consortium (http://geneontology.org/) (Woerz *et al.*, under review [3]). The results are sorted based on the number of proteins present in the dataset and are assigned to specific GO categories. Red marked processes include microtubule cytoskeleton and centrosomal/spindle pole function. A detailed overview is deposited in 10.7.2 Appendix Table 28. Figure was taken from Woerz *et al.*, under review [3].

Moreover, the Tier 2 interaction partners were categorized into functional clusters, highlighting their involvement in various cellular process. These processes include cell proliferation, cytoskeletal organization, posttranslational modification, signaling and transport (Figure 17) (Woerz *et al.*, under review [3]). Additionally, the Tier 2 proteins exhibit functions in metabolic processes, mitochondria, autophagy, and gene expression (Figure 17). Notably, we identified a total of seven interactors that have already been associated with cilia biology including HDAC2, TUBGCP2, GSK3B, KLC2, CEP70, GNAS, and STAM [72,146–151]. These results suggest a multifunctional role of ALMS1 in both cellular and ciliary processes, supporting the observation made by Álvarez-Satta in 2015 [17] (Woerz *et al.*, under review [3]).

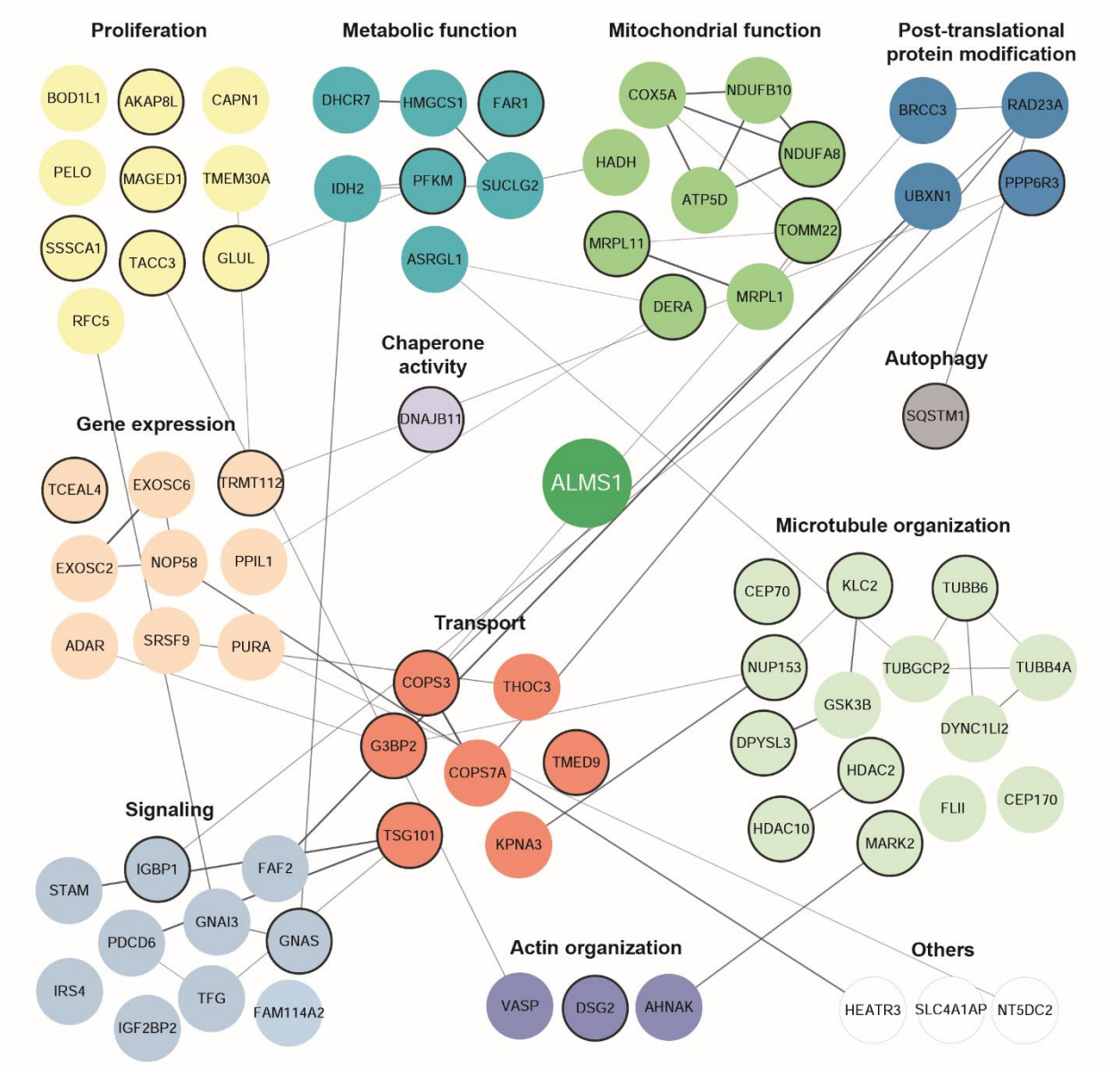

Figure 17 Network of novel ALMS1 interaction partners
A detailed protein network of potential interaction partners of ALMS1 and their respective roles in cellular processes is presented. Proteins within the network are categorized into a stringent Tier 1 (Significance A (Benjamini-Hochberg) FDR < 0.05 and Students t-test $p < 0.05$) and less stringent Tier 2 (Significance A (Benjamini-Hochberg) FDR < 0.05 and Students t-test p-value < 0.05) category. 32 proteins are grouped into Tier 1 (border paint), and additionally 47 proteins in Tier 2 (no border paint). To avoid redundancy, proteins that fulfill multiple functions are listed only once with their primary function, as documented in the UniProt Knowledgebase (using the 2023_02 released version,[152]. The network was constructed using experimental and functional interactions obtained from a curated database utilizing STRING [121]. The resulting network was visualized using Cytoscape [122], providing a comprehensive overview of the ALMS1 interaction network and its associated functions in cellular processes. Figure was taken from Woerz *et al.*, under review [3]

Next, analysis of potential ALMS1 interactors, such as AKAP8L, GSK3B and CEP70 were conducted using ALMS1 deficient cells.

7.8 ALMS1 exhibit no influence on AKAP8L expression

A novel ALMS1 interactor, A-kinase anchor protein 8-like (AKAP8L), has been identified. AKAP8L is known to play an essential role in cell cycle G2/M transition and in de-acetylation of histones during mitosis [153,154]. To check whether the AKAP8L protein is altered in hTERT-RPE1 control and ALMS1 KO cells, western blot analysis was conducted. The analysis targeted AKAP8L protein (~95 kDa) along with the housekeeping gene GAPDH (37 kDa) as a loading control (Figure 18). No difference in signal intensity was observed between the control cells and the ALMS1 KO cells (depicted here are three ALMS1 KO samples). This suggests that loss of ALMS1 does not significantly influence the expression levels of AKAP8L.

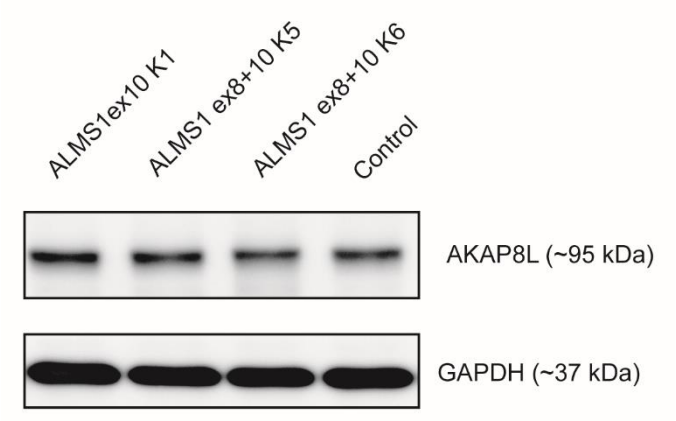

Figure 18 AKAP8L expression level unaffected upon ALMS1 loss
A Protein level of AKAP8L and GAPDH as a loading control was investigated using Western blot. hTERT-RPE1 control and three ALMS1 KOs are depicted. B Protein level intensity measurement of AKAP8L in hTERT-RPE1 control and three ALMS1 KO cells were conducted. For statistical analysis the mean was calculated. *P* values > 0.05 are not significant (ns).

7.9 ALMS1 does not influence insulin marker expression

Metabolic involvement of ALMS1 was postulated based on the development of Type 2 Diabetes in Alström syndrome patients. Insulin, a signaling molecule, binds to the insulin receptor, a type of tyrosine kinase receptor, thereby activating the pathway responsible for glucose uptake. Furthermore, ALMS1 was previously linked to GLUT4 transportation [16,155]. In this particular study, hTERT-RPE1 cells were utilized, which, according to human protein atlas data (https://www.proteinatlas.org/ENSG00000181856-SLC2A4/cell+line), lack expression of GLUT4, making it challenging to directly investigate its involvement. Nevertheless, the investigation aimed to explore the potential role of ALMS1 in insulin signaling via other GLUT transporters. Describing an alternative cilia independent mechanism of how mutated ALMS1 results in this severe disease.

Initially, hTERT-RPE1 cells were first subjected to insulin treatment to evaluate their response and ascertain the activation of insulin signaling pathways. This investigation aimed to determine

the sensitivity of hTERT-RPE1 cells to insulin and assess the subsequent activation of insulin signaling cascades.

This was achieved by treating control and ALMS1 KO cells, both in the presence and absence of insulin, and subsequently examining downstream signaling effects. It is important to note that this preliminary experiment involved only one biological replicate for each condition. An important kinase in the insulin signaling pathway is the protein kinase B/AKT. AKT gets phosphorylated twice on threonine 308 (Thr308) and serine 473 (Ser473) by 3-Phosphoinositide-dependent protein kinase 1 (PDK-1) and is subsequently activated, inducing inter alia glucose metabolism [156–158]. Control and ALMS1 KO cells without insulin stimulation showed a gradual and mild increase of AKT total protein level from left to right (Figure 19 upper left panel). Upon insulin stimulation an increase of total AKT was observed, with similar results for control and ALMS1 ex 10 KO, while comparing control to ALMS1 ex 8-10 KO 1 and KO 2 seemed to show a mild increase of AKT total (Figure 19 upper right panel). Furthermore, pAKT (Ser473) was investigated, showing a mild increase in the ALMS1 KO cells compared to the control. Insulin-induced phosphorylation of AKT at Ser473 showed in control and ALMS1 KO cells similar results (Figure 19 lower panel). This outcome needs to be interpreted with caution because only one biological replicate was used, and additional prospective experiments needs to be adjusted considering GAPDH oversaturation. Nevertheless, this initial experiment indicates, that hTERT-RPE1 cells react sensitive to insulin stimulation and that ALMS1 might interact with other GLUT transporter, which needs further und future investigation.

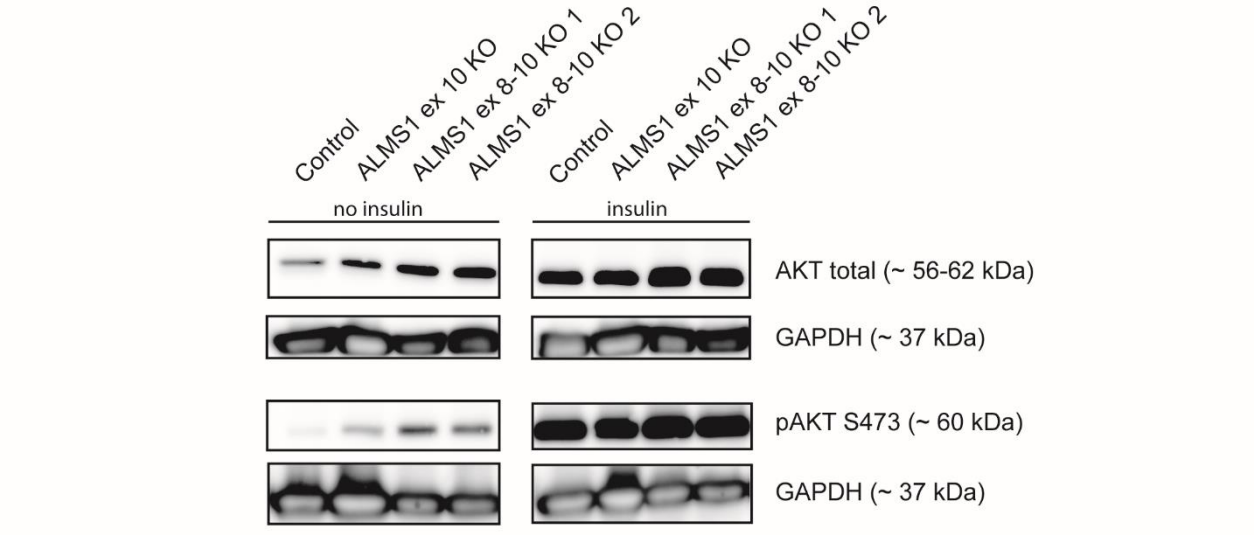

Figure 19 ALMS1 shows in a first experiment no direct influence on AKT
Protein level of AKT total and pAKT (Ser473) in insulin stimulated and unstimulated hTERT-RPE1 control and ALMS1 ex 10 KO, ALMS1 ex 8-10 KO 1, ALMS1 ex 8-10 KO 2 and the respective loading control GAPDH is depicted. One biological replicate was used.

One novel and potential ALMS1 interactor, GSK3B, that was connected to insulin signaling was found within Tier 2 identified proteins (Figure 17), harboring a negative regulatory function on glucose homeostasis and was thought to facilitate development of insulin resistance by influencing transcription factors [159,160]. Protein level investigation using western blot was performed. Thereby, lysate of hTERT-RPE1 control and ALMS1 KO cells, treated without or with insulin were generated. First, GSK3A/B total was examined. No signal difference in insulin untreated cells were observed among control and ALMS1 KO cells, while one ALMS1 KO (ALMS1 ex 8-10 KO 2) revealed a decrease in GSK3 alpha and beta (Figure 20 upper panel). In the untreated control cells, either no band or fainted bands were detected for pGSK3B, whereas the ALMS1 KO cells displayed a slight increase in band intensity. Interestingly, when the cells were treated with insulin, similar band intensities were observed in both control and ALMS1 KO cells (Figure 20 lower panel).

As GSK3B is also known to be involved as a negative regulator in Wnt signaling, a future experiment could involve studying the involvement of ALMS1 and GSK3B in Wnt signaling.

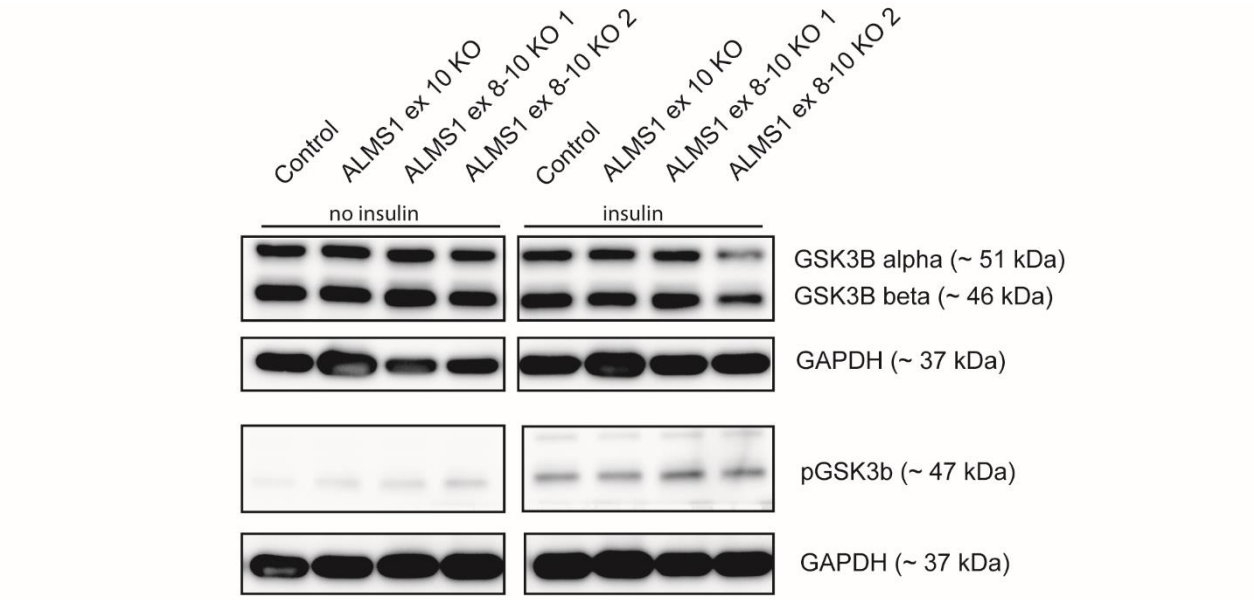

Figure 20 ALMS1 shows no explicit function on GSK3B
Western Blot analysis with one biological replicates of insulin treated and untreated hTERT-RPE1 control, ALMS1 ex 10 KO, ALMS1 ex 8-10 KO 1 and ALMS1 ex 8-10 KO 2. GSK3 total, pGSK3B and the loading control GAPDH is depicted.

Another important protein in glucose homeostasis, is the cAMP-responsive element-binding protein (CREB). It has an important role in various processes such as efficient glucose sensing and insulin exocytosis [161]. Therefore, the total protein level of CREB was investigated with insulin unstimulated and stimulated conditions in control and ALMS1 KO cells (one biological replicate). No clear results could be confirmed for ALMS1 ex 10 KO and ALMS1 ex 8-10 KO1 due to a potential blotting issue. For ALMS1 ex 8-10 KO2 no difference with and without insulin

stimulation was observed compared to the control (Figure 21). No results for pCREB (Ser133) could be obtained (data not shown). GAPDH was used as a loading control.

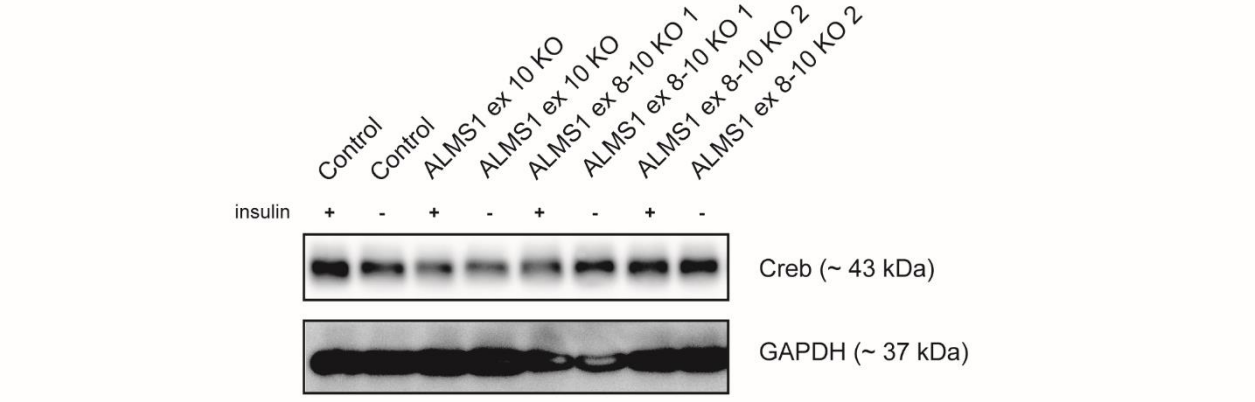

Figure 21 ALMS1 shows no clear influence on Creb
In insulin-treated and untreated hTERT-RPE1 control, ALMS1 ex 10 KO, ALMS1 ex 8-10 KO 1 and KO2, the protein level of Creb1 and GAPDH (loading control) were investigated using Western blot. One biological replicate was used.

7.10 CEP70 is a strong interaction partner of ALMS1

In protein complex analysis of ALMS1, one highly abundant interactor was identified for the first time: the centrosomal protein of 70 kDa (CEP70, ENST00000264982.8, CEP70-201, CCDS3102) protein (Figure 16 B, blue labeled). The CEP70 full length protein comprises 579 amino acids (aa). The CEP70 associates with the centrosome and BB of cilia. Previous studies showed an important function of CEP70 on microtubule stability by influencing acetylation of tubulin via HDAC6. Further, deficiency of CEP70 led to left-right defects and reduced ciliary length with an unaffected basal body in zebrafish [72]. It was shown that the coiled-coil domains of CEP70 play a role in centrosomal localization, while the TPR harboring CT end shows weak or no importance for centrosomal localization. To better understand the interplay of ALMS1 and CEP70, an independent protein complex analysis using overexpression constructs for full length CEP70 fused to a N-terminal Strep-Flag tag (NSF-CEP70) and NSF-RAF1 (control) was performed. Six biological replicates respectively were used and analyzed as described above (Figure 22 A). Novel interaction partners of CEP70 were identified (Figure 22 B) (Woerz *et al.*, under review [3]).

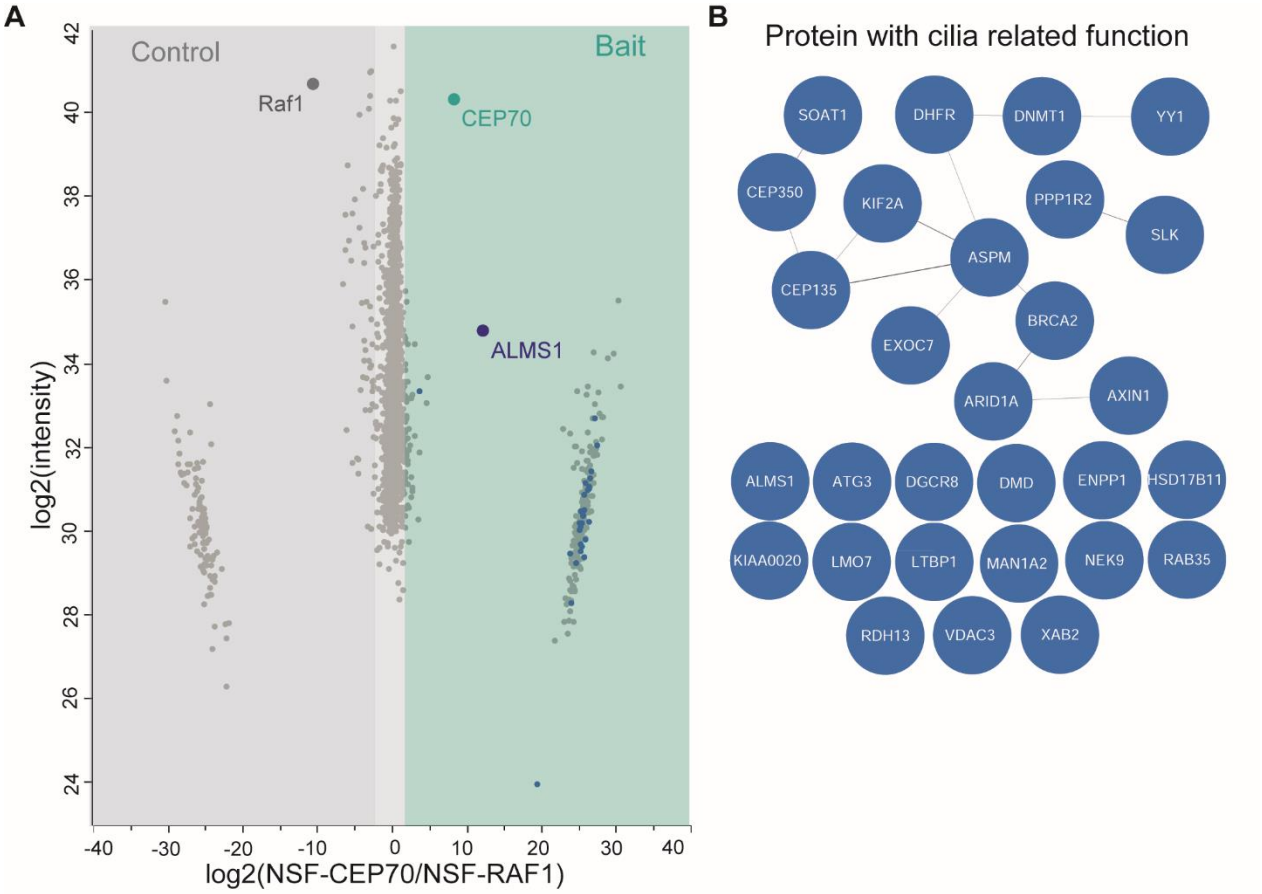

Figure 22 Novel CEP70 interaction partners identified by mass spectrometry
A, The scatter plot represents the analysis of the CEP70 protein complex, comparing six biological replicates of NSF-CEP70 (shown in cyan) and its control (NSF-RAF1, shown in grey). Mass spectrometry data was processed using MaxQuant and Perseus. The x-axis displays the log2 ratio of the mean NSF-CEP70 to the mean NSF-RAF1, while the y-axis represents log2 intensity. The CEP70 protein (the bait) is indicated by a cyan filled circle, the control is depicted in grey, and Tier 2 interactors (significance A < 0.05, Benjamini-Hochberg < 0.05) associated with cilia-related functions are marked in blue. **B**, Overview of potential Tier 2 interaction partners of CEP70 involved in cilia biology or exhibiting a cilia-related function. Figure was modified after and taken from Woerz *et al.*, under review [3].

As done before for ALMS1 interactome analysis, proteins are subdivided in Tier 1 (Significance A Benjamini-Hochberg FDR < 0.05 and Permutation based FDR < 0.05) and Tier 2 (Significance A Benjamini-Hochberg FDR < 0.05 and *p*-value < 0.05). 202 proteins are included in Tier 1 and 225 proteins in Tier 2. Among these 225 Tier 2 proteins, 29 proteins were found with cilia-related functions using UniProtKB (Figure 23 B, Figure 24) (Woerz *et al.*, under review [3]). Notably, the protein complex analysis of CEP70 revealed an interaction with another centrosomal protein CEP135, which is already documented in the BioGRID database. CEP135 plays an important role in regulating the localization of CEP250 and centriolar satellites. [162–164]. Furthermore, another centrosomal protein, the CEP350 was found as a Tier 2 protein. It is described to function as a scaffold protein being involved in centriole function and early ciliogenesis [165–167] (Woerz *et al.*, under review [3]). Moreover, other significantly enriched interaction partners were identified. These proteins are involved in various cellular processes, including transport,

mitosis, signaling processes, mitochondrial function (Woerz *et al.*, under review [3]). Additionally, they exhibit functions related to the eyes, nervous system, and glucose metabolism functions (Figure 23, see 10.7.4 Appendix Table 29). Interestingly, the protein complex analysis revealed ALMS1 with a sequence coverage of 28.3 % (Tier 1) as an interactor of CEP70, highlighting a strong association between these two proteins (see 10.8 Appendix Figure 40) (Woerz *et al.*, under review [3]). No specific clusters related to microtubules, or the centrosome were identified using the Gene Ontology Resource.

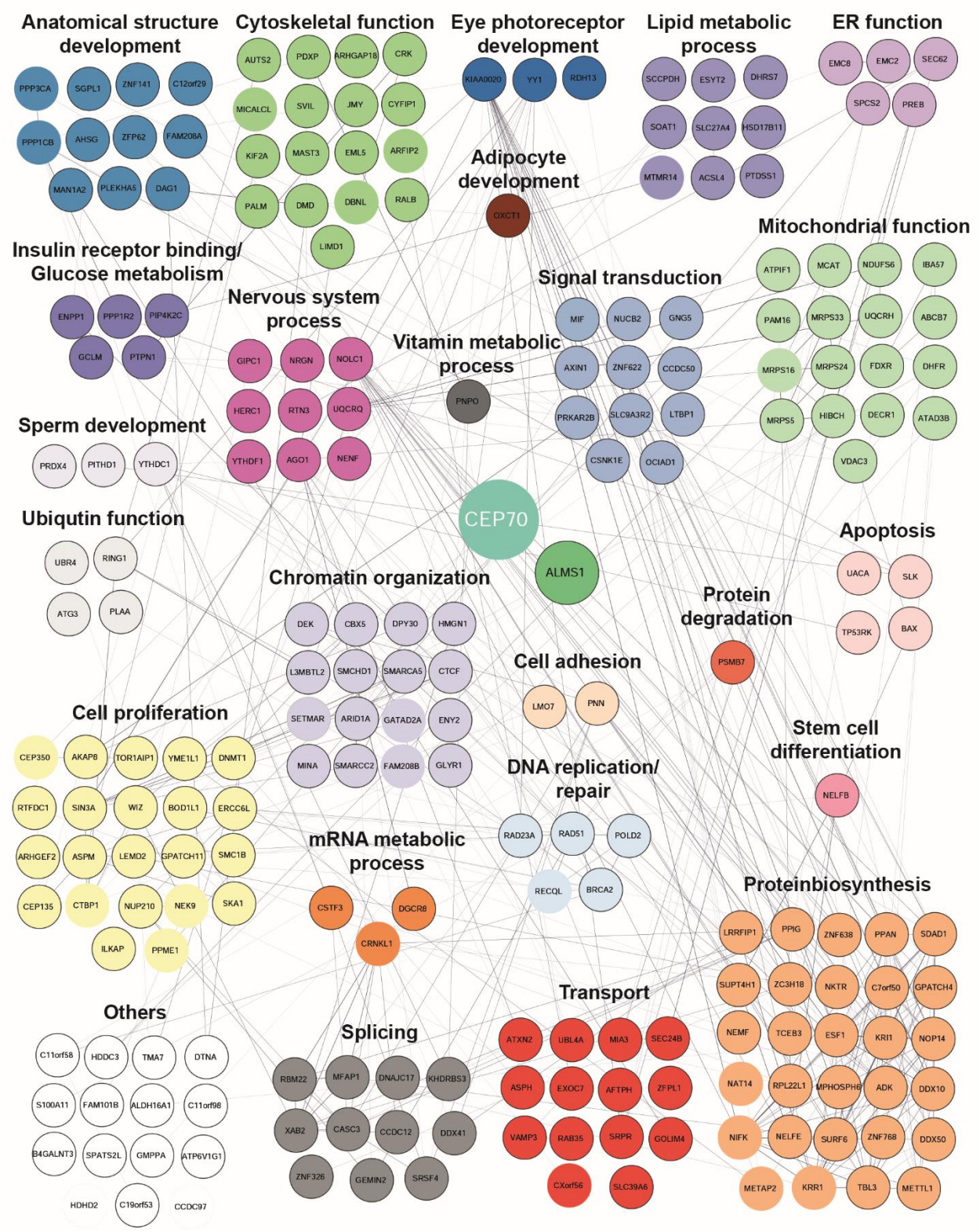

Figure 23 CEP70 interaction network

An overview of CEP70 protein interaction network, according to their function in cellular processes is presented. Proteins are grouped according to their main function in cellular processes, to my best knowledge. Proteins with unknown biological function are grouped under others. The respectively function can be found on UniProt Knowledgebase (UniProtKB) in 2022. 202 Proteins were classified into Tier 1 (Significance A (Benjamini-Hochberg) FDR < 0.05) and are depicted with black border paint (see also 10.7.4). Additional 23 proteins are grouped into Tier 2

(Significance A (Benjamini-Hochberg) FDR < 0.05 and *p*-value < 0.05) and marked with no border (see also 10.7.4). NACAP1 was excluded due to its pseudogene prediction. The network was created by leveraging experimental and functional interactions derived from a meticulously curated database using the STRING platform [121],and then visually represented in Cytoscape [122] for enhanced visualization. Figure was taken from Woerz *et al.*, under review [3].

7.11 ALMS1 and other centrosomal proteins bind TPR-CT domain of CEP70

The localization of CEP70 to the centrosome primarily relies on its N-terminal (NT) region, that contains two coiled-coil domains. Conversely, the expression of the C-terminal (CT) region harboring the TPR-domain has been reported to result in either no [74] or weak [168] centrosomal localization. Here, the ALMS1-specific interacting domain in CEP70 was investigated and defined by performing deletion analysis. Therefore, region-specific forms of CEP70 were cloned into an N-terminal Strep Flag (NSF) plasmid and utilized for affinity-based protein complex purification, followed by data-dependent analysis [120] (Woerz *et al.*, under review [3]). These results were then compared to the interactome of full length CEP70, described above, with the Scatter plot presenting the distribution of proteins found with the different fragments (Figure 24 A). The designed fragments of CEP70 contain either the two coiled-coil domain (CC1-2, 75-326 aa, Figure 24 C, middle panel) with 251 aa or the TPR domain and the CT end (TPR-CT, 327-597 aa, Figure 24 C, lower panel) (Woerz *et al.*, under review [3]).

A both-sided statistical test was employed, considering only Tier 1 based CEP70 interactors, that were previously defined by comparing CEP70 full length against the control. The deletion analysis revealed a decreased binding of 122 proteins to the CC1-2 domain, while seven proteins show a diminished binding to the TPR-CT region (Figure 24 B, see 10.7.5 and 10.7.6). Among these proteins, exhibiting reduced binding in CC1-2 samples, a total of 19 ciliary proteins were identified, including CEP135. Interestingly, ALMS1 was found to bind to the TPR-CT region, but not significant or less to CC1-2, suggesting CEP70 may localize to the centrosome/BB independently of ALMS1 (Woerz *et al.*, under review [3]). Furthermore, five proteins parallel to ALMS1 showed a significant reduction in binding to the TPR-CT form, namely UBR4, ATG3, PLAA, UACA, TP53K and BAX.

In summary, the validation of CEP70-specific interactors through affinity purification of deletion constructs provided valuable insights into the domain-specific interactions of CEP70 with its TPR-CT and CC1-2 domains. Additionally, CEP70 was found as a significant interactor of ALMS1 and vice versa for the first time. Furthermore, the identification of ALMS1 as an interactor of CEP70, binding specifically the TPR-CT domain, suggests a potential ALMS1-independent localization of CEP70 to the centrosome/BB (Woerz *et al.*, under review [3]).

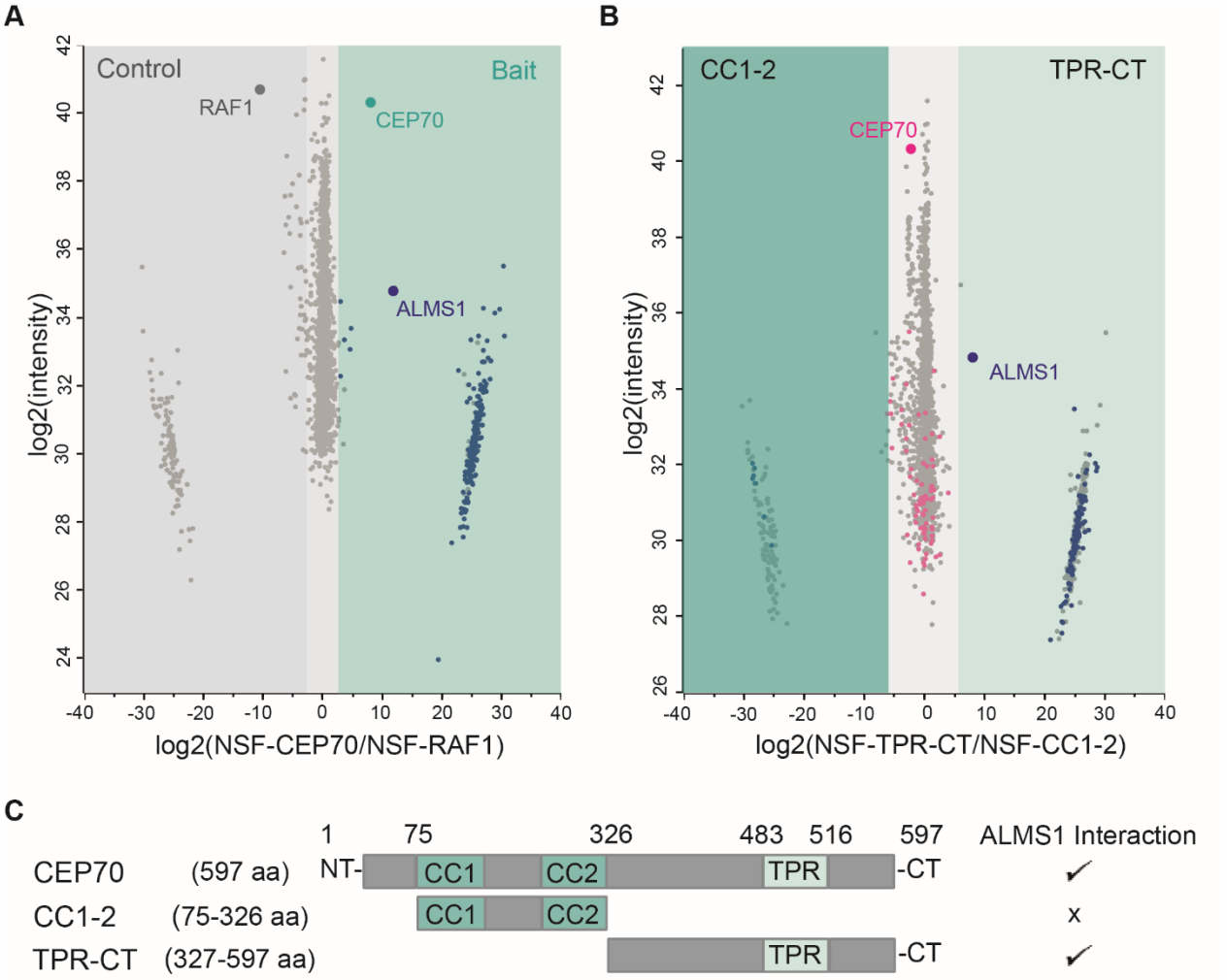

Figure 24 ALMS1 binds TPR domain and CT end of CEP70
A, Scatter plot emphasizes the distribution of proteins that were found with NSF-CEP70 (full length). The CEP70 protein (bait) is depicted in cyan, the control in grey and significant Tier 2 proteins in blue. Six biological replicates of NSF-CEP70 and NSF-RAF1 were respectively used. Max Quant and Perseus was used to analyze Mass spectrometry data. **B**, The scatter plot highlights the distribution of proteins found with either CC1-2 (displayed in mid cyan on the left side) or with the TPR-CT form of CEP70 (depicted in light cyan on the right side). Proteins identified as Tier 2 interactors in the full-length CEP70 (as shown in plot A) are indicated in pink (found in both CC1-2 and TPR-CT samples with no significant difference) or blue (exhibiting a significant difference between CC1-2 and TPR-CT).
C, A schematic overview provides an overview of the structure of CEP70 in different forms. The full-length CEP70 is composed of 597 amino acids (CEP70), while specific CEP70 forms contain either the CC1 and CC2 domains (amino acids 75-326, CC1-2) or the TPR domain with the CT end (amino acids 327-597, TPR-CT). An indication of a positive identification of ALMS1 interaction with CEP70 is represented by a checkmark (✓), whereas no interaction is denoted by an "x". The design of protein domain lengths and structures in the schematic was inspired by information obtained from the UniProt Knowledgebase (UniProtKB) 2022 release. The abbreviations used include CC (coiled coil), TPR (tetratricopeptide repeat), aa (amino acids), NT (N-terminus), CT (C-terminus), CEP70 (full-length CEP70), CC1-2 (CEP70 amino acids 75-326), and TPR-CT (CEP70 amino acids 327-597). Figure was taken and modified from Woerz *et al.*, under review [3].

Next, functional relevance of ALMS1-CEP70 interaction was investigated by performing an epistasis experiment with the downregulation of CEP70 as well as both genes.

7.12 ALMS1 loss affect cell survival in wt hTERT-RPE1 cells

To investigate if CEP70 localization at the BB is influenced upon ALMS1 loss, immunostaining of CEP70 and the ciliary marker ARL13B was conducted. When comparing the localization (Figure 25 A) and the intensity (Figure 25 B) of CEP70 in hTERT-RPE1 control and ALMS1 KO (ALMS1 ex 8-10 KO 2) cells no difference in CEP70 signal patterns were observed. This finding suggests, that CEP70 may be located upstream of ALMS1.

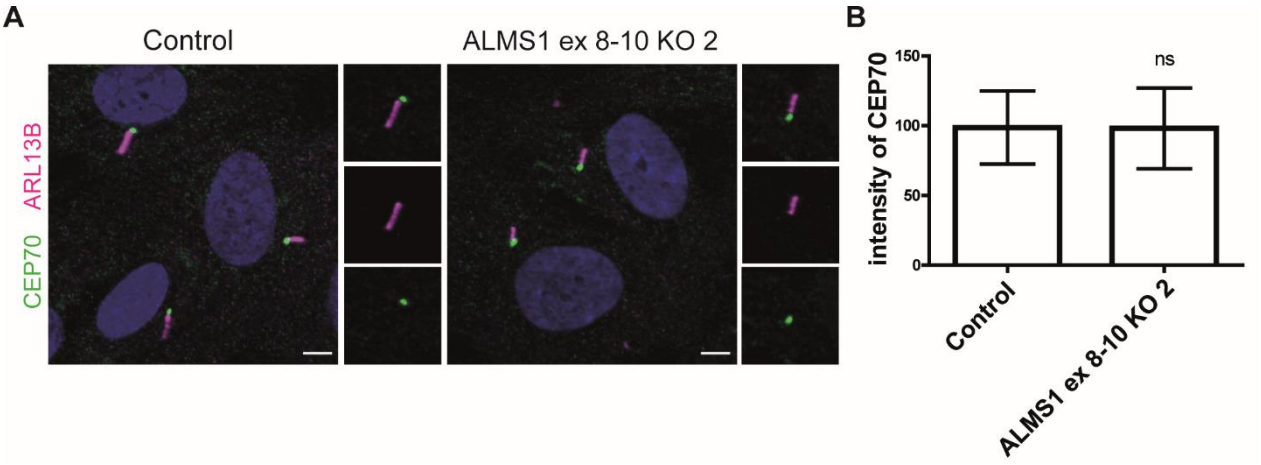

Figure 25 CEP70 localization is unaffected due to ALMS1 loss in hTERT-RPE1 cells
A, HTERT-RPE1 control and ALMS1 KO cells are depicted. Cilia (ARL13B) are marked in magenta, with the basal body (CEP70) in green. **B**, Intensity measurement was conducted with one biological replicate and 4 technical replicates. *P*-value < 0.001 are marked with *** asterisks. ApoTome, 40x magnification. Scale bar is 5 µm.

Next, ALMS1 localization to the BB upon CEP70 loss was examined by using again the CRISPR/Cas9 system (Woerz *et al.*, under review [3]). Therefore, specific sgRNAs targeting ex 5 and 6 of *CEP70* were designed as described above and cloned into the PX459 plasmid (was a gift from Feng Zhang). CRISPR/Cas9 mediated CEP70 KO were generated and verified by sequencing. However, CEP70 KO could not be confirmed using western blot or immunofluorescence staining with CEP70 antibodies, that recognize only the NT end (data not shown). Immunostaining of potential CEP70 knockout cells showed no changes in acetylated tubulin, which had been previously reported to be affected [70], suggesting unclear KO status and were therefore excluded from this study (data not shown).

At the same time, to further investigate the relevance of the interaction between ALMS1 and CEP70 in overlapping cellular processes, an epistasis experiment involving the downregulation of both genes was performed. First, double knock-out (dKO) using the CRISRP/Cas9 system was conducted. Initial attempts to generate dKO cells, lacking CEP70 and ALMS1 were unsuccessful, as no dKO could be confirmed (data not shown). Additionally, a high rate of cell loss/death was observed during the experiment. Therefore, a leveled knockdown (KD) of CEP70 was applied in wildtype (wt) and ALMS1 deficient cells.

In a first step, CEP70 siRNA (siCEP70) based KD was assessed using various concentrations ranging from 5 to 50 nM and evaluated using quantitative PCR (qPCR) (Figure 26 A, one biological replicate). There was no decrease of *CEP70* mRNA level using 5 nM siCEP70, while a gradual decrease in CEP70 expression was observed from 50 to 10 nM. A minimal CEP70 downregulation was observed with 10 nM, while a clear downregulation was observed with 30 nM and 50 nM concentrations (Figure 26, A) (Woerz *et al.*, under review [3]).

Moreover, 10 nM to 30 nM of CEP70 siRNA resulted in a decrease in cell number (Figure 26, for 30 nM see 10.9 Appendix Figure 41). To ensure comparable results, the number of cells/mL were automatically measured using TECAN and equally distributed for transfection. Loss of cells in wt and ALMS1 deficient cells transfected with scrambled (siControl) or CEP70 siRNA was investigated after 72 hrs post-transfection (24 hrs of transfection, 48 hrs starvation) by counting the remaining and attached cells after DAPI staining (Figure 26 B). No differences were observed between untreated wt and siControl treated cells with 10 nM respectively. However, significant reduction in cell number was observed when cells were treated with 10 nM CEP70 siRNA in wt cells ($F(5,66) = 43,83, < 0.05$) and in siControl treated wt cells ($F(5,66) = 34,42, < 0.05$), suggesting a potential effect on either proliferation or up-regulation of cell death upon CEP70 loss alone. Interestingly, a significant reduction in cell number with 10 nM was detected in ALMS1 KO untreated compared to untreated wt cells ($F(5,66) = 35,25, < 0.05$) or siControl treated wt cells ($F(5,66) = 25,83, < 0.05$). Furthermore, ALMS1 KO treated with siCEP70 shows a significant decrease in cell number compared to ALMS1 KO untreated ($F(5,66) = 24,33, < 0.05$) and ALMS1 siControl ($F(5,66) = 26,50, < 0.05$) treated cells (Figure 26 B). Moreover, a mild reduction without significance was observed between wt and ALMS1 KO cells treated with siCEP70, suggesting a role of both proteins in cell loss (Woerz *et al.*, under review [3]).
Moreover, untreated and 30 nM siControl treated wt cells ($F(5,102) = 23$, $p < 0.05$), as well as wt siCEP70 30 nM ($F(5,102) = 52.89$, $p < 0.001$), exhibited a significant decrease in nuclei count (see 10.9 Appendix Figure 41). There was also a significant difference in nuclei count between wt siControl 30 nM and wt siCEP70 30 nM ($F(5,102) = 29.89$, $p < 0.01$). However, no significant difference was observed between ALMS1 KO untreated and ALMS1 KO siControl 30 nM ($F(5,102) = 13.83$, $p > 0.05$), while there was a significant decrease compared to ALMS1 KO siCEP70 ($F(5,102) = 56.89$, $p < 0.001$). Additionally, ALMS1 KO siControl 30 nM compared to ALMS1 KO siCEP70 30 mM exhibited a significant decrease in nuclei count ($F(5,102) = 43.06$, $p < 0.001$). These results indicate an increased cell loss in ALMS1-deficient cells accompanied by CEP70 knockdown at 30 nM.

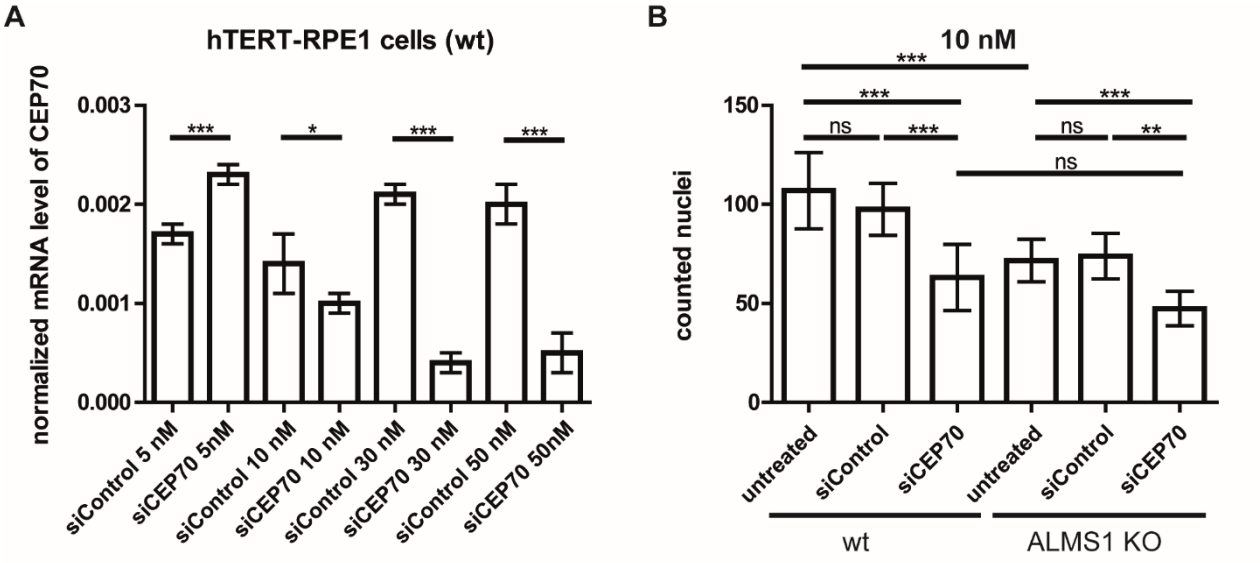

Figure 26 ALMS1 KO and CEP70 KD in wt cells lead to cell loss
A, To initiate the knockdown experiment, a pool of three CEP70 siRNAs (siCEP70) was utilized. The concentrations of siCEP70 ranged from 5 to 50 nM. The primer set for CEP70 targeted exons 9 to 11, while GAPDH served as the housekeeping gene. This experiment was performed with a sample size of n=1. **B**, For cell loss investigation, the nuclei were counted in three biological replicates. The staining was performed on untreated cells, cells treated with siCEP70, and cells treated with siControl. Both wildtype and ALMS1-deficient cells were included in the analysis. A concentration of 10 nM CEP70 siRNA was used for transfection. The data were analyzed using an ANOVA test (Tukey), and the error bars represent the standard deviation (SD). *P*-value below 0.001 are marked with *** asterisks, *p*-value below 0.01 are presented with ** asterisks, *p*-value above 0.05 are deemed not significant. Figure was taken and modified after Woerz *et al.*, under review [3].

Interestingly, phenotypic analysis of ALMS1 localization at the BB in hTERT-RPE1 wt cells treated with 10 nM siCEP70 already revealed a significant reduction of ALMS1 localization compared to wt and siControl treated cells. This result suggests a CEP70-dependent ALMS1 recruitment or stabilization at the BB (Figure 27 A, B) (Woerz *et al.*, under review [3]).

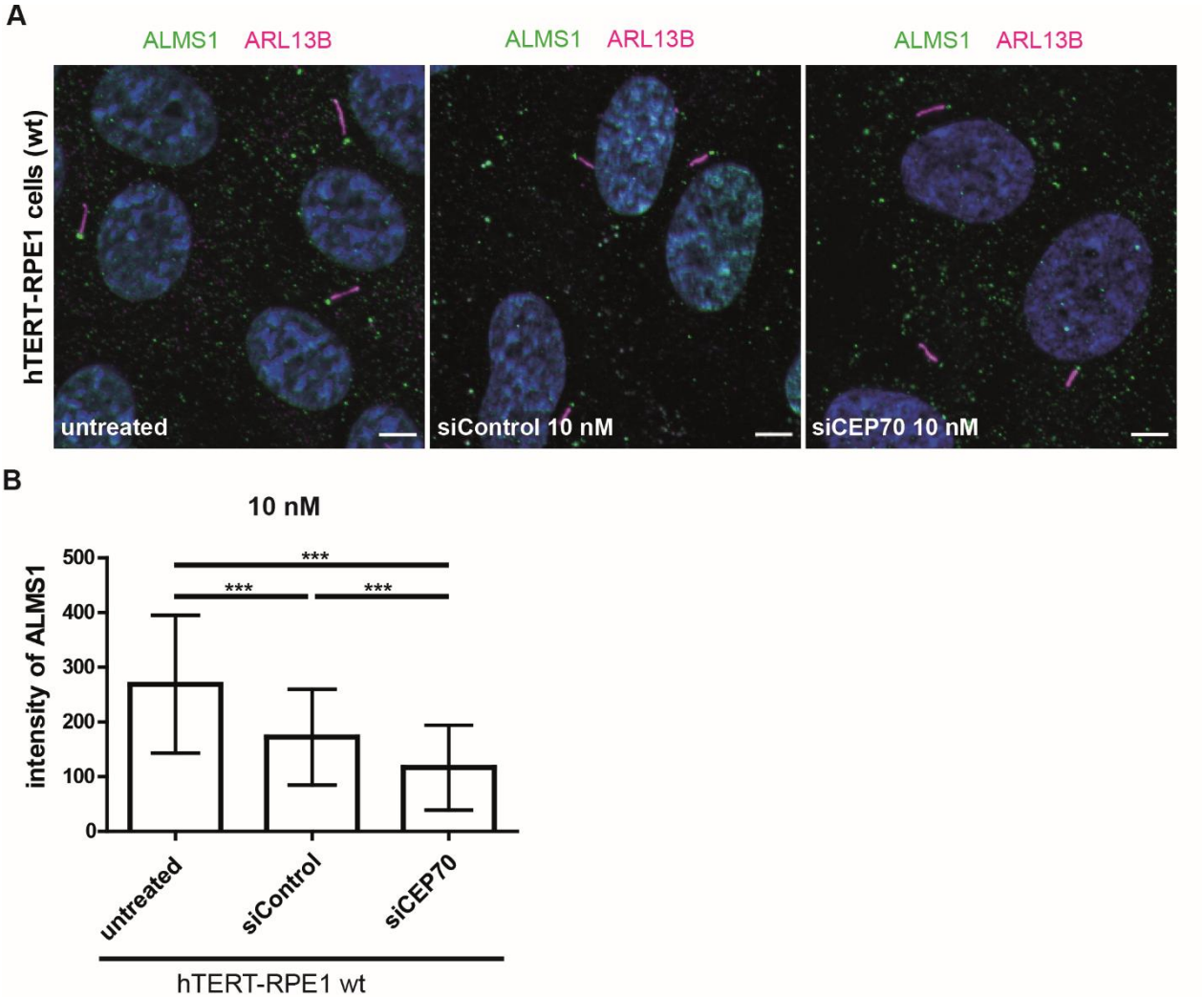

Figure 27 CEP70 KD in wt hTERT-RPE1 cells leads to reduced ALMS1 at the BB
A, Images of hTERT-RPE1 wildtype (wt) cells are presented from left to right: untreated cells, cells transfected with 10 nM siControl, and cell treated with 10 nM CEP70 siRNA. ALMS1 protein is visualized in green, and cilia are co-stained with ARL13B in magenta. The cell nuclei were stained with DAPI in blue. Microscopy pictures are made using ApoTome imaging at 40x magnification. Scale bar marks 5 µm.
B, Intensity measurement of ALMS1 at the BB of cilia were conducted by hand using Zen software (Zen blue).For untreated conditions a total number of 122 BB, for siControl treated cells 112 BB and for siCEP70 treated cells 121 BB and the respectively background were taken into statistical analysis. A one-way ANOVA (Tukey) test was performed. Error bars mark with the standard deviation (SD) are presented. Three asterisks (***) indicate $p < 0.001$. Figure was taken from and modified after Woerz *et al.*, under review [3].

7.13 CEP70 KD in wt hTERT-RPE1 cells induce apoptosis on mRNA level

In the CEP70 network analysis, proteins were found to be linked to apoptotic events, such as the pro-apoptotic marker BAX, that could partially explain the occurring phenotype in ALMS1 and CEP70 deficient hTERT-RPE1 cells. BAX was found to be involved in mitochondrial apoptotic processes by inducing mitochondrial outer membrane permeabilization (MOMP), resulting in the release of cytochrome c and other apoptotic factors [169–176]. BAX in turn gets inhibited by the pro survival protein BCL-2, which is under physiological conditions predominantly expressed

(Figure 36). This allows the cell to survive and maintain proper functions. Therefore, the association and ratio of BAX to BCL2 is of importance due to their involvement in determining cell fate in response to an apoptotic stimuli [177]. For example, an increase in the relative level of BAX with a subsequent decrease in BCL2 shifts the cell fate towards apoptosis [178,179]. In the deletion analysis, it was found, that BAX and ALMS1 bind the same CEP70 region containing the TPR domain and CT end.

An initial qPCR experiment without CEP70 downregulation was performed to investigate *BAX/BCL2* ratio in control (wt and Cas9) and three different ALMS1 KO cells (ALMS1 ex 10 KO, ALMS1 ex 8-10 KO 1, ALMS1 ex 8-10 KO 2). Normalization was first conducted against GAPDH and further to wt (Figure 28 A) or Cas9 control (Figure 28 B). The qPCR experiment utilized one biological replicate with six technical replicates. Cas9 control (transfected CRISPR/Cas9 plasmid without sgRNA; $F(4,5) = -0{,}7484$, $p < 0.05$), ALMS1 ex 8-10 KO 1 ($F(4,5) = -1{,}327$, $p < 0.05$) and ALMS1 ex 8-10 KO 2 ($F(4,5) = -1{,}139$, $p < 0.05$) showed a significant increase of *BAX/BCL2* ratio compared to wt, indicating apoptosis. Conversely, ALMS1 ex 10 KO ($F(4,5) = 0{,}3042$, $p < 0.05$) revealed a reduced *BAX/BCL2* ratio compared to wt, suggesting cell survival. Since the cells, except of wt, were transfected either with CRISPR/Cas9 plasmid with or without sgRNA, the *BAX/BCL2* expression was normalized against Cas9 control. This might help to decipher Cas9-related effects. ALMS1 ex 10 KO ($F(3,4) = 0{,}6013$, $p < 0.05$) showed a significant decrease of the *BAX/BCL2* expression level compared to Cas9, while a significant increase was observed with ALMS1 ex 8-10 KO 1 ($F(3,4) = -0{,}3328$, $p < 0.05$) and ALMS1 ex 8-10 KO 2 ($F(3,4) = -0{,}2242$, $p < 0.05$).

Further investigation focused on the interplay of BAX and BCL2 to gain insights into cell loss in CEP70 and ALMS1 deficient hTERT-RPE1 cells. A qPCR analysis was performed on wt and ALMS1 KO (ALMS1 ex 8-10 KO 2) cells, both treated with either siControl or siCEP70 at concentrations of 10 nM (Figure 28 C) and 30 nM (Figure 28 D). The analysis involved one biological replicate with six technical replicates, respectively.

When comparing wt cells treated with 10 nM siControl to wt cells treated with 10 nM siCEP70 ($F(3,4) = -0{,}4351$, $p > 0.05$), a mild increase in the *BAX/BCL2* ratio was observed, although it was not statistically significant. Additionally, no significant difference in the *BAX/BCL2* ratio was found between wt siControl 10 nM and ALMS1 KO siControl 10 nM ($F(3,4) = 0{,}4290$, $p > 0.05$), as well as between wt siControl 10 nM and ALMS1 KO siCEP70 10 nM ($F(3,4) = 0{,}4287$, $p > 0.05$). Comparing ALMS1 KO siControl with ALMS1 siCEP70 ($F(3,4) = -0{,}0003603$, $p > 0.05$) revealed no significant difference, while a significant difference in the *BAX/BCL2* ratio was observed between wt siCEP70 and ALMS1 KO siCEP70 ($F(3,4) = 0{,}8637$, $p < 0.05$) (Figure 28 C).

At higher concentration of siControl and siCEP70 (30 nM), comparing wt siControl with wt siCEP70 (F(3,4) = 0,9058, $p > 0.05$) and with ALMS1 siControl (F(3,4) = 0,7915, $p < 0.05$) showed a reduced *BAX/BCL2* ratio, indicating cell survival. A significant difference was observed between wt siCEP70 and ALMS1 KO siCEP70 (F(3,4) = -0,7926, $p < 0.05$), as well as between ALMS1 KO siControl and siCEP70 (F(3,4) = -0,6783, $p < 0.05$). However, ALMS1 KO siCEP70 (F(3,4) = 0,1132, $p > 0.05$) exhibited no significant difference in the *BAX/BCL2* ratio compared to wt siControl, suggesting cell survival or homeostasis (Figure 28 D, Figure 36).

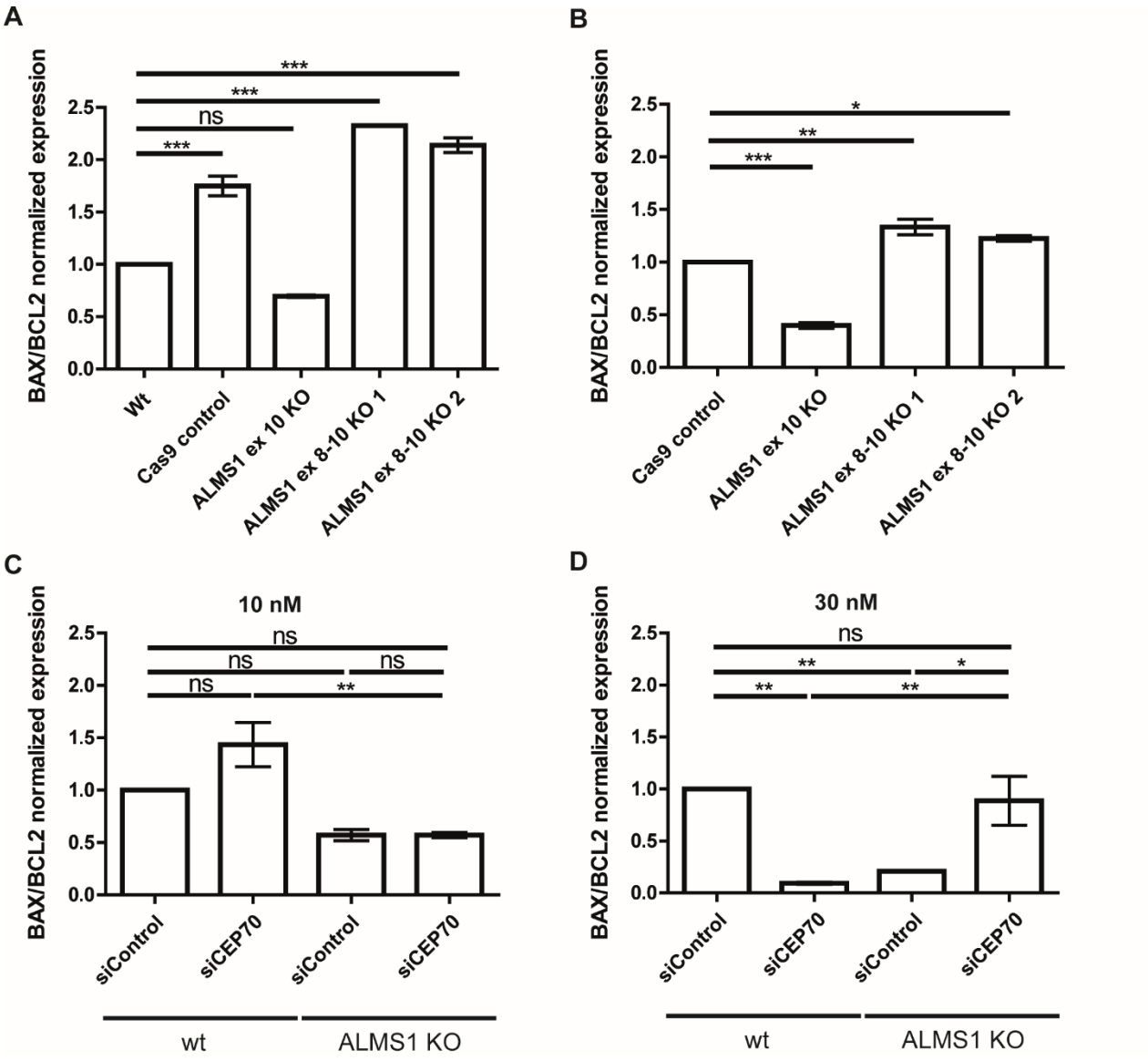

Figure 28 CEP70 KD in wt hTERT-RPE1 cells leads to cell death
A, Normalized *BAX/BCL2* expression levels were shown for two controls (wt and Cas9 control) and three ALMS1 knockout (KO) cells under ciliated conditions. GAPDH was used as the housekeeping gene for normalization. The ΔΔCt was calculated, with normalization against wt. One- way ANOVA with Post-hoc Tukey analysis was conducted, and error bars represent the standard deviation (SD). Statistical significance was indicated by asterisks: (***) mark $p < 0.001$, two asterisks (**) indicate $p < 0.01$, one asterisk (*) means $p < 0.05$ and not significant (ns) $p > 0.05$. One biological replicate (n = 1), with three technical replicated, respectively.

B, The normalized *BAX/BCL2* ratio is presented for the Cas9 control and three different ALMS1 KO cell lines. GAPDH was utilized as the housekeeping gene for normalization. The ΔΔCt method was employed to calculate the relative expression levels, normalized against the Cas9 control. One-way ANOVA (Tukey) analysis was performed, and the standard deviation (SD) is represented by error bars. Statistical significance is indicated using asterisks: three asterisks (***) for $p < 0.001$, two asterisks (**) for $p < 0.01$, one asterisk (*) for $p < 0.05$, and non-significant (ns) for $p > 0.05$. The experiment consisted of one biological replicate, with three technical replicates each. Normalized *BAX/BCL2* ratio is shown for Cas9 control and three different ALMS1 KO cells. GAPDH was used as housekeeping gene. ΔΔCt was used (normalized against Cas9 control). ANOVA (Tukey) was applied. Error bars indicate SD. Statistical significance are shown with asterisks: three asterisks (***) $p < 0.001$, two asterisks (**) $p < 0.01$, one asterisks (*) $p < 0.05$ and not significant (ns) $p > 0.05$. one biological replicate, with three technical replicated, respectively were used.
C, The mRNA expression levels of *BAX/BCL2* were assessed in wildtype (wt) and ALMS1 KO (ALMS1 ex 8-10 KO 2) cells treated with either 10 nM siControl or siCEP70. The expression levels were normalized against GAPDH and further normalized using wt siControl. Statistical analysis was performed using one-way ANOVA (Tukey) test, and the significance levels were specified as follows: *** for $p < 0.001$, ** for $p < 0.01$, * for $p < 0.05$, and ns for non-significant ($p > 0.05$). The experiment was conducted with one biological replicate and included three technical replicates.
D, The mRNA expression levels of *BAX/BCL2* were determined in wildtype (wt) and ALMS1 KO (ALMS1 ex 8-10 KO 2) cells. The cells were treated with either 30 nM siControl or siCEP70. To normalize the data, GAPDH was used as the reference gene, and further normalization was performed against wt siControl. Statistical analysis was conducted using one-way ANOVA (Tukey) test, where significance levels were denoted as follows: *** for $p < 0.001$, ** for $p < 0.01$, * for $p < 0.05$, and ns for non-significant ($p > 0.05$). The experiment included one biological replicate with three technical replicates.

The results obtained in this study provide evidence suggesting, that CEP70 influences cell death and/or cell survival based on the experimental findings presented.

7.14 Identifying retina specific interaction partners of ALMS1.

7.14.1 RFP-HA endogenously tagged ALMS1 localizes at the basal body

HEK293T cells with their high expression levels of proteins and ability to form cilia are a great source for network studies. A recent approach was established by Tina Beyer *et al.* using tissue, e.g. retina from porcine eyes, for protein pull-down and isolation to identify a tissue specific interaction network of the bait protein [180]. Therefore, tagged ALMS1 from HEK293T cells was used for tagged bait purification, with a subsequent removal of bound interaction partners with sodium dodecyl sulfate (SDS) and retina-specific affinity purification.

To identify tissue specific interaction partners, three steps are crucial to consider, such as the tag-bait affinity, the SDS concentration to minimize the influence on the bait protein structure and an animal, that shares ALMS1 protein sequence similarities to the human ALMS1.

Therefore, a tag with a high affinity to the desired beads was introduced at the CT end of the *ALMS1* gene as described for sfGFP tag. For example, a HA tag is widely used in protein purification and is suggested to have a high affinity to the beads [181,182]. This advantage is important for the SDS washing step, which should only gently clear bound proteins from the HEK293T cells, while preserving the tagged protein itself. For the retina pull-down, a combination of two tags were designed, a high bead-affinity HA tag fused to a red fluorescent protein (RFP). By utilizing RFP, the localization of tagged ALMS1 at the centrosome/BB can be visualized. For the RFP-HA tag, two linker sequences (GGGS) were added between the

homology arm and the RFP and between the RFP sequence and HA sequence to enhance flexibility and reduce protein folding changes [120,183]. Native HEK293T were transfected with the CRISPR/Cas9 plasmid containing sgRNA targeting *ALMS1* exon 23 and the repair construct with the RFP-HA tag. After single clone selection, tag insertion was first verified by PCR and gel electrophoresis. ALMS1- RFP-HA tagged single clones showed one single prominent band with the size of approximately 1676 bp (see 10.10 Appendix Figure SX 42 A). Eleven homozygous and 21 heterozygous ALMS1- RFP-HA tagged cells out of a total of 59 single clones were found (Figure 29 D). Sanger sequencing confirmed the successful insertion of the RFP-HA tag into the CT of the *ALMS1* gene (Figure 29 A, see 10.10, Appendix Figure 42 B). Again, localization studies were performed to exclude a potential effect of the rather large tag (746 bp) on the ALMS1 localization to the BB in comparison with untagged ALMS1 cells (Figure 29 B). Therefore, ALMS1-RFP-HA tagged cells were stained with the ciliary marker ARL13B, that confirmed ALMS1-RFP-HA at the BB of cilia (Figure 29 C).

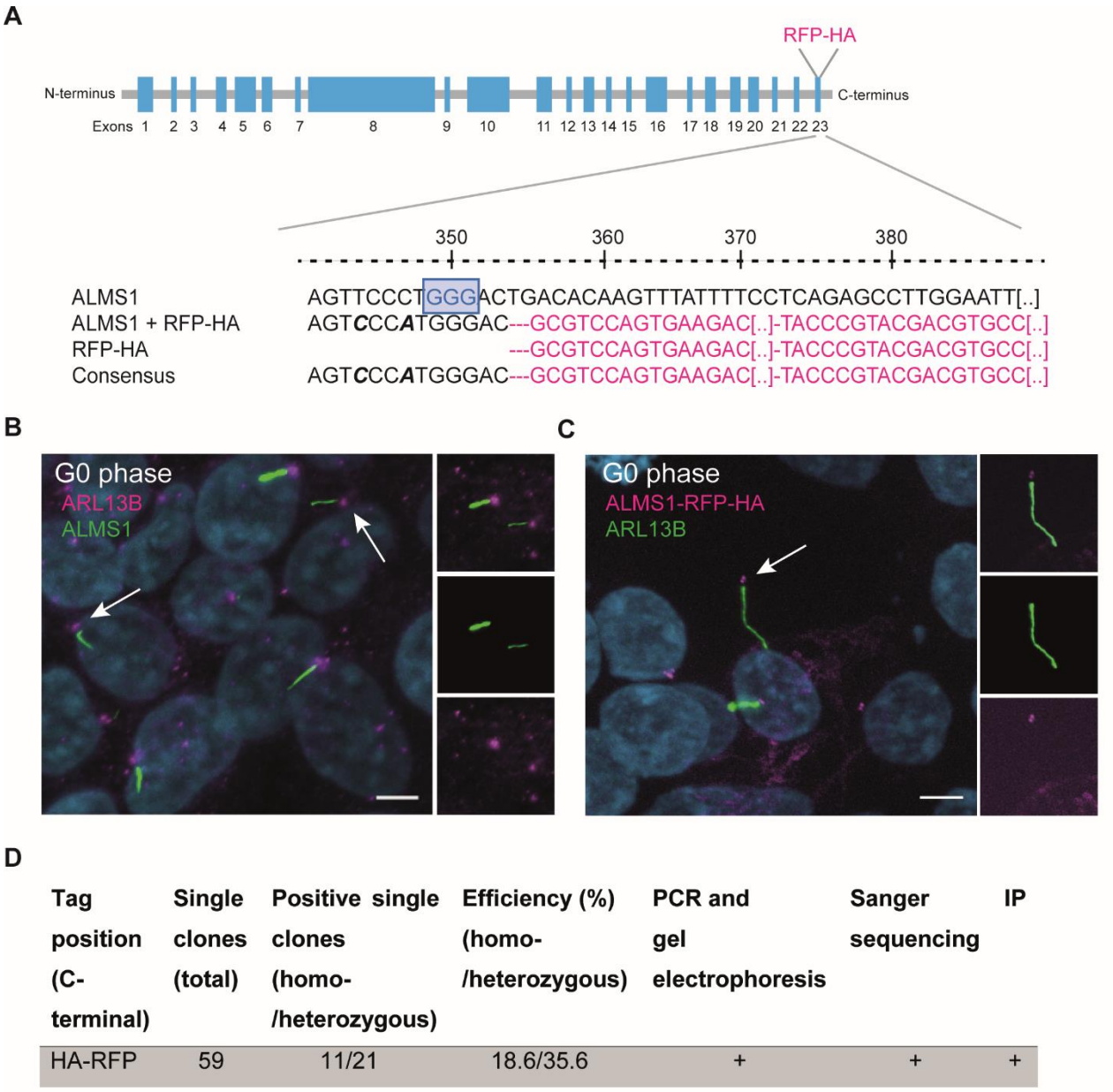

D

Tag position (C-terminal)	Single clones (total)	Positive single clones (homo-/heterozygous)	Efficiency (%) (homo-/heterozygous)	PCR and gel electrophoresis	Sanger sequencing	IP
HA-RFP	59	11/21	18.6/35.6	+	+	+

Figure 29 ALMS1-RFP-HA localizes to the BB of cilia
A, Schematic overview of another tag insertion into the C-terminus of ALMS1 confirmed by Sanger sequencing. An RFP-HA tag containing linker sequences (---) were designed and was introduced upstream of the PAM sequence (blue). From upper panel to lower panel, a small part of the tagged single clone sequence, the RFP-HA sequence and the consensus sequence are shown. [..] = continued sequence, --- = linker sequences (GGGS).
B, HEK293T wt cells in G0 phase were used for localization studies of native ALMS1 (magenta) at the basal body of cilia (green).
C, ALMS1-RFP-HA (magenta) in HEK293T cells show basal body localization under ciliated conditions. ARL13B was used as a marker for cilia and is marked in green.
D, The presented table encompasses the total number of single clones, positively tagged cells and the employed methods for verifying the inserted tag. Positively tagged ALMS1 cells were used for affinity purification followed by mass spectrometry analysis.

7.14.2 Retina specific Pull Down

The procedure of tissue-specific protein complex analysis includes several steps. First lysate of ALMS1-RFP-HA and native HEK293T cells were generated, incubated with HA beads with a

subsequent SDS wash to remove interactors originating from HEK293T cells. The cleared bait was further incubated with porcine retina lysate, followed by several washing steps and an on-bead digest. Samples were further processed for mass spectrometry and used for database dependent data analysis (Figure 30).

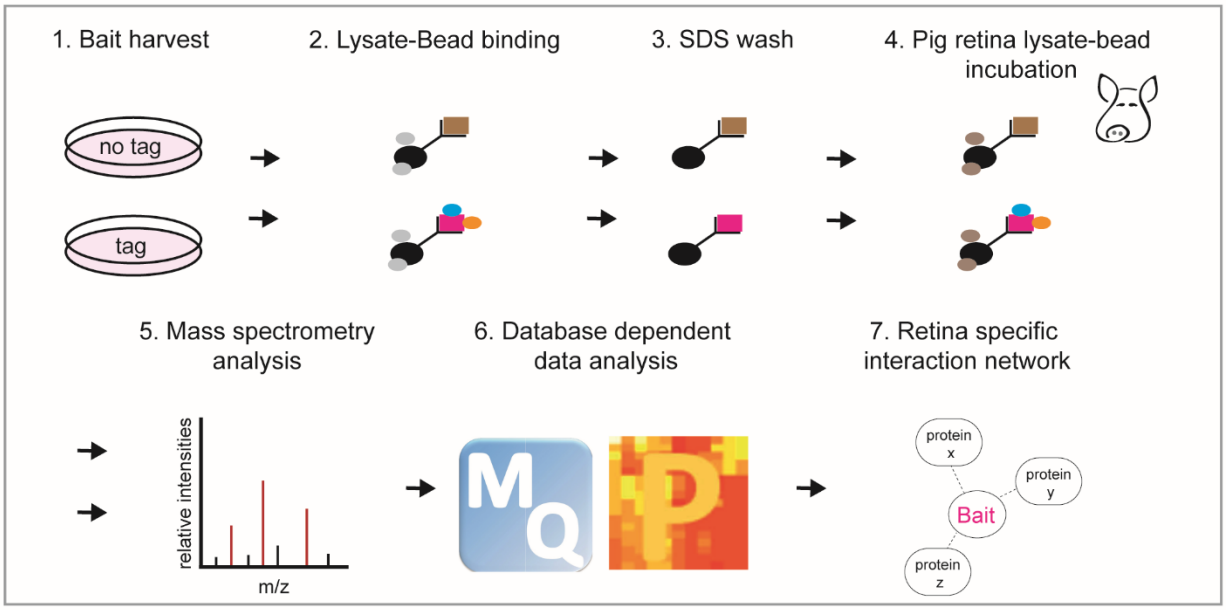

Figure 30 Workflow of Tissue-specific pull down
A workflow of tissue specific protein complex analysis is presented. First, ALMS1-RFP-HA and native HEK293T cells are harvested (1.), followed by cell lysis and bead incubation (2.). After removal of interactors originating from HEK293T cells with SDS (3.), porcine retina lysate is added to the tag bound beads (4.). After an on-bead digest, mass spectrometry analysis was conducted with database dependent data leading to a retina specific interaction network.

In preparation for tissue specific protein complex analysis, an experiment was performed with six biological replicates of only ALMS1-RFP-HA and HEK293T native cells, respectively. ALMS1 was found with a high sequence coverage (75.9 %) (see 10.10, Appendix Figure 42 C). Again, the Tier system was also applied as described above. Tier 1 proteins include nine proteins, while 60 proteins are grouped into Tier 2. No significant specific clusters linked to microtubules, or the centrosome were identified using the Gene Ontology Resource. CEP70 protein was also found with the RFP-HA tag, alongside with AKAP8L, that were also found with ALMS1-sfGFP (Figure 31 A, B). No more overlapping proteins were identified by comparing the two tags. An ALMS1-RFP-HA protein network identified proteins that are also involved inter alia in cytoskeletal function, ubiquitin function, in signaling, apoptosis, cell proliferation. Proteins, that play a role in anatomical structure development, in lipid metabolic process and carbohydrate metabolic process were found (Figure 32, see 10.10.2 Appendix Table 31,32). With the advantage of the high affinity of HA to the beads, ALMS1-RFP-HA was further used for tissue-specific protein complex analysis.

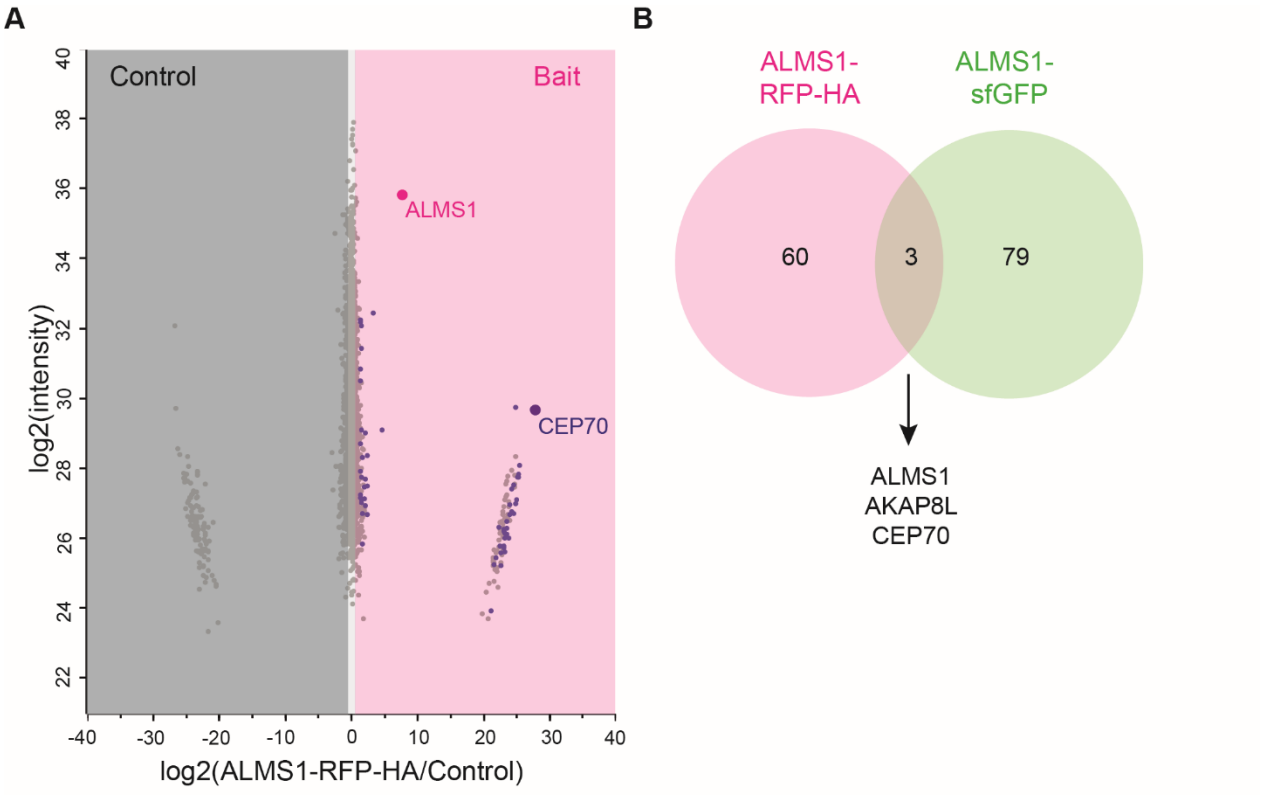

Figure 31 Protein complex analysis
A, Scatter plot indicates the distribution of all proteins identified for ALMS1-RFP-HA compared to the control (native HEK293T). On the x-axis the ratio of mean ALMS1-RFP-HA/mean control and on the y-axis the intensity is shown. ALMS1-RFP-HA is marked in magenta, and Tier 2 identified potential proteins (*p*-value) are depicted in blue. Six biological replicates of ALMS1-RFP-HA and control were used, respectively.
B, A Venn-diagram compares identified potential interactors with ALMS1-RFP-HA (left) and ALMS1-sfGFP (right), that were grouped in Tier 2 (*p*-value). Three proteins are shared in both experiments, including the bait (ALMS1) protein, AKAP8L and CEP70. While 60 Tier 2 proteins were identified with ALMS1-RFP-HA, 79 Tier 2 proteins were found with ALMS1-sfGFP.

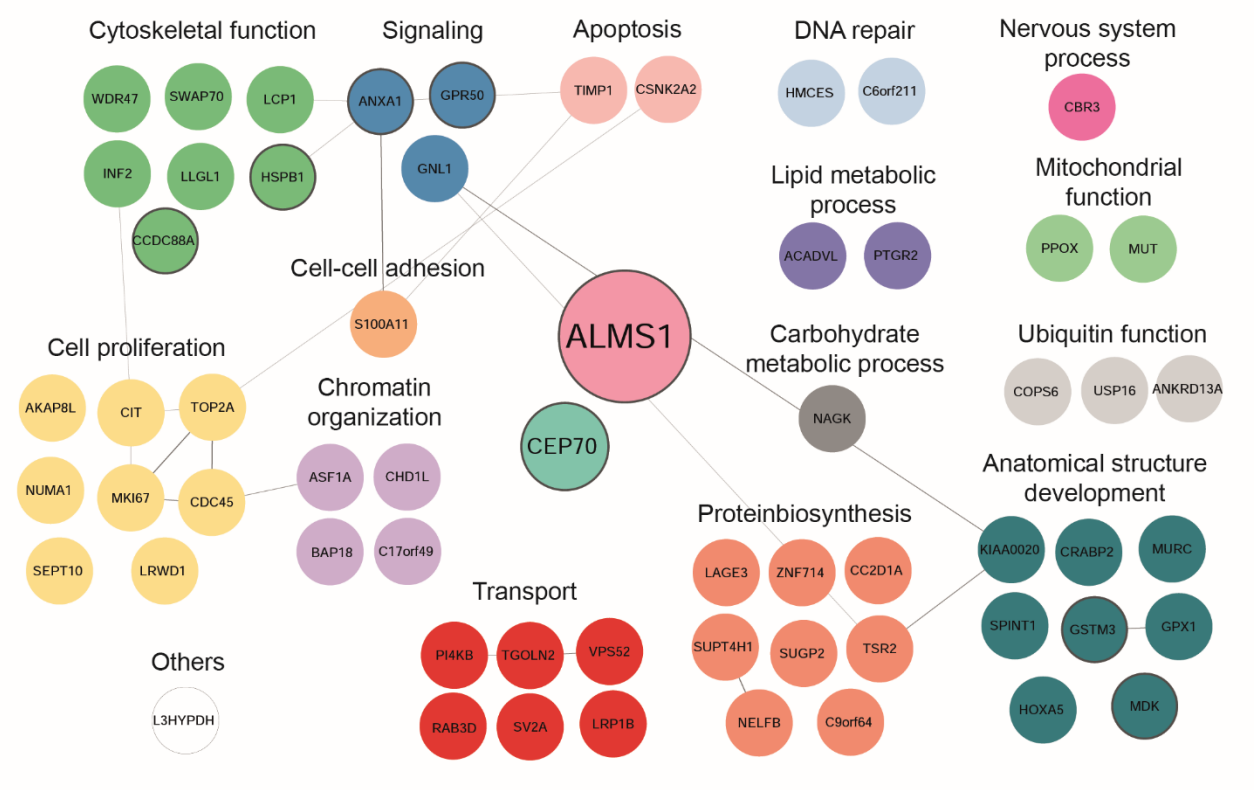

Figure 32 ALMS1-RFP-HA network
Network of potential interaction partners of ALMS1 using RPF-HA tagged cells and their respective function according to the 2023_02 released UniProt Knowledgebase version is presented [152]. Proteins are grouped based on a stringent analysis using FDR < 0.05 and significance A (Benjamini Hochberg) (Tier1) and a less stringent analysis applying *p*-value and significance A (Benjamini Hochberg) (Tier 2). Tier 1 includes nine proteins (black border paint) and Tier 2 60 proteins. Network was created using experimental and functional interactions extracted from curated database using STRING, which was further visualized in Cytoscape [121,122].

First, the concentration of the detergent SDS was determined. Here, 0.01 % SDS was sufficient to remove gently ALMS1 interactors, such as CEP70, originating from HEK293T cells. To check whether the denaturing behavior of SDS influences the bait itself, CEP70 NSF eluate was added to the SDS washed bait samples. CEP70 binds SDS treated ALMS1 bait samples, which enhanced the confidence of using 0.01 % SDS for this experiment (Figure 33).

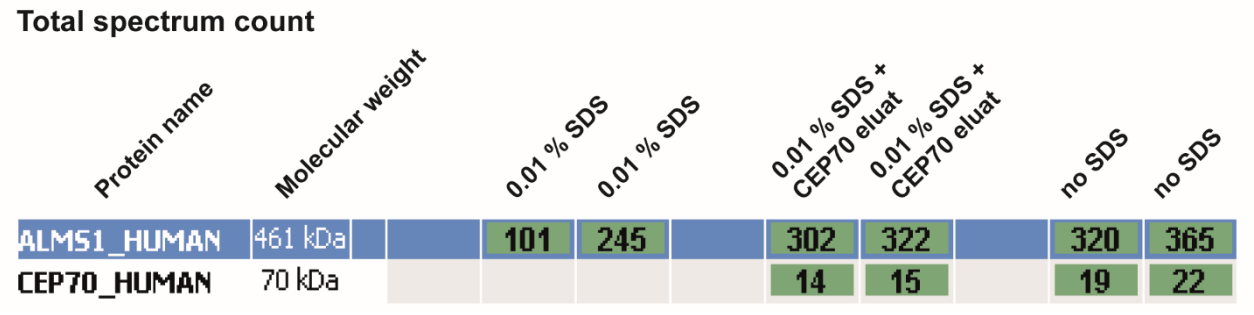

Figure 33 SDS concentration has no impact on ALMS1 binding capacity
An excerpt from the proteome software Scaffold 5 shows an overview of the total spectrum count of ALMS1-RFP-HA treated with or without 0.01 % as well as with or without eluate from CEP70. As CEP70 seems to be a strong

interaction partner of ALMS1, eluate from CEP70 was used after 0.01 % SDS washing to identify the potential influence of SDS on the binding capacity bait itself. The experiment was exerted in duplicates.

Eventually, the tissue specific protein complex analysis was conducted and analyzed using database dependent analysis. The scatter plot summarizes proteins that are abundant in the control or the bait (Figure 34).

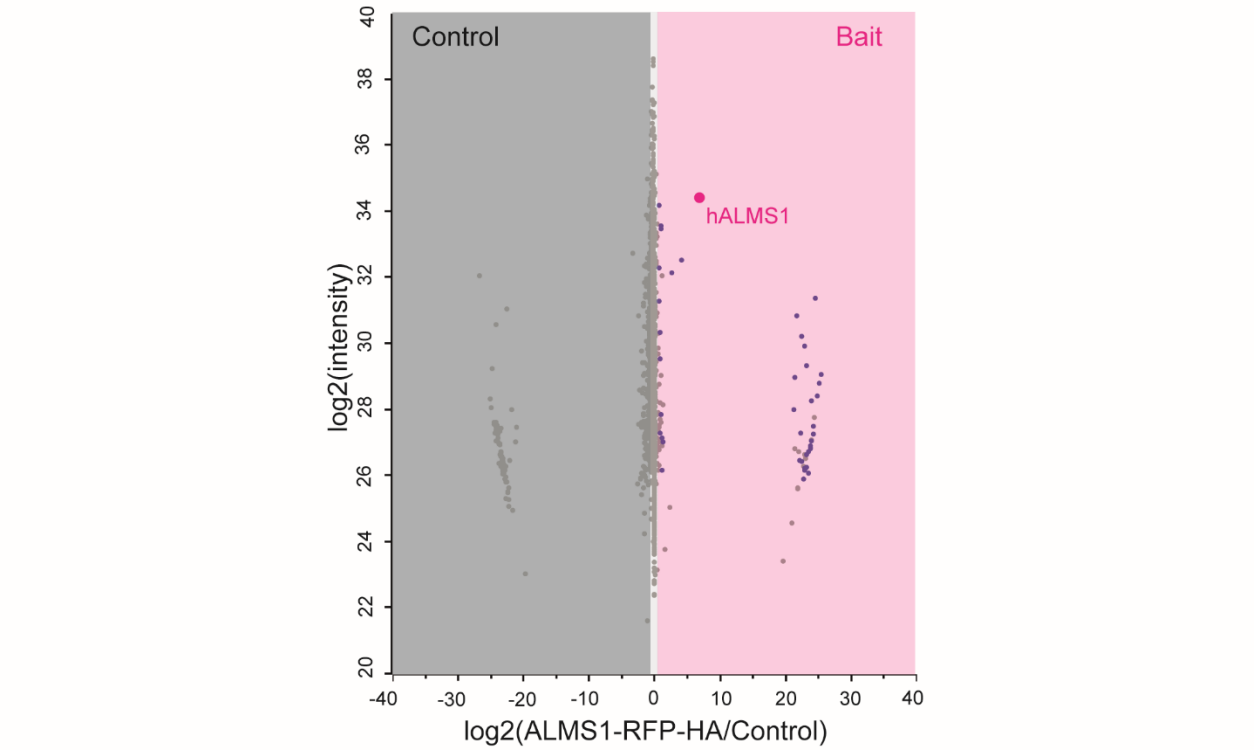

Figure 34 Scatter plot of tissue-specific pull down
The scatter plot summarizes six biological replicates of ALMS1-RFP-HA and control, both treated with 0.01 % SDS. Proteins that are more abundant in the bait (ALMS1-RFP-HA) sample are on the right side (magenta), while proteins that are more abundant in the control cells are on the left side (grey). Identified interactors are grouped according to a stringent (Tier1: significance A (Benjamini Hochberg, FDR < 0.05) and less stringent (Tier 2: significance A (Benjamini Hochberg), *p*-value 0.05) analysis. Tier 2 proteins are marked in blue. hALMS1 = human ALMS1.

Stringent analysis identified seven proteins for Tier 1, while less stringent analysis grouped 44 proteins in Tier 2 (Figure 35, see 10.10.4 Appendix Table 33). Tier 1 proteins are APIP, LRP4, EFEMP1, NQO2, FSTL, FBN1, IGFBP5 (Figure 35, bold boarder marked). Tier 2 proteins harbor various function, including cytoskeletal function, cilium organization, signaling and photoreceptor development. No overlapping proteins were identified by comparing interactors gained from HEK293T and pig retina lysate. However, Nephrocystin 4 (NPHP4) was found as an interactor of ALMS1, that was already been described. It was not identified with HEK293T cells, although it is expressed according to the Human Protein Atlas (https://www.proteinatlas.org/ENSG00000131697-NPHP4/cell+line), that highlights the importance of this method [184,185]. Furthermore, this approach enables in-depth understanding of tissue-specific and functionally relevant protein networks in a native context.

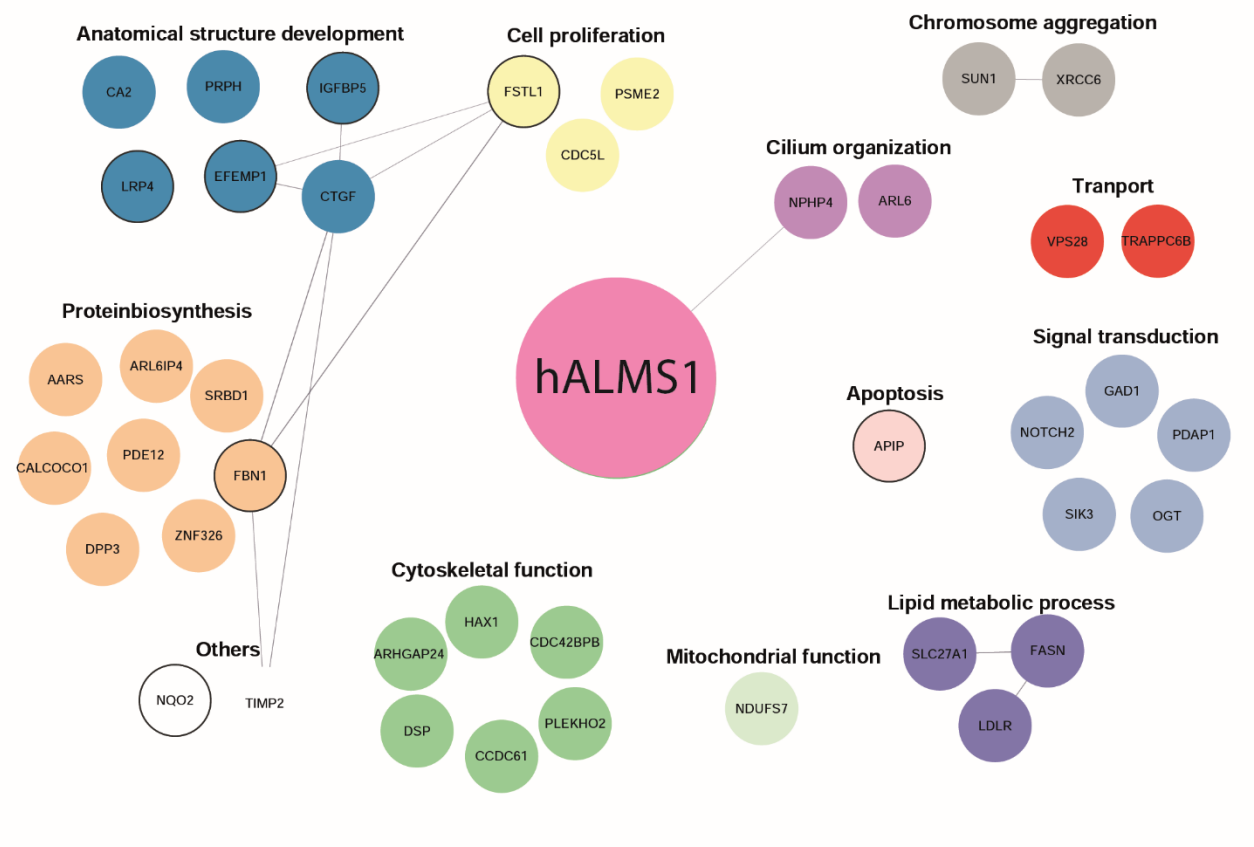

Figure 35 Retina specific ALMS1 network
Presenting a network of retina specific interaction partners of ALMS1 grouped according to their function in cellular processes. Proteins are clustered in Tier 1 and Tier 2 based groups. Tier 1 (Significance A (Benjamini-Hochberg) FDR < 0.05) and permutation-based FDR < 0.05) contains seven significantly enriched proteins (border painted in black). Tier 2 (Significance A (Benjamini-Hochberg) FDR < 0.05 and *p*-value < 0.05) contains 44 proteins, with a less stringent threshold (no border paint). Proteins, which exhibit multiple function, were listed only once with their primary function, as described on the UniProt Knowledgebase (the 2023_02 released version, [152]). This retina specific ALMS1 network was set up using experimental and functional interactions extracted from STRING, a curated database, and finally visualized in Cytoscape [121,122].

8 Discussion and Outlook

The Alström syndrome is a rare monogenic multisystem disorder, which is caused by the mutated *ALMS1* gene. However, the (patho-) mechanism is still elusive. Therefore, the aim of this thesis was to get a new insight into the function of ALMS1, its role in BB and ciliary function, as well as to elucidate the underlying mechanism in Alström syndrome. For the investigation of this aim two main analyses were applied. First, the protein complex analysis to identify interaction partners of ALMS1 and second phenotypic analysis to validate the ALMS1 interactome and the role of ALMS1 in cilia biology. HEK293T cells were used due to their high protein yield, their ability to form cilia, and their wide use in protein network studies [120,186–188]. Furthermore, indels were introduced in the *ALMS1* gene of human retinal pigment epithelial cells (hTERT-RPE1). They were chosen due to planar growth, cytoskeletal arrangement and their high ciliation rate (80-90%) [189].

8.1 Novel interaction partners of ALMS1

So far, ALMS1 interaction partners were identified by yeast-two hybrid (Y2H) system experiments, BioID studies or several affinity purifications coupled with mass spectrometry (AP-MS) experiments. Latter includes the BioPlex large-scale human interactome study based on AP-MS [16,190,191]. These studies mainly used ALMS1 fragments, covering the CT with ALMS1 motif from murine or found ALMS1 as an interactor/prey. For example, for the yeast-two hybrid system, the CT end of mouse ALMS1 was used. Disadvantages of the Y2H system include that protein-protein interaction has to occur in the nucleus to induce reporter gene activation, a high number of false positive and false negative hits are generated and differences in protein folding properties, expression and PTM can happen [192]. In this thesis, the focus was on human full-length ALMS1 protein, which is closer to the physiological protein level and does not alter protein interactions [193].

To identify and investigate functional important interaction partners, endogenously tagged ALMS1 was employed for protein complex analysis. A fluorescent tag sequence (sfGFP) at the C-terminal (CT) end of the *ALMS1* gene was introduced via the CRISPR/Cas9 method into HEK293T cells (Figure 14). An N-terminal tag was not possible due to a high GC-rich region and repetitive sequences in exon 1 (Woerz *et al.*, under review [3]). Another benefit of introducing a CT tag is that many transcript variants of ALMS1, which are in total 25, can be covered [194] (Woerz *et al.*, under review [3]). Rather than transfecting overexpression constructs, endogenous tagging enables investigation of protein function in full length and in a native context, as well as it does not alter protein interactions [193,195]. It was previously shown, that overexpression of ALMS1 displaced endogenous ALMS1 in the past [18]. Another benefit is, that

no ALMS1 antibodies are needed, which may have a low affinity to the beads and may not be specific enough [196] (Woerz *et al.*, under review [3]). The tag has a size of 711 bp, which could lead to changes in the protein folding properties, a possibly disturbed localization at the BB/centrosome, which may result in altered centrosomal and cilia biology. To reduce these risks, I decided to use sfGFP, that should not interfere with the protein folding properties of the tagged protein [197]. My results showed that despite this rather large tag, the occurring localization was not disturbed (Figure 15) (Woerz *et al.*, under review [3]).Therefore, the tagged cells are suitable for protein complex analysis, which led to a successful purification of endogenous tagged 461 kDa ALMS1 and its potential interaction partners.

The ALMS1-sfGFP interactome presented here included interactors, that are involved in the same or in similar processes as described by the before mentioned interactome studies. Hence, our data contribute to the ongoing discussion about the various ALMS1 functions in cell differentiation, energy metabolism homeostasis, cell cycle control, intracellular trafficking, and ciliary signaling pathways [16,17]. Furthermore, novel and promising ALMS1 interaction partners were identified that are involved inter alia in cell cycle, cytoskeletal and cilia-related processes. The analysis of the resulting data suggests a role of ALMS1 in ciliary basal-body membrane docking, proliferation, cytoskeletal organization, and signal transduction (Figure 17) (Woerz *et al.*, under review [3]). Additionally, mass spectrometry analysis of sfGFP tagged ALMS1 revealed that ALMS1 is indirectly involved in ciliogenesis (Woerz *et al.*, under review [3]).
Highly promising and functional relevant interaction partners were CEP70 and TUBGPC2 (Woerz *et al.*, under review [3]). CEP70, described by Shi et al in 2011, plays an important role in microtubule organization and stabilization by regulating tubulin acetylation through the interaction with histone deacetylase 6 (HDAC6) [70]. Additionally, CEP70 interacts via its coiled coil domains with γ-tubulin, ensuring proper localization to the centrosome [74]. Γ-tubulin, a member of the tubulin super-family, is crucial for the microtubule nucleating molecular machinery known as the γ-Tubulin Ring Complex (γ-TURC) at the centrosome [46]. ALMS1-sfGFP interactome data showed a component of the γ-TURC: the TUBGCP2 as a possible interactor. It codes for the γ-tubulin complex protein 2 (GCP2) and leads to a neurodevelopmental phenotype upon mutation [198]. Our results demonstrated an unaffected TUBGCP2 at the BB in ALMS1 deficient cells using localization studies, hinting towards TUBGCP2 upstream of ALMS1 (Figure 9). These findings are in line with previous results from Hearn *et al.*, who described an association of γ-tubulin and ALMS1 at the centrosome and BB of cilia and showed an unchanged γ-tubulin in ALMS1 deficient fibroblasts [116].

Another interesting ALMS1 interactor is the A-kinase anchoring protein 8 like (AKAP8L), a homolog of AKAP8. AKAPs form macromolecular complexes of cAMP pathway regulators including adenylyl cyclase (AC) and downstream effectors of cAMP like protein kinase A [199]. AKAP8L was previously shown to bind protein kinase A regulatory subunit Iα (RIα) [200]. Additionally, RIα is involved in regulating mTORC1-mediated processes [201]. Further, AKAP8L positively influences mTORC1 biology and anchors PKA [200]. The mTOR pathway regulates cell growth, cell proliferation, apoptosis, and autophagy [200,202]. Interestingly, ALMS1 was also reported to be involved in cell cycle transition [88], which might indicate, that both proteins are part of the same mechanism regulating cell cycle progression. ALMS1 KO hTERT-RPE1 whole cell lysate was investigated regarding AKAP8L protein expression (Figure 18). The ALMS1 KO demonstrated no influence on total AKAP8L protein level. However, this does not provide any conclusion if AKAP8L localization or function is altered. To investigate a functional interplay, a co-localization of ALMS1 and AKAP8L could be investigated. Intriguingly, AKAP-mediated PKA anchoring regulates contractile function in cardiomyocytes [203]. Disturbed contractility can lead to dilated cardiomyopathy [204], which is one major symptom (~60%) of Alström patients [205]. Even more interesting, the data presented in this study suggest an interaction of ALMS1 main interactor CEP70 with protein kinase A regulatory subunit IIβ (PRKAR2B) and AKAP8 (Figure 23, see 10.7.4). This emphasizes the potential role of ALMS1 and CEP70 in this tissue specific process and hints at the possibility that this mechanism has a similar impact in other tissues as well.

A recently described method by Ghetti *et al.* (2021) offers a novel approach for achieving rapid and efficient CRISPR/Cas9-mediated knock-in in hTERT-RPE1 cells, as well as in induced pluripotent stem cells (iPSCs) [206]. Implementing this method could significantly contribute to identifying interaction partners in a more specific manner, tailored to the retinal or ALMS patient context. By utilizing this technique, researchers can enhance the relevance and precision of their investigations, providing valuable insights into the molecular interactions associated with ALMS and retinal function.

8.2 ALMS1 shows no impact on insulin marker expression in hTERT-RPE1

One of the major symptoms Alström patients suffer from is diabetes type II (~90%) [110]. Interestingly, the presented ALMS1-sfGFP interactome study revealed TSG101 and STAM as interesting interactors linking ALMS1 function to the transport of Glucose transporter-4 (GLUT4) and therefore insulin signaling [207,208] (Woerz *et al.*, under review [3]). It was also shown, that ALMS1 interacts with Actinin 4 (ACTN4), which in muscle cells is involved in GLUT4 trafficking

[112]. GLUT4 is a glucose transporter that facilitates insulin regulated glucose uptake into fat and muscle cells [209]. The Tumor susceptibility gene 101 protein (TSG101), a member of the endosomal sorting complex required for transport (ESCRT)-I complex, emphasizes vesicular trafficking as well as sorting and re-distribution of GLUT4 in cardiac myocytes [207,210,211]. Signal transducing adapter molecule 1 (STAM) is a member of ESCRT-0 complex, which interacts with TSG101 of ESCRT-I complex, inducing the ESCRT mediated endosomal trafficking [150,208,212]. ALMS1 may serve here as a modulator or stabilizing scaffold protein, to facilitate proper GLUT4 transport by mediating vesicular trafficking via TSG101.

ALMS1 was also suggested being involved in glucose transport via the actin cytoskeleton [155,213], which is important for insulin stimulated GLUT4 transport. Furthermore, the ALMS1-sfGFP IP data revealed three proteins, Vasodilator-stimulated phosphoprotein (VASP), Desmoglein-2 (DSG2) and Neuroblast differentiation-associated protein AHNAK (AHNAK), that support actin organization. Therefore, investigation of the interplay of TSG101, GLUT4 transport and the actin cytoskeleton using localization studies could be performed in the future. To gain initial insights into the structural arrangement/organization of actin cytoskeleton in human retinal cells, a phalloidin staining, that binds to F-actin, can be performed. Since hTERT-RPE1 cells lack GLUT4, it would be interesting to investigate TSG101 in insulin signaling in ALMS patient derived fibroblasts or organoids (https://www.proteinatlas.org/ENSG00000181856-SLC2A4/cell+line).

A different approach that could be of use, is metabolomics, which could help to link and narrow the metabolic involvement of ALMS1 in human ciliated cells. So far, one untargeted metabolome and transcriptome study identified a connection between ALMS1 and specific metabolites by revealing three potential candidates: (N(alpha)-acetyl-dl-ornithine, N(alpha)-acetyllysine, and N-acetyl-l-aspartate (NAA)) [214]. This could link the causally metabolic function of ALMS1 to Alström syndrome.

In general, insulin (PI3K/AKT) signaling pathway is involved in glucose and lipid metabolism and homeostasis as well as cell survival and cell proliferation [156,157]. Under pathophysiological conditions of this pathway, obesity and type 2 diabetes can be evolved. It was also shown that ALMS1 loss alters TGF-β pathway, which could also influence other signaling pathways such as the p53, MAPKs and PI3K/AKT pathway [157,215–218]. Bea-Mascato *et al.* showed an inhibitory effect of TGF-β on downstream processes, such as cell proliferation, cell migration and recycling of receptors due to ALMS1 loss [215,219]. Thus, ALMS1 wildtype and KO hTERT-RPE1 cells were treated with insulin to stimulate glucose uptake and investigate any deviation of the insulin signaling pathway upon ALMS1 loss. Therefore, the level of proteins involved in

insulin and glucose signaling, such as AKT, pAKT (Figure 19), GSK3B (Figure 20), and CREB (Figure 21) were investigated.

Regarding protein kinase B (AKT), activation occurs due to phosphorylation of Thr308 and Ser473 by 3-Phosphoinositide-dependent protein kinase 1 (PDK-1), inducing inter alia glucose metabolism [156–158]. AKT involvement in insulin signaling upon ALMS1 loss is so far elusive. It was shown, that AKT activation on pre-adipocytes lead to no alterations, while in certain mice tissues exhibit enhanced activation or even inhibition of AKT due to ALMS1 loss [155,215,220]. An initial experiment with control and ALMS1 KO cells showed no direct involvement of ALMS1 on AKT expression or phosphorylation level. This variability could be either due to three AKT isoforms with different phosphorylation sites, that are present in different tissues [215,221] or an ALMS1-independent role [16].

Glycogen synthase kinase 3 (GSK3) was proven as a significant player in the emergence of insulin resistance, primarily owing to its involvement in the regulation of glycogen synthesis [160,222–224]. GSK3 comprises two homologous isoforms including GSK3α and β, with postulated distinct functions. Insulin has an inhibitory effect on GSK3 via phosphorylation resulting in glycogen synthetase (GS) activation followed by glucose storage in form of glycogen. Ablation of GSK3 leads to obesity and type 2 diabetes via inactivation of GS [225]. Interestingly, ALMS1 was identified as an interactor of GSK3β in a proximity-labeling followed by MS [226,227]. In the ALMS1 protein-protein interaction study presented here, GSK3β was also found as an interactor of ALMS1, suggesting a regulatory function of ALMS1 on GSK3β. To further investigate this interaction hTERT-RPE1 control and ALMS1 KO cells were compared on protein level regarding pGSK3β (Figure 20). The cells were either untreated or stimulated with insulin and upon initial analysis a clear increase of pGSK3β intensity from untreated to insulin treated was visible. This proves the functionality of this experiment, which is consistent with the findings that AKT phosphorylates and inactivates GSK3 [228,229]. In untreated conditions a slight increase in pGSK3β from control to ALMS1 KO can be seen, which suggests activation of downstream substrates, such as GS leading to glycogen synthesis. Unfortunately, this effect was not visible by comparing control and ALMS1 KO under insulin stimulated conditions. The observed mild increase in basal level pGSK3β could potentially be attributed to additional signaling pathways. GSK3β plays a crucial role in various pathways, including Wnt signaling, which might contribute to its altered expression [230,231]. This preliminary result suggests, either no direct link between ALMS1 and GSK3β or a mechanism independent of phosphorylation of GSK3β. An alternative hypothesis could be the occurrence of genetic compensation, wherein alterations in RNA or protein levels may serve as a compensatory

mechanism for the loss-of-function of a another gene [232]. Further, it would be interesting to investigate a potential inhibitory effect of ALMS1 on GS, resulting in insulin resistance.

Another protein, cAMP response element-binding protein (CREB1), is involved inter alia in glucose homeostasis [161,233]. For example, in pancreatic beta cells, CREB plays a role in insulin secretion. When glucose levels rise, it leads to an increase in intracellular ATP levels, which subsequently activates the enzyme adenylyl cyclase (AC). AC generates cyclic AMP (cAMP), which then activates protein kinase A (PKA). PKA phosphorylates and activates CREB, which in turn promotes the expression of genes involved in insulin secretion and beta cell function [234,235]. To investigate a potential influence on insulin dysregulation upon ALMS1 loss via CREB1, ALMS1 KO and control hTERT-RPE1 cells were stimulated with insulin or not (Figure 21). No change of CREB1 protein level was detected, which suggests no influence of ALMS1 on CREB1. However, phosphorylated CREB1 was not investigated, which might give valuable insights inter alia in glucose sensing and insulin secretion alterations [161,234,236,237].

As previously described, CEP70 was found to interact with PRKAR2B and has an influence on cAMP signaling in heart tissue, that might be the cause for dilated cardiomyopathy. Further, I hypothesized the possibility that this involvement could lead to symptoms in other tissues as well. Here, the described connection of ALMS1 close interactor CEP70 with PRKAR2B, respectively ALMS1 with GSK3, and hence their impact on cAMP signaling might influence insulin signaling as well as beta cell function and may ultimately lead to type 2 diabetes. Concluding that an affected cAMP signaling in Alström patients could explain two of their main symptoms.

In conclusion, the ALMS1 network study offers novel and interesting insights into potential interactors that connect with previously published data. No direct impact of ALMS1 on protein/expression levels of the so far investigated candidates could be confirmed in both native (wt) and ALMS1 deficient hTERT-RPE1 cells. It is important to note that the absence of GLUT4 in the utilized cell lines might contribute to this outcome, and it raises the possibility that ALMS1, as hypothesized, is essential for GLUT4 transport. In addition, the observed reaction of RPE1 cells to insulin treatment further suggests a possible interaction of ALMS1 with other members of the GLUT family. Furthermore, it is possible that ALMS1 plays a role in facilitating the appropriate localization of these interactors to ensure proper functioning, rather than exerting an inhibitory effect. Thus, additional investigations using different cell lines, such as HEK293T cells for a rapid assessment, as well as ALMS-patient derived fibroblasts or organoids, along with

localization studies, would help to reveal if ALMS1 is truly involved in insulin signaling such as GSK3β phosphorylation or GLUT4 transport.

8.3 ALMS1 function in cilia biology

First, indels were introduced into the *ALMS1* ex 8 and/or ex10 using the CRISPR/Cas9 method (Table 22, Figure 6). Therefore, exon specific sgRNAs were designed using the CCtop online tool [137] and chosen due to a low off-target effect prediction [137,238]. These off-targets are located in intergenic and intronic sequences showing three to four mismatches and were therefore neglected [239]. Characterization of the introduced indels showed for ALMS1 ex 8 a reduced ALMS1 localization at the BB with unaltered ciliary length compared to the control, suggesting a truncated ALMS1, which may represent a milder progression of patients with *ALMS1* ex 8 mutations [240] or due to genetic compensation in CRISPR/Cas9 mutants, while in knock-down models not [241] (Figure 7, Figure 8). To address this, the effect upon complete loss of ALMS1 needs to be first understood, which could help to explain truncated ALMS1 function in the future. Additionally, a truncated ALMS1 variant needs to be verified in ALMS patient derived cells to exclude potential artefacts. Therefore, the ALMS1 ex 8 mutant was excluded from the study.

In contrast to ALMS1 ex 8 KO, ALMS1 ex 10 as well as both ALMS1 ex 8-10 KO cells showed no ALMS1 localization at the BB of cilia (Figure 7, Figure 8) (Woerz *et al.*, under review [3]). A Blue Native Polyacrylamide Gel Electrophoresis (BN-PAGE), that enables separation of proteins according to their net charge, size (up to 10 MDa) and native structure, was performed with one sample of HEK293T lysate (native ALMS1) and two samples of ALMS1-sfGFP eluate (kindly conducted by PhD student Klaudia Maruszcak, AG Rapaport, Biochemistry department, University Tuebingen) [242,243]. A faint band at around 460 kDa for HEK293T cell lysate was observed, while the eluates showed inconclusive results due to lack of specific controls, such as ALMS1 deficient cells (see 10.6). In the future, additional investigation including patient-specific mutations can be investigated, once a clear phenotype in ALMS1 KO will be described, which could be used as a read-out.

ALMS1 deficient cells displays an overall mild increase in γ-tubulin (TUBGCP1 and TUBGCP2) signal at the basal body (Figure 9). However, it's important to acknowledge that these results display significant variability. Interestingly, in ALMS patient-derived fibroblasts from the skin, γ-tubulin levels appear to remain unaffected [116,119]. Notably, increased γ-tubulin levels have only been observed in cancer cells [244] . Further analyses have to be conducted to investigate and understand the specific impact of ALMS1 on γ-tubulin.

The role of ALMS1 in cilia formation is a subject of extensive discussion in ALMS1 mutant models, proposing both direct and indirect involvement [16,18,66,117–119]. In a recent study by Álvarez-Satta *et al.*, longer and bended cilia were observed in an ALMS1 knockdown model using hTERT-RPE1 cells [87], whereas my ALMS1-deficient cells displayed mostly shorter cilia (Figure 7, 8). Moreover, co-staining of ARL13B and acetylated tubulin excluded transport and localization defects of ARL13B in the ciliary membrane and confirmed ciliary shortening (Figure 7). In the beginning, the ALMS1 ex 10 KO exhibited longer cilia, which became shorter over time. Furthermore, it could be that the longer cilia of ALMS1 ex 10 KO become unstable, resulting in subsequent shortening. Alternatively, cells may require an extended timeframe to form cilia. This can be addressed by an increase of serum deprivation time. Cilia assembly is potentially influenced by factors such as a slower proliferation rate, centrosomal cohesion or impaired signaling. Unfortunately, conducting a rescue experiment to restore ciliary length remains a formidable challenge, owing to the significant size of the ALMS1 protein (~ 0.5 MDa). An ALMS1 variant lacking exon 2 fused to a N-terminal Flag tag was obtained from Addgene (Plasmid #136877) and was tested. The expression of ALMS1 variant relies on doxycycline induction. However, obtaining conclusive results proved elusive as the ALMS1 antibody epitope sequence did not align with the ALMS1 variant sequence in the plasmid. Additionally, the lack of a suitable Flag antibody for localization studies thwarted the verification of successful transfection.

Discrepancies in the observed phenotype may arise from differences in the experimental setup, including the utilization of an ALMS1 knockdown model in hTERT-RPE1 cells by Álvarez-Satta *et al.* or different serum deprivation time points. Speculation remains regarding whether genotype-phenotype correlations contribute to the variation in ciliary length, as accurately assessing isoform-specific levels of ALMS1 protein remains challenging. Consequently, distinct mutations may induce diverse phenotypic features, influencing the development and manifestations of ALMS [119,245]. Mutations that profoundly affect the structure or function of the ALMS1 protein may lead to more severe organ phenotypes.

CEP250 modulates the anchoring of the centrosomal linker and the ciliary rootlet promoting centriole cohesion. Disease involvement of CEP250 was described for cone-rod dystrophy and hearing loss (OMIM: 618358), which are also presented in Alström syndrome. It was previously shown, that CEP250 is reduced at the BB upon ALMS1 loss, which aligns with the findings obtained from ALMS1 deficient cells used in this study (Figure 10, 11). Another protein of interest, pericentriolar material 1 (PCM1), was investigated, as it is inter alia essential for centrosome assembly and function, ensuring the proper localization of key centrosomal proteins including CEP250, CETN3, PCNT, and NEK2 [133,134]. Interestingly, PCM1 remained

unaffected upon ALMS1 loss (Figure 10), indicating a potential CEP250-depedendent localization on PCM1 and ALMS1. Furthermore, previous studies have indicated that CEP250 is not directly involved in cilium formation or maintenance [246–248], while another study proposed its influence on centrosomal cohesion and cilia assembly [249]. Based on these findings, it could be hypothesized, that the reduction of CEP250 at the BB upon ALMS1 loss may contribute to a shortage in ciliary length. To further investigate this hypothesis, rescue experiments utilizing overexpression constructs for CEP250 in ALMS1-deficient cells could provide valuable insights. As already indicated, CEP250 alteration show similar phenotypic features as described in ALMS. These results suggest ALMS1 upstream of CEP250 leading to retinal degeneration and hearing loss, while other ALMS1 interacting proteins lead to different phenotypical features such as type 2 diabetes. In this case, ALMS1 might exhibit a scaffold protein function. A deletion analysis of domain specific fragments of ALMS1 might also shed light onto this postulation by identifying domain specific interaction partners and validation of their functions.

Further, positioning and anchoring of the basal body of a cilium, using rootletin was investigated (Figure 10). Rootletin is an important component of the ciliary rootlet and facilitates maintenance of centrosome cohesion and long-term stability of primary cilia [131,132,250,251]. However, in the data presented, the loss of ALMS1 did not affect rootletin compared to the control. As of now, there is no direct evidence of a direct connection between ALMS1 and rootletin function or how rootletin may influence the development of ALMS.

Retinitis pigmentosa GTPase regulator (RPGR) which mainly localizes to the ciliary gate, the transition zone, of cilia was investigated in ALMS1 deficient hTERT-RPE1 cells. RPGR is linked to progressive retinal degeneration and subsequent vision loss in retinitis pigmentosa patients. The protein is postulated to interact with transport processes and to be involved in cilia formation [252]. By comparing control to ALMS1 KO cells, a compressed RPGR was observed (Figure 12). To identify RPGR dysfunction, a known interactor of RPGR the IFT88 was investigated [253]. IFT88, a core member of IFT B complex, remained unaffected suggesting an unaffected intraflagellar transport in the presented ALMS1 KO cells, in contrast to recent findings that showed impaired ciliary transport in ALMS1$^{S1645*/S1645*}$ fibroblasts [107]. This result indicates a preserved RPGR function, despite its compressed morphology in shorter cilia. These findings could be also tissue or cell-specific and need to be further investigated with more than one ALMS-patient derived fibroblast.

Furthermore, polyglutamylated tubulin (GT335) was checked in ALMS1 KO hTERT-RPE1 cells (Figure 12). Polyglutamylation of tubulin has been implicated in several cellular processes, including microtubule stability, intracellular transport, and ciliary function [26,135,254,255]. Aberrant polyglutamylation has also been associated with certain neurodegenerative diseases,

such as Alzheimer's disease and Parkinson's disease. Upon ALMS1 loss in hTERT-RPE1 cells no difference in polyglutamylation of tubulin were observed, suggesting, shorter cilia with unaffected stability, that ensures proper IFT transport, at least for IFT88.

Additionally, to comprehensively identify differentially expressed proteins and quantify the extent of these changes in control and ALMS1 knockout (KO) hTERT-RPE1 cells, a data-dependent acquisition (DDA) or data-independent acquisition (DIA) analysis using mass spectrometry can be employed. These powerful techniques enable the detection and characterization of proteins, allowing for the identification of cell-specific protein alterations following ALMS1 loss [256–258]. The versatility of this approach makes it applicable to various tissues, facilitating the investigation of protein changes in diverse biological contexts and to identify a potential disease-causing mechanism.

8.4 CEP70 interacts with ALMS1 and vice versa

Next, to confirm the ALMS1 interaction with CEP70 a protein complex analysis for CEP70 was conducted. Therefore, CEP70 was fused to a N-terminal Strep/Flag-Tag vector (NSF-CEP70). Since an overexpression model enables the comparison of isoforms as well as domain specific fragments, that mostly cannot be effectively achieved using endogenous tags or antibodies. Transient overexpression of proteins can be advantageous, despite the risk of artifacts and of false negative or false positive results, [193]. Additionally, when it comes to detecting interactors, this approach may only be successful through ectopic expression rather than endogenous precipitations. While this could be attributed to differences in sensitivity, it highlights that ectopic expression can yield rapid and significant results, albeit with a higher potential for false positive detections [193,259]. Interestingly, among other proteins, ALMS1 was found in the CEP70 interactome data. Based on these results of two independent protein complex studies presented here, a strong interaction between ALMS1 and CEP70 can be suggested.

To gain further insights into the functional relationship between ALMS1 and CEP70, CEP70 KD in wt and ALMS1 KO (ALMS1 ex 8-10 KO 2) hTERT-RPE1 cells were performed. A gradual decrease in cell number in ALMS1 deficient cells compared to control cells was observed (Figure 26). This decline could be attributed to either a deceleration in cell cycle progression, increased detaching of cells or an increase in cell death upon loss of ALMS1. ALMS1 KO hTERT-RPE1 cells showed a decrease in cell proliferation using crystal violet, which could influence the cell fate towards cell loss (Figure 8). A previous study highlighted the role of ALMS1 in regulating various cellular processes, including the cell cycle and apoptosis, through the TGF-β pathway [87,88]. They observed an apoptosis resistance to THAP- and C2-C treatment upon ALMS1 deficiency [88]. Furthermore, it was already found that longer cilia

promote cell cycle re-entry delay and apoptosis resistance [219,260,261], while shorter cilia promote cell death in neuronal cells [262]. In ALMS1 KO cells the ciliary length was shorter and cell loss were detected. These findings suggest a potential connection between the length of cilia and cellular responses such as cell cycle regulation and apoptosis.

Furthermore, in the ALMS1 interactome study, proteins involved in cell-cell adhesion were identified, such as Desmoglein-2 (DSG2), a component of the desmosome junctions (Figure 17). It was previously linked to be involved in caspase 3-mediated apoptosis in epithelial cells [263]. While caspases play a critical role in apoptosis, recent studies suggest that caspases are not universally essential for all forms of cell death. Furthermore, caspase activation does not always result in cell death, highlighting the complex nature of cell fate regulation. [263–265]. Low levels of caspases, e.g. caspase-3, was shown in mildly stressed cells to prone cell survival [265,266]. Furthermore, caspase-3 influence cell cycle checkpoint regulators even without causing cell death. This mechanism is so far still elusive and poorly understood [265,267]. To investigate a potential DSG2 and caspase-3 involvement leading to cell loss/survival in the used hTERT-RPE1 cells, localization studies could be performed, as well as a luminescent assay to measure caspase activity. Furthermore, it could be tested whether the detached cells are still viable or death by using either propidium iodide solution or trypan blue. Another method would be mitochondrial fractioning to study cell death and signaling pathways [268,269].

The interaction analysis of CEP70 identified proteins, involved in cilia-related functions as well as in regulation of apoptosis (Figure 23). Notably, a truncated CEP70 form lacking its coiled coil (CC) domains, revealed a loss of ALMS1, other ciliary proteins, and apoptosis regulators. These findings indicate that the two CC domains of CEP70 are vital for its appropriate localization at the centrosome, independent of ALMS1 (Figure 24) [74,168] (Woerz *et al.*, under review [3]). This was further confirmed by unaffected CEP70 localization in ALMS1 KO cells (Figure 25), emphasizing the distinct centrosomal localization mechanism of CEP70. Moreover, upon CEP70 KD in hTERT-RPE1 wt cells, a significant decrease of the ALMS1 signal at the base of the cilia compared to siControl treated wt cells was observed (Figure 27) (Woerz *et al.*, under review [3]). This result suggests CEP70 upstream of ALMS1 with a potential regulatory or stabilizing function on ALMS1. To gain a deeper understanding of the relationship between CEP70 and ALMS1, it would be valuable to explore these findings in patient-derived cells. Such investigations could provide valuable insights into the connection between CEP70 and ALMS1 and the potential clinical significance of CEP70 in relevant disease contexts (Woerz *et al.*, under review [3]).

A potential link between those two proteins could be the Lys-63-specific deubiquitinase BRCC36 (BRCC3), that was identified in the ALMS1 interactome. CEP70 has to be de-ubiquitylated to ensure stable cilia formation [75], that involves the ubiquitin carboxyl-terminal hydrolase CYLD.

However, CYLD was not found in the interaction data, suggesting a transient interaction. Therefore, BRCC3 could be an interesting candidate, although a cilia-related function is so far elusive (Woerz *et al.*, under review [3]).

There are additional CEP70 interactors, that have been implicated in insulin receptor binding, suggesting a potential link to insulin resistance in ALMS patients. For example, Ectonucleotide pyrophosphatase/phosphodiesterase family member 1 (ENPP1). ENPP1 exerts its effect by inhibiting the activity of the insulin receptor (IR) and consequently impeding downstream signaling pathways [270].

To sum up, the identification of ALMS1 as an interactor of CEP70, binding specifically the TPR-CT domain, suggest a potential ALMS1 independent localization of CEP70 to the centrosome/BB.

The differential binding of various proteins and their involvement in apoptosis regulation, ubiquitin function, and CEP70-dependent cell death highlight their significance in the context of CEP70's cellular function (Woerz *et al.*, under review [3]).

8.5 CEP70 KD induces apoptotic events on mRNA level in hTERT-RPE1

To investigate a potential apoptotic event, the *BAX/BCL2* ratio on mRNA level was examined for control and three ALMS1 KO hTERT-RPE1 cells, either with or without CEP70 downregulation (Figure 28). Upon normalization to the Cas9 control, the *BAX/BCL2* ratio of two ALMS1 KO cells (ALMS1 ex 8-10 KO 1 and 2) indicate an already occurring apoptotic event, while only one ALMS1 KO (ALMS1 ex 10 KO) demonstrated a pro-survival ratio. Zulato *et al.* [219] and Bea-Mascato *et al.* [88] suggested an apoptosis resistance in ALMS1 deficient cells, which could be in line with ALMS1 ex 10 KO. However, the two other ALMS1 KOs (ALMS1 ex 8-10 KO 1 and KO 2) revealed an apoptotic event on mRNA level. The precise apoptosis effect upon ALMS1 loss on protein level is so far elusive and needs further investigation in the future. However, an increased cell death accompanied by a decreased cell proliferation rate was identified in ALMS1 deficient β-cells of zebrafish models [271]. It could be hypothesized, that specific mutations in the *ALMS1* gene may trigger apoptotic events in a tissue specific manner, which might lead to a more severe and progressive phenotype in ALMS patients, particularly early photoreceptor degeneration. This hypothesis could be further supported by previous studies, that linked apoptosis to retinal degeneration [272].

Next, the *BAX/BCL2* ratio was investigated, by downregulating CEP70 in wt and ALMS1 deficient cells (here: ALMS1 ex 8-10 KO 2). In this experiment, CEP70 knockdown (KD) (10nM) in native hTERT-RPE1 cells shows an increase in *BAX/BCL2* ratio on mRNA level, while

knockdown of CEP70 in ALMS1 deficient cells leads to a shift towards cell survival. With utilizing 30 nM siCEP70 in wt and ALMS1 KO cells, no apoptotic event was suggested on *BAX/BCL2* mRNA level. However, the cell loss in ALMS1 KO cells with an additional CEP70 KD, which was described earlier, needs to be also considered, implying the concentration of 30 nM might be too high. No marker for successful transfection was used, which makes it unclear if the remaining cells have a CEP70 KD. Therefore, a fluorescently labeled siRNA could be used [273]. Additionally, it has to be considered, that already a potential apoptotic effect of the Cas9 control (Figure 28 A) was detected. Given that the siControl, a commercially available non-targeting DsiRNA (DS NC1, IDT), also already demonstrated an effect on cell loss and staining efficacy, an additional control, such as the DsiRNA with a scrambled sequence could be utilized (DS ScrambledNeg, IDT). Additionally, optimizing and evaluating the transfection method is crucial, as some reagents may offer improved efficiency [274,275].

The results obtained in this study provide evidence suggesting, that CEP70 influences cell death and/or cell survival based on the experimental findings presented (Figure 36). Controversially, it was previously shown, that despite the centrosomal localization of CEP70, it is crucial for development and cell cycle regulation. Notably, CEP70 has been shown to play a diverse role in different organisms, such as regulating centriole amplification in multi-ciliated cells in *Xenopus* [168], participating in flagella formation and spermatogenesis in mice [276], and controlling left-right development and ciliogenesis in zebrafish [72] (Woerz *et al.*, under review [3]).

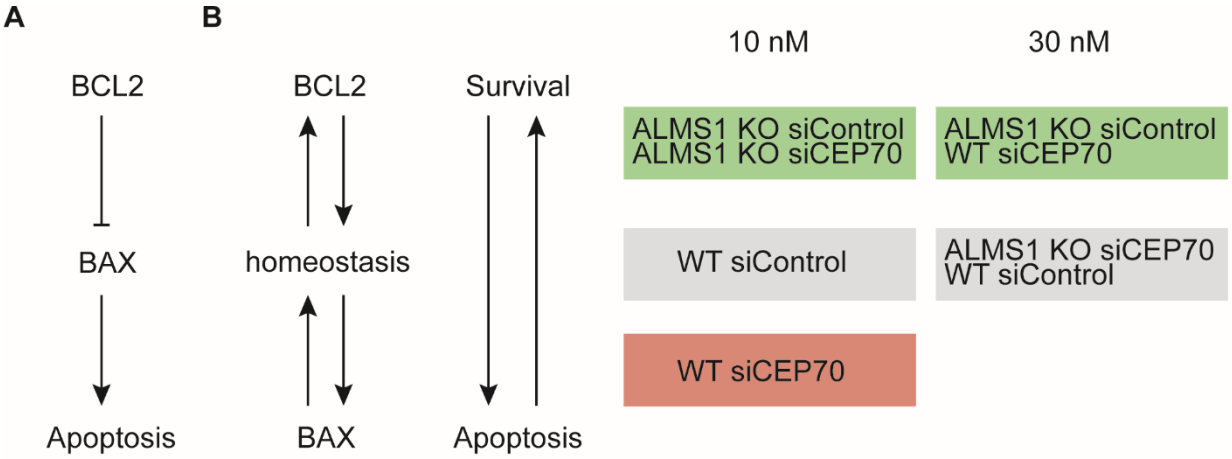

Figure 36 Simplified BAX-BCL2 interaction in relation to gained results
A, A simplified representation of the relationship of BCL2 and BAX in cell fate. BCL2 inhibits BAX, promoting cell survival, while suppression of BCL2 activity releases the inhibition on BAX, leading to cell death.
B, In the left panel, a simplified overview illustrates the relationship between BCL2 and BAX. The experimental setup involved wildtype (wt) and ALMS1 knockout (KO) cells treated with two different concentrations of siControl or siCEP70. Based on the observed outcome of this experiment, the cells are categorized into three groups: cell-survival (depicted by light green), homeostasis (shown as light grey), and apoptosis (represented by light red).

8.6 Retina-specific interaction partners of ALMS1

In this thesis, another endogenous tag, RFP-HA, was employed to identify retina-specific interaction partners of ALMS1. An initial ALMS1-RFP-HA protein complex analysis without retina revealed novel and potential ALMS1 interaction partners, that are linked inter alia to cytoskeletal function, signaling, cell proliferation, and apoptosis. By comparing the ALMS1-RFP-HA and the ALMS1-sfGFP data an overlap of two proteins (CEP70 and AKAP8L) was identified (Figure 31). The observed differences could be partially explained through the application of two different methods, in-solution digest vs on-bead digest [277]. While the on-bead digest methodology involves direct digestion of proteins on the beads, the in-solution digest method involves digestion of eluted proteins within a solution. Additionally, the initial experimental setup had some limitations, as the ALMS1-RFP-HA cells were not starved prior to lysate generation, and no phosphatase inhibitor cocktails were added to the TBS wash buffer. These factors might have led to the loss of certain protein complexes, potentially affecting the identification of ALMS1 interaction partners, that were found with ALMS1-sfGFP.

In a next step, retina-specific interaction partners were identified by performing a retina specific pull down (Figure 35). ALMS1 was already shown to localize at the BB of cilia in ciliated cells. A localization study of ALMS1 and GT335 in human retina presented their presence in the photoreceptor segment (Appendix Figure 44). This supports the retina specific interactome investigation of ALMS1 with ALMS1-RFP-HA tagged HEKT cells. ALMS1 is not well conserved among species, which makes an investigation challenging [18]. Since amounts of up to 4 mg with a minimum of 2 mg are necessary for retinal pull down [180], it is not possible to use organoids or human eyes due to limitation in quantities, availability, long generation times and costs. Therefore, the porcine eye was used for retina lysate generation, due to protein sequence similarities of porcine and human ALMS1 protein (see 10.10.5). By performing the retina pull down, novel and potential retina specific ALMS1 interaction partners were identified, harboring functions inter alia in cell proliferation, cytoskeletal function, signal transduction, cilium organization and transport. Among these potential ALMS1 interactors, CEP70 remains unidentified, suggesting a tissue-specific function other than in the retina. However, another interesting interaction partner, the protein nephrocystin-4/nephroretinin (NPHP4), was found. NPHP4 mutations are linked to Nephronophthisis (NPHP), showing similarities with other ciliopathies, such as the Alström syndrome [111]. NPHP4 localizes to centrosome and basal body, like ALMS1, and is suggested to be essential for proper photoreceptor ribbon synapse maintenance as well as outer segment assembly [278]. Therefore, a co-localization would be of interest to decipher their concomitant roles, for example in centrosomal localization, in sensory

signal transduction and cytoskeletal organization [278–280]. Another protein that was found is centrosomal protein CCDC61 (CCDC61), which is important for cytoskeletal function and cell proliferation by ensuring centriole cohesion and positioning independently of CEP250 and rootletin [281]. CCDC61 was also described as a paralog of Spindle assembly abnormal protein 6 homolog (SAS6) protein, which is necessary for centriole biogenesis ensuring the 9 fold symmetry of centrioles [282]. Despite the unaltered γ-tubulin in the ALMS1 deficient cells, it would be interesting if ALMS1 exhibits a role in BB structure maintenance.

Another interesting protein, that was identified with this experiment, is ADP-ribosylation factor-like protein 6 (ARL6/BBS3). ARL6 was already described for Bardet-Biedl syndrome (BBS) by modulating ciliogenesis and Wnt signaling pathway [283]. Based on the similarities of ALMS and BBS phenotype, it would be interesting to investigate the localization of ARL6 as well as Wnt signaling in ALMS1 deficient cells [283]. This could identify novel functions of ALMS1 and could also help to explain partially the ciliary phenotype presented in this study.

Another interesting protein is Neurogenic locus notch homolog protein 2 (NOTCH2), which is involved in cell proliferation, cell differentiation and cell fate [284,285]. Interestingly, a previous study has indicated a potential association between ALMS1 and Notch signaling. ALMS1 deficiency has been linked to disrupted Notch receptor trafficking via late endosomes, resulting in an overactivation of the Notch signaling pathway [286]. Remarkably, this defect appears to be independent of the recycling process, as both the membrane and ciliary localization of the Notch receptor remain unaffected [16,286]. This overactivated Notch signaling pathway has been associated with certain phenotypic features of Alström syndrome, including inter alia insulin resistance [16].

Furthermore, this experiment gives valuable information on retina specific ALMS1 interactions as well as information to derive new hypotheses. Interaction partners, that are involved in development could also hint towards a potential role of ALMS1 in developmental processes. For the first time, photoreceptor precursor cells (PPCs, kindly generated and provided by Pietro di Angeli, AG Wissinger, Molecular Genetics Laboratory, Institute for Ophthalmic Research) [287] were stained for ALMS1 and cilia (ARL13B). Surprisingly, ALMS1 can be found at the BB of cilia in PPCs, towards a potential developmental involvement of ALMS1 (see 10.12 Appendix Figure 45). This finding provides a new cell model to study ALMS1.

This thesis represents a significant contribution to our understanding of ALMS1's functions, particularly in the context of cilia-related processes. For the first time, potential interaction partners of full-length ALMS1 were identified (Woerz *et al.*, under review [3]). Moreover, a domain-specific interaction between ALMS1 and CEP70 was described with a modulatory

function of CEP70 on ALMS1 as well as an influencing and modulating role of ALMS1 and CEP70 in cell survival (Woerz *et al.*, under review [3]). Additionally, the study indicates and suggests, that ALMS1 may possess multiple functions, potentially stabilizing, modulating, and regulating other proteins.

In the future, a combination of ultrastructure expansion microscopy (U-ExM) with super-resolution microscopy holds great potential for visualizing and identifying the preserved ultrastructure organization within the centrosome as well as (co-) localization of potential interaction partners of ALMS1 at the centrosome [288,289]. Assessing the potential involvement of ALMS1 in more dynamic processes might be interesting, particularly protein biosynthesis, which is important for cell differentiation or endocytosis for energy metabolism [290–292]. Furthermore, ALMS1's impact on signaling processes like insulin, Wnt, Notch, and others could be explored by employing inhibitors and activators for further investigation. This might help to identify the precise localization and interaction of ALMS1 and its potential binding partners, paving the way for a deeper understanding of ALMS1 and centrosome-related processes.

To strengthen these findings, validation of gained results and in-depth analyses using patient-derived fibroblasts and/or organoids are essential. Given the variability of phenotypic features in ALMS patients, these models offer unique advantages in studying and identifying dysfunctions specific to ALMS1-dependent mechanisms, including cytoskeletal arrangement and cilia-dependent signaling. Furthermore, exploring the functional relevance of the identified interaction partners in the context of ALMS will lead to a deeper understanding of ALMS1's role in the disease.

Overall, this thesis expanded our knowledge on ALMS1, opening new avenues for further research to understand the precise molecular function of ALMS1, which potentially pave the way for the development of therapeutic strategies.

9 List of references

[1] F. Hoffmann, S. Bolz, K. Junger, F. Klose, T. Schubert, F. Woerz, K. Boldt, M. Ueffing, T. Beyer, TTC30A and TTC30B Redundancy Protects IFT Complex B Integrity and Its Pivotal Role in Ciliogenesis, Genes (Basel). 13 (2022). https://doi.org/10.3390/genes13071191.

[2] S. Cevik, X. Peng, T. Beyer, M.S. Pir, F. Yenisert, F. Woerz, F. Hoffmann, B. Altunkaynak, B. Pir, K. Boldt, A. Karaman, M. Cakiroglu, S.S. Oner, Y. Cao, M. Ueffing, O.I. Kaplan, WDR31 displays functional redundancy with GTPase-activating proteins (GAPs) ELMOD and RP2 in regulating IFT complex and recruiting the BBSome to cilium, Life Sci. Alliance. 6 (2023) e202201844. https://doi.org/10.26508/lsa.202201844.

[3] F. Woerz, F. Hoffmann, S. Antony, S. Bolz, M.A. Jarboui, K. Junger, K. Franziska, I.F. Stehle, K. Boldt, U. Marius, T. Beyer, Interactome analysis reveals a link of the novel ALMS1-CEP70 complex to centrosomal clusters, Under Rev. Mol. Cell. Proteomics. (n.d.).

[4] T. Leonhard, G.D. Diwan, F. Klose, I.F. Stehle, K. Junger, M. Seda, S. Bolz, F. Woerz, R.B. Russell, K. Boldt, D. Jenkins, M. Ueffing, T. Beyer, Ciliopathy-associated missense mutations in IFT140 are hypomorphic and have edgetic effects on protein interaction networks, BioRxiv. (2023) 2023.01.18.523235. https://doi.org/10.1101/2023.01.18.523235.

[5] W.F. Marshall, S. Nonaka, Cilia: Tuning in to the Cell's Antenna, Curr. Biol. (2006). https://doi.org/10.1016/j.cub.2006.07.012.

[6] S. Hoyer-Fender, Primary and Motile Cilia: Their Ultrastructure and Ciliogenesis BT - Cilia and Nervous System Development and Function, in: K.L. Tucker, T. Caspary (Eds.), Springer Netherlands, Dordrecht, 2013: pp. 1–53. https://doi.org/10.1007/978-94-007-5808-7_1.

[7] Y. Texier, N. Kinkl, K. Boldt, M. Ueffing, From quantitative protein complex analysis to disease mechanism, Vision Res. 75 (2012) 108–111. https://doi.org/https://doi.org/10.1016/j.visres.2012.08.016.

[8] X. Shi, G. Garcia, J.C. Van De Weghe, R. McGorty, G.J. Pazour, D. Doherty, B. Huang, J.F. Reiter, Super-resolution microscopy reveals that disruption of ciliary transition-zone architecture causes Joubert syndrome, Nat. Cell Biol. 19 (2017).

https://doi.org/10.1038/ncb3599.

[9] J.F. Reiter, M.R. Leroux, Genes and molecular pathways underpinning ciliopathies, Nat. Rev. Mol. Cell Biol. 18 (2017) 533–547. https://doi.org/10.1038/nrm.2017.60.

[10] S.T. Christensen, L.B. Pedersen, L. Schneider, P. Satir, Sensory Cilia and integration of signal transduction in human health and disease, Traffic. 8 (2007) 97–109. https://doi.org/10.1111/j.1600-0854.2006.00516.x.

[11] P. Satir, L.B. Pedersen, S.T. Christensen, The primary cilium at a glance, J. Cell Sci. 123 (2010) 499–503. https://doi.org/10.1242/jcs.050377.

[12] T. Hearn, G.L. Renforth, C. Spalluto, N.A. Hanley, K. Piper, S. Brickwood, C. White, V. Connolly, J.F.N. Taylor, I. Russell-Eggitt, D. Bonneau, M. Walker, D.I. Wilson, Mutation of ALMS1, a large gene with a tandem repeat encoding 47 amino acids, causes Alström syndrome, Nat. Genet. (2002). https://doi.org/10.1038/ng874.

[13] J.D. Marshall, S. Beck, P. Maffei, J.K. Naggert, N.J.K. Marshall, Jan D., Beck, Sebastian, Maffei, Pietro, Alström Syndrome, Eur. J. Hum. Genet. 15 (2007) 1193–1202. https://doi.org/10.1038/sj.ejhg.5201933.

[14] J. D. Marshall, P. Maffei, G. B. Collin, J. K. Naggert, Alstrom Syndrome: Genetics and Clinical Overview, Curr. Genomics. 12 (2012) 225–235. https://doi.org/10.2174/138920211795677912.

[15] J.D. Marshall, THE ALSTRÖM SYNDROME HANDBOOK ~ a Guide to Understanding, Managing, and Treating Alström Syndrome, Alström Syndrome International. Mount Desert, ME 04660 USA, 2013.

[16] T. Hearn, ALMS1 and Alström syndrome: a recessive form of metabolic, neurosensory and cardiac deficits, J. Mol. Med. 97 (2019). https://doi.org/10.1007/s00109-018-1714-x.

[17] M. Álvarez-Satta, S. Castro-Sánchez, D. Valverde, Alström syndrome: current perspectives, Appl. Clin. Genet. 8 (2015) 171–179. https://doi.org/10.2147/TACG.S56612.

[18] V.J. Knorz, C. Spalluto, M. Lessard, T.L. Purvis, F.F. Adigun, G.B. Collin, N.A. Hanley, D.I. Wilson, T. Hearn, Centriolar association of ALMS1 and likely centrosomal functions of the ALMS motif-containing proteins C10orf90 and KIAA1731, Mol. Biol. Cell. (2010). https://doi.org/10.1091/mbc.E10-03-0246.

[19] P. Beales, P.K. Jackson, Cilia - the prodigal organelle, Cilia. 1 (2012) 1.

https://doi.org/10.1186/2046-2530-1-1.

[20] Long Huan and Huang Kaiyao, Transport of Ciliary Membrane Proteins, Front. Cell Dev. Biol. 7:381 (2020). https://doi.org/10.3389/fcell.2019.00381.

[21] F. Wörz, ALMS1 interactome identification and its role in ciliogenesis using CRISPR/Cas9 gene editing and protein complex analysis, unpublished Master thesis, Molecular Medicine, Eberhard Karls Universität Tübingen, 2018.

[22] P. Satir, S.T. Christensen, Structure and function of mammalian cilia, Histochem. Cell Biol. (2008). https://doi.org/10.1007/s00418-008-0416-9.

[23] S. Hoyer-Fender, Centriole maturation and transformation to basal body, Semin. Cell Dev. Biol. 21 (2010) 142–147. https://doi.org/https://doi.org/10.1016/j.semcdb.2009.07.002.

[24] Z. Zhang, N. Danné, B. Meddens, I. Heller, E.J.G. Peterman, Direct imaging of intraflagellar-transport turnarounds reveals that motors detach, diffuse, and reattach to opposite-direction trains, Proc. Natl. Acad. Sci. 118 (2021) e2115089118. https://doi.org/10.1073/pnas.2115089118.

[25] S.N. van der Burght, S. Rademakers, J.-L. Johnson, C. Li, G.-J. Kremers, A.B. Houtsmuller, M.R. Leroux, G. Jansen, Ciliary Tip Signaling Compartment Is Formed and Maintained by Intraflagellar Transport, Curr. Biol. 30 (2020) 4299-4306.e5. https://doi.org/https://doi.org/10.1016/j.cub.2020.08.032.

[26] T. Kanamaru, A. Neuner, B. Kurtulmus, G. Pereira, Balancing the length of the distal tip by septins is key for stability and signalling function of primary cilia, EMBO J. 41 (2022) e108843. https://doi.org/https://doi.org/10.15252/embj.2021108843.

[27] C.J. Haycraft, B. Banizs, Y. Aydin-Son, Q. Zhang, E.J. Michaud, B.K. Yoder, Gli2 and Gli3 Localize to Cilia and Require the Intraflagellar Transport Protein Polaris for Processing and Function, PLOS Genet. 1 (2005) e53. https://doi.org/10.1371/journal.pgen.0010053.

[28] L.B. Pedersen, A. Akhmanova, Kif7 keeps cilia tips in shape, Nat. Cell Biol. 16 (2014) 623–625. https://doi.org/10.1038/ncb2997.

[29] A.R. Nager, J.S. Goldstein, V. Herranz-Pérez, D. Portran, F. Ye, J.M. Garcia-Verdugo, M. V. Nachury, An Actin Network Dispatches Ciliary GPCRs into Extracellular Vesicles to Modulate Signaling, Cell. (2017). https://doi.org/10.1016/j.cell.2016.11.036.

[30] S.C. Phua, S. Chiba, M. Suzuki, E. Su, E.C. Roberson, G. V. Pusapati, M. Setou, R.

Rohatgi, J.F. Reiter, K. Ikegami, T. Inoue, Dynamic Remodeling of Membrane Composition Drives Cell Cycle through Primary Cilia Excision, Cell. (2017). https://doi.org/10.1016/j.cell.2016.12.032.

[31] G. Wang, H.-B. Hu, Y. Chang, Y. Huang, Z.-Q. Song, S.-B. Zhou, L. Chen, Y.-C. Zhang, M. Wu, H.-Q. Tu, J.-F. Yuan, N. Wang, X. Pan, A.-L. Li, T. Zhou, X.-M. Zhang, K. He, H.-Y. Li, Rab7 regulates primary cilia disassembly through cilia excision, J. Cell Biol. (2019). https://doi.org/10.1083/jcb.201811136.

[32] R.W. Young, THE RENEWAL OF PHOTORECEPTOR CELL OUTER SEGMENTS, J. Cell Biol. 33 (1967) 61–72. https://doi.org/10.1083/jcb.33.1.61.

[33] O.P. Kocaoglu, Z. Liu, F. Zhang, K. Kurokawa, R.S. Jonnal, D.T. Miller, Photoreceptor disc shedding in the living human eye, Biomed. Opt. Express. 7 (2016) 4554–4568. https://doi.org/10.1364/BOE.7.004554.

[34] M. Taschner, S. Bhogaraju, E. Lorentzen, Architecture and function of IFT complex proteins in ciliogenesis, Differentiation. 83 (2012) S12–S22. https://doi.org/https://doi.org/10.1016/j.diff.2011.11.001.

[35] A. Dummer, C. Poelma, M.C. DeRuiter, M.J.T.H. Goumans, B.P. Hierck, Measuring the primary cilium length: Improved method for unbiased high-throughput analysis, Cilia. 5 (2016). https://doi.org/10.1186/s13630-016-0028-2.

[36] S. Bhogaraju, B.D. Engel, E. Lorentzen, Intraflagellar transport complex structure and cargo interactions, Cilia. (2013). https://doi.org/10.1186/2046-2530-2-10.

[37] B. Prevo, J.M. Scholey, E.J.G. Peterman, Intraflagellar transport: mechanisms of motor action, cooperation, and cargo delivery, FEBS J. 284 (2017). https://doi.org/10.1111/febs.14068.

[38] J.L. Wingfield, K.F. Lechtreck, E. Lorentzen, Trafficking of ciliary membrane proteins by the intraflagellar transport/BBSome machinery, Essays Biochem. 62 (2018). https://doi.org/10.1042/EBC20180030.

[39] W. Fu, L. Wang, S. Kim, J. Li, B.D. Dynlacht, Role for the IFT-A Complex in Selective Transport to the Primary Cilium, Cell Rep. 17 (2016) 1505–1517. https://doi.org/https://doi.org/10.1016/j.celrep.2016.10.018.

[40] G. Garcia, D.R. Raleigh, J.F. Reiter, How the Ciliary Membrane Is Organized Inside-Out

to Communicate Outside-In, Curr. Biol. 28 (2018) R421–R434. https://doi.org/https://doi.org/10.1016/j.cub.2018.03.010.

[41] V. Singla, J.F. Reiter, The primary cilium as the cell's antenna: Signaling at a sensory organelle, Science (80-.). (2006). https://doi.org/10.1126/science.1124534.

[42] J.M. Gerdes, E.E. Davis, N. Katsanis, The Vertebrate Primary Cilium in Development, Homeostasis, and Disease, Cell. (2009). https://doi.org/10.1016/j.cell.2009.03.023.

[43] H. Ishikawa, W.F. Marshall, Ciliogenesis: Building the cell's antenna, Nat. Rev. Mol. Cell Biol. 12 (2011) 222–234. https://doi.org/10.1038/nrm3085.

[44] K. Szymanska, C.A. Johnson, The transition zone: An essential functional compartment of cilia, Cilia. 1 (2012) 1. https://doi.org/10.1186/2046-2530-1-10.

[45] H.R. Dawe, H. Farr, K. Gull, Centriole/basal body morphogenesis and migration during ciliogenesis in animal cells, J. Cell Sci. (2007). https://doi.org/10.1242/jcs.03305.

[46] S. Jaiswal, H. Kasera, S. Jain, S. Khandelwal, P. Singh, Centrosome: A Microtubule Nucleating Cellular Machinery, J. Indian Inst. Sci. 101 (2021) 5–18. https://doi.org/10.1007/s41745-020-00213-1.

[47] M. Alvarado-Kristensson, Γ-Tubulin As a Signal-Transducing Molecule and Meshwork With Therapeutic Potential, Signal Transduct. Target. Ther. 3 (2018) 1–6. https://doi.org/10.1038/s41392-018-0021-x.

[48] H. May-Simera, K. Nagel-Wolfrum, U. Wolfrum, Cilia - The sensory antennae in the eye, Prog. Retin. Eye Res. 60 (2017) 144–180. https://doi.org/10.1016/j.preteyeres.2017.05.001.

[49] M. V. Nachury, E.S. Seeley, H. Jin, Trafficking to the Ciliary Membrane: How to Get Across the Periciliary Diffusion Barrier?, Annu. Rev. Cell Dev. Biol. (2010). https://doi.org/10.1146/annurev.cellbio.042308.113337.

[50] A. Molla-Herman, R. Ghossoub, T. Blisnick, A. Meunier, C. Serres, F. Silbermann, C. Emmerson, K. Romeo, P. Bourdoncle, A. Schmitt, S. Saunier, N. Spassky, P. Bastin, A. Benmerah, The ciliary pocket: An endocytic membrane domain at the base of primary and motile cilia, J. Cell Sci. (2010). https://doi.org/10.1242/jcs.059519.

[51] Y. Liang, D. Meng, B. Zhu, J. Pan, Mechanism of ciliary disassembly, Cell. Mol. Life Sci. 73 (2016). https://doi.org/10.1007/s00018-016-2148-7.

[52] S. Yang, J. Zhou, D. Li, Functions and Diseases of the Retinal Pigment Epithelium, Front. Pharmacol. 12 (2021). https://www.frontiersin.org/articles/10.3389/fphar.2021.727870.

[53] A. Reichenbach, A. Bringmann, Glia of the human retina, Glia. 68 (2020) 768–796. https://doi.org/https://doi.org/10.1002/glia.23727.

[54] M. Hoon, H. Okawa, L. Della Santina, R.O.L. Wong, Functional architecture of the retina: Development and disease, Prog. Retin. Eye Res. 42 (2014) 44–84. https://doi.org/10.1016/j.preteyeres.2014.06.003.

[55] M. Ptito, M. Bleau, J. Bouskila, The Retina: A Window into the Brain, Cells. 10 (2021). https://doi.org/10.3390/cells10123269.

[56] R.S. Molday, O.L. Moritz, Photoreceptors at a glance, J. Cell Sci. 128 (2015) 4039–4045. https://doi.org/10.1242/jcs.175687.

[57] J. Chen, A.P. Sampath, Chapter 14 - Structure and Function of Rod and Cone Photoreceptors, in: S.J. Ryan, S.R. Sadda, D.R. Hinton, A.P. Schachat, S.R. Sadda, C.P. Wilkinson, P. Wiedemann, A.P.B.T.-R. (Fifth E. Schachat (Eds.), W.B. Saunders, London, 2013: pp. 342–359. https://doi.org/https://doi.org/10.1016/B978-1-4557-0737-9.00014-X.

[58] D. Mustafi, A.H. Engel, K. Palczewski, Structure of cone photoreceptors, Prog. Retin. Eye Res. 28 (2009) 289–302. https://doi.org/10.1016/j.preteyeres.2009.05.003.

[59] J.S. Wang, V.J. Kefalov, The Cone-specific visual cycle, Prog. Retin. Eye Res. 30 (2011) 115–128. https://doi.org/10.1016/j.preteyeres.2010.11.001.

[60] O. Yildiz, H. Khanna, Ciliary signaling cascades in photoreceptors, Vision Res. 75 (2012) 112–116. https://doi.org/10.1016/j.visres.2012.08.007.

[61] Q. Liu, A. Lyubarsky, J.H. Skalet, E.N. Pugh, E.A. Pierce, RP1 is required for the correct stacking of outer segment discs, Investig. Ophthalmol. Vis. Sci. 44 (2003) 4171–4183. https://doi.org/10.1167/iovs.03-0410.

[62] H. Khanna, Photoreceptor Sensory Cilium: Traversing the Ciliary Gate, Cells. 4 (2015) 674–686. https://doi.org/10.3390/cells4040674.

[63] P. Gönczy, G.N. Hatzopoulos, Centriole assembly at a glance, J. Cell Sci. 132 (2019). https://doi.org/10.1242/jcs.228833.

[64] Z. Carvalho-Santos, J. Azimzadeh, J.B. Pereira-Leal, M. Bettencourt-Dias, Evolution: Tracing the origins of centrioles, cilia, and flagella, J. Cell Biol. 194 (2011) 165–175.

https://doi.org/10.1083/jcb.201011152.

[65] V. Joukov, A. De Nicolo, The Centrosome and the Primary Cilium: The Yin and Yang of a Hybrid Organelle, Cells. 8 (2019) 701. https://doi.org/10.3390/cells8070701.

[66] S. Graser, Y.-D. Stierhof, S.B. Lavoie, O.S. Gassner, S. Lamla, M. Le Clech, E.A. Nigg, Cep164, a novel centriole appendage protein required for primary cilium formation, J. Cell Biol. 179 (2007) 321–330. https://doi.org/10.1083/jcb.200707181.

[67] M. Hirono, Cartwheel assembly, Philos. Trans. R. Soc. Lond. B. Biol. Sci. 369 (2014) 20130458. https://doi.org/10.1098/rstb.2013.0458.

[68] A. Kumari, D. Panda, Regulation of microtubule stability by centrosomal proteins, IUBMB Life. 70 (2018) 602–611. https://doi.org/10.1002/iub.1865.

[69] A. Kumar, V. Rajendran, R. Sethumadhavan, R. Purohit, CEP proteins: the knights of centrosome dynasty, Protoplasma. 250 (2013) 965–983. https://doi.org/10.1007/s00709-013-0488-9.

[70] X. Shi, Y. Yao, Y. Wang, Y. Zhang, Q. Huang, J. Zhou, M. Liu, D. Li, Cep70 regulates microtubule stability by interacting with HDAC6, FEBS Lett. 589 (2015) 1771–1777. https://doi.org/https://doi.org/10.1016/j.febslet.2015.06.017.

[71] G. Shiratsuchi, R. Kamiya, M. Hirono, Scaffolding function of the Chlamydomonas procentriole protein CRC70, a member of the conserved Cep70 family, J. Cell Sci. 124 (2011) 2964–2975. https://doi.org/10.1242/jcs.084715.

[72] C.J. Wilkinson, M. Carl, W.A. Harris, Cep70 and Cep131 contribute to ciliogenesis in zebrafish embryos, BMC Cell Biol. 10 (2009) 17. https://doi.org/10.1186/1471-2121-10-17.

[73] J.S. Andersen, C.J. Wilkinson, T. Mayor, P. Mortensen, E.A. Nigg, M. Mann, Proteomic characterization of the human centrosome by protein correlation profiling, Nature. 426 (2003) 570–574. https://doi.org/10.1038/nature02166.

[74] X. Shi, X. Sun, M. Liu, D. Li, R. Aneja, J. Zhou, CEP70 protein interacts with γ-tubulin to localize at the centrosome and is critical for mitotic spindle assembly, J. Biol. Chem. 286 (2011) 33401–33408. https://doi.org/10.1074/jbc.M111.252262.

[75] Y. Yang, J. Ran, M. Liu, D. Li, Y. Li, X. Shi, D. Meng, J. Pan, G. Ou, R. Aneja, S.-C. Sun, J. Zhou, CYLD mediates ciliogenesis in multiple organs by deubiquitinating Cep70 and

inactivating HDAC6, Cell Res. 24 (2014) 1342–1353. https://doi.org/10.1038/cr.2014.136.

[76] I. Sánchez, B.D. Dynlacht, Cilium assembly and disassembly, Nat. Cell Biol. 18 (2016). https://doi.org/10.1038/ncb3370.

[77] H. Goto, H. Inaba, M. Inagaki, Mechanisms of ciliogenesis suppression in dividing cells, Cell. Mol. Life Sci. 74 (2017) 881–890. https://doi.org/10.1007/s00018-016-2369-9.

[78] D.K. Breslow, A.J. Holland, Mechanism and Regulation of Centriole and Cilium Biogenesis, Annu. Rev. Biochem. 88 (2019) 691–724. https://doi.org/10.1146/annurev-biochem-013118-111153.

[79] W. Wang, B.M. Jack, H.H. Wang, M.A. Kavanaugh, R.L. Maser, P. V Tran, Intraflagellar Transport Proteins as Regulators of Primary Cilia Length, Front. Cell Dev. Biol. 9 (2021). https://www.frontiersin.org/articles/10.3389/fcell.2021.661350.

[80] H.W. Ko, The primary cilium as a multiple cellular signaling scaffold in development and disease, BMB Rep. 45 (2012) 427–432. https://www.bmbreports.org/journal/view.html?doi=.

[81] A. Vertii, H.-F.F. Hung, H. Hehnly, S. Doxsey, Human basal body basics, Cilia. 5 (2016) 13. https://doi.org/10.1186/s13630-016-0030-8.

[82] L. Wang, B.D. Dynlacht, The regulation of cilium assembly and disassembly in development and disease, Dev. 145 (2018). https://doi.org/10.1242/dev.151407.

[83] H. Zhao, Z. Khan, C.J. Westlake, Ciliogenesis membrane dynamics and organization, Semin. Cell Dev. Biol. 133 (2023) 20–31. https://doi.org/https://doi.org/10.1016/j.semcdb.2022.03.021.

[84] S. Shakya, C.J. Westlake, Recent advances in understanding assembly of the primary cilium membrane, Fac. Rev. 10 (2021) 16. https://doi.org/10.12703/r/10-16.

[85] D. Huangfu, A. Liu, A.S. Rakeman, N.S. Murcia, L. Niswander, K. V Anderson, Hedgehog signalling in the mouse requires intraflagellar transport proteins, Nature. 426 (2003) 83–87. https://doi.org/10.1038/nature02061.

[86] K.C. Corbit, P. Aanstad, V. Singla, A.R. Norman, D.Y.R. Stainier, J.F. Reiter, Vertebrate Smoothened functions at the primary cilium, Nature. (2005). https://doi.org/10.1038/nature04117.

[87] M. Álvarez-Satta, M. Lago-Docampo, B. Bea-Mascato, C. Solarat, S. Castro-Sánchez,

S.T. Christensen, D. Valverde, ALMS1 Regulates TGF-β Signaling and Morphology of Primary Cilia, Front. Cell Dev. Biol. 9 (2021) 623829. https://doi.org/10.3389/fcell.2021.623829.

[88] B. Bea-Mascato, E. Neira-Goyanes, A. Iglesias-Rodríguez, D. Valverde, Depletion of ALMS1 affects TGF-β signalling pathway and downstream processes such as cell migration and adhesion capacity, Front. Mol. Biosci. 9 (2022). https://www.frontiersin.org/articles/10.3389/fmolb.2022.992313.

[89] C.A. Clement, K.D. Ajbro, K. Koefoed, M.L. Vestergaard, I.R. Veland, M.P.R. Henriques de Jesus, L.B. Pedersen, A. Benmerah, C.Y. Andersen, L.A. Larsen, S.T. Christensen, TGF-β Signaling Is Associated with Endocytosis at the Pocket Region of the Primary Cilium, Cell Rep. 3 (2013) 1806–1814. https://doi.org/https://doi.org/10.1016/j.celrep.2013.05.020.

[90] S. Habbig, M.P. Bartram, R.U. Müller, R. Schwarz, N. Andriopoulos, S. Chen, J.G. Sägmüller, M. Hoehne, V. Burst, M.C. Liebau, H.C. Reinhardt, T. Benzing, B. Schermer, NPHP4, a cilia-associated protein, negatively regulates the Hippo pathway, J. Cell Biol. 193 (2011) 633–642. https://doi.org/10.1083/jcb.201009069.

[91] G. Wheway, L. Nazlamova, J.T. Hancock, Signaling through the primary cilium, Front. Cell Dev. Biol. 6 (2018). https://doi.org/10.3389/fcell.2018.00008.

[92] H.L. May-Simera, M.W. Kelley, Cilia, Wnt signaling, and the cytoskeleton, Cilia. (2012). https://doi.org/10.1186/2046-2530-1-7.

[93] P. Foerster, M. Daclin, S. Asm, M. Faucourt, A. Boletta, A. Genovesio, N. Spassky, mTORC1 signaling and primary cilia are required for brain ventricle morphogenesis, Development. 144 (2017) 201–210. https://doi.org/10.1242/dev.138271.

[94] Y. Omori, T. Chaya, S. Yoshida, S. Irie, T. Tsujii, T. Furukawa, Identification of G Protein-Coupled Receptors (GPCRs) in Primary Cilia and Their Possible Involvement in Body Weight Control, PLoS One. 10 (2015) e0128422. https://doi.org/10.1371/journal.pone.0128422.

[95] Z. Anvarian, K. Mykytyn, S. Mukhopadhyay, L.B. Pedersen, S.T. Christensen, Cellular signalling by primary cilia in development, organ function and disease, Nat. Rev. Nephrol. 15 (2019) 199–219. https://doi.org/10.1038/s41581-019-0116-9.

[96] D.K. Song, J.H. Choi, M.S. Kim, Primary cilia as a signaling platform for control of energy

metabolism, Diabetes Metab. J. 42 (2018) 117–127. https://doi.org/10.4093/dmj.2018.42.2.117.

[97] A. Zullo, D. Iaconis, A. Barra, A. Cantone, N. Messaddeq, G. Capasso, P. Dollé, P. Igarashi, B. Franco, Kidney-specific inactivation of Ofd1 leads to renal cystic disease associated with upregulation of the mTOR pathway, Hum. Mol. Genet. 19 (2010) 2792–2803. https://doi.org/10.1093/hmg/ddq180.

[98] Y. Nishimura, K. Kasahara, T. Shiromizu, M. Watanabe, M. Inagaki, Primary Cilia as Signaling Hubs in Health and Disease, Adv. Sci. 6 (2019) 1801138. https://doi.org/https://doi.org/10.1002/advs.201801138.

[99] R. Pala, N. Alomari, S.M. Nauli, Primary Cilium-Dependent Signaling Mechanisms, Int. J. Mol. Sci. 18 (2017). https://doi.org/10.3390/ijms18112272.

[100] S.T. Christensen, C.A. Clement, P. Satir, L.B. Pedersen, Primary cilia and coordination of receptor tyrosine kinase (RTK) signalling, J. Pathol. 226 (2012) 172–184. https://doi.org/https://doi.org/10.1002/path.3004.

[101] S.T. Christensen, S.K. Morthorst, J.B. Mogensen, L.B. Pedersen, Primary cilia and coordination of receptor tyrosine kinase (RTK) and transforming growth factor β (TGF-β) signaling, Cold Spring Harb. Perspect. Biol. 9 (2017). https://doi.org/10.1101/cshperspect.a028167.

[102] L. Schneider, C.A. Clement, S.C. Teilmann, G.J. Pazour, E.K. Hoffmann, P. Satir, S.T. Christensen, PDGFRαα Signaling Is Regulated through the Primary Cilium in Fibroblasts, Curr. Biol. 15 (2005) 1861–1866. https://doi.org/https://doi.org/10.1016/j.cub.2005.09.012.

[103] F.M. Schmid, K.B. Schou, M.J. Vilhelm, M.S. Holm, L. Breslin, P. Farinelli, L.A. Larsen, J.S. Andersen, L.B. Pedersen, S.T. Christensen, IFT20 modulates ciliary PDGFRα signaling by regulating the stability of Cbl E3 ubiquitin ligases, J. Cell Biol. 217 (2017) 151–161. https://doi.org/10.1083/jcb.201611050.

[104] N.L. Stevenson, D.J.M. Bergen, A. Xu, E. Wyatt, F. Henry, J. McCaughey, L. Vuolo, C.L. Hammond, D.J. Stephens, Regulator of calcineurin-2 is a centriolar protein with a role in cilia length control, J. Cell Sci. 131 (2018) jcs212258. https://doi.org/10.1242/jcs.212258.

[105] L. Sánchez-Bellver, V. Toulis, G. Marfany, On the Wrong Track: Alterations of Ciliary Transport in Inherited Retinal Dystrophies, Front. Cell Dev. Biol. 9 (2021). https://www.frontiersin.org/articles/10.3389/fcell.2021.623734.

[106] A. Grochowsky, M. Gunay-Aygun, Clinical characteristics of individual organ system disease in non-motile ciliopathies, Transl. Sci. Rare Dis. 4 (2019) 1–23. https://doi.org/10.3233/TRD-190033.

[107] J. Eintracht, E. Forsythe, H. May-Simera, M. Moosajee, Translational readthrough of ciliopathy genes BBS2 and ALMS1 restores protein, ciliogenesis and function in patient fibroblasts, EBioMedicine. 70 (2021) 103515. https://doi.org/https://doi.org/10.1016/j.ebiom.2021.103515.

[108] C.H. ALSTROM, B. Hallgren, L.B. Nilsson, H. Asander, Retinal degeneration combined with obesity, diabetes mellitus and neurogenous deafness: a specific syndrome (not hitherto described) distinct from the Laurence-Moon-Bardet-Biedl syndrome: a clinical, endocrinological and genetic examination based on a lar, Acta Psychiatr. Neurol. Scand. Suppl. 129 (1959) 1–35.

[109] R. Forsyth, M. Gunay-aygun, Bardet-Biedl Syndrome Overview, 2003rd, Upda ed., GeneReviews(R), Seattle (WA): University of Washington, Seattle; 1993-2023, 2020. https://www.ncbi.nlm.nih.gov/books/NBK1363/.

[110] R.B. Paisey, R. Steeds, T. Barrett, D. Williams, T. Geberhiwot, M. Gunay-Aygun, Alström Syndrome., GeneReviews® [Internet]. (2003).

[111] G.B. Collin, J.D. Marshall, A. Ikeda, W.V. So, I. Russell-Eggitt, P. Maffei, S. Beck, C.F. Boerkoel, N. Sicolo, M. Martin, P.M. Nishina, J.K. Naggert, Mutations in ALMS1 cause obesity, type 2 diabetes and neurosensory degeneration in Alström syndrome, Nat. Genet. (2002). https://doi.org/10.1038/ng867.

[112] G.B. Collin, J.D. Marshall, B.L. King, G. Milan, P. Maffei, D.J. Jagger, J.K. Naggert, The Alström syndrome protein, ALMS1, interacts with α-actinin and components of the endosome recycling pathway, PLoS One. 7 (2012) e37925–e37925. https://doi.org/10.1371/journal.pone.0037925.

[113] D. Izquierdo, W.-J. Wang, K. Uryu, M.-F.B. Tsou, Stabilization of Cartwheel-less Centrioles for Duplication Requires CEP295-Mediated Centriole-to-Centrosome Conversion, Cell Rep. 8 (2014) 957–965. https://doi.org/https://doi.org/10.1016/j.celrep.2014.07.022.

[114] C.-W. Chang, W.-B. Hsu, J.-J. Tsai, C.-J.C. Tang, T.K. Tang, CEP295 interacts with microtubules and is required for centriole elongation, J. Cell Sci. 129 (2016) 2501–2513.

https://doi.org/10.1242/jcs.186338.

[115] J.D. Marshall, J. Muller, G.B. Collin, G. Milan, S.F. Kingsmore, D. Dinwiddie, E.G. Farrow, N.A. Miller, F. Favaretto, P. Maffei, H. Dollfus, R. Vettor, J.K. Naggert, Alström Syndrome: Mutation Spectrum of ALMS1, Hum. Mutat. 36 (2015) 660–668. https://doi.org/10.1002/humu.22796.

[116] T. Hearn, C. Spalluto, V.J. Phillips, G.L. Renforth, N. Copin, N.A. Hanley, D.I. Wilson, Subcellular localization of ALMS1 supports involvement of centrosome and basal body dysfunction in the pathogenesis of obesity, insulin resistance, and type 2 diabetes, Diabetes. 54 (2005) 1581–1587. https://doi.org/10.2337/diabetes.54.5.1581.

[117] G. Li, R. Vega, K. Nelms, N. Gekakis, C. Goodnow, P. McNamara, H. Wu, N.A. Hong, R. Glynne, A Role for Alström Syndrome Protein, Alms1, in Kidney Ciliogenesis and Cellular Quiescence, PLOS Genet. 3 (2007) e8.

[118] G.B. Collin, J.D. Marshall, B.L. King, G. Milan, P. Maffei, D.J. Jagger, J.K. Naggert, The alström syndrome protein, ALMS1, interacts with α-actinin and components of the endosome recycling pathway, PLoS One. 7 (2012). https://doi.org/10.1371/journal.pone.0037925.

[119] J.H. Chen, T. Geberhiwot, T.G. Barrett, R. Paisey, R.K. Semple, Refining genotype–phenotype correlation in Alström syndrome through study of primary human fibroblasts, Mol. Genet. Genomic Med. 5 (2017) 390–404. https://doi.org/10.1002/mgg3.296.

[120] C.J. Gloeckner, K. Boldt, M. Ueffing, Strep/FLAG tandem affinity purification (SF-TAP) to study protein interactions, Curr. Protoc. Protein Sci. (2009) 1–19. https://doi.org/10.1002/0471140864.ps1920s57.

[121] D. Szklarczyk, R. Kirsch, M. Koutrouli, K. Nastou, F. Mehryary, R. Hachilif, A.L. Gable, T. Fang, N.T. Doncheva, S. Pyysalo, P. Bork, L.J. Jensen, C. von Mering, The STRING database in 2023: protein–protein association networks and functional enrichment analyses for any sequenced genome of interest, Nucleic Acids Res. 51 (2023) D638–D646. https://doi.org/10.1093/nar/gkac1000.

[122] P. Shannon, A. Markiel, O. Ozier, N.S. Baliga, J.T. Wang, D. Ramage, N. Amin, B. Schwikowski, T. Ideker, Cytoscape: a software environment for integrated models of biomolecular interaction networks., Genome Res. 13 (2003) 2498–2504. https://doi.org/10.1101/gr.1239303.

[123] C. Doornbos, R. van Beek, E.M.H.F. Bongers, D. Lugtenberg, P.H.M. Klaren, L.E.L.M. Vissers, R. Roepman, M.M. Oud, Cell-based assay for ciliopathy patients to improve accurate diagnosis using ALPACA, Eur. J. Hum. Genet. 29 (2021) 1677–1689. https://doi.org/10.1038/s41431-021-00907-9.

[124] J. Schindelin, I. Arganda-Carreras, E. Frise, V. Kaynig, M. Longair, T. Pietzsch, S. Preibisch, C. Rueden, S. Saalfeld, B. Schmid, J.-Y. Tinevez, D.J. White, V. Hartenstein, K. Eliceiri, P. Tomancak, A. Cardona, Fiji: an open-source platform for biological-image analysis, Nat. Methods. 9 (2012) 676–682. https://doi.org/10.1038/nmeth.2019.

[125] F.A. Ran, P.D. Hsu, J. Wright, V. Agarwala, D.A. Scott, F. Zhang, Genome engineering using the CRISPR-Cas9 system, Nat. Protoc. 8 (2013) 2281–2308. https://doi.org/10.1038/nprot.2013.143.

[126] J.T. den Dunnen, R. Dalgleish, D.R. Maglott, R.K. Hart, M.S. Greenblatt, J. McGowan-Jordan, A.-F. Roux, T. Smith, S.E. Antonarakis, P.E.M. Taschner, HGVS Recommendations for the Description of Sequence Variants: 2016 Update, Hum. Mutat. 37 (2016) 564–569. https://doi.org/https://doi.org/10.1002/humu.22981.

[127] K. He, K. Ling, J. Hu, The emerging role of tubulin posttranslational modifications in cilia and ciliopathies, Biophys. Reports. 6 (2020) 89–104. https://doi.org/10.1007/s41048-020-00111-0.

[128] N. Forcioli-Conti, D. Estève, A. Bouloumié, C. Dani, P. Peraldi, The size of the primary cilium and acetylated tubulin are modulated during adipocyte differentiation: Analysis of HDAC6 functions in these processes, Biochimie. 124 (2016) 112–123. https://doi.org/https://doi.org/10.1016/j.biochi.2015.09.011.

[129] T. Mitani, J. Punetha, I. Akalin, D. Pehlivan, M. Dawidziuk, Z. Coban Akdemir, S. Yilmaz, E. Aslan, J. V Hunter, H. Hijazi, C.M. Grochowski, S.N. Jhangiani, E. Karaca, J.M. Fatih, P. Iwanowski, T. Gambin, P. Wlasienko, A. Goszczanska-Ciuchta, M. Bekiesinska-Figatowska, M. Hosseini, S. Arzhangi, H. Najmabadi, J.A. Rosenfeld, H. Du, D. Marafi, S. Blaser, R. Teitelbaum, R. Silver, J.E. Posey, H.-H. Ropers, R.A. Gibbs, W. Wiszniewski, J.R. Lupski, D. Chitayat, K. Kahrizi, P. Gawlinski, Bi-allelic Pathogenic Variants in TUBGCP2 Cause Microcephaly and Lissencephaly Spectrum Disorders, Am. J. Hum. Genet. 105 (2019) 1005–1015. https://doi.org/https://doi.org/10.1016/j.ajhg.2019.09.017.

[130] R. Shen, Z. Zhang, Y. Zhuang, X. Yang, L. Duan, A novel TUBG1 mutation with neurodevelopmental disorder caused by malformations of cortical development, Biomed

Res. Int. 2021 (2021) 6644274. https://doi.org/10.1155/2021/6644274.

[131] S. Bahe, Y.-D. Stierhof, C.J. Wilkinson, F. Leiss, E.A. Nigg, Rootletin forms centriole-associated filaments and functions in centrosome cohesion, J. Cell Biol. 171 (2005) 27–33. https://doi.org/10.1083/jcb.200504107.

[132] I. V. Nechipurenko, A. Olivier-Mason, A. Kazatskaya, J. Kennedy, I.G. McLachlan, M.G. Heiman, O.E. Blacque, P. Sengupta, A Conserved Role for Girdin in Basal Body Positioning and Ciliogenesis, Dev. Cell. 38 (2016) 493–506. https://doi.org/10.1016/j.devcel.2016.07.013.

[133] A. Dammermann, A. Merdes, Assembly of centrosomal proteins and microtubule organization depends on PCM-1, J. Cell Biol. 159 (2002) 255–266. https://doi.org/10.1083/jcb.200204023.

[134] R.S. Hames, R.E. Crookes, K.R. Straatman, A. Merdes, M.J. Hayes, A.J. Faragher, A.M. Fry, Dynamic Recruitment of Nek2 Kinase to the Centrosome Involves Microtubules, PCM-1, and Localized Proteasomal Degradation, Mol. Biol. Cell. 16 (2005) 1711–1724. https://doi.org/10.1091/mbc.e04-08-0688.

[135] D.R. Mitchell, Polyglutamylation: The GLU that Makes Microtubules Sticky, Curr. Biol. 20 (2010) R234–R236. https://doi.org/10.1016/j.cub.2010.01.008.

[136] A.B. Jaykumar, P.S. Caceres, K.N. King-Medina, T.-D. Liao, I. Datta, D. Maskey, J.K. Naggert, M. Mendez, W.H. Beierwaltes, P.A. Ortiz, Role of Alström syndrome 1 in the regulation of blood pressure and renal function, JCI Insight. 3 (2018). https://doi.org/10.1172/jci.insight.95076.

[137] M. Stemmer, T. Thumberger, M. Del Sol Keyer, J. Wittbrodt, J.L. Mateo, CCTop: An intuitive, flexible and reliable CRISPR/Cas9 target prediction tool, PLoS One. 10 (2015) 1–11. https://doi.org/10.1371/journal.pone.0124633.

[138] C. Zhang, R. Quan, J. Wang, Development and application of CRISPR/Cas9 technologies in genomic editing, Hum. Mol. Genet. 27 (2018) R79–R88. https://doi.org/10.1093/hmg/ddy120.

[139] X. He, C. Tan, F. Wang, Y. Wang, R. Zhou, D. Cui, W. You, H. Zhao, J. Ren, B. Feng, Knock-in of large reporter genes in human cells via CRISPR/Cas9-induced homology-dependent and independent DNA repair, Nucleic Acids Res. 44 (2016) e85–e85. https://doi.org/10.1093/nar/gkw064.

[140] J. Cox, M. Mann, MaxQuant enables high peptide identification rates, individualized p.p.b.-range mass accuracies and proteome-wide protein quantification, Nat. Biotechnol. 26 (2008) 1367–1372. https://doi.org/10.1038/nbt.1511.

[141] S. Tyanova, T. Temu, P. Sinitcyn, A. Carlson, M.Y. Hein, T. Geiger, M. Mann, J. Cox, The Perseus computational platform for comprehensive analysis of (prote)omics data, Nat. Methods. 13 (2016) 731–740. https://doi.org/10.1038/nmeth.3901.

[142] M.G. Aslanyan, C. Doornbos, G.D. Diwan, Z. Anvarian, T. Beyer, K. Junger, S.E.C. van Beersum, R.B. Russell, M. Ueffing, A. Ludwig, K. Boldt, L.B. Pedersen, R. Roepman, A targeted multi-proteomics approach generates a blueprint of the ciliary ubiquitinome, Front. Cell Dev. Biol. 11 (2023). https://www.frontiersin.org/articles/10.3389/fcell.2023.1113656.

[143] D.U. Mick, R.B. Rodrigues, R.D. Leib, C.M. Adams, A.S. Chien, S.P. Gygi, M. V. Nachury, Proteomics of Primary Cilia by Proximity Labeling, Dev. Cell. (2015). https://doi.org/10.1016/j.devcel.2015.10.015.

[144] M. Ashburner, C.A. Ball, J.A. Blake, D. Botstein, H. Butler, J.M. Cherry, A.P. Davis, K. Dolinski, S.S. Dwight, J.T. Eppig, M.A. Harris, D.P. Hill, L. Issel-Tarver, A. Kasarskis, S. Lewis, J.C. Matese, J.E. Richardson, M. Ringwald, G.M. Rubin, G. Sherlock, Gene Ontology: tool for the unification of biology, Nat. Genet. 25 (2000) 25–29. https://doi.org/10.1038/75556.

[145] Carbon, Seth, Eric Douglass, Benjamin M. Good, Deepak R. Unni, Nomi L. Harris, Christopher J. Mungall, Siddartha Basu, The Gene Ontology resource: enriching a GOld mine, Nucleic Acids Res. 49 (2021) D325–D334. https://doi.org/10.1093/nar/gkaa1113.

[146] H.Y. Chen, R.A. Kelley, T. Li, A. Swaroop, Primary cilia biogenesis and associated retinal ciliopathies, Semin. Cell Dev. Biol. 110 (2021) 70–88. https://doi.org/https://doi.org/10.1016/j.semcdb.2020.07.013.

[147] S. Shankar, Z.-T. Hsu, A. Ezquerra, C.-C. Li, T.-L. Huang, E. Coyaud, R. Viais, C. Grauffel, B. Raught, C. Lim, J. Lüders, S.-Y. Tsai, K.-C. Hsia, A γ-tubulin complex-dependent pathway suppresses ciliogenesis by promoting cilia disassembly, Cell Rep. 41 (2022) 111642. https://doi.org/https://doi.org/10.1016/j.celrep.2022.111642.

[148] B. Zhang, T. Zhang, G. Wang, G. Wang, W. Chi, Q. Jiang, C. Zhang, GSK3β-Dzip1-Rab8 Cascade Regulates Ciliogenesis after Mitosis, PLOS Biol. 13 (2015) e1002129.

https://doi.org/10.1371/journal.pbio.1002129.

[149] L. Lu, Q. Liu, L. Zhi, X. Che, B. Xiao, M. Cui, M. Yu, B. Yang, J. Zhang, B. Zhang, Establishment of a Ciliogenesis-Associated Signaling Model for Polycystic Kidney Disease, Kidney Blood Press. Res. 46 (2021) 693–701. https://doi.org/10.1159/000517408.

[150] J. Hu, S.G. Wittekind, M.M. Barr, STAM and Hrs Down-Regulate Ciliary TRP Receptors, Mol. Biol. Cell. 18 (2007) 3277–3289. https://doi.org/10.1091/mbc.e07-03-0239.

[151] J. Yang, T. Li, The ciliary rootlet interacts with kinesin light chains and may provide a scaffold for kinesin-1 vesicular cargos, Exp. Cell Res. 309 (2005) 379–389. https://doi.org/https://doi.org/10.1016/j.yexcr.2005.05.026.

[152] T.U. Consortium, UniProt: the Universal Protein Knowledgebase in 2023, Nucleic Acids Res. 51 (2023) D523–D531. https://doi.org/10.1093/nar/gkac1052.

[153] Y. Li, G.D. Kao, B.A. Garcia, J. Shabanowitz, D.F. Hunt, J. Qin, C. Phelan, M.A. Lazar, A novel histone deacetylase pathway regulates mitosis by modulating Aurora B kinase activity, Genes & Dev. 20 (2006) 2566–2579. https://doi.org/10.1101/gad.1455006.

[154] S.B. Martins, T. Eide, R.L. Steen, T. Jahnsen, S. Skalhegg B, P. Collas, HA95 is a protein of the chromatin and nuclear matrix regulating nuclear envelope dynamics, J. Cell Sci. 113 (2000) 3703–3713. https://doi.org/10.1242/jcs.113.21.3703.

[155] F. Favaretto, G. Milan, G.B. Collin, J.D. Marshall, F. Stasi, P. Maffei, R. Vettor, J.K. Naggert, GLUT4 defects in adipose tissue are early signs of metabolic alterations in alms1GT/GT, a mouse model for obesity and insulin resistance, PLoS One. 9 (2014). https://doi.org/10.1371/journal.pone.0109540.

[156] R. Miao, X. Fang, J. Wei, H. Wu, X. Wang, J. Tian, Akt: A Potential Drug Target for Metabolic Syndrome, Front. Physiol. 13 (2022). https://www.frontiersin.org/articles/10.3389/fphys.2022.822333.

[157] X. Huang, G. Liu, J. Guo, Z. Su, The PI3K/AKT pathway in obesity and type 2 diabetes, Int. J. Biol. Sci. 14 (2018) 1483–1496. https://doi.org/10.7150/ijbs.27173.

[158] O. V Leontieva, Z.N. Demidenko, M. V Blagosklonny, Rapamycin reverses insulin resistance (IR) in high-glucose medium without causing IR in normoglycemic medium, Cell Death Dis. 5 (2014) e1214–e1214. https://doi.org/10.1038/cddis.2014.178.

[159] G.I. Welsh, C.G. Proud, Glycogen synthase kinase-3 is rapidly inactivated in response to insulin and phosphorylates eukaryotic initiation factor eIF-2B, Biochem. J. 294 (1993) 625–629. https://doi.org/10.1042/bj2940625.

[160] S. Patel, B.W. Doble, K. MacAulay, E.M. Sinclair, D.J. Drucker, J.R. Woodgett, Tissue-Specific Role of Glycogen Synthase Kinase 3β in Glucose Homeostasis and Insulin Action, Mol. Cell. Biol. 28 (2008) 6314–6328. https://doi.org/10.1128/MCB.00763-08.

[161] S. Dalle, J. Quoyer, E. Varin, S. Costes, Roles and Regulation of the Transcription Factor CREB in Pancreatic β-Cells, Curr. Mol. Pharmacol. 4 (2011) 187–195. https://doi.org/http://dx.doi.org/10.2174/1874467211104030187.

[162] B. Kurtulmus, W. Wang, T. Ruppert, A. Neuner, B. Cerikan, L. Viol, R. Dueñas-Sánchez, O.J. Gruss, G. Pereira, WDR8 is a centriolar satellite and centriole-associated protein that promotes ciliary vesicle docking during ciliogenesis, J. Cell Sci. 129 (2016) 621–636. https://doi.org/10.1242/jcs.179713.

[163] K. Kim, S. Lee, J. Chang, K. Rhee, A novel function of CEP135 as a platform protein of C-NAP1 for its centriolar localization, Exp. Cell Res. 314 (2008) 3692–3700. https://doi.org/https://doi.org/10.1016/j.yexcr.2008.09.016.

[164] J. Kleylein-Sohn, J. Westendorf, M. Le Clech, R. Habedanck, Y.-D. Stierhof, E.A. Nigg, Plk4-Induced Centriole Biogenesis in Human Cells, Dev. Cell. 13 (2007) 190–202. https://doi.org/https://doi.org/10.1016/j.devcel.2007.07.002.

[165] T. Eguether, M.A. Ermolaeva, Y. Zhao, M.C. Bonnet, A. Jain, M. Pasparakis, G. Courtois, A.-M. Tassin, The deubiquitinating enzyme CYLD controls apical docking of basal bodies in ciliated epithelial cells, Nat. Commun. 5 (2014) 4585. https://doi.org/10.1038/ncomms5585.

[166] O.R. Karasu, A. Neuner, E.S. Atorino, G. Pereira, E. Schiebel, The central scaffold protein CEP350 coordinates centriole length, stability, and maturation, J. Cell Biol. 221 (2022) e202203081. https://doi.org/10.1083/jcb.202203081.

[167] T. Kanie, K.L. Abbott, N.A. Mooney, E.D. Plowey, J. Demeter, P.K. Jackson, The CEP19-RABL2 GTPase Complex Binds IFT-B to Initiate Intraflagellar Transport at the Ciliary Base, Dev. Cell. 42 (2017) 22-36.e12. https://doi.org/https://doi.org/10.1016/j.devcel.2017.05.016.

[168] S.K. Kim, E. Brotslaw, V. Thome, J. Mitchell, R. Ventrella, C. Collins, B. Mitchell, A role for

Cep70 in centriole amplification in multiciliated cells, Dev. Biol. 471 (2021) 10–17. https://doi.org/https://doi.org/10.1016/j.ydbio.2020.11.011.

[169] E. Schmitt, C. Paquet, M. Beauchemin, J. Dever-Bertrand, R. Bertrand, Characterization of Bax-ς, a Cell Death-Inducing Isoform of Bax, Biochem. Biophys. Res. Commun. 270 (2000) 868–879. https://doi.org/https://doi.org/10.1006/bbrc.2000.2537.

[170] H. Zhang, J.K. Kim, C.A. Edwards, Z. Xu, R. Taichman, C.-Y. Wang, Clusterin inhibits apoptosis by interacting with activated Bax, Nat. Cell Biol. 7 (2005) 909–915. https://doi.org/10.1038/ncb1291.

[171] E. Gavathiotis, M. Suzuki, M.L. Davis, K. Pitter, G.H. Bird, S.G. Katz, H.-C. Tu, H. Kim, E.H.-Y. Cheng, N. Tjandra, L.D. Walensky, BAX activation is initiated at a novel interaction site, Nature. 455 (2008) 1076–1081. https://doi.org/10.1038/nature07396.

[172] P.E. Czabotar, E.F. Lee, G. V Thompson, A.Z. Wardak, W.D. Fairlie, P.M. Colman, Mutation to Bax beyond the BH3 Domain Disrupts Interactions with Pro-survival Proteins and Promotes Apoptosis*, J. Biol. Chem. 286 (2011) 7123–7131. https://doi.org/https://doi.org/10.1074/jbc.M110.161281.

[173] F. Edlich, S. Banerjee, M. Suzuki, M.M. Cleland, D. Arnoult, C. Wang, A. Neutzner, N. Tjandra, R.J. Youle, Bcl-xL Retrotranslocates Bax from the Mitochondria into the Cytosol, Cell. 145 (2011) 104–116. https://doi.org/https://doi.org/10.1016/j.cell.2011.02.034.

[174] Z.N. Oltval, C.L. Milliman, S.J. Korsmeyer, Bcl-2 heterodimerizes in vivo with a conserved homolog, Bax, that accelerates programed cell death, Cell. 74 (1993) 609–619. https://doi.org/https://doi.org/10.1016/0092-8674(93)90509-O.

[175] T. Chittenden, C. Flemington, A.B. Houghton, R.G. Ebb, G.J. Gallo, B. Elangovan, G. Chinnadurai, R.J. Lutz, A conserved domain in Bak, distinct from BH1 and BH2, mediates cell death and protein binding functions., EMBO J. 14 (1995) 5589–5596. https://doi.org/https://doi.org/10.1002/j.1460-2075.1995.tb00246.x.

[176] K.O. Tan, N.Y. Fu, S.K. Sukumaran, S.-L. Chan, J.H. Kang, K.L. Poon, B.S. Chen, V.C. Yu, MAP-1 is a mitochondrial effector of Bax, Proc. Natl. Acad. Sci. 102 (2005) 14623–14628. https://doi.org/10.1073/pnas.0503524102.

[177] A. Peña-Blanco, A.J. García-Sáez, Bax, Bak and beyond — mitochondrial performance in apoptosis, FEBS J. 285 (2018) 416–431. https://doi.org/https://doi.org/10.1111/febs.14186.

[178] T.E. Vaskivuo, F. Stenbäck, J.S. Tapanainen, Apoptosis and apoptosis-related factors Bcl-2, Bax, tumor necrosis factor-α, and NF-κB in human endometrial hyperplasia and carcinoma, Cancer. 95 (2002) 1463–1471. https://doi.org/https://doi.org/10.1002/cncr.10876.

[179] C. Gao, A.-Y. Wang, Significance of Increased Apoptosis and Bax Expression in Human Small Intestinal Adenocarcinoma, J. Histochem. Cytochem. 57 (2009) 1139–1148. https://doi.org/10.1369/jhc.2009.954446.

[180] T. Beyer, F. Klose, A. Kuret, F. Hoffmann, R. Lukowski, M. Ueffing, K. Boldt, Tissue- and isoform-specific protein complex analysis with natively processed bait proteins, J. Proteomics. 231 (2021) 103947. https://doi.org/10.1016/j.jprot.2020.103947.

[181] F. Kuhnert, A. Stefanski, N. Overbeck, L. Drews, A.S. Reichert, K. Stühler, A.P.M. Weber, Rapid Single-Step Affinity Purification of HA-Tagged Plant Mitochondria1 [OPEN], Plant Physiol. 182 (2020) 692–706. https://doi.org/10.1104/pp.19.00732.

[182] M.E. Kimple, A.L. Brill, R.L. Pasker, Overview of Affinity Tags for Protein Purification, Curr. Protoc. Protein Sci. 73 (2013) 9.9.1-9.9.23. https://doi.org/https://doi.org/10.1002/0471140864.ps0909s73.

[183] V.P. Reddy Chichili, V. Kumar, J. Sivaraman, Linkers in the structural biology of protein–protein interactions, Protein Sci. 22 (2013) 153–167. https://doi.org/https://doi.org/10.1002/pro.2206.

[184] M. Uhlen, P. Oksvold, L. Fagerberg, E. Lundberg, K. Jonasson, M. Forsberg, M. Zwahlen, C. Kampf, K. Wester, S. Hober, H. Wernerus, L. Björling, F. Ponten, Towards a knowledge-based Human Protein Atlas, Nat. Biotechnol. 28 (2010) 1248–1250. https://doi.org/10.1038/nbt1210-1248.

[185] Human Protein Atlas proteinatlas.org, Version 22.0. (2022). proteinatlas.org.

[186] V. Jäger, K. Büssow, A. Wagner, S. Weber, M. Hust, A. Frenzel, T. Schirrmann, High level transient production of recombinant antibodies and antibody fusion proteins in HEK293 cells, BMC Biotechnol. 13 (2013) 52. https://doi.org/10.1186/1472-6750-13-52.

[187] O. Bernatik, P. Pejskova, D. Vyslouzil, K. Hanakova, Z. Zdrahal, L. Cajanek, Phosphorylation of multiple proteins involved in ciliogenesis by Tau Tubulin kinase 2, Mol. Biol. Cell. 31 (2020) 1032–1046. https://doi.org/10.1091/mbc.E19-06-0334.

[188] K. Takahashi, T. Nagai, S. Chiba, K. Nakayama, K. Mizuno, Glucose deprivation induces primary cilium formation through mTORC1 inactivation, J. Cell Sci. 131 (2018) jcs208769. https://doi.org/10.1242/jcs.208769.

[189] P. Zhang, A.A. Kiseleva, V. Korobeynikov, H. Liu, M.B. Einarson, E.A. Golemis, Microscopy-Based Automated Live Cell Screening for Small Molecules That Affect Ciliation, Front. Genet. 10 (2019) 75. https://doi.org/10.3389/fgene.2019.00075.

[190] E.L. Huttlin, R.J. Bruckner, J.A. Paulo, J.R. Cannon, L. Ting, K. Baltier, G. Colby, F. Gebreab, M.P. Gygi, H. Parzen, J. Szpyt, S. Tam, G. Zarraga, L. Pontano-Vaites, S. Swarup, A.E. White, D.K. Schweppe, R. Rad, B.K. Erickson, R.A. Obar, K.G. Guruharsha, K. Li, S. Artavanis-Tsakonas, S.P. Gygi, J.W. Harper, Architecture of the human interactome defines protein communities and disease networks, Nature. 545 (2017) 505–509. https://doi.org/10.1038/nature22366.

[191] E.L. Huttlin, L. Ting, R.J. Bruckner, F. Gebreab, M.P. Gygi, J. Szpyt, S. Tam, G. Zarraga, G. Colby, K. Baltier, R. Dong, V. Guarani, L.P. Vaites, A. Ordureau, R. Rad, B.K. Erickson, M. Wühr, J. Chick, B. Zhai, D. Kolippakkam, J. Mintseris, R.A. Obar, T. Harris, S. Artavanis-Tsakonas, M.E. Sowa, P. De Camilli, J.A. Paulo, J.W. Harper, S.P. Gygi, The BioPlex Network: A Systematic Exploration of the Human Interactome, Cell. 162 (2015) 425–440. https://doi.org/https://doi.org/10.1016/j.cell.2015.06.043.

[192] A. Brückner, C. Polge, N. Lentze, D. Auerbach, U. Schlattner, Yeast Two-Hybrid, a Powerful Tool for Systems Biology, Int. J. Mol. Sci. 10 (2009) 2763–2788. https://doi.org/10.3390/ijms10062763.

[193] T.J. Gibson, M. Seiler, R.A. Veitia, The transience of transient overexpression, Nat. Methods. 10 (2013) 715–721. https://doi.org/10.1038/nmeth.2534.

[194] F. Cunningham, J.J.E. Allen, J.J.E. Allen, J. Alvarez-Jarreta, M.R. Amode, I.M. Armean, O. Austine-Orimoloye, A.G. Azov, I. Barnes, R. Bennett, A. Berry, J. Bhai, A. Bignell, K. Billis, S. Boddu, L. Brooks, M. Charkhchi, C. Cummins, L. Da Rin Fioretto, C. Davidson, K. Dodiya, S. Donaldson, B. El Houdaigui, T. El Naboulsi, R. Fatima, C.G. Giron, T. Genez, J.G. Martinez, C. Guijarro-Clarke, A. Gymer, M. Hardy, Z. Hollis, T. Hourlier, T. Hunt, T. Juettemann, V. Kaikala, M. Kay, I. Lavidas, T. Le, D. Lemos, J.C. Marugán, S. Mohanan, A. Mushtaq, M. Naven, D.N. Ogeh, A. Parker, A. Parton, M. Perry, I. Piližota, I. Prosovetskaia, M.P. Sakthivel, A.I.A. Salam, B.M. Schmitt, H. Schuilenburg, D. Sheppard, J.G. Pérez-Silva, W. Stark, E. Steed, K. Sutinen, R. Sukumaran, D. Sumathipala, M.-M.

Suner, M. Szpak, A. Thormann, F.F. Tricomi, D. Urbina-Gómez, A. Veidenberg, T.A. Walsh, B. Walts, N. Willhoft, A. Winterbottom, E. Wass, M. Chakiachvili, B. Flint, A. Frankish, S. Giorgetti, L. Haggerty, S.E. Hunt, G.R. IIsley, J.E. Loveland, F.J. Martin, B. Moore, J.M. Mudge, M. Muffato, E. Perry, M. Ruffier, J. Tate, D. Thybert, S.J. Trevanion, S. Dyer, P.W. Harrison, K.L. Howe, A.D. Yates, D.R. Zerbino, P. Flicek, Ensembl 2022; currently release 109 - Feb 2023, Nucleic Acids Res. 50, curren (2022) D988–D995. https://doi.org/10.1093/nar/gkab1049.

[195] M.K. Schwinn, L.S. Steffen, K. Zimmerman, K. V Wood, T. Machleidt, A Simple and Scalable Strategy for Analysis of Endogenous Protein Dynamics, Sci. Rep. 10 (2020) 8953. https://doi.org/10.1038/s41598-020-65832-1.

[196] A.-C. Gingras, R. Aebersold, B. Raught, Advances in protein complex analysis using mass spectrometry, J. Physiol. 563 (2005) 11–21. https://doi.org/https://doi.org/10.1113/jphysiol.2004.080440.

[197] J.-D. Pédelacq, S. Cabantous, T. Tran, T.C. Terwilliger, G.S. Waldo, Engineering and characterization of a superfolder green fluorescent protein, Nat. Biotechnol. 24 (2006) 79–88. https://doi.org/10.1038/nbt1172.

[198] S. Gungor, Y. Oktay, S. Hiz, Á. Aranguren-Ibáñez, I. Kalafatcilar, A. Yaramis, E. Karaca, U. Yis, E. Sonmezler, B. Ekinci, M. Aslan, E. Yilmaz, B. Özgör, S. Balaraju, N. Szabo, S. Laurie, S. Beltran, D.G. MacArthur, D. Hathazi, A. Töpf, A. Roos, H. Lochmuller, I. Vernos, R. Horvath, Autosomal recessive variants in TUBGCP2 alter the γ-tubulin ring complex leading to neurodevelopmental disease, IScience. 24 (2020) 101948. https://doi.org/10.1016/j.isci.2020.101948.

[199] T.A. Baldwin, C.W. Dessauer, Function of Adenylyl Cyclase in Heart: the AKAP Connection, J. Cardiovasc. Dev. Dis. 5 (2018). https://doi.org/10.3390/jcdd5010002.

[200] C.H. Melick, D. Meng, J.L. Jewell, A-kinase anchoring protein 8L interacts with mTORC1 and promotes cell growth, J. Biol. Chem. 295 (2020) 8096–8105. https://doi.org/https://doi.org/10.1074/jbc.AC120.012595.

[201] M. Mavrakis, J. Lippincott-Schwartz, C.A. Stratakis, I. Bossis, Depletion of type IA regulatory subunit (RIα) of protein kinase A (PKA) in mammalian cells and tissues activates mTOR and causes autophagic deficiency, Hum. Mol. Genet. 15 (2006) 2962–2971. https://doi.org/10.1093/hmg/ddl239.

[202] Z. Zou, T. Tao, H. Li, X. Zhu, mTOR signaling pathway and mTOR inhibitors in cancer: progress and challenges, Cell Biosci. 10 (2020) 31. https://doi.org/10.1186/s13578-020-00396-1.

[203] M.A. Fink, D.R. Zakhary, J.A. Mackey, R.W. Desnoyer, C. Apperson-Hansen, D.S. Damron, M. Bond, AKAP-Mediated Targeting of Protein Kinase A Regulates Contractility in Cardiac Myocytes, Circ. Res. 88 (2001) 291–297. https://doi.org/10.1161/01.RES.88.3.291.

[204] V. De Paris, F. Biondi, D. Stolfo, M. Merlo, G. Sinagra, Pathophysiology BT - Dilated Cardiomyopathy : From Genetics to Clinical Management, in: G. Sinagra, M. Merlo, B. Pinamonti (Eds.), Springer International Publishing, Cham, 2019: pp. 17–25. https://doi.org/10.1007/978-3-030-13864-6_3.

[205] S. Dedeoglu, E. Dede, F. Oztunc, A. Gedikbasi, G. Yesil, R. Dedeoglu, Mutation identification and prediction for severe cardiomyopathy in Alström syndrome, and review of the literature for cardiomyopathy, Orphanet J. Rare Dis. 17 (2022) 359. https://doi.org/10.1186/s13023-022-02483-7.

[206] S. Ghetti, M. Burigotto, A. Mattivi, G. Magnani, A. Casini, A. Bianchi, A. Cereseto, L.L. Fava, CRISPR/Cas9 ribonucleoprotein-mediated knockin generation in hTERT-RPE1 cells, STAR Protoc. 2 (2021) 100407. https://doi.org/https://doi.org/10.1016/j.xpro.2021.100407.

[207] K. Essandoh, S. Deng, X. Wang, Y. Li, Q. Li, X. Mu, T. Peng, G.-C. Fan, Tsg101 Is Involved in the Sorting and Re-Distribution of Glucose Transporter-4 to the Sarcolemma Membrane of Cardiac Myocytes, Cells. 9 (2020). https://doi.org/10.3390/cells9091936.

[208] H. Takahashi, J.R. Mayers, L. Wang, J.M. Edwardson, A. Audhya, Hrs and STAM Function Synergistically to Bind Ubiquitin-Modified Cargoes In Vitro, Biophys. J. 108 (2015) 76–84. https://doi.org/https://doi.org/10.1016/j.bpj.2014.11.004.

[209] J. Stöckli, D.J. Fazakerley, D.E. James, GLUT4 exocytosis, J. Cell Sci. 124 (2011) 4147–4159. https://doi.org/10.1242/jcs.097063.

[210] S.I. Buschow, J.M.P. Liefhebber, R. Wubbolts, W. Stoorvogel, Exosomes contain ubiquitinated proteins, Blood Cells, Mol. Dis. 35 (2005) 398–403. https://doi.org/https://doi.org/10.1016/j.bcmd.2005.08.005.

[211] C. Théry, M. Boussac, P. Véron, P. Ricciardi-Castagnoli, G. Raposo, J. Garin, S.

Amigorena, Proteomic Analysis of Dendritic Cell-Derived Exosomes: A Secreted Subcellular Compartment Distinct from Apoptotic Vesicles1, J. Immunol. 166 (2001) 7309–7318. https://doi.org/10.4049/jimmunol.166.12.7309.

[212] M. Colombo, C. Moita, G. van Niel, J. Kowal, J. Vigneron, P. Benaroch, N. Manel, L.F. Moita, C. Théry, G. Raposo, Analysis of ESCRT functions in exosome biogenesis, composition and secretion highlights the heterogeneity of extracellular vesicles, J. Cell Sci. 126 (2013) 5553–5565. https://doi.org/10.1242/jcs.128868.

[213] F. Dassie, F. Favaretto, S. Bettini, M. Parolin, M. Valenti, F. Reschke, T. Danne, R. Vettor, G. Milan, P. Maffei, Alström syndrome: an ultra-rare monogenic disorder as a model for insulin resistance, type 2 diabetes mellitus and obesity, Endocrine. 71 (2021) 618–625. https://doi.org/10.1007/s12020-021-02643-y.

[214] R. Sönmez Flitman, B. Khalili, Z. Kutalik, R. Rueedi, A. Brümmer, S. Bergmann, Untargeted Metabolome- and Transcriptome-Wide Association Study Suggests Causal Genes Modulating Metabolite Concentrations in Urine, J. Proteome Res. 20 (2021) 5103–5114. https://doi.org/10.1021/acs.jproteome.1c00585.

[215] B. Bea-Mascato, E. Gómez-Castañeda, Y.E. Sánchez-Corrales, S. Castellano, D. Valverde, Loss of the centrosomal protein ALMS1 alters lipid metabolism and the regulation of extracellular matrix-related processes, BioRxiv. (2022) 2022.11.02.514847. https://doi.org/10.1101/2022.11.02.514847.

[216] K.W. Finnson, Y. Almadani, A. Philip, Non-canonical (non-SMAD2/3) TGF-β signaling in fibrosis: Mechanisms and targets, Semin. Cell Dev. Biol. 101 (2020) 115–122. https://doi.org/https://doi.org/10.1016/j.semcdb.2019.11.013.

[217] S. Patel, J. Tang, J.M. Overstreet, S. Anorga, F. Lian, A. Arnouk, R. Goldschmeding, P.J. Higgins, R. Samarakoon, Rac-GTPase promotes fibrotic TGF-β1 signaling and chronic kidney disease via EGFR, p53, and Hippo/YAP/TAZ pathways, FASEB J. 33 (2019) 9797–9810. https://doi.org/https://doi.org/10.1096/fj.201802489RR.

[218] R.A. Rahimi, E.B. Leof, TGF-β signaling: A tale of two responses, J. Cell. Biochem. 102 (2007) 593–608. https://doi.org/https://doi.org/10.1002/jcb.21501.

[219] E. Zulato, F. Favaretto, C. Veronese, S. Campanaro, J.D. Marshall, S. Romano, A. Cabrelle, G.B. Collin, B. Zavan, A.S. Belloni, E. Rampazzo, J.K. Naggert, G. Abatangelo, N. Sicolo, P. Maffei, G. Milan, R. Vettor, ALMS1-deficient fibroblasts over-express extra-

cellular matrix components, display cell cycle delay and are resistant to apoptosis, PLoS One. (2011). https://doi.org/10.1371/journal.pone.0019081.

[220] I. Huang-Doran, R.K. Semple, Knockdown of the Alström syndrome-associated gene Alms1 in 3T3-L1 preadipocytes impairs adipogenesis but has no effect on cell-autonomous insulin action, Int. J. Obes. 34 (2010) 1554–1558. https://doi.org/10.1038/ijo.2010.92.

[221] Y. Liao, M.-C. Hung, Physiological regulation of Akt activity and stability, Am. J. Transl. Res. 2 (2010) 19–42. http://europepmc.org/abstract/MED/20182580.

[222] J. Lee, M.-S. Kim, The role of GSK3 in glucose homeostasis and the development of insulin resistance, Diabetes Res. Clin. Pract. 77 (2007) S49–S57. https://doi.org/https://doi.org/10.1016/j.diabres.2007.01.033.

[223] M.L. Latif, T.S. Pillay, Differential detection of phosphorylated glycogen synthase kinase 3 α and β depending on blocking conditions, Anal. Biochem. 379 (2008) 136–137. https://doi.org/10.1016/j.ab.2008.04.033.

[224] S.R. McGlashan, E.C. Cluett, C.G. Jensen, C.A. Poole, Primary Cilia in osteoarthritic chondrocytes: From chondrons to clusters, Dev. Dyn. (2008). https://doi.org/10.1002/dvdy.21501.

[225] L. Wang, J. Li, L. Di, Glycogen synthesis and beyond, a comprehensive review of GSK3 as a key regulator of metabolic pathways and a therapeutic target for treating metabolic diseases, Med. Res. Rev. 42 (2022) 946–982. https://doi.org/https://doi.org/10.1002/med.21867.

[226] K.W. Cormier, B. Larsen, A.-C. Gingras, J.R. Woodgett, Interactomes of Glycogen Synthase Kinase-3 Isoforms, J. Proteome Res. 22 (2023) 977–989. https://doi.org/10.1021/acs.jproteome.2c00825.

[227] X. Liu, K. Salokas, F. Tamene, Y. Jiu, R.G. Weldatsadik, T. Öhman, M. Varjosalo, An AP-MS- and BioID-compatible MAC-tag enables comprehensive mapping of protein interactions and subcellular localizations, Nat. Commun. 9 (2018) 1188. https://doi.org/10.1038/s41467-018-03523-2.

[228] X. Fang, S.X. Yu, Y. Lu, R.C. Bast, J.R. Woodgett, G.B. Mills, Phosphorylation and inactivation of glycogen synthase kinase 3 by protein kinase A, Proc. Natl. Acad. Sci. 97 (2000) 11960–11965. https://doi.org/10.1073/pnas.220413597.

[229] M.A. Hermida, J. Dinesh Kumar, N.R. Leslie, GSK3 and its interactions with the PI3K/AKT/mTOR signalling network, Adv. Biol. Regul. 65 (2017) 5–15. https://doi.org/https://doi.org/10.1016/j.jbior.2017.06.003.

[230] D. Wu, W. Pan, GSK3: a multifaceted kinase in Wnt signaling, Trends Biochem. Sci. 35 (2010) 161–168. https://doi.org/https://doi.org/10.1016/j.tibs.2009.10.002.

[231] E. Beurel, S.F. Grieco, R.S. Jope, Glycogen synthase kinase-3 (GSK3): Regulation, actions, and diseases, Pharmacol. Ther. 148 (2015) 114–131. https://doi.org/https://doi.org/10.1016/j.pharmthera.2014.11.016.

[232] M.A. El-Brolosy, D.Y.R. Stainier, Genetic compensation: A phenomenon in search of mechanisms, PLOS Genet. 13 (2017) e1006780. https://doi.org/10.1371/journal.pgen.1006780.

[233] K. Benchoula, I.S. Parhar, P. Madhavan, W.E. Hwa, CREB nuclear transcription activity as a targeting factor in the treatment of diabetes and diabetes complications, Biochem. Pharmacol. 188 (2021) 114531. https://doi.org/https://doi.org/10.1016/j.bcp.2021.114531.

[234] E. Blanchet, S. Van de Velde, S. Matsumura, E. Hao, J. LeLay, K. Kaestner, M. Montminy, Feedback Inhibition of CREB Signaling Promotes Beta Cell Dysfunction in Insulin Resistance, Cell Rep. 10 (2015) 1149–1157. https://doi.org/https://doi.org/10.1016/j.celrep.2015.01.046.

[235] A. Steven, M. Friedrich, P. Jank, N. Heimer, J. Budczies, C. Denkert, B. Seliger, What turns CREB on? And off? And why does it matter?, Cell. Mol. Life Sci. 77 (2020) 4049–4067. https://doi.org/10.1007/s00018-020-03525-8.

[236] S. Naqvi, K.J. Martin, J.S.C. Arthur, CREB phosphorylation at Ser133 regulates transcription via distinct mechanisms downstream of cAMP and MAPK signalling, Biochem. J. 458 (2014) 469–479. https://doi.org/10.1042/BJ20131115.

[237] L. Qi, M. Saberi, E. Zmuda, Y. Wang, J. Altarejos, X. Zhang, R. Dentin, S. Hedrick, G. Bandyopadhyay, T. Hai, J. Olefsky, M. Montminy, Adipocyte CREB Promotes Insulin Resistance in Obesity, Cell Metab. 9 (2009) 277–286. https://doi.org/https://doi.org/10.1016/j.cmet.2009.01.006.

[238] M. Labuhn, F.F. Adams, M. Ng, S. Knoess, A. Schambach, E.M. Charpentier, A. Schwarzer, J.L. Mateo, J.-H. Klusmann, D. Heckl, Refined sgRNA efficacy prediction improves large- and small-scale CRISPR–Cas9 applications, Nucleic Acids Res. 46

(2018) 1375–1385. https://doi.org/10.1093/nar/gkx1268.

[239] H.J. Lee, H.J. Kim, S.J. Lee, Mismatch Intolerance of 5′-Truncated sgRNAs in CRISPR/Cas9 Enables Efficient Microbial Single-Base Genome Editing, Int. J. Mol. Sci. 22 (2021). https://doi.org/10.3390/ijms22126457.

[240] J.D. Marshall, E.G. Hinman, G.B. Collin, S. Beck, R. Cerqueira, P. Maffei, G. Milan, W. Zhang, D.I. Wilson, T. Hearn, P. Tavares, R. Vettor, C. Veronese, M. Martin, W.V. So, P.M. Nishina, J.K. Naggert, Spectrum of ALMS1 variants and evaluation of genotype-phenotype correlations in Alström syndrome, Hum. Mutat. (2007). https://doi.org/10.1002/humu.20577.

[241] A. Rossi, Z. Kontarakis, C. Gerri, H. Nolte, S. Hölper, M. Krüger, D.Y.R. Stainier, Genetic compensation induced by deleterious mutations but not gene knockdowns, Nature. 524 (2015) 230–233. https://doi.org/10.1038/nature14580.

[242] V. Strecker, Z. Wumaier, I. Wittig, H. Schägger, Large pore gels to separate mega protein complexes larger than 10 MDa by blue native electrophoresis: Isolation of putative respiratory strings or patches, Proteomics. 10 (2010) 3379–3387. https://doi.org/https://doi.org/10.1002/pmic.201000343.

[243] H. Eubel, H.-P. Braun, Ah. Millar, Blue-native PAGE in plants: a tool in analysis of protein-protein interactions, Plant Methods. 1 (2005) 11. https://doi.org/10.1186/1746-4811-1-11.

[244] C.D. Katsetos, E. Dráberová, A. Legido, P. Dráber, Tubulin targets in the pathobiology and therapy of glioblastoma multiforme. II. γ-tubulin, J. Cell. Physiol. 221 (2009) 514–520. https://doi.org/https://doi.org/10.1002/jcp.21884.

[245] B. Bea-Mascato, D. Valverde, Genotype–phenotype associations in Alström syndrome: a systematic review and meta-analysis, J. Med. Genet. (2023) jmg-2023-109175. https://doi.org/10.1136/jmg-2023-109175.

[246] M. Panic, S. Hata, A. Neuner, E. Schiebel, The Centrosomal Linker and Microtubules Provide Dual Levels of Spatial Coordination of Centrosomes, PLOS Genet. 11 (2015) e1005243. https://doi.org/10.1371/journal.pgen.1005243.

[247] S. Floriot, C. Vesque, S. Rodriguez, F. Bourgain-Guglielmetti, A. Karaiskou, M. Gautier, A. Duchesne, S. Barbey, S. Fritz, A. Vasilescu, M. Bertaud, M. Moudjou, S. Halliez, V. Cormier-Daire, J. E.L. Hokayem, E.A. Nigg, L. Manciaux, R. Guatteo, N. Cesbron, G. Toutirais, A. Eggen, S. Schneider-Maunoury, D. Boichard, J. Sobczak-Thépot, L. Schibler,

C-Nap1 mutation affects centriole cohesion and is associated with a Seckel-like syndrome in cattle, Nat. Commun. 6 (2015) 6894. https://doi.org/10.1038/ncomms7894.

[248] A.-M. Flanagan, E. Stavenschi, S. Basavaraju, D. Gaboriau, D.A. Hoey, C.G. Morrison, Centriole splitting caused by loss of the centrosomal linker protein C-NAP1 reduces centriolar satellite density and impedes centrosome amplification, Mol. Biol. Cell. 28 (2017) 736–745. https://doi.org/10.1091/mbc.e16-05-0325.

[249] A. Loukil, K. Tormanen, C. Sütterlin, The daughter centriole controls ciliogenesis by regulating Neurl-4 localization at the centrosome, J. Cell Biol. 216 (2017) 1287–1300. https://doi.org/10.1083/jcb.201608119.

[250] S. Graser, Y.-D. Stierhof, E.A. Nigg, Cep68 and Cep215 (Cdk5rap2) are required for centrosome cohesion, J. Cell Sci. 120 (2007) 4321–4331. https://doi.org/10.1242/jcs.020248.

[251] J. Yang, J. Gao, M. Adamian, X.-H. Wen, B. Pawlyk, L. Zhang, M.J. Sanderson, J. Zuo, C.L. Makino, T. Li, The Ciliary Rootlet Maintains Long-Term Stability of Sensory Cilia, Mol. Cell. Biol. 25 (2005) 4129–4137. https://doi.org/10.1128/MCB.25.10.4129-4137.2005.

[252] M. Gakovic, X. Shu, I. Kasioulis, S. Carpanini, I. Moraga, A.F. Wright, The role of RPGR in cilia formation and actin stability, Hum. Mol. Genet. 20 (2011) 4840–4850. https://doi.org/10.1093/hmg/ddr423.

[253] Q. Zhang, J.C. Giacalone, C. Searby, E.M. Stone, B.A. Tucker, V.C. Sheffield, Disruption of RPGR protein interaction network is the common feature of RPGR missense variations that cause XLRP, Proc. Natl. Acad. Sci. 116 (2019) 1353–1360. https://doi.org/10.1073/pnas.1817639116.

[254] S. Bodakuntla, A. Schnitzler, C. Villablanca, C. Gonzalez-Billault, I. Bieche, C. Janke, M.M. Magiera, Tubulin polyglutamylation is a general traffic-control mechanism in hippocampal neurons, J. Cell Sci. 133 (2020) jcs241802. https://doi.org/10.1242/jcs.241802.

[255] S. Gadadhar, S. Bodakuntla, K. Natarajan, C. Janke, The tubulin code at a glance, J. Cell Sci. 130 (2017) 1347–1353. https://doi.org/10.1242/jcs.199471.

[256] A. Hu, W.S. Noble, A. Wolf-Yadlin, Technical advances in proteomics: new developments in data-independent acquisition [version 1; peer review: 3 approved], F1000Research. 5

(2016). https://doi.org/10.12688/f1000research.7042.1.

[257] Y. Kawashima, E. Watanabe, T. Umeyama, D. Nakajima, M. Hattori, K. Honda, O. Ohara, Optimization of Data-Independent Acquisition Mass Spectrometry for Deep and Highly Sensitive Proteomic Analysis, Int. J. Mol. Sci. 20 (2019). https://doi.org/10.3390/ijms20235932.

[258] R. Bruderer, O.M. Bernhardt, T. Gandhi, Y. Xuan, J. Sondermann, M. Schmidt, D. Gomez-Varela, L. Reiter, Optimization of Experimental Parameters in Data-Independent Mass Spectrometry Significantly Increases Depth and Reproducibility of Results*, Mol. Cell. Proteomics. 16 (2017) 2296–2309. https://doi.org/https://doi.org/10.1074/mcp.RA117.000314.

[259] T. Beyer, S. Bolz, K. Junger, N. Horn, M. Moniruzzaman, Y. Wissinger, M. Ueffing, K. Boldt, CRISPR/Cas9-mediated Genomic Editing of Cluap1/IFT38 Reveals a New Role in Actin Arrangement, Mol. Cell. Proteomics. 17 (2018) 1285–1294. https://doi.org/10.1074/mcp.RA117.000487.

[260] J.E. Bae, G.M. Kang, S.H. Min, D.S. Jo, Y.K. Jung, K. Kim, M.S. Kim, D.H. Cho, Primary cilia mediate mitochondrial stress responses to promote dopamine neuron survival in a Parkinson's disease model, Cell Death Dis. 10 (2019). https://doi.org/10.1038/s41419-019-2184-y.

[261] S. Kim, N.A. Zaghloul, E. Bubenshchikova, E.C. Oh, S. Rankin, N. Katsanis, T. Obara, L. Tsiokas, Nde1-mediated inhibition of ciliogenesis affects cell cycle re-entry, Nat. Cell Biol. 13 (2011) 351–360. https://doi.org/10.1038/ncb2183.

[262] B.K.A. Choi, P.M. D'Onofrio, A.P. Shabanzadeh, P.D. Koeberle, Stabilization of primary cilia reduces abortive cell cycle re-entry to protect injured adult CNS neurons from apoptosis, PLoS One. 14 (2019) e0220056. https://doi.org/10.1371/journal.pone.0220056.

[263] N. Cirillo, M. Lanza, A. De Rosa, M. Cammarota, A. La Gatta, F. Gombos, A. Lanza, The most widespread desmosomal cadherin, desmoglein 2, is a novel target of caspase 3-mediated apoptotic machinery, J. Cell. Biochem. 103 (2008) 598–606. https://doi.org/https://doi.org/10.1002/jcb.21431.

[264] M.C. Abraham, S. Shaham, Death without caspases, caspases without death, Trends Cell Biol. 14 (2004) 184–193. https://doi.org/https://doi.org/10.1016/j.tcb.2004.03.002.

[265] E. Eskandari, C.J. Eaves, Paradoxical roles of caspase-3 in regulating cell survival,

proliferation, and tumorigenesis, J. Cell Biol. 221 (2022) e202201159. https://doi.org/10.1083/jcb.202201159.

[266] H. Khalil, N. Peltzer, J. Walicki, J.-Y. Yang, G. Dubuis, N. Gardiol, W. Held, P. Bigliardi, B. Marsland, L. Liaudet, C. Widmann, Caspase-3 Protects Stressed Organs against Cell Death, Mol. Cell. Biol. 32 (2012) 4523–4533. https://doi.org/10.1128/MCB.00774-12.

[267] Y. Yosefzon, D. Soteriou, A. Feldman, L. Kostic, E. Koren, S. Brown, R. Ankawa, E. Sedov, F. Glaser, Y. Fuchs, Caspase-3 Regulates YAP-Dependent Cell Proliferation and Organ Size, Mol. Cell. 70 (2018) 573-587.e4. https://doi.org/https://doi.org/10.1016/j.molcel.2018.04.019.

[268] P.-C. Liao, C. Bergamini, R. Fato, L.A. Pon, F. Pallotti, Chapter 1 - Isolation of mitochondria from cells and tissues, in: L.A. Pon, E.A.B.T.-M. in C.B. Schon (Eds.), Mitochondria, 3rd Ed., Academic Press, 2020: pp. 3–31. https://doi.org/https://doi.org/10.1016/bs.mcb.2019.10.002.

[269] B. Liu, Z. Jian, Q. Li, K. Li, Z. Wang, L. Liu, L. Tang, X. Yi, H. Wang, C. Li, T. Gao, Baicalein protects Human melanocytes from H2O2-induced apoptosis via inhibiting mitochondria-dependent caspase activation and the p38 MAPK pathway, Free Radic. Biol. Med. 53 (2012) 183–193. https://doi.org/https://doi.org/10.1016/j.freeradbiomed.2012.04.015.

[270] B.A. Maddux, I.D. Goldfine, Membrane glycoprotein PC-1 inhibition of insulin receptor function occurs via direct interaction with the receptor alpha-subunit., Diabetes. 49 (2000) 13–19. https://doi.org/10.2337/diabetes.49.1.13.

[271] J.E. Nesmith, T.L. Hostelley, C.C. Leitch, M.S. Matern, S. Sethna, R. McFarland, S. Lodh, C.J. Westlake, R. Hertzano, Z.M. Ahmed, N.A. Zaghloul, Genomic knockout of alms1 in zebrafish recapitulates Alström syndrome and provides insight into metabolic phenotypes, Hum. Mol. Genet. 28 (2019). https://doi.org/10.1093/hmg/ddz053.

[272] C.E. Remé, C. Grimm, F. Hafezi, A. Wenzel, T.P. Williams, Apoptosis in the Retina: The Silent Death of Vision, Physiology. 15 (2000) 120–124. https://doi.org/10.1152/physiologyonline.2000.15.3.120.

[273] A. Paganin-Gioanni, E. Bellard, J.M. Escoffre, M.P. Rols, J. Teissié, M. Golzio, Direct visualization at the single-cell level of siRNA electrotransfer into cancer cells, Proc. Natl. Acad. Sci. 108 (2011) 10443–10447. https://doi.org/10.1073/pnas.1103519108.

[274] H. Dana, G.M. Chalbatani, H. Mahmoodzadeh, R. Karimloo, O. Rezaiean, A. Moradzadeh, N. Mehmandoost, F. Moazzen, A. Mazraeh, V. Marmari, M. Ebrahimi, M.M. Rashno, S.J. Abadi, E. Gharagouzlo, Molecular Mechanisms and Biological Functions of siRNA., Int. J. Biomed. Sci. 13 (2017) 48–57.

[275] F. Safari, S. Rahmani Barouji, A.M. Tamaddon, Strategies for Improving siRNA-Induced Gene Silencing Efficiency., Adv. Pharm. Bull. 7 (2017) 603–609. https://doi.org/10.15171/apb.2017.072.

[276] Q. Liu, Q. Guo, W. Guo, S. Song, N. Wang, X. Chen, A. Sun, L. Yan, J. Qiao, Loss of CEP70 function affects acrosome biogenesis and flagella formation during spermiogenesis, Cell Death Dis. 12 (2021) 478. https://doi.org/10.1038/s41419-021-03755-z.

[277] B. Turriziani, A. Garcia-Munoz, R. Pilkington, C. Raso, W. Kolch, A. Von Kriegsheim, On-Beads Digestion in Conjunction with Data-Dependent Mass Spectrometry: A Shortcut to Quantitative and Dynamic Interaction Proteomics, Biology (Basel). 3 (2014) 320–332. https://doi.org/10.3390/biology3020320.

[278] J. Won, C.M. de Evsikova, R.S. Smith, W.L. Hicks, M.M. Edwards, C. Longo-Guess, T. Li, J.K. Naggert, P.M. Nishina, NPHP4 is necessary for normal photoreceptor ribbon synapse maintenance and outer segment formation, and for sperm development, Hum. Mol. Genet. 20 (2011) 482–496. https://doi.org/10.1093/hmg/ddq494.

[279] A.R. Jauregui, M.M. Barr, Functional characterization of the C. elegans nephrocystins NPHP-1 and NPHP-4 and their role in cilia and male sensory behaviors, Exp. Cell Res. 305 (2005) 333–342. https://doi.org/https://doi.org/10.1016/j.yexcr.2005.01.008.

[280] M.T.F. Wolf, J. Lee, F. Panther, E.A. Otto, K.-L. Guan, F. Hildebrandt, Expression and Phenotype Analysis of the Nephrocystin-1 and Nephrocystin-4 Homologs in Caenorhabditiselegans, J. Am. Soc. Nephrol. 16 (2005). https://journals.lww.com/jasn/Fulltext/2005/03000/Expression_and_Phenotype_Analysis_of_the.17.aspx.

[281] V. Pizon, N. Gaudin, M. Poteau, C. Cifuentes-Diaz, R. Demdou, V. Heyer, B. Reina San Martin, J. Azimzadeh, hVFL3/CCDC61 is a component of mother centriole subdistal appendages required for centrosome cohesion and positioning, Biol. Cell. 112 (2020) 22–37. https://doi.org/https://doi.org/10.1111/boc.201900038.

[282] T. Ochi, V. Quarantotti, H. Lin, J. Jullien, I. Rosa e Silva, F. Boselli, D.D. Barnabas, C.M. Johnson, S.H. McLaughlin, S.M. V Freund, A.N. Blackford, Y. Kimata, R.E. Goldstein, S.P. Jackson, T.L. Blundell, S.K. Dutcher, F. Gergely, M. van Breugel, CCDC61/VFL3 Is a Paralog of SAS6 and Promotes Ciliary Functions, Structure. 28 (2020) 674-689.e11. https://doi.org/https://doi.org/10.1016/j.str.2020.04.010.

[283] C.J. Wiens, Y. Tong, M.A. Esmail, E. Oh, J.M. Gerdes, J. Wang, W. Tempel, J.B. Rattner, N. Katsanis, H.-W. Park, M.R. Leroux, Bardet-Biedl Syndrome-associated Small GTPase ARL6 (BBS3) Functions at or near the Ciliary Gate and Modulates Wnt Signaling*, J. Biol. Chem. 285 (2010) 16218–16230. https://doi.org/https://doi.org/10.1074/jbc.M109.070953.

[284] B. Zhou, W. Lin, Y. Long, Y. Yang, H. Zhang, K. Wu, Q. Chu, Notch signaling pathway: architecture, disease, and therapeutics, Signal Transduct. Target. Ther. 7 (2022) 95. https://doi.org/10.1038/s41392-022-00934-y.

[285] K. Hori, A. Sen, S. Artavanis-Tsakonas, Notch signaling at a glance, J. Cell Sci. 126 (2013) 2135–2140. https://doi.org/10.1242/jcs.127308.

[286] C.C. Leitch, S. Lodh, V. Prieto-Echagüe, J.L. Badano, N.A. Zaghloul, Basal body proteins regulate Notch signaling through endosomal trafficking, J. Cell Sci. 127 (2014) 2407–2419. https://doi.org/10.1242/jcs.130344.

[287] S. Zhou, A. Flamier, M. Abdouh, N. Tétreault, A. Barabino, S. Wadhwa, G. Bernier, Differentiation of human embryonic stem cells into cone photoreceptors through simultaneous inhibition of BMP, TGFβ and Wnt signaling, Development. 142 (2015) 3294–3306. https://doi.org/10.1242/dev.125385.

[288] D. Gambarotto, V. Hamel, P. Guichard, Chapter 4 - Ultrastructure expansion microscopy (U-ExM), in: P. Guichard, V.B.T.-M. in C.B. Hamel (Eds.), Expans. Microsc. Cell Biol., Academic Press, 2021: pp. 57–81. https://doi.org/https://doi.org/10.1016/bs.mcb.2020.05.006.

[289] D. Gambarotto, F.U. Zwettler, M. Le Guennec, M. Schmidt-Cernohorska, D. Fortun, S. Borgers, J. Heine, J.-G. Schloetel, M. Reuss, M. Unser, E.S. Boyden, M. Sauer, V. Hamel, P. Guichard, Imaging cellular ultrastructures using expansion microscopy (U-ExM), Nat. Methods. 16 (2019) 71–74. https://doi.org/10.1038/s41592-018-0238-1.

[290] M. Buszczak, R.A.J. Signer, S.J. Morrison, Cellular Differences in Protein Synthesis Regulate Tissue Homeostasis, Cell. 159 (2014) 242–251.

https://doi.org/https://doi.org/10.1016/j.cell.2014.09.016.

[291] M. Piper, S. Salih, C. Weinl, C.E. Holt, W.A. Harris, Endocytosis-dependent desensitization and protein synthesis–dependent resensitization in retinal growth cone adaptation, Nat. Neurosci. 8 (2005) 179–186. https://doi.org/10.1038/nn1380.

[292] K. Müntjes, S.K. Devan, A.S. Reichert, M. Feldbrügge, Linking transport and translation of mRNAs with endosomes and mitochondria, EMBO Rep. 22 (2021) e52445. https://doi.org/https://doi.org/10.15252/embr.202152445.

[293] F. Corpet, Multiple sequence alignment with hierarchical clustering, Nucleic Acids Res. 16 (1988) 10881–10890. https://doi.org/10.1093/nar/16.22.10881.

10 Appendix

10.1 Sequences of *ALMS1* exon 8, 10, 23

10.1.1 *ALMS1* exon 8 (ENSE00003712451)

GAGACACTTCTAAAGGAGGCATAGCTAAAGTTACTCAATCCAACTTGAAGTCAGGCATCACT
ACCACTCCTGTTGATTCAGACATTGGATCTCATTTATCCTTGTCCCTTGAGGACCTGTCTCA
GTTGGCTGTAAGTTCTCCTCTAGAAACTACTACTGGTCAACACACTGATACTCTCAACCAAA
AGACATTAGCAGATACTCATCTAACTGAAGAGACTCTGAAAGTCACAGCTATTCCTGAACCA
GCTGACCAGAAGACTGCAACACCAACAGTACTCTCTAGTTCCCACTCACATAGGGGGAAGC
CCAGCATTTTCTACCAGCAGGGCTTGCCAGACAGTCATCTAACTGAAGAGGCTTTGAAAGT
TTCAGCTGCTCCTGGACTAGCTGACCAGACAACTGGCATGTCAACTCTAACCTCTACTTCCT
ACTCACATAGAGAGAAGCCTGGTACTTTTTACCAACAAGAGTTACCAGAGAGTAACTTAACC
GAAGAGCCTTTGGAAGTTTCAGCTGCTCCTGGCCCAGTGGAGCAGAAGACGGGAATACCT
ACAGTATCCTCTACATCCCACTCACATGTAGAGGACCTCCTCTTTTTCTATCGACAGACCTT
GCCAGATGGTCATCTAACTGATCAGGCTCTGAAAGTCTCAGCTGTGTCTGGACCAGCTGAC
CAGAAGACTGGGACAGCAACAGTACTCTCTACTCCCCACTCACATAGAGAGAAGCCTGGTA
TTTTTTACCAACAAGAGTTCGCAGACAGTCATCAAACTGAAGAGACTCTTACTAAAGTTTCA
GCCACTCCTGGACCAGCTGACCAGAAGACTGAGATACCAGCAGTACAGTCTAGTTCTTACT
CACAAAGAGAAAAGCCTAGTATTTTGTACCCACAGGACTTAGCAGACAGTCATCTACCTGAA
GAGGGTCTGAAAGTTTCAGCTGTTGCTGGACCAGCTGACCAGAAGACTGGCCTACCAACA
GTACCCTCTAGTGCATACTCACACAGAGAGAAGCTCCTTGTTTTCTACCAACAGGCCTTGCT
GGACAGCCATCTACCCGAAGAGGCTCTGAAAGTTTCAGCTGTTTCTGGACCAGCTGACGGA
AAGACTGGGACACCAGCTGTAACCTCTACTTCCTCTGCGTCCTCTTCACTTGGAGAAAAGC
CCAGTGCTTTCTATCAGCAGACCTTACCCAATAGTCATCTAACTGAAGAGGCTCTGAAAGTA
TCAATTGTTCCTGGACCAGGTGATCAGAAGACTGGGATACCCTCAGCACCATCTAGTTTCTA
CTCACACAGAGAGAAGCCCATTATTTTTTCCCAGCAGACCCTGCCAGACTTTCTTTTCCCTG
AAGAAGCTCTGAAGGTTTCAGCTGTTTCTGTATTGGCTGCCCAGAAGACTGGGACACCAAC
AGTGTCCTCTAATTCTCACTCACATAGCGAGAAATCTAGTGTTTTCTACCAGCAAGAGTTGC
CAGACAGTGATCTACCTAGAGAATCTCTGAAAATGTCTGCTATTCCTGGACTGACTGACCAG
AAGACTGTCCCAACACCAACAGTACCTTCAGGTTCCTTCTCACATAGAGAGAAGCCCAGTA
TTTTCTATCAACAGGAGTGGCCAGATAGTTATGCAACTGAAAAGGCTCTGAAAGTTTCAACT
GGCCCTGGACCAGCTGACCAGAAGACTGAGATACCAGCAGTACAGTCTAGTTCTTACCCAC
AGAGGGAGAAGCCTAGTGTTTTGTACCCACAGGTGTTATCAGACAGTCATCTACCTGAAGA
GAGTCTGAAAGTTTCAGCCTTCCCTGGACCAGCTGACCAGATGACTGACACACCAGCAGTA

CCGTCTACTTTCTACTCACAAAGAGAGAAGCCTGGTATTTTCTACCAACAGACCTTGCCAGA
GAGTCATCTGCCTAAAGAGGCTCTGAAAATTTCAGTAGCTCCTGGACTAGCAGACCAGAAG
ACTGGCACACCAACTGTAACCTCAACTTCCTACTCACAACATAGAGAAAAGCCCAGCATTTT
CCACCAGCAGGCCTTGCCAGGTACTCATATACCTGAAGAGGCTCAGAAAGTTTCAGCTGTT
ACTGGACCAGGTAACCAGAAGACTTGGATACCAAGAGTACTTTCTACCTTCTACTCACAAAG
AGAGAAACCTGGTATTTTCTATCAACAGACCTTGCCAGGTAGTCACATACCTGAAGAGGCA
CAGAAAGTTTCACCTGTTCTTGGACCAGCTGACCAGAAGACTGGGACACCAACTCCAACCT
CTGCTTCTTACTCACACACAGAGAAGCCTGGTATTTTCTACCAACAGGTCTTGCCAGATAAT
CATCCAACTGAAGAGGCTCTGAAAATTTCAGTTGCCTCTGAACCAGTTGACCAGACAACTG
GCACACCAGCTGTAACCTCTACTTCCTACTCACAATATAGAGAGAAGCCCAGCATTTTCTAC
CAACAGTCGTTGCCAAGTAGTCATCTAACTGAAGAGGCTAAGAATGTTTCAGCGGTTCCTG
GACCAGCTGACCAGAAGACTGTGATACCAATTTTACCCTCTACTTTCTACTCACACACAGAG
AAGCCTGGTGTTTTCTACCAACAGGTCTTGCCACATAGTCATCCAACTGAAGAGGCTCTGA
AAATTTCAGTTGCCTCTGAACCAGTTGACCAGACAACTGGCACACCAACTGTAACCTCTACT
TCTTACTCACAACATACAGAGAAGCCGAGTATTTTCTACCAACAGTCGTTGCCAGGTAGTCA
TCTAACTGAAGAGGCTAAGAACGTTTCAGCGGTTCCTGGACCAGGTGACCGGAAGACTGG
GATACCAACTTTACCCTCTACTTTCTACTCACACACAGAGAAGCCTGGTAGTTTCTACCAAC
AGGTCTTGCCACATAGTCATCTACCTGAAGAGGCTTTGGAAGTTTCAGTTGCTCCTGGACC
AGTTGACCAGACGATTGGCACACCAACTGTAACCTCCCCTTCCAGCTCATTTGGAGAGAAG
CCCATTGTTATCTACAAACAGGCCTTTCCAGAGGGTCATCTACCTGAAGAGTCTCTGAAAGT
TTCAGTTGCTCCTGGACCAGTTGGCCAGACAACTGGCGCACCAACTATAACCTCTCCTTCC
TACTCACAACATAGAGCAAAGTCTGGCAGTTTCTACCAACTGGCATTGCTAGGTAGTCAAAT
ACCTGAAGAGGCTCTCAGAGTTTCTTCTGCTCCTGGACCAGCTGACCAGACAACTGGCATA
CCAACCATAACCTCTACTTCCTACTCATTTGGAGAGAAGCCGATTGTTAACTACAAACAGGC
CTTTCCAGATGGTCATCTACCTGAAGAGGCTCTGAAAGTTTCCATTGTTTCTGGACCTACTG
AAAAAAAGACTGACATACCAGCAGGACCTTTAGGTTCCAGTGCACTTGGAGAGAAGCCCAT
TACTTTCTACCGGCAGGCTCTGCTAGACAGTCCTCTAAATAAAGAGGTTGTGAAAGTTTCAG
CTGCTCCTGGACCAGCTGACCAGAAGACTGAGACATTACCAGTACATTCTACTAGCTACTC
AAATAGGGGGAAGCCTGTCATTTTCTACCAGCAGACCCTATCAGACAGTCATTTACCTGAA
GAAGCTCTGAAAGTTCCACCTGTTCCTGGACCAGATGCCCAGAAGACTGAGACACCATCAG
TATCCTCTAGTTTATACTCATATAGAGAGAAGCCCATTGTCTTCTACCAACAGGCCCTGCCA
GACAGTGAGCTAACTCAAGAAGCTCTGAAAGTTTCAGCTGTTCCTCAACCAGCTGACCAGA
AGACTGGGTTATCTACTGTAACTTCCTCTTTCTATTCACATACAGAGAAGCCTAATATTTCTT
ACCAGCAAGAGTTGCCAGATAGTCATCTAACTGAAGAGGCTCTGAAAGTTTCAAATGTTCCT
GGACCAGCTGACCAGAAGACTGGGGTATCAACAGTAACCTCTACTTCCTACTCACACAGAG

AGAAGCCCATTGTTTCCTACCAGCGAGAGTTGCCGCATTTTACTGAAGCAGGTTTGAAAATT
TTAAGAGTTCCTGGACCAGCTGACCAGAAGACTGGAATAAACATCCTGCCCTCTAATTCCTA
CCCACAGAGAGAGCACTCTGTCATTTCTTATGAGCAGGAGTTGCCAGATCTTACTGAAGTA
ACTTTGAAAGCAATAGGGGTTCCTGGGCCTGCTGACCAGAAGACTGGGATACAAATAGCAT
CCTCTAGTTCCTACTCAAATAGAGAGAAGGCCAGTATTTTTCATCAGCAGGAGTTGCCAGAT
GTTACTGAAGAAGCTTTAAATGTTTTTGTTGTTCCTGGACAAGGTGACCGGAAGACTGAGAT
ACCAACAGTACCTTTAAGTTACTACTCACGTAGAGAGAAGCCCAGTGTTATCTCTCAACAGG
AGTTGCCAGACAGTCATCTCACAGAAGAGGCTCTGAAAGTTTCACCTGTTTCTATACCAGCA
GAGCAGAAGACTGGGATACCAATAGGACTGTCTAGTTCCTACTCACATTCACATAAAGAGA
AACTCAAGATTTCAACTGTGCATATACCAGATGACCAGAAAACTGAGTTTCCAGCAGCTACC
CTTAGTTCCTACTCACAAATAGAGAAGCCCAAGATTTCAACTGTGATTGGACCAAATGACCA
GAAGACTCCATCCCAGACAGCTTTTCATAGTTCCTATTCTCAAACAGTAAAGCCCAATATTTT
ATTTCAACAGCAGTTGCCAGATAGAGATCAAAGTAAAGGTATTCTAAAGATTTCAGCTGTCC
CTGAACTAACTGATGTGAATACTGGAAAACCAGTATCTCTCTCTAGTTCTTATTTTCACAGAG
AGAAATCGAATATTTTCAGTCCACAGGAATTGCCAGGTAGTCATGTAACTGAAGATGTGCTG
AAGGTTTCAACAATTCCTGGACCAGCTGGCCAGAAAACAGTATTACCAACAGCTCTTCCTAG
TTCCTTTTCACATCGAGAGAAACCAGATATTTTCTATCAAAAGGATTTGCCAGATAGACATCT
AACTGAAGATGCTCTAAAGATCTCAAGTGCTCTTGGGCAAGCTGATCAAATTACCGGATTAC
AAACAGTTCCCTCTGGTACTTACTCACATGGTGAGAATCACAAGCTTGTTTCAGAACATGTC
CAAAGGCTAATAGATAATTTGAATTCTTCTGACTCCAGTGTTAGCTCAAATAATGTGCTTTTA
AATTCTCAGGCTGATGACAGAGTTGTAATAAATAAACCAGAATCTGCAGGTTTTAGAGATGT
TGGCTCTGAAGAAATCCAGGATGCAGAAAATAGTGCTAAAACTCTTAAGGAAATTCGGACA
CTTTTGATGGAGGCAGAAAATATGGCACTGAAACGATGCAATTTTCCTGCTCCCCTTGCCC
GTTTCAGAGATATTAGTGATATTTCATTTATACAATCTAAGAAGGTGGTTTGCTTCAAAGAAC
CCTCTTCCACGGGTGTATCTAATGGTGATTTGCTTCACAGACAGCCATTCACAGAGGAAAG
CCCAAGCAGCAGGTGCATACAGAAGGATATTGGCACACAGACGAATTTGAAATGCCGGAG
AGGCATTGAAAATTGGGAGTTTATTAGTTCAACTACAGTTAGAAGTCCTCTACAGGAAGCAG
AGAGCAAAGTCAGTATGGCATTAGAAGAAACTCTTAGGCAATATCAAGCAGCCAAATCTGTA
ATGAGGTCTGAACCTGAAGGGTGTAGTGGAACCATTGGGAATAAAATTATTATCCCTATGAT
GACTGTCATAAAAAGTGATTCAAGTAGTGATGCCAGTGATGGAAATGGTTCCTGCTCGTGG
GACAGTAATTTACCAGAGTCTTTGGAATCAGTTTCTGATGTTCTTCTAAACTTCTTTCCATAT
GTTTCACCCAAGACAAGTATAACAGATAGCAGGGAGGAAGAGGGTGTGTCAGAGAGTGAG
GATGGTGGTGGTAGCAGTGTAGATTCACTGGCTGCACATGTGAAAAACCTTCTGCAATGTG
AATCCTCACTGAATCATGCTAAAGAAATACTCAGAAATGCAGAGGAAGAGGAAAGCCGGGT
ACGAGCACATG

10.1.2 *ALMS1* exon 10 (ENSE00003528865)

GGTTTACAGAGTCCACGGGGAATGGGATGCAAGCCAGAAGCTGTATGTAGTCACATTATTA
TTGAGAGCCATGAAAAGGGATGTTTCCGGACTCTAACTTCTGAACATCCACAACTAGATAGA
CACCCTTGTGCTTTCAGATCTGCTGGACCCTCAGAAATGACCAGAGGACGGCAGAACCCAT
CATCATGCAGAGCCAAGCATGTCAACCTTTCTGCATCCTTAGACCAGAACAACTCCCATTTC
AAAGTTTGGAATTCCTTGCAGTTAAAAAGTCATTCCCCATTTCAGAACTTTATACCTGATGAA
TTCAAAATCAGCAAAGGTCTTCGAATGCCATTCGATGAAAAGATGGACCCTTGGCTGTCAG
AATTAGTAGAACCTGCTTTTGTGCCACCTAAAGAAGTGGATTTTCATTCTTCATCACAAATGC
CGTCCCCAGAACCCATGAAAAAGTTTACTACCTCCATCACTTTTTCATCTCACCGACATTCT
AAATGCATTTCCAATTCCTCTGTTGTTAAGGTTGGTGTTACTGAAGGTAGCCAGTGTACTGG
AGCATCTGTGGGGGTATTTAATTCTCATTTCACTGAAGAACAAAATCCTCCCAGAGATCTTA
AACAGAAAACCTCTTCCCCTTCATCATTTAAAATGCATAGTAATTCACAAGATAAAGAAGTGA
CTATTTTAGCAGAAGGTAGAAGGCAAAGCCAAAAATTACCTGTTGATTTTGAGCGTTCTTTT
CAAGAAGAAAAACCCTTAGAAAGATCAGATTTTACAGGCAGTCATTCTGAGCCCAGTACCA
GGGCAAATTGTAGCAATTTCAAGGAAATTCAGATTTCTGATAACCATACCCTTATTAGCATG
GGCAGACCAAGTTCCACCCTAGGAGTAAACAGATCGAGTTCCAGACTAGGAGTAAAAGAGA
AGAATGTAACTATAACTCCAGATCTTCCTTCTTGCATTTTTCTTGAACAACGAGAGCTCTTTG
AACAAAGCAAAGCCCCACGTGCAGATGACCATGTGAGGAAACACCATTCTCCCTCTCCTCA
ACATCAGGATTATGTAGCTCCAGACCTTCCTTCTTGCATTTTTCTTGAACAACGAGAACTCTT
TGAACAGTGCAAAGCCCCATATGTAGATCATCAAATGAGAGAAAACCATTCTCCCCTTCCTC
AAGGTCAGGATTCTATAGCTTCAGACCTTCCGTCTCCCATTTCTCTTGAACAATGCCAAAGC
AAAGCGCCAGGTGTAGATGACCAAATGAATAAACACCATTTTCCCCTTCCTCAAGGTCAGG
ATTGTGTAGTGGAAAAGAATAATCAACATAAGCCTAAATCACACATTTCTAATATAAATGTTG
AAGCCAAGTTCAATACTGTGGTCTCCCAGTCAGCCCCAAATCACTGTACATTAGCAGCATCT
GCATCTACTCCTCCTTCAAATAGAAAAGCACTTTCTTGTGTTCATATAACTCTTTGTCCCAAG
ACTTCTTCCAAGTTGGATAGTGGAACTTTAGATGAAAGATTCCATTCATTGGATGCTGCTTC
TAAAGCGAGGATGAATAGTGAGTTTAACTTTGACTTACATACTGTATCTTCGAGATCACTGG
AACCAACCTCCAAATTATTGACCAGTAAACCTGTAGCACAGGATCAAGAATCTTTAGGTTTT
CTAGGACCTAAATCTTCACTGGATTTCCAAGTCGTACAGCCTTCTCTTCCAGACAGTAACAC
TATTACTCAGGACTTGAAAACCATACCTTCTCAGAATAGCCAGATAGTAACCTCCAGGCAAA
TACAAGTGAACATTTCAGATTTCGAAGGACATTCCAATCCAGAGGGGACCCCAGTATTTGCA
GATCG

10.1.3 *ALMS1* exon 23 (ENSE00003744901)

AGAGTGACCAATCAACTTCTGGGGAGAAAAGTTCCCTGGGACTGACACAAGTTTATTTTCCT
CAGAGCCTTGGAATTCTATTTTATGAACCTAGAGAAGCAGAATCCTTACTTTTGTGAGTCTG
GTTGAATAAAGCTTATTCTTTGTCCATGTGTATTTTAGAAATAGTAACTTCTAAAGAGTCTGG
AACAAAGTGGTGATTAAAATTCCTAATGGTTTGGGAGCAATACTTTCTGCATAGTGGCCTTG
TCCAATGGCCTGTGTGTTACAATGATATGATCATTTCTCAAGAATAAGTCCCTTTTTGTATGT
GTTTTTATACTTTTAGAAAATAAAAACTTTAGATTAACTC

10.2 Predicted off-target effects

10.2.1 Low prediction on off-target effects for sgRNA *ALMS1* exon 23, 8, 10

Table 23 Predicted off-target effects: sgRNA *ALMS1* exon 23
sgRNAs were designed using CCTop and were selected due to low off-target prediction. The table presents 20 off-targets, with the highest risk. Exons (E) are marked in red, Introns (I) in yellow and intergenic sequences in (-) green. Table was taken from Woerz *et al.*, under review [3].

Coordinates	strand	MM	target_seq	PAM	distance		gene name	gene id
chr2:73609585-73609607	+	0	TCTGGGGA[GAAAAGTTCCCT]	GGG	0	E	ALMS1	ENSG00000116127
chr7:39506451-39506473	+	4	**ATCT**GGGA[GAAAAGTTCCCT]	AGG	13356	-	POU6F2	ENSG00000106536
chr6:67688885-67688907	+	4	T**AGT**GG**T**A[GAAAAGTTCCCT]	GGG	63421	-	Y_RNA	ENSG00000206672
chr18:53753297-53753319	-	3	**A**CTGG**A**GA[G**G**AAAGTTCCCT]	AGG	NA	-	NA	NA
chr11:5199273-5199295	+	4	TC**A**G**TTT**A[GAAAAGTTCCCT]	TGG	440	-	OR51V1	ENSG00000176742
chr6:39240540-39240562	-	4	**CT**TG**A**GGA[G**T**AAAGTTCCCT]	GGG	11090	-	KCNK5	ENSG00000164626
chr14:65997912-65997934	-	4	**AT**TGGG**A**A[**C**AAAAGTTCCCT]	GGG	6521	I	CTD-2014B16.3	ENSG00000258847
chr10:123892280-123892302	+	4	T**TCT**GGGA[G**T**AAAGTTCCCT]	GGG	296	I	CPXM2	ENSG00000121898
chr10:75893633-75893655	+	4	T**G**TGT**G**T**T**[GAAAAGTTCCCT]	GGG	10108	I	C10orf11	ENSG00000148655
chrX:52978988-52979010	-	4	**G**CTGG**CC**A[G**C**AAAGTTCCCT]	TGG	13007	I	FAM156A	ENSG00000268350
chr17:41327061-41327083	-	4	TC**A**GG**CC**A[G**G**AAAGTTCCCT]	GGG	24	I	TBC1D3P7	ENSG00000233014
chr10:130485965-130485987	-	3	T**G**TGG**A**GA[GAAA**G**GTTCCCT]	AGG	2811	-	RP11-540N6.1	ENSG00000236303
chr22:35354089-35354111	+	1	TCTGGGGA[GAAAAG**G**TCCCT]	GGG	6095	-	TOM1	ENSG00000100284
chr5:12878319	+	3	**AT**TGGGGA[GAAAA**C**TTCC	TG	40362	I	CTC-	ENSG00000248

1-128783213			CT]	G			573M9.1	634
chr8:124380736-124380758	-	4	TC**AA**GG**A**A[GAA**C**AGTTCCCT]	TGG	8044	-	TMEM65	ENSG00000164983
chr2:149788325-149788347	-	4	**AA**TGGGGA[GA**TG**AGTTCCCT]	GGG	15835	I	AC007364.1	ENSG00000162947
chr8:41674694-41674716	-	4	**G**C**A**GGG**A**A[GAAAA**C**TTCCCT]	GGG	1782	I	ANK1	ENSG00000029534
chr11:117745399-117745421	-	4	**CAA**GGGGA[GAAAAG**C**TCCCT]	TGG	31370	I	DSCAML1	ENSG00000177103
chr1:119175437-119175459	+	4	TC**A**G**A**GGA[**C**AAA**G**GTTCCCT]	GGG	5931	I	RP11-418J17.1	ENSG00000231365
chrX:132084802-132084824	-	4	**G**CTGG**CC**A[GAAAA**C**TTCCCT]	AGG	217	I	FRMD7	ENSG00000165694

Table 24 Predicted off-target effects: sgRNA *ALMS1* exon 8
sgRNAs were designed with CCTop and were picked due to low off-target prediction. The present table shows 20 off-targets, with the highest risk. Exons (E) are highlighted in red, while introns (I) are marked in yellow and intergenic sequences in (-) green. Table was taken from Woerz *et al.*, under review [3].

Coordinates	strand	MM	target_seq	PAM	distance		gene name	gene id
chr2:73453892-73453917	+	0	TATAACAGATA[GCAGGGAGGAAG]	AGG	0	E	ALMS1	ENSG00000116127
chr10:59553566-59553591	-	4	T**GG**AACAGA**G**A[G**G**AGGGAGGAAG]	AGG	1688	-	MRPL50P4	ENSG00000235469
chr9:107375341-107375366	+	4	TATAA**A**AG**GG**A[GCA**A**GGAGGAAG]	AGG	43147	-	RAD23B	ENSG00000119318
chrY:12112710-12112735	-	4	TATAA**A**AGA**A**A[G**GG**GGGAGGAAG]	GGG	NA	-	NA	NA
chr5:71509080-71509105	+	3	TATAA**A**AGATA[G**A**AGGGA**T**GAAG]	AGG	360	I	BDP1	ENSG00000145734
chr9:68759298-68759323	+	4	TATA**G**CA**T**A**A**A[GCAGGGAG**T**AAG]	GGG	16641	I	PIP5K1B	ENSG00000107242
chr16:17969552-17969577	-	4	**G**ATAA**A**AGATA[GCAGG**C**A**T**GAAG]	GGG	1864	I	CTA-481E9.4	ENSG00000259929
chr15:295914	-	4	**C**ATAACAG**G**TA[GCAGG**T**AGG	GG	1822	-	RP11-	ENSG00000259

23-29591448			ATG]	G	8		300A12.2	814
chr2:239006889-239006914	+	4	TATATCAGACA[GCAGGAAGGAGG]	AGG	33879	-	AC114788.1	ENSG00000211566
chr19:30766564-30766589	-	4	TATAAGAGATG[GAAGGGAGGAAT]	TGG	53026	-	ZNF536	ENSG00000198597
chr8:126681920-126681945	+	4	TAAAACAGAAA[GCAGGGAGCATG]	TGG	5507	I	RP11-89K10.1	ENSG00000254286

Table 25 Predicted off-target effects: sgRNA *ALMS1* exon 10
sgRNAs were designed using CCTop and were chosen with low off-target prediction. In this table 20 off-targets, with the highest risk, are depicted. Exons (E) are depicted in red, Introns (I) in yellow and intergenic sequences in (-) green. Table was taken from Woerz *et al.*, under review [3].

Coordinates	strand	MM	target_seq	PAM	distance		gene name	gene id
chr2:73490479-73490501	+	0	TAACCATA[CCCTTATTAGCA]	TGG	0	E	ALMS1	ENSG00000116127
chrX:13282113-13282135	+	4	AAAACCTA[ACCTTATTAGCA]	TGG	5294	I	GS1-600G8.5	ENSG00000235385
chr10:65095253-65095275	+	3	TATCCACA[CCATTATTAGCA]	TGG	28392	-	RP11-252C24.3	ENSG00000282906
chr12:63854927-63854949	+	4	AAACCTTT[CTCTTATTAGCA]	GGG	10044	I	SRGAP1	ENSG00000196935
chrX:53352221-53352243	+	4	CCACCACA[CCCCTATTAGCA]	TGG	10716	-	RP6-29D12.2	ENSG00000234413
chr2:105343534-105343556	+	4	TAAATATT[CCTTTATTAGCA]	AGG	311	I	C2orf49	ENSG00000135974
chrX:111675757-111675779	-	4	TTCCCATA[CATTTATTAGCA]	AGG	5339	I	ALG13	ENSG00000101901
chr8:137454746-137454768	+	4	GAATCATA[CATTTATTAGCA]	TGG	29725	-	ZYXP1	ENSG00000274572
chr14:23710784-23710806	+	4	TTTCTATA[CCCTTCTTAGCA]	TGG	18232	-	RP11-388E23.2	ENSG00000258464
chr16:8613848-8613870	+	4	TCACTATA[CACCTATTAGCA]	TGG	7813	-	METTL22	ENSG00000067365
chr10:16045742-16045764	-	4	TTACCACA[CACCTATTAGCA]	TGG	25652	-	FTLP19	ENSG00000237913
chr2:99859286-99859308	+	4	GAACCACA[TCCTTTTTAGCA]	TGG	21762	I	AFF3	ENSG00000144218
chr5:78044294-78044316	-	4	TTATCATA[GCCTTAGTAGCA]	TGG	156	I	CTD-2179L22.1	ENSG00000253558
chr2:59186123-59186145	+	3	GAACCATA[CCCTGAGTAGCA]	AGG	31563	-	AC007131.1	ENSG00000222030
chr6:13007643	+	4	TAACTTTA[TCCTTATAAGC	TG	2104	I	L3MBTL3	ENSG00000198

2-130076454			A]	G				45
chr19:47805134-47805156	-	4	**A**AACCA**A**A[CC**A**TTAT**C**AGCA]	GGG	1445	I	TPRX1	ENSG00000178928
chr1:61159505-61159527	+	4	T**G**ACCA**C**A[CCCT**G**A**G**TAGCA]	AGG	26477	I	NFIA	ENSG00000162599
chr6:8376736-8376758	-	4	T**G**ACCA**C**A[CCCT**G**A**G**TAGCA]	AGG	33715	-	RP11-203H2.2	ENSG00000234763
chr1:4427563-4427585	-	4	TAAC**T**A**C**A[CCCT**G**A**C**TAGCA]	AGG	2874	-	RP5-1166F10.1	ENSG00000235054
chr8:74307346-74307368	-	4	T**T**ACC**T**TA[CCCTT**CA**TAGCA]	GGG	7493	I	JPH1	ENSG00000104369

10.3 Sequences of CEP70 exon 5, 6

10.3.1 CEP70 exon 5 (ENSE00003686624)

ATCTCATCATTTTTGACAAACAGTCATCACAAAGGATGAGACAGAATTTGAAATTGTTGGTG
GAAGAAACATCATGTCAACAGAACATGATACAGGAGCTTATAGAAACTAATCAACAGCTTAG

10.3.2 CEP70 exon 6 (ENSE00003676297)

AAATGAACTTCAGCTAGAGCAAAGCCGAGCAGCCAATCAAGAACAACGAGCTAATGACTTG
GAACAAATTATGGAAAGTGTGAAATCCAAAATTGGTGAATTGGAGGATGAATCACTAAGTAG
GGCTTGCCACCAACAGAATAAAATAAAAGATCTTCAAAAGGAGCAGAAAACTTTACAG

10.4 Additional information of endogenous sfGFP tag verification

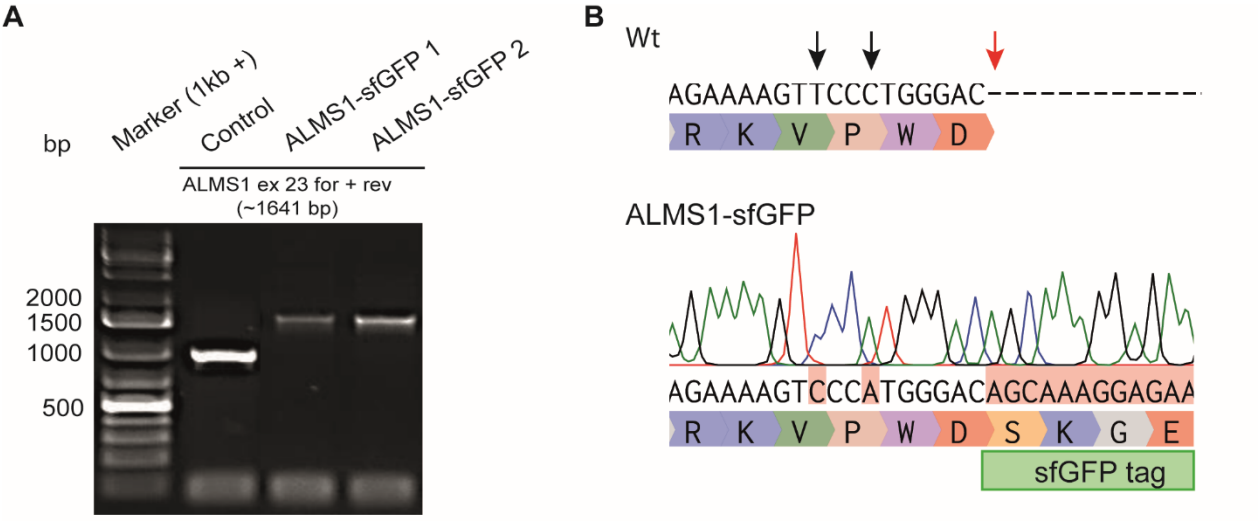

C

Tag (CT)	Single clones (total)	Positive single clones (homo-/heterozygous)	Efficiency (%) (homo-/heterozygous)	PCR and gel electrophoresis	Sanger sequencing	IP
sfGFP	49	7/11	14.3/22.44	+	+	+

D

sfGFP - AP	Sequence coverage (%)	Tier 1	Tier 2
ALMS1 (bait)	50.6	+	+

Figure 37 Additional information for endogenous tag verification
A, Gel electrophoreses of PCR products was conducted with C-terminal tagged sfGFP single clones. A forward and reverse primer for *ALMS1* exon 23 were used for all samples. *ALMS1*-sfGFP positive single clones show one prominent band at a height of approximately 1641 bp, respectively. Control shows a band at approximately 930 bp. Pictures was modified after Wörz, unpublished Master thesis 2018 [21]
B, The depiction provides the nucleotide and amino acid sequences of ALMS1 wt in the top panel, and ALMS1-sfGFP in the bottom panel. Within the sequences, black arrows indicate the presence of wobbled nucleotides. A distinct red arrow signifies the specific insertion site where the sfGFP sequence has been incorporated. Wt sequence was supplied by ensemble.org (ENST00000613296.6, ALMS1-205, CCDS42697)
C, The summary table presents an overview of the total number of received single clones, the number of positively tagged single clones as well as the efficiency of the tag insertion. Verification of tag insertion (+ = positive) was performed using PCR and Sanger sequencing. Successfully tagged ALMS1 single clones were used for affinity purification followed by mass spectrometry analysis. Table was modified after Wörz unpublished Master thesis 2018 [21].
D, After database dependent data analysis using MaxQuant and Perseus, ALMS1 was found with a sequence coverage of 50.6 %. Identified proteins were classified in Tier system (Tier 1 and Tier 2), as previously described. "+" indicates Tier 1 or Tier 2 positive proteins were identified.
Figure was modified and taken from Woerz *et al.*, under review [3].

10.5 Protein coverage of ALMS1-sfGFP

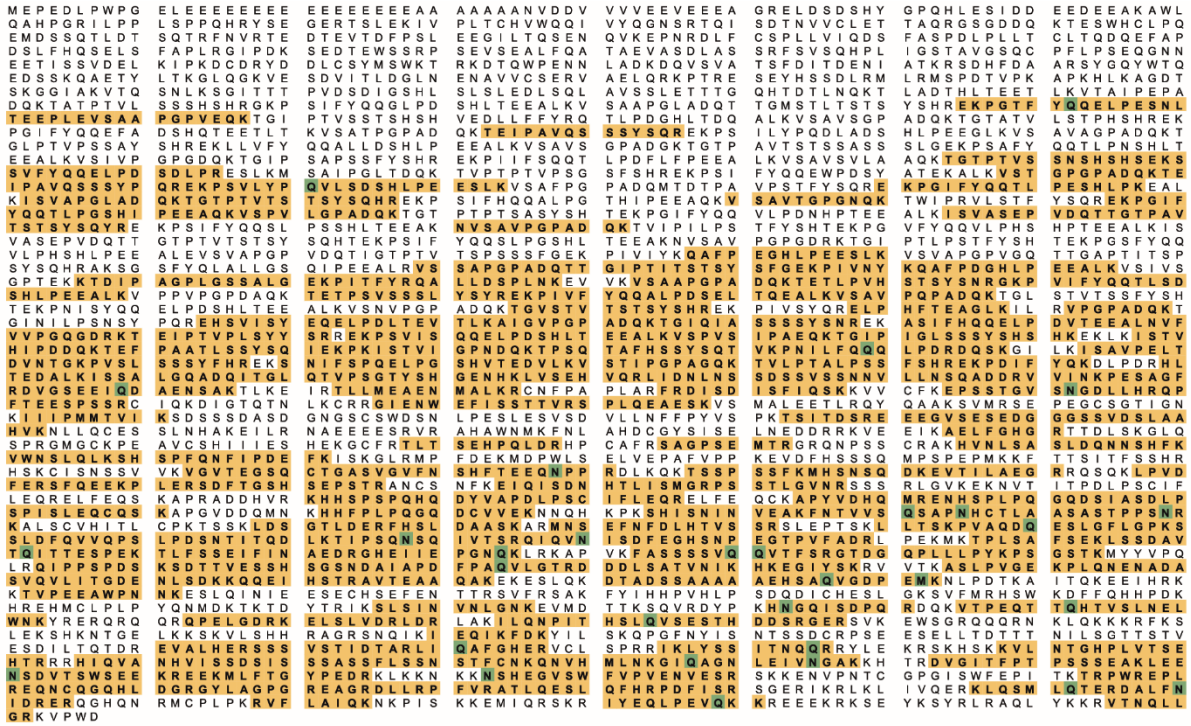

Figure 38 Protein coverage of ALMS1-sfGFP using Scaffold
The program Scaffold provided the localization of identified exclusive unique peptides on the ALMS1 protein (homo sapiens, 461 kDa). The amino acids (aa), that matched the MS/MS spectrum are emphasized in yellow, and post-translational modified aa are shown in green. Figure was taken from Woerz *et al.*, under review [3].

10.6 Blue Native Page- ALMS1-sfGFP

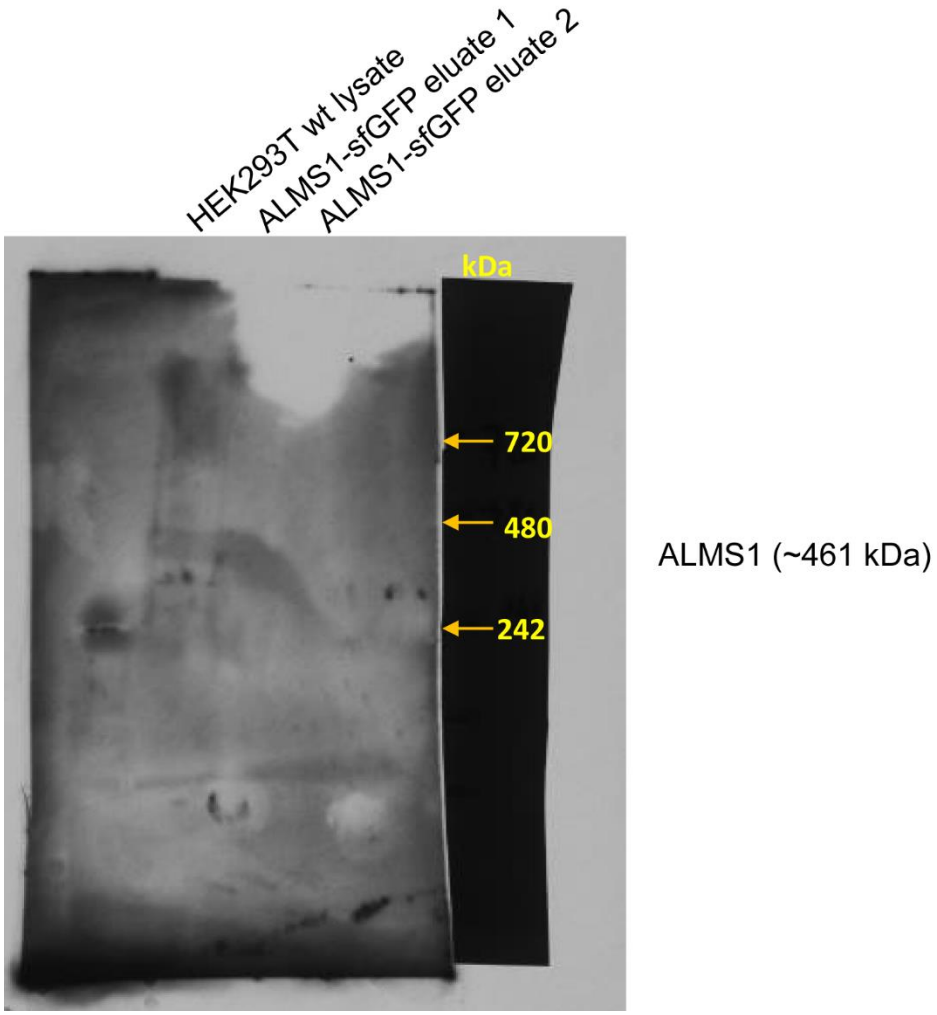

Figure 39 Blue Native Page with ALMS1-sfGFP eluate and HEK293T wt lysate
A first Blue Native Page was performed by PhD candidate Klaudia Maruszczak (AG Rapaport) with lysate of native HEK293T cells and eluate of ALMS1-sfGFP. ALMS1 antibody from Novusbio (rb) 1:500 was used. Ladder is indicated in yellow.

10.7 Novel ALMS1 and CEP70 interactors

10.7.1 MaxQuant settings ALMS1 sf-GFP

Parameter	Value	Max. peptide mass [Da]	4600
Version	1.6.1.0	Min. peptide length for unspecific search	8
User name	mpcadmin	Max. peptide length for unspecific search	25
Machine name	ADMIN-PC	Razor protein FDR	True
Date of writing	03.11.2019 19:02	Disable MD5	False
Fixed modifications	Carbamidomethyl (C)	Max mods in site table	3
Include contaminants	True	Match unidentified features	False
PSM FDR	0.01	MS/MS tol. (FTMS)	20 ppm

XPSM FDR	0.01	Top MS/MS peaks per Da interval. (FTMS)	12
Protein FDR	0.01	Da interval. (FTMS)	100
Site FDR	0.01	MS/MS deisotoping (FTMS)	True
Use Normalized Ratios For Occupancy	True	MS/MS deisotoping tolerance (FTMS)	7
Min. peptide Length	7	MS/MS deisotoping tolerance unit (FTMS)	ppm
Min. score for unmodified peptides	0	MS/MS higher charges (FTMS)	True
Min. score for modified peptides	40	MS/MS water loss (FTMS)	True
Min. delta score for unmodified peptides	0	MS/MS ammonia loss (FTMS)	True
Min. delta score for modified peptides	6	MS/MS dependent losses (FTMS)	True
Min. unique peptides	0	MS/MS recalibration (FTMS)	False
Min. razor peptides	1	MS/MS tol. (ITMS)	0.5 Da
Min. peptides	1	Top MS/MS peaks per Da interval. (ITMS)	8
Use only unmodified peptides and	False	Da interval. (ITMS)	100
Peptides used for protein quantification	Razor	MS/MS deisotoping (ITMS)	False
Discard unmodified counterpart peptides	True	MS/MS deisotoping tolerance (ITMS)	0.15
Label min. ratio count	2	MS/MS deisotoping tolerance unit (ITMS)	Da
Use delta score	False	MS/MS higher charges (ITMS)	True
iBAQ	False	MS/MS water loss (ITMS)	True
iBAQ log fit	False	MS/MS ammonia loss (ITMS)	True
Match between runs	False	MS/MS dependent losses (ITMS)	True
Find dependent peptides	False	MS/MS recalibration (ITMS)	False
Fasta file	C:\Databases\SP-human-2014-11.fasta	MS/MS tol. (TOF)	40 ppm
First search fasta file	C:\Databases\first.search\human.first.search.fasta	Top MS/MS peaks per Da interval. (TOF)	10
Decoy mode	revert	Da interval. (TOF)	100
Include contaminants	True	MS/MS deisotoping (TOF)	True
Advanced ratios	True	MS/MS deisotoping tolerance (TOF)	0.01
Fixed andromeda index folder		MS/MS deisotoping tolerance unit (TOF)	Da
Temporary folder		MS/MS higher charges (TOF)	True

Combined folder location		MS/MS water loss (TOF)	True
Second peptides	True	MS/MS ammonia loss (TOF)	True
Stabilize large LFQ ratios	True	MS/MS dependent losses (TOF)	True
Separate LFQ in parameter groups	False	MS/MS recalibration (TOF)	False
Require MS/MS for LFQ comparisons	True	MS/MS tol. (Unknown)	0.5 Da
Calculate peak properties	False	Top MS/MS peaks per Da interval. (Unknown)	8
Main search max. combinations	200	Da interval. (Unknown)	100
Advanced site intensities	True	MS/MS deisotoping (Unknown)	False
LFQ norm for sites and peptides	False	MS/MS deisotoping tolerance (Unknown)	0.15
Write msScans table	True	MS/MS deisotoping tolerance unit (Unknown)	Da
Write msmsScans table	True	MS/MS higher charges (Unknown)	True
Write ms3Scans table	True	MS/MS water loss (Unknown)	True
Write allPeptides table	True	MS/MS ammonia loss (Unknown)	True
Write mzRange table	True	MS/MS dependent losses (Unknown)	True
Write pasefMsmsScans table	True	MS/MS recalibration (Unknown)	False
Write accumulatedPasefMsmsScans table	True	Site tables	Oxidation (M)Sites.txt

10.7.2 List of ALMS1 interactors (ALMS1-sfGFP)

Table 26 Novel ALMS1-sfGFP interactors (Tier 1)
An immunoprecipitation was conducted with endogenously sfGFP-tagged ALMS1 in HEK293T cells and wildtype control cells. The table summarizes identified ALMS1 interactors with their gene names, the ratio (sfGFP_x/y_Control) and their -log2 median *p*-values and of eight biological replicates. In this table, Tier 1 (Sig A <0.05 and Permutation based FDR *p*<0.05) interactors are listed. Table was taken from Woerz *et al.*, under review [3].

Gene names	**Ratio**	**p-value ($-\log_2$)**	**Gene names**	**Ratio**	**p-value ($-\log_2$)**
AKAP8L	19.6766	3.51828	MAGED1	18.6421	3.45215
ALMS1	26.7639	18.7674	MARK2	17.8854	2.43684
CEP70	22.5945	15.5859	MRPL11	2.54852	2.19002
COPS3	19.1441	2.39132	NDUFA8	18.6528	2.35508
DERA	18.9257	3.54381	NUP153	17.7311	2.32062
DNAJB11	19.0595	24.9926	PFKM	18.9086	3.64041

DPYSL3	20.4316	21.0363	PPP6R3	18.9321	3.43913
DSG2	18.0544	2.39281	SQSTM1	18.5036	2.67901
FAR1	18.7341	2.67953	SSSCA1	19.6951	2.72143
G3BP2	19.3687	2.81733	TACC3	17.5629	2.67966
GLUL	18.6806	2.35097	TCEAL4	17.6424	2.40903
GNAS	18.3735	2.32031	TMED9	19.0528	2.35898
HDAC10	23.0334	3.55545	TOMM22	19.4518	2.4247
HDAC2	19.1937	3.79566	TRMT112	20.7562	2.71212
IGBP1	17.6647	2.67885	TSG101	18.8482	2.38638
KLC2	18.3873	3.80341	TUBB6	21.0721	3.16611

Table 27 Novel ALMS1-sfGFP interactors (Tier 2)
Tier 2 (Sig A <0.05 and *p*-value <0.05) interactors are listed. Tier 2 also includes Tier 1 interactors. Table was taken from Woerz *et al.*, under review [3].

Gene names	**Ratio**	**p-value ($-\log_2$)**	**Gene names**	**Ratio**	**p-value ($-\log_2$)**
ADAR	17.4363	1.72134	KLC2	18.3873	3.80341
AHNAK	3.135	1.80802	KPNA3	18.6659	1.63513
AKAP8L	19.6766	3.51828	MAGED1	18.6421	3.45215
ALMS1	26.7639	18.7674	MARK2	17.8854	2.43684
ASRGL1	19.034	1.77514	MRPL1	19.291	1.74768
ATP5D	21.637	1.69644	MRPL11	2.54852	2.19002
BOD1L1	17.8084	1.63484	NDUFA8	18.6528	2.35508
BRCC3	17.0099	1.69963	NDUFB10	17,7955	1.72275
CAPN1	19.1771	1.6608	NOP58	18.1496	1.63545
CEP170	17.5944	1.74162	NT5DC2	18.6254	1.74471
CEP70	22.5945	15.5859	NUP153	17.7311	2.32062
COPS3	19.1441	2.39132	PDCD6	20.0884	1.75573
COPS7A	18.7941	1.70131	PELO	17.3091	1.70123
COX5A	18.2069	1.65435	PFKM	18.9086	3.64041
DERA	18.9257	3.54381	PPIL1	19.913	1.68036
DHCR7	19.5302	1.78032	PPP6R3	18.9321	3.43913
DNAJB11	19.0595	24.9926	PURA	17.9674	1.63382
DPYSL3	20.4316	21.0363	RAD23A	19.2547	1.64552
DSG2	18.0544	2.39281	RFC5	19.2058	1.70806

DYNC1LI2	18.4545	1.70777	SLC4A1AP	17.4949	1.63163
EXOSC2	18.399	1.70174	SQSTM1	18.5036	2.67901
EXOSC6	18.6213	1.74209	SRSF9	18.7254	1.62052
FAF2	18.4544	1.67408	SSSCA1	19.6951	2.72143
FAM114A2	17.4237	1.69699	STAM	18.1576	1.70306
FAR1	18.7341	2.67953	SUCLG2	19.1531	1.6336
FLII	17.6975	1.6501	TACC3	17.5629	2.67966
G3BP2	19.3687	2.81733	TCEAL4	17.6424	2.40903
GLUL	18.6806	2.35097	TFG	20.3008	1.62216
GNAI3	19.9552	1.72531	THOC3	19.4705	1.71437
GNAS	18.3735	2.32031	TMED9	19.0528	2.35898
GSK3B	18.3641	1.66393	TMEM30A	17.3481	1.66455
HADH	19.33	1.70287	TOMM22	19.4518	2.4247
HDAC10	23.0334	3.55545	TRMT112	20.7562	2.71212
HDAC2	19.1937	3.79566	TSG101	18.8482	2.38638
HEATR3	17.8742	1,58552	TUBB4A	21.037	1.89741
HMGCS1	20.9135	1.91024	TUBB6	21.0721	3.16611
IDH2	18.8767	1.75657	TUBGCP2	17.2795	1.7098
IGBP1	17.6647	2.67885	UBXN1	20.0795	1.79532
IGF2BP2	19.2822	1.82533	VASP	16.5983	1.68848
IRS4	2.52312	1.67687			

Table 28 Go enrichment analysis ALMS1

GO enrichment analysis was conducted utilizing the knowledgebase provided by the Gene Ontology Consortium (http://geneontology.org/). Analysis type: PANTHER Overrepresentation Test (Released 20221013); Annotation Version and Release Date: GO Ontology database DOI: 10.5281/zenodo.6799722 Released 2022-07-01; Reference List: Homo sapiens (all genes in database); Test-Type FISHER; Correction FDR**.** Table was taken from Woerz *et al.*, under review [3].

GO cellular component complete	**Homo sapiens - REFLIST (20589)**	**upload_1 (79)**	**upload_1 (expected)**	**upload_1 (over/under)**	**upload_1 (fold Enrichment)**	**upload_1 (raw P-value)**	**upload_1 (FDR)**
VCP-NPL4-UFD1 AAA ATPase complex (GO:0034098)	8	2	0.03	+	65.16	6.36E-04	4.64E-02
host cellular	9	2	0.03	+	57.92	7.76E-	5.11E-

component (GO:0018995)						04	02
host cell (GO:0043657)	9	2	0.03	+	57.92	7.76E-04	4.95E-02
spindle pole (GO:0000922)	173	5	0.66	+	7.53	6.03E-04	4.56E-02
mitochondrial protein-containing complex (GO:0098798)	293	8	1.12	+	7.12	1.96E-05	2.67E-03
spindle (GO:0005819)	428	8	1.64	+	4.87	2.59E-04	2.41E-02
microtubule (GO:0005874)	471	8	1.81	+	4.43	4.85E-04	3.81E-02
centrosome (GO:0005813)	634	10	2.43	+	4.11	1.67E-04	1.71E-02
microtubule organizing center (GO:0005815)	840	11	3.22	+	3.41	3.79E-04	3.09E-02
microtubule cytoskeleton (GO:0015630)	1374	16	5.27	+	3.03	6.10E-05	7.33E-03
supramolecular fiber (GO:0099512)	1047	12	4.02	+	2.99	6.58E-04	4.64E-02
supramolecular polymer (GO:0099081)	1056	12	4.05	+	2.96	7.09E-04	4.83E-02
catalytic complex (GO:1902494)	1686	19	6.47	+	2.94	1.69E-05	2.46E-03
nuclear protein-containing complex (GO:0140513)	1276	14	4.9	+	2.86	3.46E-04	2.94E-02

mitochondrion (GO:0005739)	1671	17	6.41	+	2.65	1.79E-04	1.74E-02
cytoskeleton (GO:0005856)	2401	21	9.21	+	2.28	2.74E-04	2.43E-02
protein-containing complex (GO:0032991)	5771	47	22.14	+	2.12	7.77E-09	1.59E-05
cytosol (GO:0005829)	5458	44	20.94	+	2.1	5.27E-08	2.69E-05
nucleoplasm (GO:0005654)	4130	32	15.85	+	2.02	3.08E-05	3.94E-03
organelle lumen (GO:0043233)	5614	42	21.54	+	1.95	1.44E-06	3.28E-04
intracellular organelle lumen (GO:0070013)	5614	42	21.54	+	1.95	1.44E-06	2.95E-04
membrane-enclosed lumen (GO:0031974)	5614	42	21.54	+	1.95	1.44E-06	2.68E-04
intracellular non-membrane-bounded organelle (GO:0043232)	5225	39	20.05	+	1.95	6.03E-06	1.03E-03
non-membrane-bounded organelle (GO:0043228)	5226	39	20.05	+	1.94	6.05E-06	9.50E-04
nuclear lumen (GO:0031981)	4494	33	17.24	+	1.91	9.33E-05	1.00E-02
nucleus (GO:000563	7682	47	29.48	+	1.59	9.31E-05	1.06E-02

4)							
cytoplasm (GO:0005737)	12097	70	46.42	+	1.51	1.19E-08	8.11E-06
intracellular membrane-bounded organelle (GO:0043231)	12154	68	46.63	+	1.46	2.42E-07	8.25E-05
intracellular organelle (GO:0043229)	13254	73	50.86	+	1.44	1.04E-08	1.06E-05
membrane-bounded organelle (GO:0043227)	13230	71	50.76	+	1.4	3.64E-07	1.06E-04
organelle (GO:0043226)	14064	73	53.96	+	1.35	5.79E-07	1.48E-04
intracellular anatomical structure (GO:0005622)	14945	76	57.34	+	1.33	7.81E-08	3.19E-05

10.7.3 MaxQuant setting CEP70

Parameter	Value
Version	1.6.1.0
User name	mpcadmin
Machine name	ADMIN-PC
Date of writing	01/28/2023 18:11:34
Fixed modifications	Carbamidomethyl (C)
Include contaminants	True
PSM FDR	0.01
XPSM FDR	0.01
Protein FDR	0.01
Site FDR	0.01
Use Normalized Ratios For Occupancy	True
Min. peptide Length	7
Min. score for unmodified peptides	0
Min. score for modified peptides	40
Min. delta score for unmodified peptides	0
Min. delta score for modified peptides	6
Min. unique peptides	0
Min. razor peptides	1
Min. peptides	1
Use only unmodified peptides and	False
Peptides used for protein quantification	Razor
Discard unmodified counterpart peptides	True
Label min. ratio count	2
Use delta score	False
iBAQ	False
iBAQ log fit	False
Match between runs	True
Matching time window	0.7
Max. peptide mass [Da]	4600
Min. peptide length for unspecific search	8
Max. peptide length for unspecific search	25
Razor protein FDR	True
Disable MD5	False
Max mods in site table	3
Match unidentified features	True
MS/MS tol. (FTMS)	20 ppm
Top MS/MS peaks per Da interval. (FTMS)	12
Da interval. (FTMS)	100
MS/MS deisotoping (FTMS)	True
MS/MS deisotoping tolerance (FTMS)	7
MS/MS deisotoping tolerance unit (FTMS)	ppm
MS/MS higher charges (FTMS)	True
MS/MS water loss (FTMS)	True
MS/MS ammonia loss (FTMS)	True
MS/MS dependent losses (FTMS)	True
MS/MS recalibration (FTMS)	False
MS/MS tol. (ITMS)	0.5 Da
Top MS/MS peaks per Da interval. (ITMS)	8
Da interval. (ITMS)	100
MS/MS deisotoping (ITMS)	False
MS/MS deisotoping tolerance (ITMS)	0.15
MS/MS deisotoping tolerance unit (ITMS)	Da
MS/MS higher charges (ITMS)	True
MS/MS water loss (ITMS)	True
MS/MS ammonia loss (ITMS)	True
MS/MS dependent losses (ITMS)	True
MS/MS recalibration	False

[min]		(ITMS)	
Alignment time window [min]	20	MS/MS tol. (TOF)	40 ppm
Find dependent peptides	False	Top MS/MS peaks per Da interval. (TOF)	10
Fasta file	C:\Databases\swissprot_human_2021_05_TB.fasta	Da interval. (TOF)	100
Decoy mode	revert	MS/MS deisotoping (TOF)	True
Include contaminants	True	MS/MS deisotoping tolerance (TOF)	0.01
Advanced ratios	True	MS/MS deisotoping tolerance unit (TOF)	Da
Fixed andromeda index folder		MS/MS higher charges (TOF)	True
Temporary folder		MS/MS water loss (TOF)	True
Combined folder location		MS/MS ammonia loss (TOF)	True
Second peptides	True	MS/MS dependent losses (TOF)	True
Stabilize large LFQ ratios	True	MS/MS recalibration (TOF)	False
Separate LFQ in parameter groups	False	MS/MS tol. (Unknown)	0.5 Da
Require MS/MS for LFQ comparisons	False	Top MS/MS peaks per Da interval. (Unknown)	8
Calculate peak properties	False	Da interval. (Unknown)	100
Main search max. combinations	200	MS/MS deisotoping (Unknown)	False
Advanced site intensities	True	MS/MS deisotoping tolerance (Unknown)	0.15
LFQ norm for sites and peptides	False	MS/MS deisotoping tolerance unit (Unknown)	Da
Write msScans table	True	MS/MS higher charges (Unknown)	True
Write msmsScans table	True	MS/MS water loss (Unknown)	True
Write ms3Scans table	True	MS/MS ammonia loss (Unknown)	True
Write allPeptides table	True	MS/MS dependent losses (Unknown)	True
Write mzRange table	True	MS/MS recalibration (Unknown)	False
Write pasefMsmsScans table	True	Site tables	Oxidation (M)Sites.txt
Write accumulatedPasefMsmsScans table	True		

10.7.4 List of CEP70 interactors

Table 29 Novel CEP70 interactors (Tier 1)
An immunoprecipitation was conducted with overexpression constructs NSF-CEP70 and NSF-RAF1 in HEK293T. The table summarizes identified CEP70 interactors with their gene names, the ratio (CEP70_x/y_RAF1) and their -log2 median *p*-values of six biological replicates. Tier 1 proteins are listed, including the proteins NACAP1 and L1RE1, which was not identified in homo sapiens using string. Table was taken from Woerz *et al.*, under review [3].

Gene names	Ratio	p-value ($-\log_2$)	Gene names	Ratio	p-value ($-\log_2$)
ABCB7	25.2716	3.65742	MIF	27.1729	21.5083
ACSL4	24.6142	19.5801	MINA	25.4826	3.80551
ADK	24.9438	18.9229	MPHOSPH6	24.7016	3.56912
AFTPH	24.9992	21.087	MRPS24	24.8593	2.29583
AGO1	24.9892	3.57061	MRPS33	24.9712	3.56987
AHSG	27.2943	22.5144	MRPS5	25.6198	2.11071
AKAP8	21.6644	14.0186	NACAP1	26.0796	3.68989
ALDH16A1	25.6673	3.57066	NDUFS6	25.1445	2.29566
ALMS1	12.0578	3.00457	NELFB	25.1923	19.8738
ARHGAP18	26.4041	2.29548	NELFE	3.03217	1.80316
ARHGEF2	24.2743	3.56752	NEMF	24.221	17.8037
ARID1A	25.1728	20.3704	NENF	25.2904	2.01237
ASPH	24.8878	2.25335	NKTR	26.953	21.2186
ASPM	25.6941	19.1346	NOLC1	27.6067	18.7053
ATAD3B	2.92521	7.23432	NOP14	26.0568	20.0002
ATG3	25.1388	2.27109	NRGN	23.6788	19.9643
ATP6V1G1	24.2891	16.8476	NUCB2	26.0149	2.2955
ATPIF1	28.2028	19.3636	NUP210	25.9116	2.35917
ATXN2	25.6189	3.57053	OCIAD1	27.0417	3.91943
AUTS2	23.5367	18.9735	OXCT1	24.7845	2.01409
AXIN1	19.4388	2.29546	PALM	25.7367	3.56752
B4GALNT3	30.5683	4.84693	PAM16	25.4216	2.02646
BAX	25.7342	2.30988	PDXP	24.2674	3.56968
BOD1L1	26.8791	22.1762	PIP4K2C	24.1663	2.29556
BRCA2	26.3389	3.59187	PITHD1	25.567	2.34542
C11orf98	25.6602	2.25988	PLAA	25.1435	3.55058
C12orf29	25.9816	16.3044	PLEKHA5	25.7558	2.29586
C19orf53	25.4504	18.1598	PNN	27.7669	2.54866

C7orf50	4.55379	1.98157	PNPO	25.0923	13.0894
CASC3	25.8537	3.55188	POLD2	25.0548	3.5706
CBX5	24.4297	2.29387	PPAN	26.2021	16.3931
CCDC12	24.9779	21.3183	PPIG	25.1781	3.57041
CCDC50	25.5141	21.0103	PPP1R2	26.2653	20.4602
CEP135	25.3543	19.8792	PRDX4	26.8223	19.2773
CEP70	8.09268	12.5164	PREB	26.2951	2.31529
CRK	24.9807	3.56783	PRKAR2B	29.6645	23.0216
CSNK1E	25.0786	2.09107	PSMB7	26.9772	2.67454
CSTF3	25.706	21.0793	PTDSS1	24.2263	2.29574
CTCF	23.7459	23.22	PTPN1	25.6452	19.947
CYFIP1	25.1166	3.57721	RAB35	25.7375	3.57053
DAG1	24.9092	2.29567	RAD23A	26.0684	2.29579
DDX10	24.7998	2.32641	RAD51	27.2874	3.65512
DDX41	30.2721	3.67801	RALB	25.2185	2.1076
DDX50	25.2512	2.29583	RBM22	25.3893	2.29558
DECR1	25.0788	2.29501	RDH13	23.9199	2.29525
DEK	26.0802	18.1957	RING1	25.9972	2.31049
DGCR8	25.1134	16.5606	RPL22L1	24.6441	3.57058
DHFR	23.8241	2.2933	RTFDC1	26.1915	2.41315
DHRS7	26.3805	2.29578	RTN3	25.0888	2.29562
DMD	27.0458	1.99999	S100A11	25.9421	3.56947
DNAJC17	24.9025	19.3229	SCCPDH	26.0178	2.35343
DNMT1	26.475	2.39141	SDAD1	22.8368	2.28144
DPY30	24.1579	2.17177	SEC24B	24.4071	2.29578
DTNA	25.5984	2.29462	SEC62	25.9998	18.6008
EMC2	25.0187	2.29565	SGPL1	24.6461	2.12867
EMC8	24.9634	19.1635	SIN3A	25.0969	3.60008
EML5	24.9433	2.16537	SKA1	26.5625	2.42222
ENPP1	26.2259	18.509	SLC27A4	27.4428	16.698
ENY2	24.9829	3.57073	SLC39A6	23.0438	1.4252
ERCC6L	24.7139	3.61605	SLC9A3R2	24.862	3.57038
ESF1	24.3109	3.56887	SLK	26.1956	20.0867

ESYT2	24.7615	2.18119	SMAP	26.9264	19.5531
EXOC7	25.2424	18.8086	SMARCA5	25.9058	2.3911
FAM101B	25.0685	2.29575	SMARCC2	25.8784	2.32678
FAM208A	25.3443	2.29579	SMC1B	26.7911	20.5192
FDXR	23.6574	2.02687	SMCHD1	23.9406	2.29539
GCLM	24.9837	19.9559	SOAT1	24.9852	2.29519
GEMIN2	25.8406	3.57008	SPATS2L	24.6388	2.2956
GIPC1	25.4184	2.07381	SPCS2	25.9022	2.35668
GLYR1	25.5026	19.3234	SRPR	26.6465	3.71915
GMPPA	23.212	2.29586	SRSF4	25.8677	3.68148
GNG5	26.0692	3.60338	SUPT4H1	25.2318	3.5703
GOLIM4	23.5718	19.8094	SURF6	26.8422	2.29574
GPATCH11	26.2952	19.0831	SVIL	24.7916	18.5786
GPATCH4	26.0001	18.4873	TBL3	27.0149	2.34584
HDDC3	25.2699	3.60504	TCEB3	26.4221	2.57909
HERC1	4.74474	1.79419	TMA7	26.4603	19.1969
HIBCH	26.3818	2.37231	TOR1AIP1	25.0779	2.29482
HMGN1	23.3232	13.118	TP53RK	25.1332	1.99311
HSD17B11	25.1918	2.29493	UACA	23.9673	24.6129
IBA57	24.4154	1.96067	UBL4A	25.1342	3.54849
ILKAP	24.5602	3.56803	UBR4	24.6722	3.56962
JMY	28.1047	17.4056	UQCRH	25.2134	3.42636
KHDRBS3	25.0193	2.29555	UQCRQ	24.6817	17.8928
KIAA0020	3.62285	1.51039	VAMP3	24.6677	2.29475
KIF2A	25.8995	3.7585	VDAC3	25.4046	2.26942
KRI1	24.204	2.29256	WIZ	25.3266	2.34273
L1RE1	25.5739	3.62106	XAB2	27.4176	4.0102
L3MBTL2	25.3395	3.57059	YME1L1	26.3386	3.59928
LEMD2	25.5098	3.56425	YTHDC1	23.7772	2.29487
LIMD1	24.5737	25.0698	YTHDF1	25.1166	18.1559
LMO7	24.6148	2.29585	YY1	25.4473	3.58169
LRRFIP1	25.973	2.38722	ZC3H18	25.1185	3.87519
LTBP1	25.463	2.2957	ZFP62	25.5161	14.4244

MAN1A2	25.8359	3.56782	ZFPL1	26.5958	19.2232
MAST3	28.8416	3.98953	ZNF141	25.3681	2.2947
MCAT	25.3796	3.53068	ZNF326	25.0232	2.29512
METTL1	25.0451	3.78467	ZNF622	25.5296	20.1343

Table 30 Novel CEP70 interaction partners (Tier 2)
Tier 2 (Sig A <0.05 and *p*-value <0.05) interactors are listed with their gene names, their ratio (CEP70_x/y_RAF1) and respective *p*-value (log_2). Table was taken from Woerz *et al.*, under review [3].

Gene names	Ratio	p-value ($-log_2$)	Gene names	Ratio	p-value ($-log_2$)
ABCB7	25.2716	3.65742	MICALCL	25.5451	2.33689
ACSL4	24.6142	19.5801	MIF	27.1729	21.5083
ADK	24.9438	18.9229	MINA	25.4826	3.80551
AFTPH	24.9992	21.087	MPHOSPH6	24.7016	3.56912
AGO1	24.9892	3.57061	MRPS16	25.6413	1.37088
AHSG	27.2943	22.5144	MRPS24	24.8593	2.29583
AKAP8	21.6644	14.0186	MRPS33	24.9712	3.56987
ALDH16A1	25.6673	3.57066	MRPS5	25.6198	2.11071
ALMS1	12.0578	3.00457	MTMR14	23.8853	1.31404
ARFIP2	24.6429	1.35695	NACAP1	26.0796	3.68989
ARHGAP18	26.4041	2.29548	NAT14	25.3938	1.32244
ARHGEF2	24.2743	3.56752	NDUFS6	25.1445	2.29566
ARID1A	25.1728	20.3704	NEK9	25.6364	1.32387
ASPH	24.8878	2.25335	NELFB	25.1923	19.8738
ASPM	25.6941	19.1346	NELFE	3.03217	1.80316
ATAD3B	2.92521	7.23432	NEMF	24.221	17.8037
ATG3	25.1388	2.27109	NENF	25.2904	2.01237
ATP6V1G1	24.2891	16.8476	NIFK	26.1516	1.37233
ATPIF1	28.2028	19.3636	NKTR	26.953	21.2186
ATXN2	25.6189	3.57053	NOLC1	27.6067	18.7053
AUTS2	23.5367	18.9735	NOP14	26.0568	20.0002
AXIN1	19.4388	2.29546	NRGN	23.6788	19.9643
B4GALNT3	30.5683	4.84693	NUCB2	26.0149	2.2955
BAX	25.7342	2.30988	NUP210	25.9116	2.35917
BOD1L1	26.8791	22.1762	OCIAD1	27.0417	3.91943

BRCA2	26.3389	3.59187	OXCT1	24.7845	2.01409
C11orf98	25.6602	2.25988	PALM	25.7367	3.56752
C12orf29	25.9816	16.3044	PAM16	25.4216	2.02646
C19orf53	25.4504	18.1598	PDXP	24.2674	3.56968
C7orf50	4.55379	1.98157	PIP4K2C	24.1663	2.29556
CASC3	25.8537	3.55188	PITHD1	25.567	2.34542
CBX5	24.4297	2.29387	PLAA	25.1435	3.55058
CCDC12	24.9779	21.3183	PLEKHA5	25.7558	2.29586
CCDC50	25.5141	21.0103	PNN	27.7669	2.54866
CCDC97	25.7888	1.34239	PNPO	25.0923	13.0894
CEP135	25.3543	19.8792	POLD2	25.0548	3.5706
CEP350	26.6426	1.34089	PPAN	26.2021	16.3931
CEP70	8.09268	12.5164	PPIG	25.1781	3.57041
CRK	24.9807	3.56783	PPME1	25.3946	1.35676
CRNKL1	25.4225	1.35997	PPP1CB	26.1918	1.33898
CSNK1E	25.0786	2.09107	PPP1R2	26.2653	20.4602
CSTF3	25.706	21.0793	PPP3CA	24.744	1.32627
CTBP1	25.5192	1.33784	PRDX4	26.8223	19.2773
CTCF	23.7459	23.22	PREB	26.2951	2.31529
CXorf56	25.6284	1.36377	PRKAR2B	29.6645	23.0216
CYFIP1	25.1166	3.57721	PSMB7	26.9772	2.67454
DAG1	24.9092	2.29567	PTDSS1	24.2263	2.29574
DBNL	25.013	1.32651	PTPN1	25.6452	19.947
DDX10	24.7998	2.32641	RAB35	25.7375	3.57053
DDX41	30.2721	3.67801	RAD23A	26.0684	2.29579
DDX50	25.2512	2.29583	RAD51	27.2874	3.65512
DECR1	25.0788	2.29501	RALB	25.2185	2.1076
DEK	26.0802	18.1957	RBM22	25.3893	2.29558
DGCR8	25.1134	16.5606	RDH13	23.9199	2.29525
DHFR	23.8241	2.2933	RECQL	25.4444	1.32833
DHRS7	26.3805	2.29578	RING1	25.9972	2.31049
DMD	27.0458	1.99999	RPL22L1	24.6441	3.57058
DNAJC17	24.9025	19.3229	RTFDC1	26.1915	2.41315

DNMT1	26.475	2.39141	RTN3	25.0888	2.29562
DPY30	24.1579	2.17177	S100A11	25.9421	3.56947
DTNA	25.5984	2.29462	SCCPDH	26.0178	2.35343
EMC2	25.0187	2.29565	SDAD1	22.8368	2.28144
EMC8	24.9634	19.1635	SEC24B	24.4071	2.29578
EML5	24.9433	2.16537	SEC62	25.9998	18.6008
ENPP1	26.2259	18.509	SETMAR	24.3546	1.3212
ENY2	24.9829	3.57073	SGPL1	24.6461	2.12867
ERCC6L	24.7139	3.61605	SIN3A	25.0969	3.60008
ESF1	24.3109	3.56887	SKA1	26.5625	2.42222
ESYT2	24.7615	2.18119	SLC27A4	27.4428	16.698
EXOC7	25.2424	18.8086	SLC39A6	23.0438	1.4252
FAM101B	25.0685	2.29575	SLC9A3R2	24.862	3.57038
FAM208A	25.3443	2.29579	SLK	26.1956	20.0867
FAM208B	26.3407	1.33759	SMAP	26.9264	19.5531
FDXR	23.6574	2.02687	SMARCA5	25.9058	2.3911
GATAD2A	24.735	1.33456	SMARCC2	25.8784	2.32678
GCLM	24.9837	19.9559	SMC1B	26.7911	20.5192
GEMIN2	25.8406	3.57008	SMCHD1	23.9406	2.29539
GIPC1	25.4184	2.07381	SMCR7L	25.4071	1.36671
GLYR1	25.5026	19.3234	SOAT1	24.9852	2.29519
GMPPA	23.212	2.29586	SPATS2L	24.6388	2.2956
GNG5	26.0692	3.60338	SPCS2	25.9022	2.35668
GOLIM4	23.5718	19.8094	SRPR	26.6465	3.71915
GPATCH11	26.2952	19.0831	SRSF4	25.8677	3.68148
GPATCH4	26.0001	18.4873	SUPT4H1	25.2318	3.5703
HDDC3	25.2699	3.60504	SURF6	26.8422	2.29574
HDHD2	25.084	1.34798	SVIL	24.7916	18.5786
HERC1	4.74474	1.79419	TBL3	27.0149	2.34584
HIBCH	26.3818	2.37231	TCEB3	26.4221	2.57909
HMGN1	23.3232	13.118	TMA7	26.4603	19.1969
HSD17B11	25.1918	2.29493	TOR1AIP1	25.0779	2.29482
IBA57	24.4154	1.96067	TP53RK	25.1332	1.99311

ILKAP	24.5602	3.56803	UACA	23.9673	24.6129
JMY	28.1047	17.4056	UBL4A	25.1342	3.54849
KHDRBS3	25.0193	2.29555	UBR4	24.6722	3.56962
KIAA0020	3.62285	1.51039	UQCRH	25.2134	3.42636
KIF2A	25.8995	3.7585	UQCRQ	24.6817	17.8928
KRI1	24.204	2.29256	VAMP3	24.6677	2.29475
KRR1	24.6107	1.38514	VDAC3	25.4046	2.26942
L1RE1	25.5739	3.62106	WIZ	25.3266	2.34273
L3MBTL2	25.3395	3.57059	XAB2	27.4176	4.0102
LEMD2	25.5098	3.56425	YME1L1	26.3386	3.59928
LIMD1	24.5737	25.0698	YTHDC1	23.7772	2.29487
LMO7	24.6148	2.29585	YTHDF1	25.1166	18.1559
LRRFIP1	25.973	2.38722	YY1	25.4473	3.58169
LTBP1	25.463	2.2957	ZC3H18	25.1185	3.87519
MAN1A2	25.8359	3.56782	ZFP62	25.5161	14.4244
MAST3	28.8416	3.98953	ZFPL1	26.5958	19.2232
MCAT	25.3796	3.53068	ZNF141	25.3681	2.2947
METAP2	25.4303	1.3124	ZNF326	25.0232	2.29512
METTL1	25.0451	3.78467	ZNF622	25.5296	20.1343
MFAP1	26.0588	3.89402	ZNF638	24.0039	22.2959
MIA3	24.7491	3.56968	ZNF768	26.4245	19.3848

10.7.5 List of domain specific interactors

A deletion analysis using MS was performed with overexpression constructs NSF-CEP70 CC1-2 and NSF-CEP70 NSF in HEK293T. The table shows domain specific interactors with their gene names, the ratio (CEP70 CC1-2_x/y_CEP70) and their -log2 median *p*-values of six biological replicates. Tier 1 proteins are listed. A both sided statistical test was conducted and only CEP70 interactors, that were already determined in 10.7.4 (Tier 1) were regarded. Red marked proteins indicate ciliary proteins, that are significantly enriched in CEP70 full length and changed in CEP70-CC1-2 fragment. Table was taken from Woerz *et al.*, under review [3].

Gene names	**Ratio**	**p-value ($-\log_2$)**	**Gene names**	**Ratio**	**p-value ($-\log_2$)**
ABCB7	-25.2716	2.18992	METTL1	-25.0451	18.2999
ACSL4	-24.6142	19.2791	MICALCL	-25.5451	3.43937
ADK	-24.9438	18.6219	MRPS33	-24.9712	3.26884
AFTPH	-24.9992	20.786	MRPS5	-25.6198	1.73129
AGO1	-24.9892	1.74737	NACAP1	-26.0796	3.37907

AHSG	-27.2943	22.2134	NELFE	-27.6255	3.39077
AKAP8	-21.6644	13.7176	NEMF	-24.221	3.22024
ALDH16A1	-25.6673	3.26963	NENF	-25.2904	1.74599
ALMS1	-8.58553	2.04163	NKTR	4.21582	10.3355
ARHGAP18	-26.4041	1.99445	NRGN	-23.6788	19.6633
ARID1A	-25.1728	3.27647	NUP210	-25.9116	3.31104
ASPM	-25.6941	18.8336	OCIAD1	-27.0417	3.56589
ATAD3B	-2.84899	6.74656	OXCT1	-24.7845	3.26524
ATG3	-25.1388	3.27098	PALM	-25.7367	3.26649
ATP6V1G1	-24.2891	16.5466	PAM16	-25.4216	3.26823
AUTS2	-23.5367	18.6725	PDXP	-24.2674	3.26865
AXIN1	-19.4388	1.99443	PIP4K2C	-24.1663	1.99453
B4GALNT3	-30.5683	18.1867	PITHD1	-25.567	3.28265
BAX	-25.7342	3.25568	PLAA	-25.1435	2.13204
BRCA2	-26.3389	2.05319	PLEKHA5	-25.7558	1.99483
C12orf29	-25.9816	3.45017	PNPO	-25.0923	12.7884
C19orf53	-25.4504	2.94413	POLD2	-25.0548	1.72758
C7orf50	3.56192	8.72694	PPAN	3.7915	6.59248
CBX5	-24.4297	1.99284	PPIG	-25.1781	3.26938
CCDC12	-24.9779	3.46731	PPP1R2	-26.2653	3.39716
CCDC50	-25.5141	20.7093	PREB	-26.2951	2.02632
CEP135	-25.3543	19.5782	PRKAR2B	-29.6645	22.7206
CRK	-24.9807	3.2668	PSMB7	-26.9772	18.5521
CSNK1E	-25.0786	3.26944	PTDSS1	-24.2263	1.99471
CSTF3	-25.706	3.18407	PTPN1	-25.6452	2.08068
DDX10	5.42838	1.34474	RAB35	-25.7375	3.2695
DECR1	-25.0788	1.99398	RAD23A	-26.0684	1.99476
DHFR	-23.8241	1.99227	RALB	-25.2185	3.26836
DHRS7	-26.3805	1.07669	S100A11	-25.9421	3.26844
DNAJC17	-24.9025	19.0219	SDAD1	6.56151	1.60118
DNMT1	-4.12023	1.64167	SEC24B	-24.4071	1.99475
DTNA	-25.5984	1.99359	SEC62	-25.9998	18.2998
EMC8	-24.9634	18.8625	SIN3A	-25.0969	2.09256

EML5	-24.9433	3.26842	SKA1	-26.5625	20.1845
ENPP1	-26.2259	18.208	SLC27A4	-27.4428	3.53133
ENY2	-24.9829	3.2697	SLC39A6	-23.0438	3.26729
ERCC6L	-24.7139	18.0247	SLC9A3R2	-24.862	1.77865
ESYT2	-24.7615	2.04396	SMAP	-26.9264	19.2521
FAM101B	-25.0685	1.99472	SMC1B	-26.7911	20.2182
FDXR	-23.6574	3.26771	SOAT1	-24.9852	1.99416
GIPC1	-25.4184	3.26931	SPCS2	-25.9022	2.02498
GLYR1	-25.5026	19.0224	SUPT4H1	-25.2318	3.26927
GMPPA	-23.212	1.99483	SVIL	-24.7916	3.61552
GNG5	-26.0692	3.35404	TMA7	-26.4603	3.31171
GOLIM4	-23.5718	19.5084	TOR1AIP1	-25.0779	1.99379
GPATCH11	-26.2952	2.00133	TP53RK	-25.1332	3.2677
HMGN1	-23.3232	12.817	UACA	-23.9673	3.36947
HSD17B11	-25.1918	1.9939	UBR4	-24.6722	1.85761
IBA57	-24.4154	3.26953	UQCRH	-25.2134	3.25113
ILKAP	-24.5602	1.80463	UQCRQ	-24.6817	17.5918
JMY	-28.1047	1.92855	VAMP3	-24.6677	1.99372
KHDRBS3	-25.0193	1.99452	VDAC3	-25.4046	3.26812
KIAA0020	4.40715	6.29731	WIZ	-25.3266	3.22953
KRI1	3.93592	1.28514	YME1L1	-26.3386	3.27907
L3MBTL2	-25.3395	1.77688	YTHDC1	-23.7772	1.99384
LEMD2	-25.5098	3.26322	YTHDF1	-25.1166	17.8548
LIMD1	-24.5737	24.7688	YY1	-25.4473	2.0279
LRRFIP1	-25.973	3.42684	ZFPL1	-26.5958	3.67785
LTBP1	-25.463	1.99467	ZNF141	2.87385	1.18777
MAN1A2	-25.8359	3.26679	ZNF638	-24.0039	3.98038

10.7.6 List of CEP70 TPR-CT interactors

A deletion analysis with CEP70 was conducted with overexpression constructs NSF-CEP70 TPR-CT and NSF-CEP70 NSF in HEK293T using MS analysis. The table presents identified CEP70 TPR-CT specific interactors with their gene names, the ratio (CEP70 TPR-CT_x/y_CEP70) and their -log2 median *p*-values of six biological replicates. Tier 1 proteins are presented. A both sided statistical test was deployed, and only CEP70 interaction partners, that were defined before, were considered (see 10.7.4, Tier 1). Table was taken from Woerz *et al.*, under review [3].

Gene names	**Ratio**	**p-value ($-\log_2$)**	**Gene names**	**Ratio**	**p-value ($-\log_2$)**

AFTPH	-24.9992	20.786	JMY	-28.1047	17.1046
ATAD3B	-1.26872	3.35164	MPHOSPH6	-24.7016	1.90625
B4GALNT3	-5.64771	8.81255	NKTR	-1.06223	4.06372
HERC1	-4.29313	6.34792	OCIAD1	1.72008	2.75357

10.8 ALMS1 protein coverage in CEP70 NSF sample

Figure 40 Identification of ALMS1 protein coverage in one CEP70-NSF sample
Identified peptides (exclusive unique peptides) of the ALMS1 protein (homo sapiens, 461 kDa) are highlighted in yellow in an exemplary CEP70 NSF sample provided by the program Scaffold. Amino acids matched to MS/MS spectrum are shown in yellow, while post-translational modified amino acids are depicted in green. Figure was taken from Woerz *et al.*, under review [3].

10.9 Nuclei count of 30 nM siRNA treated wt and ALMS1 KO cells

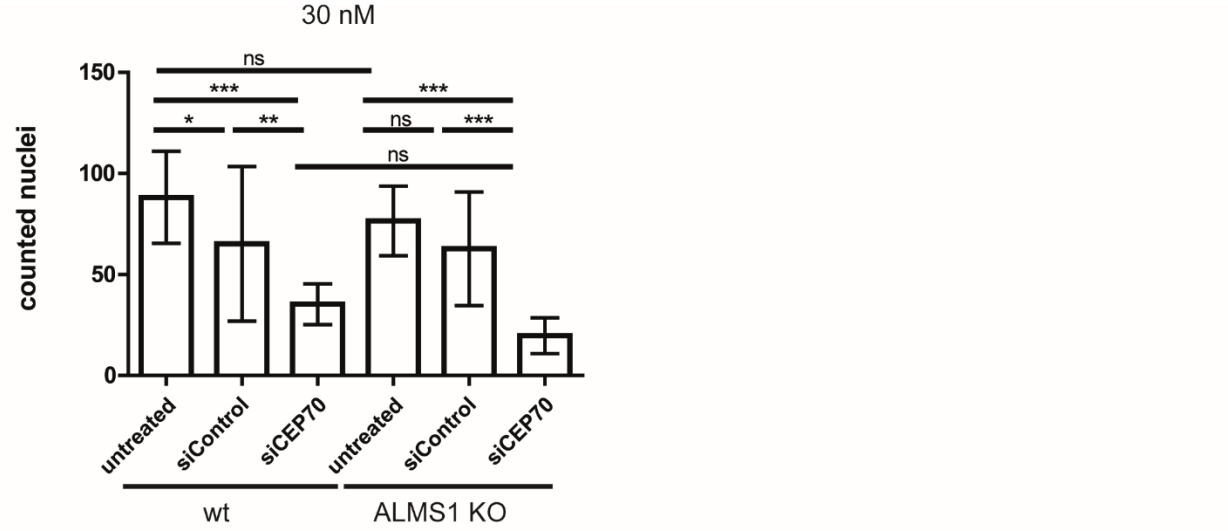

Figure 41 CEP70 KD shows increased cell loss in wt in hTERT-RPE1 cells
To assess cell loss, the nuclei were quantified in three independent experiments. The analysis included untreated cells, cells treated with siCEP70, and cells treated with siControl. Both wildtype and ALMS1-deficient cells were examined. Transfection of 30 nM CEP70 siRNA was performed for all experiments. Statistical analysis was conducted using ANOVA (Tukey), and the standard deviation (SD) was represented by error bars. Significance levels were indicated as follows: $p < 0.001$ denoted by *** asterisks, $p < 0.01$ denoted by ** asterisks, and $p > 0.05$ considered non-significant.

10.10 Identification of retina specific ALMS1 interactor

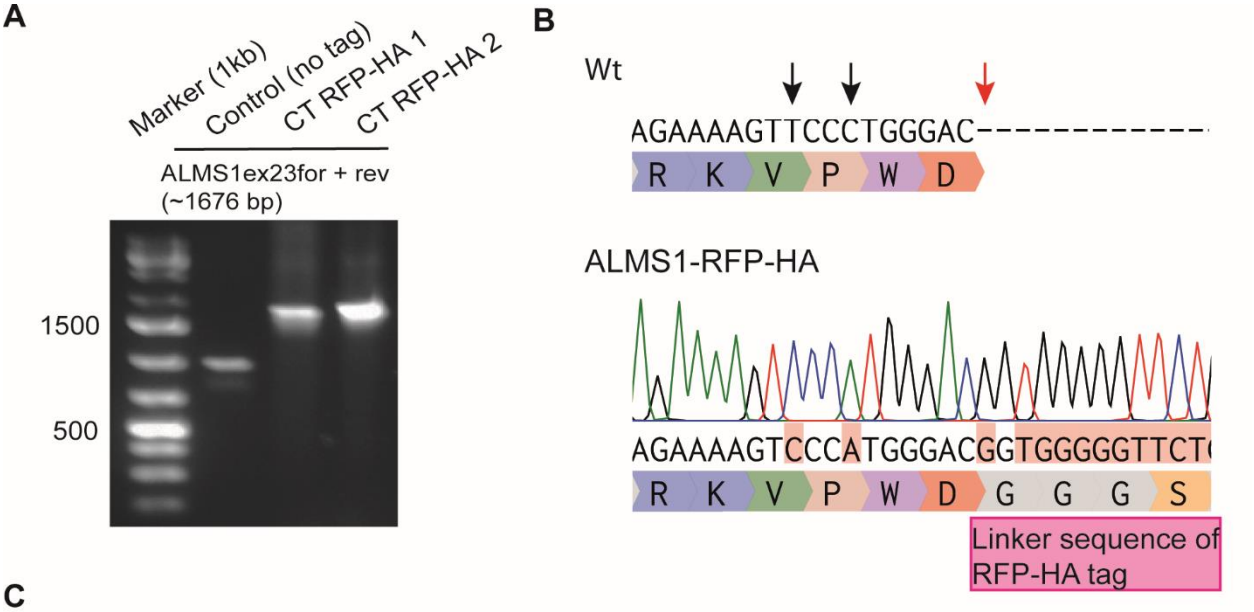

C

RFP-HA AP	Sequence coverage (%)	Tier 1	Tier 2
ALMS1 (bait)	75.9	+	+

Figure 42 Verification of endogenously RFP-HA tagged ALMS1
A, PCR with single clones was performed, followed by a gel electrophoresis. ALMS1 econ 23 forward and reverse primer were used to verify tag insertion. Control cells show a band at approximately 950 bp, while homozygous tag insertion exhibit one prominent band at a height of 1676 bp.

B Homozygously tagged ALMS1 cells were send in for sequencing, confirming tag insertion. Black arrows specify the wobble nucleotides, and the red arrow indicates the insertion site of RFP-HA tag. Wt sequence was used from ensemble.org (ENST00000613296.6, ALMS1-205, CCDS42697).
C Sequence coverage of ALMS1 in ALMS1-RFP-HA tagged cells identified by Perseus analysis. Identified potential protein interactors are categorized into Tier system as described above.

10.10.1 MaxQuant setting ALMS1-RFP-HA

Parameter	Value	Max. peptide mass [Da]	4600
Version	1.6.1.0	Min. peptide length for unspecific search	8
User name	mpcadmin	Max. peptide length for unspecific search	25
Machine name	ADMIN-PC	Razor protein FDR	True
Date of writing	12/17/2021 01:10:22	Disable MD5	False
Fixed modifications	Carbamidomethyl (C)	Max mods in site table	3
Include contaminants	True	Match unidentified features	True
PSM FDR	0.01	MS/MS tol. (FTMS)	20 ppm
XPSM FDR	0.01	Top MS/MS peaks per Da interval. (FTMS)	12
Protein FDR	0.01	Da interval. (FTMS)	100
Site FDR	0.01	MS/MS deisotoping (FTMS)	True
Use Normalized Ratios For Occupancy	True	MS/MS deisotoping tolerance (FTMS)	7
Min. peptide Length	7	MS/MS deisotoping tolerance unit (FTMS)	ppm
Min. score for unmodified peptides	0	MS/MS higher charges (FTMS)	True
Min. score for modified peptides	40	MS/MS water loss (FTMS)	True
Min. delta score for unmodified peptides	0	MS/MS ammonia loss (FTMS)	True
Min. delta score for modified peptides	6	MS/MS dependent losses (FTMS)	True
Min. unique peptides	0	MS/MS recalibration (FTMS)	False
Min. razor peptides	1	MS/MS tol. (ITMS)	0.5 Da
Min. peptides	1	Top MS/MS peaks per Da interval. (ITMS)	8
Use only unmodified peptides and	False	Da interval. (ITMS)	100
Peptides used for protein quantification	Razor	MS/MS deisotoping (ITMS)	False
Discard unmodified counterpart peptides	True	MS/MS deisotoping tolerance (ITMS)	0.15
Label min. ratio count	2	MS/MS deisotoping tolerance unit (ITMS)	Da
Use delta score	False	MS/MS higher charges (ITMS)	True
iBAQ	False	MS/MS water loss (ITMS)	True

iBAQ log fit	False	MS/MS ammonia loss (ITMS)	True
Match between runs	True	MS/MS dependent losses (ITMS)	True
Matching time window [min]	0.7	MS/MS recalibration (ITMS)	False
Alignment time window [min]	20	MS/MS tol. (TOF)	40 ppm
Find dependent peptides	False	Top MS/MS peaks per Da interval. (TOF)	10
Fasta file	C:\Databases\swissprot_human_2021_05_TB.fasta	Da interval. (TOF)	100
Decoy mode	revert	MS/MS deisotoping (TOF)	True
Include contaminants	True	MS/MS deisotoping tolerance (TOF)	0.01
Advanced ratios	True	MS/MS deisotoping tolerance unit (TOF)	Da
Fixed andromeda index folder		MS/MS higher charges (TOF)	True
Temporary folder		MS/MS water loss (TOF)	True
Combined folder location		MS/MS ammonia loss (TOF)	True
Second peptides	True	MS/MS dependent losses (TOF)	True
Stabilize large LFQ ratios	True	MS/MS recalibration (TOF)	False
Separate LFQ in parameter groups	False	MS/MS tol. (Unknown)	0.5 Da
Require MS/MS for LFQ comparisons	False	Top MS/MS peaks per Da interval. (Unknown)	8
Calculate peak properties	False	Da interval. (Unknown)	100
Main search max. combinations	200	MS/MS deisotoping (Unknown)	False
Advanced site intensities	True	MS/MS deisotoping tolerance (Unknown)	0.15
LFQ norm for sites and peptides	False	MS/MS deisotoping tolerance unit (Unknown)	Da
Write msScans table	True	MS/MS higher charges (Unknown)	True
Write msmsScans table	True	MS/MS water loss (Unknown)	True
Write ms3Scans table	True	MS/MS ammonia loss (Unknown)	True
Write allPeptides table	True	MS/MS dependent losses (Unknown)	True
Write mzRange table	True	MS/MS recalibration (Unknown)	False
Write pasefMsmsScans table	True	Site tables	Oxidation (M)Sites.txt
Write	True		

accumulatedPasefMsm
sScans table

10.10.2 List of ALMS1 interactors (ALMS1-RFP-HA)

Table 31 Tier 1 protein (ALMS1-RFP-HA)
An immunoprecipitation was performed with endogenously tagged RFP-HA ALMS1 in HEK293T cells and wildtype control cells. The table shows identified ALMS1 interactors with their gene names, the ratio (RPF_HA_x/y_Control) and their -log2 median *p*-values of six biological replicates. In this table, Tier 1 (Sig A <0.05 and Permutation based FDR p<0.05) interactors are listed.

Gene names	Ratio	p-value ($-log_2$)	Gene names	Ratio	p-value ($-log_2$)
ALMS1	7.4303	10.4217	GPR50	1.4853	4.9271
ANXA1	25.1318	18.5733	GSTM3	1.4994	5.6923
BAP18	2.0243	8.7483	HSPB1	1.4520	4.8744
CCDC88A	22.6266	18.9564	MDK	3.3409	5.1617
CEP70	27.4799	18.4862	GPR50	1.4853	4.9271

Table 32 Tier 2 proteins (ALMS1-RFP-HA)
The table presents identified ALMS1 interactors with their gene names, the ratio (RPF_HA_x/y_Control) and their -log2 median *p*-values and of eight biological replicates. Here, Tier 2 (Sig A <0.05 and *p*-value <0.05) identified interactors are listed.

Gene names	Ratio	p-value ($-log_2$)	Gene names	Ratio	p-value ($-log_2$)
ACADVL	24.9183	2.62149	LCP1	25.4218	3.8749
AKAP8L	1.29058	3.59143	LLGL1	1.67846	1.68609
ALMS1	7.43028	10.4217	LRP1B	1.32891	1.75237
ANKRD13A	23.2578	1.34518	LRWD1	22.6162	2.05113
ANXA1	25.1318	18.5733	MDK	3.34091	5.16165
ARMT1	2.02415	1.6192	MKI67	23.2259	2.33669
ASF1A	24.2788	1.33653	MURC	25.3266	3.56919
BAP18	2.02433	8.74831	MUT	22.4732	1.33228
C9orf64	1.50878	1.66101	NAGK	23.487	2.08545
CBR3	24.8038	1.60721	NELFB	1.28252	1.61588
CC2D1A	23.4489	2.34447	NUMA1	23.7615	1.3241
CCDC88A	22.6266	18.9564	PI4KB	21.5334	1.60769
CDC45	22.3652	1.60787	PPOX	2.33427	1.74851
CEP70	27.4799	18.4862	PTGR2	21.172	1.36042
CHD1L	1.92306	1.67652	RAB3D	1.30594	1.61707
CIT	2.44838	1.6853	S100A11	1.30673	3.21104
COPS6	1.4063	1.60192	SEPT10	2.03019	1.71263
CRABP2	1.34193	2.80613	SPINT1	24.8402	3.55806
CSNK2A2	2.3271	1.66583	SUGP2	23.8914	1.36467
GNL1	24.5803	2.3944	SUPT4H1	23.8832	1.34077
GPR50	1.48526	4.92713	SV2A	25.2195	2.29094
GPX1	1.92365	1.73038	SWAP70	21.9152	1.6074
GSTM3	1.49937	5.69225	TGOLN2	23.1217	1.39242
HMCES	23.1186	1.32947	TIMP1	1.68166	1.68388
HOXA5	24.1658	1.35639	TOP2A	4.64738	1.86122

HSPB1	1.45197	4.87437	TSR2	1.32193	1.56244
INF2	23.5426	3.56974	USP16	23.0651	2.04297
KIAA0020	1.66028	1.6894	VPS52	24.477	2.29563
L3HYPDH	22.9846	2.0941	WDR47	23.2315	1.60781
LAGE3	1.5386	1.60663	ZNF714	1.43047	1.63967

10.10.3 MaxQuant setting Retina Pull Down

Parameter	Value	Max. peptide mass [Da]	4600
Version	1.6.1.0	Min. peptide length for unspecific search	8
User name	mpcadmin	Max. peptide length for unspecific search	25
Machine name	ADMIN-PC	Razor protein FDR	True
Date of writing	10/21/2022 11:47:32	Disable MD5	False
Fixed modifications	Carbamidomethyl (C)	Max mods in site table	3
Include contaminants	True	Match unidentified features	True
PSM FDR	0.01	MS/MS tol. (FTMS)	20 ppm
XPSM FDR	0.01	Top MS/MS peaks per Da interval. (FTMS)	12
Protein FDR	0.01	Da interval. (FTMS)	100
Site FDR	0.01	MS/MS deisotoping (FTMS)	True
Use Normalized Ratios For Occupancy	True	MS/MS deisotoping tolerance (FTMS)	7
Min. peptide Length	7	MS/MS deisotoping tolerance unit (FTMS)	ppm
Min. score for unmodified peptides	0	MS/MS higher charges (FTMS)	True
Min. score for modified peptides	40	MS/MS water loss (FTMS)	True
Min. delta score for unmodified peptides	0	MS/MS ammonia loss (FTMS)	True
Min. delta score for modified peptides	6	MS/MS dependent losses (FTMS)	True
Min. unique peptides	0	MS/MS recalibration (FTMS)	False
Min. razor peptides	1	MS/MS tol. (ITMS)	0.5 Da
Min. peptides	1	Top MS/MS peaks per Da interval. (ITMS)	8
Use only unmodified peptides and	False	Da interval. (ITMS)	100
Peptides used for protein quantification	Razor	MS/MS deisotoping (ITMS)	False
Discard unmodified counterpart peptides	True	MS/MS deisotoping tolerance (ITMS)	0.15

Label min. ratio count	2	MS/MS deisotoping tolerance unit (ITMS)	Da
Use delta score	False	MS/MS higher charges (ITMS)	True
iBAQ	False	MS/MS water loss (ITMS)	True
iBAQ log fit	False	MS/MS ammonia loss (ITMS)	True
Match between runs	True	MS/MS dependent losses (ITMS)	True
Matching time window [min]	0.7	MS/MS recalibration (ITMS)	False
Alignment time window [min]	20	MS/MS tol. (TOF)	40 ppm
Find dependent peptides	False	Top MS/MS peaks per Da interval. (TOF)	10
Fasta file	C:\Databases\FWO-ALMS1_uniprot-proteome susscrofa 20201028.fasta	Da interval. (TOF)	100
Decoy mode	revert	MS/MS deisotoping (TOF)	True
Include contaminants	True	MS/MS deisotoping tolerance (TOF)	0.01
Advanced ratios	True	MS/MS deisotoping tolerance unit (TOF)	Da
Fixed andromeda index folder		MS/MS higher charges (TOF)	True
Temporary folder		MS/MS water loss (TOF)	True
Combined folder location		MS/MS ammonia loss (TOF)	True
Second peptides	True	MS/MS dependent losses (TOF)	True
Stabilize large LFQ ratios	True	MS/MS recalibration (TOF)	False
Separate LFQ in parameter groups	False	MS/MS tol. (Unknown)	0.5 Da
Require MS/MS for LFQ comparisons	False	Top MS/MS peaks per Da interval. (Unknown)	8
Calculate peak properties	False	Da interval. (Unknown)	100
Main search max. combinations	200	MS/MS deisotoping (Unknown)	False
Advanced site intensities	True	MS/MS deisotoping tolerance (Unknown)	0.15
LFQ norm for sites and peptides	False	MS/MS deisotoping tolerance unit (Unknown)	Da
Write msScans table	True	MS/MS higher charges (Unknown)	True
Write msmsScans table	True	MS/MS water loss (Unknown)	True
Write ms3Scans	True	MS/MS ammonia loss	True

table		(Unknown)	
Write allPeptides table	True	MS/MS dependent losses (Unknown)	True
Write mzRange table	True	MS/MS recalibration (Unknown)	False
Write pasefMsmsScans table	True	Site tables	Oxidation (M)Sites.txt
Write accumulatedPasefMsmsScans table	True		

10.10.4 List of ALMS1 interactors (Retina Pull Down)

Table 33 Tier 1 protein (Retina specific interactors)
The tables present an overview of significant enriched proteins received by a tissue specific protein complex analysis using porcine retina and RFP-HA tagged ALMS1 from HEK293T cells.
The table presents potential ALMS1 interactors with their gene names, the ratio (RPF_HA_x/y_Control) and their -log2 median *p*-values of six biological replicates. Here, Tier 1 (Sig A <0.05 and Permutation based FDR p<0.05) interactors are shown.

Gene names	Ratio	p-value ($-\log_2$)	Gene names	Ratio	p-value ($-\log_2$)
APIP	0.9956	3.7348	IGFBP5	21.3012	3.585
EFEMP1	21.6857	3.5469	LRP4	22.8143	3.5569
FBN1	24.572	16.6883	NQO2	24.1433	19.5594
FSTL1	22.3792	3.55952			

Table 34 Tier 2 proteins (Retina specific interactors)
Potential retina specific ALMS1 interactors with a less stringent analysis are grouped in Tier 2 (Sig A <0.05 and *p*-value <0.05) Gene names, the ratio (RPF_HA_x/y_Control) and their log2 median *p*-values are shown.

Gene names	Ratio	p-value ($-\log_2$)	Gene names	Ratio	p-value ($-\log_2$)
AARS1	0.691241	2.43028	LDLR	4.15183	1.87291
APIP	0.995615	3.73475	LOC100158003	0.632766	3.24075
ARHGAP24	22.8841	2.29893	LRP4	22.8143	3.5569
ARL6	0.992101	1.58418	NDUFS7	24.7452	2.18679
ARL6IP4	22.1212	1.60763	NOTCH2	1.01902	2.76616
CA2	24.2125	2.29572	NPHP4	1.05293	1.59009
CALCOCO1	25.3426	1.31534	NQO2	24.1433	19.5594
CCDC61	23.0488	1.3233	OGT	0.757307	1.53869
CCN2	23.0919	2.29513	PDAP1	22.4292	1.31796
CDC42BPB	25.0927	1.33613	PDE12	23.8096	2.04193
CDC5L	0.799206	1.74883	PLEKHO2	0.836922	1.55062
DPP3	23.8181	2.03428	PRPH	23.7351	2.28996
DSP	21.3158	1.38385	PSME2	22.8142	2.02849
EFEMP1	21.6857	3.54686	SIK3	1.28665	1.62932
EGF-like domain-containing	0.644296	2.04417	SLC27A1	23.1572	1.3245

protein					
FASN	2.66032	3.08075	SRBD1	23.5043	1.36882
FBN1	24.572	16.6883	SUN1	22.7746	2.25101
FSTL1	22.3792	3.55952	TIMP2	23.9835	2.04289
GAD1 GAD67	23.1231	1.32	TRAPPC6B	23.5361	2.29571
hALMS1	6.75895	2.24275	VPS28	24.7898	2.24785
HAX1	1.06577	1.59988	XRCC6	22.2736	1.60777
IGFBP5	21.3012	3.585	ZNF326	23.8855	2.04518

10.10.5 Protein sequence of human and porcine ALMS1

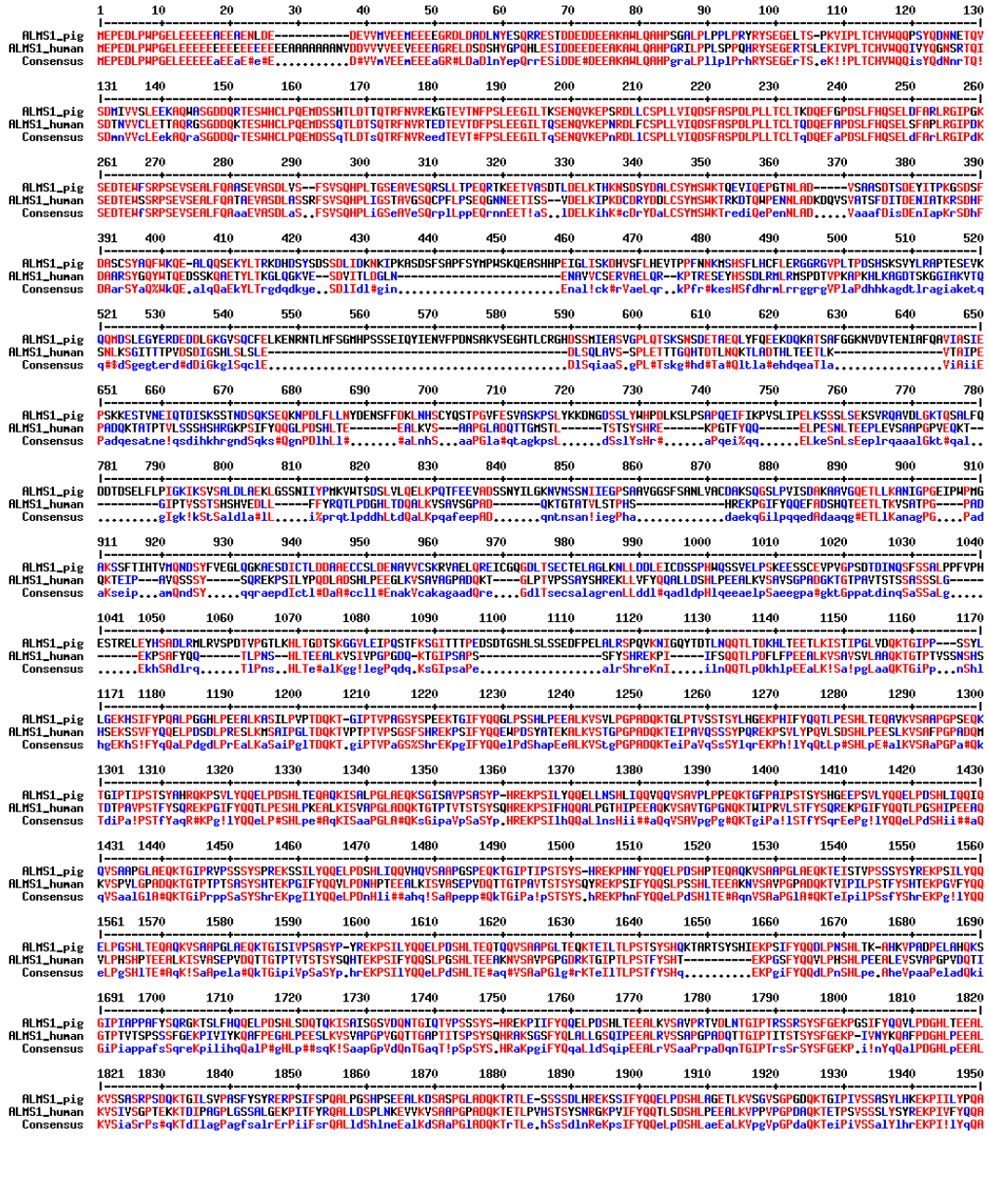

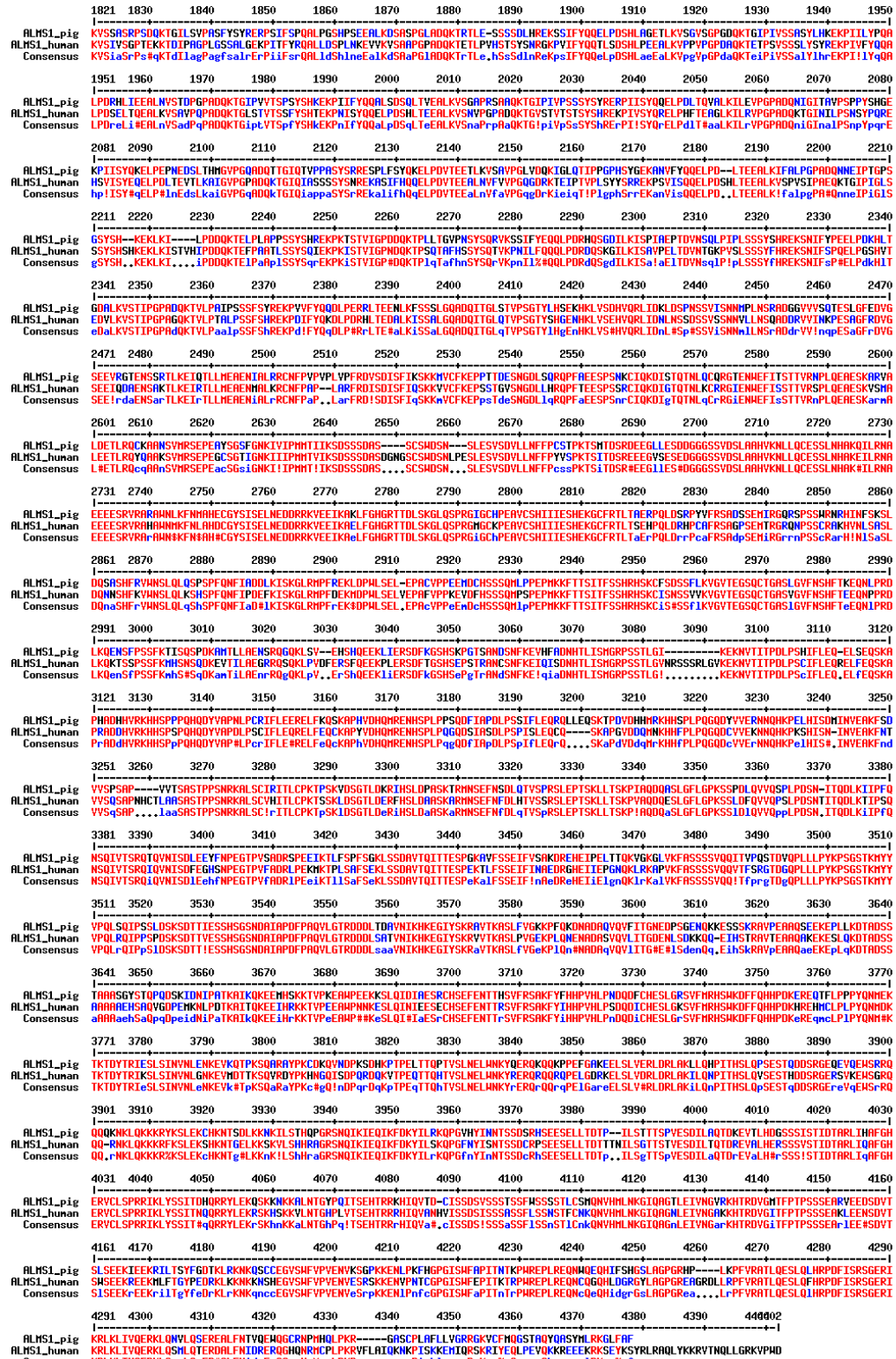

Figure 43 Alignment of human vs. sus scrofa ALMS1 protein sequence

Protein sequences of human and porcine ALMS1 were used from ensemble.org and aligned with MultAlin [293]. Compliances are depicted in red, while differences of single amino acid are in blue or of larger regions are in black. Ensemble.org provided protein sequences of pig-largewhite (ENSSSCT00025093656.1, ALMS1-204, 4332 aa) and human ALMS1 (ENST00000613296.6, ALMS1-205). Ensemble release 109- Feb 2023.

10.11 ALMS1 localizes at the BB of cilia in human retina

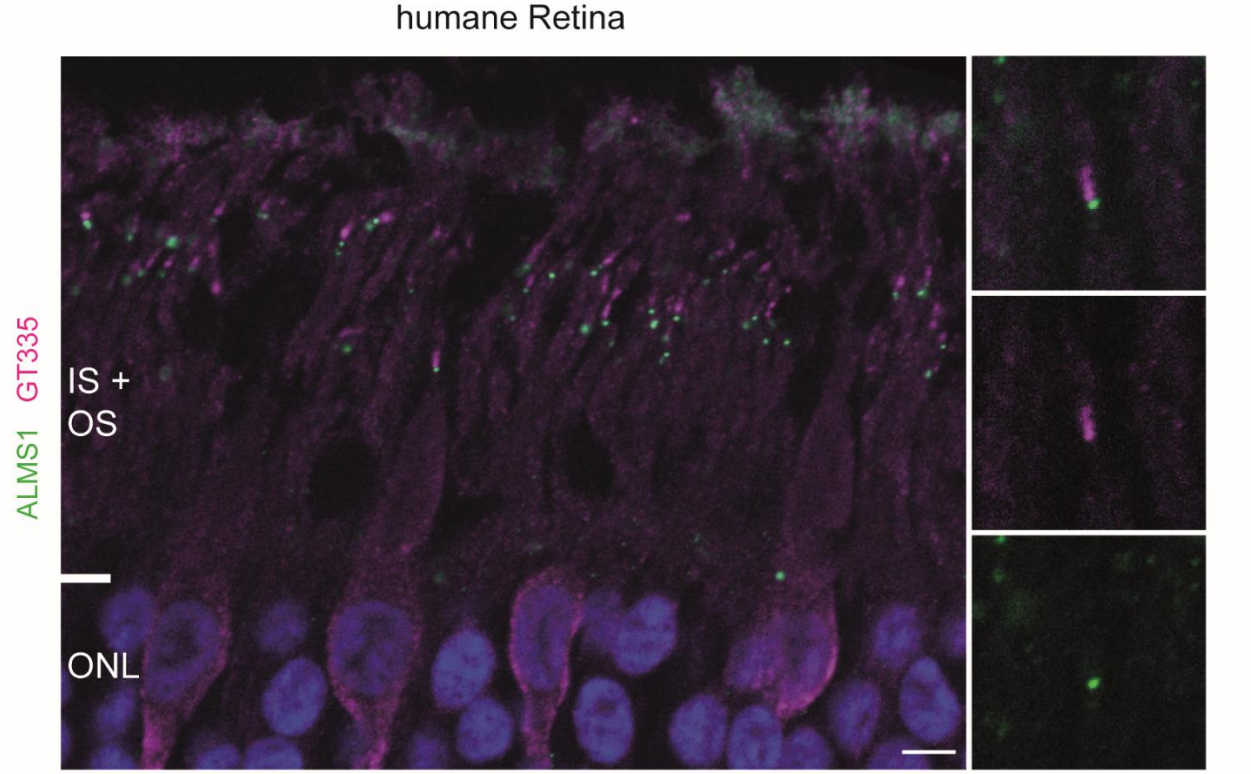

Figure 44 ALMS1 localizes at the cilium in human retina
Microscopy picture of human retina was kindly provided by Sylvia Bolz and was stained by Christine Henes. Nuclei are marked in blue. ALMS1 is depicted in green and GT335, indicating ciliary localization, in magenta. Scale bar is set to 5 µm.

10.12 ALMS1 localizes at the BB of photoreceptor precursor cells

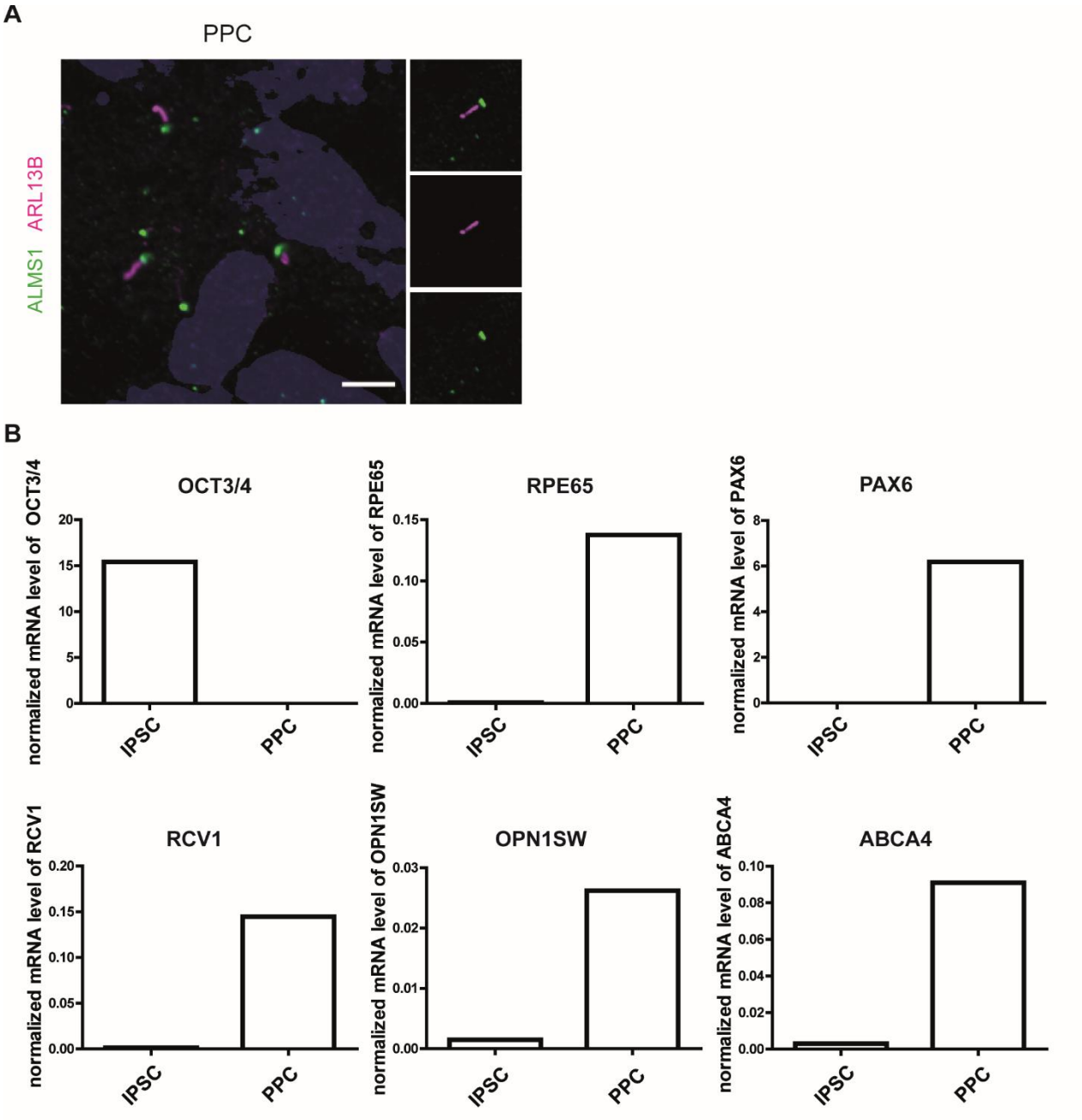

Figure 45 PPC as a potential model for ALMS1 research
A, Photoreceptor precursor cells (PPC, 30 days old) control cells were kindly provided by Pietro De Angeli. ALMS1 is depicted in green, ARL13B in magenta and DAPI in blue. Scale bar measures 5 µm.
B, Validation of PPC was done using qPCR and marker for IPSC and PPC and normalized against GUSB. N=1